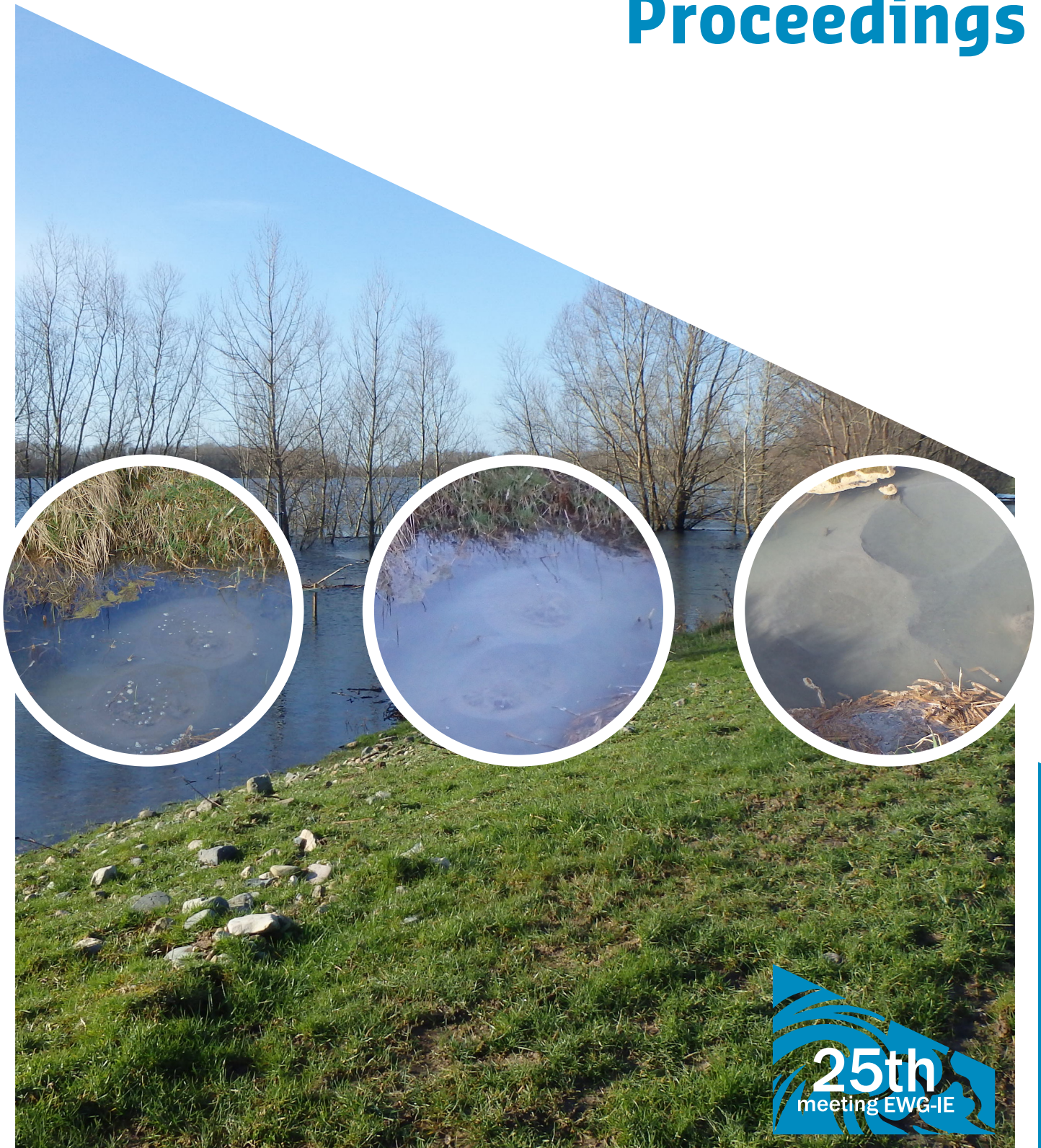


# 25th Meeting

## European Working Group on Internal Erosion in Embankment Dams & their Foundations

# Proceedings



**The information contained in this publication regarding commercial projects or firms may not be used for advertising or promotional purposes and may not be construed as an endorsement of any product or firm by the organizing committee of the 25th Meeting of the European Working Group. The organizing committee of the 25th Meeting of the European Working Group does not accept any responsibility for the statements made or the opinions expressed in this publication.**

**Copyright ©2017 Deltares**

**Proceedings of the 25th meeting of the Working Group on Internal Erosion in embankment dams and their foundations**

**Edited by: V.M. van Beek and A.R. Koelewijn**

**ISBN: 978-90-827468-1-5**



**Proceedings**  
**September 4-7**  
**Delft , The Netherlands**

25th Meeting European Working Group  
on Internal Erosion in Embankment  
Dams & their Foundations



## Organizing committee

Dr. Vera van Beek  
Dr. André Koelewijn  
Mr. Jan Jaap Heerema  
Prof. Dr. Adam Bezuijen  
Prof. Dr. Cristina Jommi  
Prof. Dr. Stéphane Bonelli

Deltares, The Netherlands  
Deltares, The Netherlands  
Rijkswaterstaat, The Netherlands  
Ghent University, Belgium  
Delft University of Technology, The Netherlands  
IRSTEA, France



## Reviewers

Prof. Dr. Adam Bezuijen  
Ms. Maaïke Blauw  
Mr. Jan Blinde  
Dr. Marcel Bottema  
Mr. Ulrich Förster  
Mr. Jan Jaap Heerema  
Dr. Marc Hijma  
Dr. Gijs Hoffmans  
Prof. Dr. Cristina Jommi  
Dr. Wim Kanning

Dr. André Koelewijn  
Mr. John Lambert  
Dr. Maria Konstantinou  
Dr. Pierre Philippe  
Dr. Esther Rosenbrand  
Ms. Maria Luisa Taccari  
Mr. Frans van den Berg  
Mr. Harry van Essen  
Ms. Kristine Vandenboer  
Dr. Ane Wiersma



# Contents

1. **Internal erosion in dams and dikes: a comparison**  
A.R. Koelewijn & R. Bridle
12. **Fine-tuning the evaluation of suffusion of silt-sand-gravel soils – a comparative study of LTU and UNSW tests**  
H. Rönnqvist
21. **Pipe depth measurement in small-scale backward erosion piping experiments**  
K. Vandenboer, V.M. van Beek & A. Bezuijen
29. **Physical measurements of the backward erosion piping process**  
B.A. Robbins & V.M. van Beek
38. **Contribution for assessing filter efficiency in zoned dams**  
A. Benamar, S. Azirou & A. Tahakourt
48. **Development of a coaxial cell for porosity measurements during contact erosion experiments**  
T. Bittner, T. Bore, A. Scheuermann, M. Bajodek & K.J. Witt
58. **Erosion behaviour of gap-graded soils due to upward flow**  
R. Correia dos Santos, L. Caldeira & E. Maranhã das Neves
69. **Historical information and advanced tools for flood protection and structures management**  
S. Aielli, S. Parodi, S. Pavan & A. Rosso
79. **Numerical simulation of the groundwater flow leading to sand boil reactivation in the Po River**  
M.F. García Martínez, M. Marchi, L. Tonni, G. Gottardi, A. Bezuijen & A. Rosso
88. **The influence of the leakage length on the initiation of backward erosion piping**  
A. Bezuijen
97. **Evaluation of Dutch backward erosion piping models and a future perspectives**  
V.M. van Beek & G.J.C.M. Hoffmans
114. **Stress-strain behavior of soils having undergone different amounts of internal erosion**  
S. Li, A.R. Russell & D. Muir Wood
123. **Large triaxial device for suffusion erodibility and mechanical behavior characterization of coarse soils**  
D. Marot, F. Bendahmane, R. Andrianatrehina & R. Gelet
133. **Resistance to erosion of lime treated soils and perspectives for coastal dikes**  
M. De Baecque, C. Chevalier, S. Palma Lopes, M. Le Feuvre, P. Reiffsteck, I. Charles & G. Herrier

- 143. Experiences on the use of polymer coated steel net for the protection of dykes against the intrusion of beavers**  
P. Di Pietro
- 150. Merging criteria for the definition of a local pore and the CSD computation of granular materials**  
F. Seblany, U. Homberg & E. Vincens & P. Winkler & K.J. Witt
- 160. Online Alarming for Internal Erosion**  
J. Dornstädter, A. Fabritius & B. Heinemann

# Internal erosion in dams and dikes: a comparison

A.R. Koelewijn

*Deltares, Delft, Netherlands*

R. Bridle

*Dam Safety Ltd, Great Missenden, United Kingdom*

**Abstract:** Dams and dikes are both water-retaining earth embankments. These are vulnerable to internal erosion but specific differences lead to varying vulnerabilities to different types of internal erosion:

- Dams are usually zoned, with potential filtering capability to arrest piping if it is initiated, while dikes are more commonly unzoned and incapable of arresting erosion.
- Dams are usually higher than dikes, therefore the pressures are higher and leakages are more damaging.
- Dams have usually been built to their present height in one stage, dikes have often been improved over time, with a present crest height considerably higher than the initial height. In case of a significant raise, the original design assumptions no longer apply and modifications to the existing structure to provide sufficient safety may be costly.
- Dams have a limited crest length, while dikes may extend for hundreds of kilometres. This poses quite different possibilities and challenges for inspection and monitoring.
- Dams are built across a stream to block it, while dikes are built along it and only guide the stream. For the design and construction of dams the flow must be sufficiently blocked, including through the foundation. Many dikes on untreated sandy foundations are vulnerable to backward erosion.
- Dams always require provisions to pass the flow, for dikes this is rare. Concentrated leak erosion along culverts and spillways often poses a threat to dams but rarely to dikes.

Each of the above points will be illustrated by practical cases, focusing on the various mechanisms of internal erosion which are dealt with first.

Keywords: Internal erosion; dams; dikes, levees, flood and canal embankments; case histories; monitoring; remediation.

## 1 INTRODUCTION

The recent publication of ICOLD (International Commission on Large Dams) Bulletin 164 on internal erosion in existing dams, dikes and levees and their foundations (ICOLD 2016, 2015) has brought together knowledge and experience from research and practice to provide guidance on the causes of internal erosion and how to investigate, analyze, remediate and monitor earth water-retaining embankments to protect them against failure by internal erosion. ICOLD Bulletin 164 is referred to as 'the Bulletin' in this paper.

The ICOLD European Club Working Group on Internal Erosion (EWGIE) has played a central role in bringing this knowledge together. At its heart is the major advance in understanding of the mechanisms of internal erosion, an issue which has previously been dealt with by disconnected research programs, and approached in practice by qualitative and quantitative risk assessment. The mechanics of internal erosion, which apply to all types of earth water-retaining embankments, are described in the following section. Subsequent sections compare how internal erosion affects, and is dealt with, in dikes and embankment dams.

## **2 INTERNAL EROSION MECHANICS**

### **2.1 Internal erosion occurs when hydraulic forces exceed resistance**

Recent advances in understanding show that internal erosion occurs in earth water-retaining embankments when the hydraulic forces imposed by water flowing through openings or seeping through pore spaces exceed the ability of the soils in the embankments or their foundations to resist them.

### **2.2 Four mechanisms of initiation of internal erosion**

As detailed in the Bulletin, internal erosion is initiated by one of the following four mechanisms:

1. Concentrated leak erosion in which water flowing through cracks or openings erodes soil particles from the walls of the cracks or openings.
2. Contact erosion which occurs at the interface of coarse and fine soil layers when the velocity of water flowing through the coarse layer is sufficient to erode soil particles from the fine layer.
3. Suffusion in which water flowing through the pores in gap-graded soils erodes fine particles through the pore spaces in the matrix of coarse particles.
4. Backward erosion which occurs in sandy foundations below earth embankments able to ‘hold a roof’ above backward erosion pipes that initiate in the foundation sand at the downstream toe of the embankment and progress upstream (‘backwards’), eventually breaking through into the reservoir or waterway retained by the embankment.

The Bulletin makes it possible to estimate the hydraulic load, usually expressed as the water level in the reservoir or waterway, at which internal erosion will initiate. The highest hydraulic loads usually occur during floods.

### **2.3 Four phases to failure by internal erosion**

Internal erosion proceeds towards failure in four phases, as follows:

1. Initiation by one of the four initiating mechanisms listed above when the hydraulic load, usually expressed as hydraulic gradient and water level, exceeds the ability of soils in the embankment to resist it
2. Continuation as eroded particles continue to move after erosion is initiated. Erosion may be arrested at this phase if there are effective filters or fill capable of filtering downstream of the eroding zone, usually the core in a zoned earth embankment. In unzoned embankments (often called ‘homogeneous’ dams or embankments) no other zones are present; consequently unzoned embankments are markedly more vulnerable to internal erosion failure than zoned embankments.
3. Progression, as the erosion forms erosion pipes or enlarges cracks or openings
4. Breach, when collapse of the embankment occurs as erosion pipes enlarge, or excess flow causes collapse of the crest or instability of the downstream slope.

### **2.4 Filtering capabilities of fills in zoned embankments**

Chapter 7 in Volume 1 of the Bulletin explains how to assess whether the fills and filters, if any, in zoned embankments would be capable of filtering eroded particles, and thereby arresting erosion and preventing continuation towards failure. The ‘filter erosion boundaries’ concept (Foster, 2007) can be applied to determine whether the fills in the zones downstream of the eroding zone, usually the core, are no-, some- or excessive-erosion filters, arresting erosion after increasing amounts of sediment-laden leakage and damage, including sinkholes in excessive-erosion ‘filters’. Fills or filters coarser than excessive-erosion filters cannot arrest erosion, and erosion if initiated would continue unchecked towards failure.

The Bulletin includes an example of an investigation to examine if the glacial till shoulder fill of a typical British dam would filter and arrest erosion of particles from the puddled clay core.

The capability of filters in embankments constructed with filter zones before reliable filter criteria (e.g. Sherard and Dunnigan, 1989) became available should be examined using the filter erosion

boundaries approach. The Bulletin includes an example of ineffective widely graded filters at Churchill Falls Dike, which allowed erosion to continue, at normal water levels (i.e. at low hydraulic loads), to the extent that sinkholes formed. Water levels were drawn down before failure occurred, but the filters were at best excessive-erosion filters, or more likely were so coarse that erosion would have continued to failure if the water level had not been drawn down.

Most dikes were built long before filters were applied. With increasing water levels, effects of subsidence and higher demands on flood safety, major improvement works on existing dikes may be needed to address issues resulting from the lack of a proper filter in the embankment and its foundation. The International Levee Handbook provides extensive advice with practical examples, like the Natomas Levee near Sacramento, USA (CIRIA, 2013:1028-1030, 1056-1058).

## 2.5 No filtering capability in unzoned ('homogeneous') embankments

Unzoned dams have no filtering capacity because there are no more-or-less vertical zones downstream of an eroding zone which might provide some kind of filter. This is illustrated in Figure 1 where the concern is contact erosion (CE) at the interface between more-or-less horizontal layers of coarse and fine fills in an unzoned dam. If contact erosion initiated, eroded particles from the fine layer would be carried through the coarse layer to the downstream face, possibly leading to settlement, overtopping and collapse.

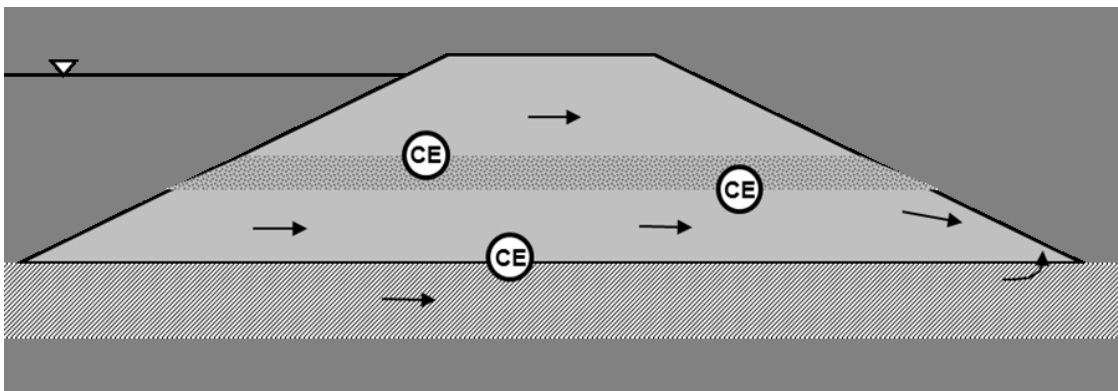


Figure 1. Showing vulnerability of an unzoned dam to contact erosion (CE) at the interfaces between coarse and fine layers. Eroded fine particles could be carried to the downstream face, possibly resulting in crest settlement, overtopping and collapse (from Beguin et al, 2009).

## 3 PROTECTING UNZONED EMBANKMENTS AGAINST INTERNAL EROSION

Many waterway embankments and older dams are unzoned, often with variable heterogeneous fill, sometimes with layers of widely differing grading. Volume 2 of the Bulletin includes examples of unzoned canal embankments where unchecked suffusion caused increased leakage at Jonage Dike and settlement at Kelms Dike. The increasing leakage was identified by routine measurements of drainage flow and the settlement by routine leveling along the crest. The embankments were remediated by grouting over the lengths affected.

Remediation is dealt with in Chapter 10 of Volume 1 and Chapter 5 of Volume 2 of the Bulletin. Alternatives to grouting include 'barriers' – sheet piles, diaphragm walls and secant piles – or filters – usually within filtered berms constructed over the full height of the downstream slope of unzoned dams and embankments to filter eroded particles there.

Barriers are often a convenient alternative where the foundations are also vulnerable to internal erosion. Examples from Volume 2 of the Bulletin include Shikwamkwa replacement dam where a deep plastic concrete cut-off wall through the foundation and the lower fill linked to the fine silty sand core.

The 70 km of the Feather River flood management embankments in California, USA, were remediated by various combinations of embankment core and cut-offs through lower fill and into the foundations. At many dams and embankments, short barriers are installed along the crest to block cracks formed by desiccation or differential settlement.

In addition to providing previously unzoned embankments with filtering capacity, filtered berms also reduce seepage velocity in coarser layers, thereby reducing the hydraulic load imposed, possibly below that required to initiate erosion. However the downstream filters may restrict drainage capacity and thereby increase pore pressure in the embankments. This may adversely affect their stability. Also, eroded particles accumulated on the inner filter impose hydraulic pressure on the berm, which must be designed as a 'weighted' berm providing sufficient resistance against the hydraulic forces to prevent fracture or uplift of the berm.

Volume 2 of the Bulletin describes the filtered berm added to Matahina Dam in New Zealand. This berm was particularly carefully designed because it is to continue to provide filtering capability in the event of cracking of the fill when movement occurs along an active fault during earthquakes. The filter materials were selected to be incapable of holding cracks and thereby remain effective when such movement and cracking occurs.

## **4 INFLUENCE OF HEIGHT ON INTERNAL EROSION POTENTIAL**

### **4.1 Height and consequences of failures of dams and dikes**

The most significant consequence of the height of dams and dikes is that if failure occurs, the flood wave from high structures will be deep and likely to cause loss of life in the floodplain downstream; casualties are less likely to occur in the shallow flood wave from low structures. It is the custom to design dams to high safety standards intended to impose a very low probability of loss of life downstream. Many flood management dikes are designed to cost-benefit criteria. However, loss of life from failures of non-dam embankments, at New Orleans for example after the Hurricane Katrina embankment failures, is leading to a change and in USA the 'loss of life' criterion is now being applied to these situations too.

In France there was loss of life during floods from failures in the 200 km of flood embankments in Rhone delta. The situation has been examined by Mallet et al. (2014) and Mallet and Fry (2016) by quantitative risk analysis using the mechanics detailed in the Bulletin to identify probability of failure by concentrated leak erosion, particularly at incompletely sealed badger burrows, and by backward erosion on lengths of embankments on sandy foundations. In places there was an unacceptably high probability of failure. Remedial work is progressing to reduce the annual probability of failure to 1 in 10,000-years or lower, a high standard as demanded by the potential of failures to cause fatalities.

### **4.2 Height and hydraulic loads causing internal erosion**

The hydraulic loads that initiate internal erosion, other than suffusion, can be estimated from the methods given in the Bulletin, verified if appropriate by laboratory testing. The hydraulic load initiating suffusion must be determined by testing. The loads are expressed as hydraulic gradient ( $H/L$ ), and  $L$ , the width of the embankment, is normally known, allowing  $H$ , the water level that would initiate internal erosion, to be readily determined.

High dams and low dikes are both subject to the hydraulic loads, particularly when water level is high during floods, that may initiate erosion. However high dams often include narrow cores, low permeability zones, supported by wide high permeability zones in the shoulder fills. This subjects the cores to high gradients, which may become 'critical', sufficient to initiate erosion during extreme floods, and unless they are protected by effective filters, the erosive forces may rapidly enlarge cracks, accelerate suffusion, erode fine materials from coarse to fine interfaces, or form continuous backward erosion pipes, leading to rapid failure.

With some caveats regarding seasonal and other changes in cracking in embankments, existing embankments have demonstrated that they are resistant to internal erosion to the highest water level, usually the highest flood level, to which they have ever been subjected.

However, without investigation and analysis using the Bulletin, it is not possible to know, or pre-empt by monitoring and surveillance, the water level that will cause an embankment to fail. Failure will occur during an extreme flood, more severe than any experienced previously, with quantities of flow that cannot be diverted by emptying pipes or similar. Progression to failure will be rapid. In case of an acceptable annual probability of failure in the order of magnitude of 1 in 10,000 years, the flood level will nearly always be higher than any historical flood level. If analysis shows that internal erosion failure will occur at an unacceptably low water level, remediation will be required. A surveillance and monitoring regime can then be deployed to confirm that the remediated embankment remains in the condition that the remediation was designed to achieve.

## 5 HEIGHT INCREASES LEADING TO BACKWARD EROSION

A major difference between dams and dikes is that dams are hardly ever raised after initial completion, and if they are, usually a thorough redesign is made. Dikes on the other hand are often raised, especially in past centuries, when the main concern was with the attained crest height only. As a result, other failure mechanisms have often been neglected. This especially holds for sand layers in the foundation, underneath the original base of the dike. Knowledge about the main cause of internal erosion there was lacking at the time many dikes were built. Besides, the original height of the dike may have been insufficient to cause backward erosion.

After several attempts to describe the phenomenon of backward erosion (e.g. Clibborn and Beresford (1902) and Bligh (1907)) came close, but erred with respect to the influence of the weight of the overlying construction, in 1910 Bligh managed to capture the essence, including a practical rule for the required ratio of  $H/L$  ( $H$ =hydraulic head,  $L$ =horizontal seepage length) to be safe, with coefficients depending on the type of granular material in the foundation. This was based on his (undocumented) experience on masonry weirs in India, but it holds for any granular layer underneath a cohesive layer able to 'hold a roof' above the sandy foundation.

Based upon the forces exerted on individual grains by the seepage flow in an already existing backward erosion pipe, Sellmeijer (1988) showed why sand boils behind pipes of limited length will not lead to failure, provided that a critical head (corresponding to a critical pipe length) is not exceeded. He also showed the dependence on scale: the larger a dike, the smaller the maximum allowable ratio of  $H/L$  becomes for an otherwise given situation. In other words: Bligh's rule is less safe for larger constructions.

Recently, Van Beek (2015) explained the process at the head of the pipe ('primary erosion'), while Sellmeijer focused on the enlarging of a pipe only ('secondary erosion'). Besides, Sellmeijer's theory describes a two-dimensional configuration only – corresponding to a longitudinally uniform outflow situation at the toe of the dam or dike – while in reality three-dimensional situations are often found, e.g. a single outlet through a confining layer of a local depression or a drainage ditch leading away from the structure.

Knowledge of the causes of potential failure helps to devise prevention measures. The large scale field tests ( $L=15$  m) at the IJkdijk in 2009 and supporting laboratory tests (Van Beek et al., 2011) have led to the following measures against backward erosion that were all successfully tested in similar tests at the IJkdijk in 2012, although failure was not reached (Koelewijn, 2014):

- A controllable horizontal drainage tube under the embankment, installed e.g. by horizontal directional drilling, to intercept and drain water, reducing the flow velocity and avoiding erosion;
- A vertically inserted permeable geotextile to block particles without hindering groundwater flow. Pipes will occur as usual but will not pass beyond the geotextile, nor under it;
- A coarse granular filter, meeting all filter criteria with respect to the base soil, covered by an impervious layer. The effectiveness is roughly similar to that of the geotextile.

In the past five years, these techniques have all been developed further. The controllable drainage tube has been applied in a dike rehabilitation project over a length of 100 m at a dike along the IJssel river near Veessen (the Netherlands), as a cost-effective alternative saving an old farmhouse, considered typical for the area from a cultural-historical perspective. The situation is indicated in Figure 2.



Figure 2. Alignment of controllable drainage tube near Veessen

The vertically inserted geotextile has been applied at four different locations in the main dike along the Lek river between Hagestein and Opheusden in the Netherlands. These sections have lengths of 100 to 500 meters (Förster et al., 2015). Field tests have been carried out at a dike of secondary importance to investigate various failure mechanisms associated with this solution (Koelewijn et al., 2017a). Two other applications are in preparation, as well as large-scale tests to determine the critical head of this system.

For the coarse sand barrier such large-scale tests are part of a thorough test program carried out from Summer 2017 until Autumn 2018, in preparation of applications on real dikes (Koelewijn et al., 2017b).

## 6 INFLUENCES OF THE LENGTH OF DAMS AND DIKES

Long embankments present challenges in investigations to determine foundation conditions and in long-term surveillance and monitoring. While it is feasible to investigate the footprint of a dam in adequate detail to provide sufficient information to design for foundation watertightness and stability, this may not be feasible along long lengths of flood management and waterways embankments. An understanding of the river geomorphology can simplify matters. Figure 3 shows how river meandering and its consequences have formed differing river channels cut into the older alluvium, which have subsequently been infilled with sand and other alluvium, and often covered with a fine-grained soil or clay blanket, usually called ‘the confining layer’, at the surface.

The floodplain deposits of major rivers such as the Mississippi, for example, seem less complex than that in Figure 3, and may be sensibly the same for many miles. Within the older floodplain deposits, the river course has meandered in more recent times, leaving modern alluvium within the remnant channels. Reports of incidents of Mississippi floods in 2011 (Shrewbridge, 2016), and 1993 (Navin, 2016), seem to show that these materials are more vulnerable to backward erosion than the older floodplain deposits. Consequently, identifying the locations of such deposits by geomorphological studies (including from aerial photos, LIDAR, etc) would limit the extent of investigations and concentrate analyses on the vulnerable reaches of long embankments.

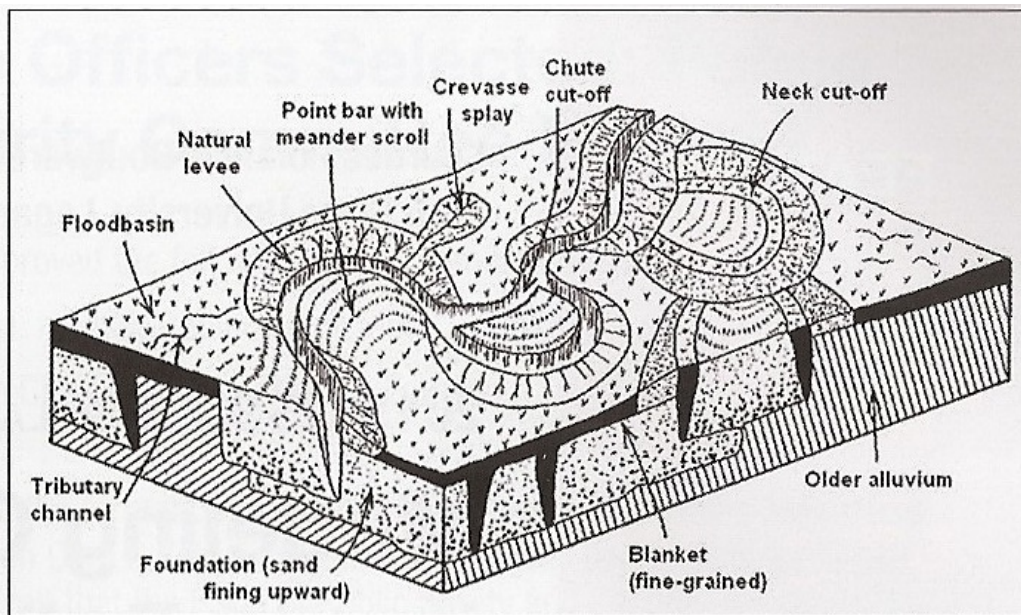


Figure 3. Geomorphic features in meandering river environment (from Polanco-Boulware 2015)

As explained in Bridle (2015) and in Chapter 6 of Volume 2 of the Bulletin, surveillance of long embankments requires regular walkovers by experienced observers at a frequency related to the importance of the embankment and potential for causing loss of life. Optical fibers provide a convenient means of monitoring the performance of long embankments. They are often installed and read by specialists once or twice a year, but this does little to alleviate the responsibility placed on observers to detect malfunction, deformation and leakage, as soon as it occurs. Monitoring by continuous reading of optical fibers would identify new leakages, and if the appropriate fiber is installed, identify new deformations, as they occur.

Dornstädter (1997) explains how soil temperature probe measurements detect seepage, based on Kappelmeyer (1957). Leakage quantities can be determined by measurement of temperature changes over optical fibers, using analytical techniques developed by Johansson (1997). Johansson and Sjødahl (2007) give examples. Radzicki and Bonelli (2010) developed the impulse response method to eliminate influences of air temperatures from the analyses for a canal dike with a constant water level. Bersan (2015) analyzed temperature measurements from one of the backward erosion experiments at the IJkdijk trial to demonstrate the possibilities of optical fibers.

The advantage of the optical fiber approach is that it can measure for leakage and locate its position to about one meter over long lengths, many kilometers, along a canal, for example, while the costs are not as prohibitive as they would be if monitoring by pore pressure meters was adopted. Fibers can also be installed in locations where direct measurement is not possible, below water level at the toe of a dam, for example. Recently, measurements with both pore pressure meters and optical fiber were obtained for a near-failure situation as reached in a research project carried out in the Willemspolder field laboratory for the vertically inserted geotextile. Here, new ditches were excavated immediately downstream of a dike of secondary importance, where sand boils already occurred occasionally in a ditch some 20 meters behind the dike. Correlations could be made between pore pressure readings, field observations and temperature measurements from two optical fibers (Koelewijn et al., 2017a).

## 7 INVESTIGATION, ANALYSIS AND REMEDIATION TO PROTECT OLD STRUCTURES AGAINST INTERNAL EROSION

### 7.1 Investigations and analyses

Investigations and tests to provide information for analyses are dealt with in Chapter 3 and Chapter 4 of Volume 2 of the Bulletin. Engineering analysis is dealt with in Volume 1; Chapter 9 suggests eight steps for engineering assessment. All analyses require knowledge of the embankment geometry, and the dimensions and materials in the zones, layers and strata in the embankment and foundations. The soil parameters required are summarized in Table 1 (taken from Bridle, 2015):

Table 1: Summary of soil and other parameters needed for internal erosion analyses

Initiating mechanism	Soil properties
Backward erosion	Foundation: Grading, permeability Fill: capable of 'holding a roof' (clay or fine silt)
Contact erosion	Both foundation and fill: Gradings of each layer to check for coarse – fine interfaces. Permeability and hydraulic gradient (and thickness) of coarse layers to estimate Darcy velocity
Suffusion	Fill (usually only, but beware some foundation materials may be suffusive): Grading, tests to estimate gradient at which suffusion will initiate, e.g. Benamar et al. (2012); in some cases tests at measured confining stress and gradient, as Fannin et al. (2008) may be warranted.
Concentrated leaks	Fill, particularly at crest and alongside spillway walls; foundations, particularly near culverts: Grading and Atterberg limits to define soil types. Main challenge is estimating location, depth and width of cracks and openings, but parametric studies may show that crack dimensions could not be eroded. Hydraulic fracture may occur in low stress zones e.g. fill above old river channels or canyons. In zoned dams, downstream fills may arrest erosion by filtering. Consider filter 'collars' to protect at spillways and culverts. Hydraulic gradient across cracks should be estimated from maximum flood level at upstream side. Hydraulic shear strength from tables in Bulletin for first estimates, from Hole Erosion Test (plastic soils) and Jet Erosion Test (non-plastic soils) as necessary.

The challenges in relation to concentrated leak erosion are included in the table. The main challenges in determining soil parameters for the other mechanisms are:

- Collecting full samples from non-plastic soils below water table;
- Measuring in-situ permeability in the relatively coarse soils in which contact erosion and backward erosion occur.

The use of special samplers, e.g. Bishop (1948); or sonic drilling and similar may make it possible to collect full samples below water table.

In-situ permeability is difficult to determine, and may vary locally within strata and change as water level changes. In-situ permeability can be measured directly at the base of advancing boreholes and by piezo-cone adaptations of the Cone Penetration Test. In-situ permeability can also be measured in piezometers. A direct and effective determination of permeability is by back calculation from direct measurement of leakage quantities through known areas of susceptible materials. The simplest means of determining leakage quantities is from direct measurement of discharge from collection systems measured over V-notch weirs, for example. The leakage is visible in ditches and in measurement chambers. If erosion is occurring, the eroded particles will probably be visible. The water level in weir

chambers can be measured automatically and transmitted and read remotely, if required. Leakage quantities can be determined by measurement of temperature changes over optical fibers, as discussed in relation to the influence of the length of dams and dikes.

## 7.2 Acting on results of internal erosion analyses

It is not possible to know if an embankment is adequately or inadequately resistant to internal erosion without carrying out analyses. The internal erosion analyses will estimate the water level at which internal erosion leading to failure will occur. In some cases this water level will be high enough, and its probability of occurrence low enough, for no remediation to be needed. In such cases, a suitable surveillance and monitoring system will be required to check that the dam's future condition and performance continue to be satisfactory. In other cases remediation will be needed to improve the dam's condition and its ability to resist internal erosion, after which an appropriate surveillance and monitoring scheme must be put in place.

## 7.3 Remediation

The two main remediation options to protect embankments against internal erosion are barriers or filters. The general issues are discussed in Chapter 10 in Volume 1 and more details are given for remediation to address the four modes of internal erosion in Chapter 5 of Volume 2. Some of the case histories in Chapter 2 of Volume 2 include descriptions of remedial measures. Examples of remediation have been mentioned in other sections of this paper.

# 8 INFLUENCES OF CULVERTS AND SPILLWAYS PASSING THROUGH EMBANKMENTS

Culverts and spillways and other conduits (sometimes collectively called 'penetrations' e.g. FEMA (2005)) passing through dams and dikes are commonly the site of failures by internal erosion. Such failures seem to occur in both high dams and low dikes. Some of the failures in the dikes in the Rhone delta mentioned earlier occurred where pipes passed under the dikes.

As reported in Volume 2 of the Bulletin, at Warmwithens dam, about 10 m high, a newly tunneled replacement low level outlet conduit was quickly washed out as the reservoir refilled on completion of the tunneling. This is thought to be the result of hydraulic fracture as the fill above the tunnel, which had been loosened by the 'ground loss' that inevitably occurs as tunneling proceeds, settled slightly as it was wetted up on refilling. Reservoir water rushed into the crack and 'floated' out the fill above the new tunnel, completely emptying the reservoir during a morning. Ferguson et al. (2013) examined the stress conditions around culverts and the potential for hydraulic fracture and cracking.

Dikes rarely have spillways, but the 15 m high unzoned Situ Gintung dam failed at the spillway position as the reservoir refilled rapidly after a drought. This is thought to have been initiated by water entering desiccation cracks below the spillway that remained open during refilling. The resulting uplift from the reservoir water was sufficient to rupture the masonry floor of the spillway allowing water to rush through the cracks and wash out the fill at the spillway position. Between 100 and 200 people were drowned in the sudden onrush of water released by the failure.

The Bulletin in Chapter 5 of Volume 2 makes recommendations on construction details to limit the possibility of washouts at low-level conduits and high level overflows. The principle is to seal by building conduits into the foundation or cut-offs below overflow channels to below the depth of desiccation cracks, for example, but to allow for leaks and arrest erosion by providing filter collars around conduits and overflow structures downstream of the seal. Care must be taken to provide sufficiently large capacity drainage outlets from the filter collars to avoid uplift and rupture from water accumulating at reservoir pressure below conduits or below overflow channel floors. The International Levee Handbook deals with practical design solutions for these issues in Section 9.15.4 (CIRIA, 2013:1165-1179).

## 9 CONCLUSIONS AND RECOMMENDATIONS

In their vulnerability and response to internal erosion dams and dikes have much in common. Both behave in response to the mechanisms of the four modes of internal erosion. Internal erosion initiates when the hydraulic load, usually expressed as water level, exceeds the ability of the soils in the embankment to resist them.

Failures of dams are often considered more dangerous than dike failures, but application of a ‘loss of life’ criterion may give similar outcomes and seems more appropriate in the light of the tragic loss of life in New Orleans and elsewhere resulting from inundation after dike failures. Higher demands and an increase of knowledge on the failure modes seems to have the largest impact on the oldest structures, often dikes. Remediation measures are more cost-effective if they interrupt failure modes instead of simply applying sufficient volume. The greater extent of dikes as compared to dams makes comprehensive monitoring more of a challenge for the former. The emerging use of the optical fibers may prove very useful in this regard.

Effective remediation of old structures against internal erosion requires proper investigation and analysis of the current situation, as outlined in both volumes of the recent ICOLD Bulletin on internal erosion (ICOLD, 2015, 2016), applicable to both dams and dikes. Penetrations like culverts and spillways provide challenges of their own. In this regard, the Internal Levee Handbook (CIRIA, 2013) may prove its value too.

## REFERENCES

- Beguin, R., Guidoux, C., Faure, Y.H. and Ho, C.C. (2009). Stability conditions and erosion rates at the contacts between two soils subjected to a water flow parallel to the interface. *Presentation at ICOLD European Working Group on Internal Erosion, St Petersburg, April.*
- Bersan, S. (2015). *Piping detection in dike foundations by distributed temperature sensing. Understanding the development of thermal anomalies.* PhD thesis, University of Padua.
- Bishop, A.W. (1948). A new sampling tool for use in cohesionless sands below ground water level, *Géotechnique* 1:125-131.
- Bligh, W.G. (1907). *The Practical design of Irrigation Works*, Constable, London.
- Bligh, W.G. (1910). Dams, barrages and weirs on porous foundations. *Engineering News*, 64(26), 708-710.
- Bridle, R. (2015). Using ICOLD Bulletin 164 to investigate, analyze and monitor the vulnerability of dams to internal erosion. *Proceedings, XVI Dam Monitoring International Conference, TKZ2015, Wierchomla, Poland, Wintera J. and Wity A. (eds)*, 29 September - 2 October 2015, 15-25.
- CIRIA, French Ministry of Ecology, USACE (2013) *The International Levee Handbook*, C731, CIRIA, London (ISBN: 978-0-86017-734-0). Go to: [www.ciria.org](http://www.ciria.org)
- Clibborn, J., and Beresford, J.S. (1902). *Experiment on passage of water through sand*, Government of India, Central Printing Office.
- Dornstädter, J. (1997). Detection of internal erosion in embankment dams. *Nineteenth International Congress on Large Dams, Florence. Q73, R7 Vol II*, 87-101. International Commission on Large Dams, Paris.
- FEMA (2005). *Technical Manual: Conduits through Embankment Dams*. Go to: <http://www.fema.gov/media-library/assets/documents/3875?id=1827>
- Ferguson, K.A., Soudakh, M. and Sossenkina, E. (2013). Potential for cracking around outlet culverts and its impact on seepage safety. *Proceedings of the 2013 Annual Conference, United States Society on Dams (USSD)*, Phoenix, February.
- Förster, U., Bezuijen, A., and Berg, S.G. van den (2015). Vertically inserted geotextile used for strengthening levees against erosion. *Proceedings 16th European Conference on Soil Mechanics and Geotechnical Engineering*, Edinburgh, September 2015, 1995-2000.
- Foster, M.A. (2007). Application of no, excessive and continuing erosion criteria to existing dams. In *Internal erosion of dams and their foundations*, R. Fell and J-J. Fry (eds), Taylor and Francis, 103-114.
- ICOLD (2015). *Internal erosion of existing dams, levees and dikes, and their foundations, Volume 1: Internal erosion processes and engineering assessment*. International Commission on Large Dams, Paris. Preprint 19 February 2015 from: <http://www.icold-cigb.org>.

- ICOLD (2016). *Internal erosion of existing dams, levees and dikes, and their foundations, Volume 2: Case histories, investigations, testing, remediation and surveillance*. International Commission on Large Dams, Paris. Preprint 6 May 2016 from: <http://www.icold-cigb.org>.
- Johansson, S. (1997). Seepage monitoring in earth embankment dams. *Doctoral Thesis, TRITA-AMI PhD 1014, ISBN 91-7170-792-1*, Royal Institute of Technology, Stockholm.
- Johansson, S. and Sjudahl, P. (2007). Seepage measurements and internal erosion detection using the Passive Temperature Method. *Assessment of the Risk of Internal Erosion of Water Retaining Structures: Dams, Dykes and Levees. Intermediate Report of the Working Group of ICOLD*, Deutsches Talsperren Komitee, Technical University of Munich, No.114 ISBN 1437-3513, ISBN 978-3-9404476-04-3, 186-192.
- Kappelmeyer, O. (1957). The use of near surface temperature measurements for discovering anomalies due to causes at depth. *Geophysical Prospecting*, The Hague, Vol. 3, 239-258.
- Koelewijn, A.R., De Vries, G., Van Lottum, H. Förster, U., Van Beek, V.M. and Bezuijen, A. (2014). Full scale testing of piping prevention measures: three tests at the IJkdijk, *8th International Conference on Physical Modelling in Geotechnics*, Perth, January, 891-897.
- Koelewijn, A.R., Taccari, M.L. and Van Beek, V.M. (2017a). A field experiment with fibre optics detecting groundwater flow and piping behind a summer dike, *Proceedings 85th Annual Meeting of International Commission on Large Dams*, Prague, July.
- Koelewijn, A., Van Beek, V., Förster, U. and Bezuijen, A. (2017b). The development of a coarse sand barrier as an effective measure against piping underneath dikes, *Proceedings 19th International Conference on Soil Mechanics and Geotechnical Engineering*, Seoul, September.
- Mallet, T. and Fry, J-J. (2016). Probability of failure of an embankment by backward erosion using the formulas of Sellmeijer and Hoffmans. *Proceedings, ICOLD Symposium on Appropriate Technology, Johannesburg, May, USB*, 2b-149-158, and presentation.
- Mallet, T., Outalmit, K. and Fry, J-J. (2014). Probability of failure of an embankment by internal erosion using the Hole Erosion Test. *Proceedings of the Symposium on Dams in Global Environmental Challenges, ICOLD Annual Meeting*, Bali, VI 278-VI 287.
- Navin, M. (2016). Kaskaskia Island and Bois Brule Levee breaches during the 1993 Mississippi River flood, *USSD International Symposium on the Mechanics of Internal Erosion for Dams and Levees*, Salt Lake City, August.
- Poulanco-Boulware, L. (2015). Modeling geomorphic features in levee reliability analyses. *USSD Newsletter*, July, 19-24.
- Rosenbrand, E., Van Beek, V., Vandenboer, K., Konstantinou, M., Van Esch, J., Noordam, A. and Bezuijen, A. (2017). Numerical modeling of small-scale experiments for a coarse sand barrier as a measure against backward erosion piping below levees, *25th Meeting of the European Working Group on Internal Erosion*, Delft, September.
- Radzicki, K., and Bonelli, S. (2010). Thermal seepage monitoring in the earth dams with impulse response function analysis model. *8th ICOLD European Club Symposium, Innsbruck, Austria*, 649-654.
- Sellmeijer, J.B. (1988). *On the mechanism of piping under impervious structures*, PhD thesis, TU Delft.
- Sherard, J.L. and Dunnigan, L.P. (1989). Critical filters for impervious soils. *J. Geotech. Eng. ASCE*, 115(7):927-947.
- Shrewbridge, S. (2016). USACE levee research, design and performance history: internal erosion and risk-informed levee design. *USSD International Symposium on the Mechanics of Internal Erosion for Dams and Levees*, Salt Lake City, August.
- Van Beek, V.M. (2015). *Backward erosion piping, initiation and progression*. PhD thesis, TU Delft.
- Van Beek, V.M., Knoeff, H. and Sellmeijer, H. (2011). Observations on the process of backward erosion piping in small-, medium- and full-scale experiments. *European Journal of Environmental and Civil Engineering*, 15(8):1115-1137.
- Van Beek, V.M., Koelewijn A.R., Negrinelli, G. and Förster, U. (2015). A coarse sand barrier as an effective piping measure, *Geotechniek* 19(September):4-7.

## Fine-tuning the evaluation of suffusion of silt-sand-gravel soils – a comparative study of LTU and UNSW tests

H. Rönnqvist

*RQV Teknik AB*

**Abstract:** Swedish embankment dams are usually constructed with core soils of glacial till. A widely graded soil sourced from moraine deposits, till comprises many fractions, from silt and sand to gravel and stones, all crushed and mixed by the action of glaciation. Interestingly, this type of soil is remarkably similar to that in other parts of the world that were once glaciated: typically cohesionless and practically non-plastic. Statistics reveal that these core soils undergo internal erosion incidents more frequently than other soil types; however, they are less likely to fail. This indicates vulnerability to the initiation of internal erosion but resistance to its progression, suggesting a potential self-filtering ability that arrests the continuation. Almost simultaneously, Australia's UNSW carried out GBE-suffusion tests on silt-sand-gravel soils that were similar in gradation to the glacial tills tested at Sweden's LTU for suffusion. This paper makes a comparative assessment of these two studies, with the objective of improving and fine-tuning the existing evaluation tools for silt-sand-gravel soils in dams.

Keywords: suffusion, internal erosion, glacial till, dams.

### 1 INTRODUCTION

Dam materials comprising broadly graded silt-sand-gravel soil, especially glacial till, have been the core soil used in many notable sinkhole-afflicted dams in the past (Sherard, 1979). Sinkholes are typically the ultimate manifestation of internal erosion, a process initiated by the mechanisms of concentrated leak erosion, backward erosion, contact erosion, and suffusion erosion (ICOLD, 2013).

Glacial till, a soil used for dam fills in many parts of the world that once were glaciated, appears to be particularly susceptible to internal erosion (Ravaska, 1997; Sherard, 1979; Foster, 1999; Foster et al., 2000). The reason for this was unclear and perhaps to an extent still is; however, early on, Sherard (1979) attributed it to "internal instability". At the time, this claim was somewhat controversial, since it was immediately rebutted by Leps (1979) as impossible. Leps (1979) argued that the coarser particles would be suspended in the soil matrix, which would eliminate internal instability. This is true, but as will be discussed in this paper, there are times when these soils may indeed be vulnerable. Later, Sherard's claim was challenged by Milligan (2003) who instead put the blame on the soil's likely segregation problems. This was thought provoking, indeed, and probably true. Subsequently, as reported by Nilsson and Norstedt (2004), in the late 1980s, while consulting on a sinkhole incident that occurred in a Swedish dam a few years prior, James Sherard refined his statement to say that the internal instability of these types of soils stems from their insufficient content of sand-sized particles, which would render the coarser fractions incapable of preventing the progressive loss of fines. This agrees with what we know today about the internal instability of soils (Kenney and Lau, 1985, 1986; Skempton and Brogan, 1994; Wan and Fell, 2004; Rönnqvist, 2015, Douglas et al., 2016).

Table 1. Compilation of tests and soil and erosion parameters (after Douglas et al, 2016; Rönnqvist, 2015).

	Test number	Fines (d<0,075 mm) (%)	Finer fraction (F <sub>p</sub> ) (%)	Filter EOS wrt CE <sup>1</sup>	Postulated erosion mechanism	Internal erosion amount
Douglas et al., (2016)	1, 1R, 1B, 1Row	17	30	= CE	GBE	Medium
	2, 2A	36 <sup>2</sup>	n/a	> CE = CE	GBE	Very minor-Major
	4, 4A	15	30	> CE = CE	Suffusion	Major
	6, 6A, 6B	15	25	= CE > CE < CE	Suffusion (GBE @ CE filter)	Major
	6Bmod	11	20	< CE	Suffusion	Medium
	7, 7A	15	29	= CE > CE	Suffusion	Major
	8, 8A	15	35	> CE = CE	Suffusion (Very minor GBE @ CE)	Major
	9	21 <sup>2</sup>	n/a	= CE	Internally unstable	No erosion
	10, 10A	15	30	> CE = CE	GBE	Medium-Major
	11, 11A	17	41	= CE > CE	Suffusion	Major
	13	0	55	> CE	GBE	Minor-Medium
	14, 14A	15	25	= CE < CE	Suffusion (GBE @ CE filter)	Major
	15, 15B	26 <sup>2</sup>	n/a	> CE	Internally unstable	No erosion
	17	11	27	= CE	Suffusion	Major
	18	14	40	= CE	Suffusion	Major
	19, 19B, 19B	24 <sup>2</sup>	49	< CE = CE > CE	Internally unstable (suffusion @ >CE filter)	No erosion - Major
	21	7	n/a	= CE	GBE	Very minor
	WB1	13	27	< CE	Suffusion	Major
	W9	11	15	< CE	Suffusion	Major
	WA3	9	17	< CE	Suffusion	Major
Rönnqvist (2015)	BE1	34	50	<< CE	Stable	Minor
	BE2	22	32		Stable	Minor
	BE3	17	29		Suffusion	Minor
	BE4	13	25		Suffusion	Major
	RA1	37	45	<< CE	Stable	Very minor
	GR1	30	40	<< CE	Stable	Very minor
	GR2	19	32		GBE	Minor
	GR3	10	20		Suffusion	Medium
	GR4	18	31		Stable	Very minor
	ST1	17	31		Stable	Minor
ST2	10	40	<< CE	GBE	Major	
ST3	4	17		Suffusion	Major	

<sup>1</sup> Downstream filter coarseness in relation to continuing erosion boundary: “=CE”: test against an EOS=4.75 mm base mesh (D<sub>15</sub> = 43 mm). “>CE”: test against an EOS 9.5 mm base mesh (D<sub>15</sub> = 86 mm). “<CE”: test against an EOS 2,36 mm base mesh (D<sub>15</sub> = 21 mm). “<<CE”: test against a granular filter (D<sub>15</sub> = 1.0 mm).

<sup>2</sup> No gradation data available for passing weight < 20 %.

Two recent studies of suffusion, occurring almost simultaneously at the University of New South Wales (UNSW) and the Luleå University of Technology (LTU), the latter carried out by the author. The studies are described in Douglas et al. (2016) and Rönnqvist et al. (2017). In this paper, the findings of these experimental programmes are compared, and from the cumulative knowledge attained from the testing of 32 soils, an attempt is made at fine-tuning the evaluation of suffusion of this soil type.

## 2 GBE VERSUS SUFFUSION

Backward erosion occurs if there is an unfiltered seepage exit, e.g., at an interface with an inadequate filter (ICOLD, 2013). Assuming that the driving force is attained, the erosion will progress backwards towards the source of the water through the detachment of soil particles. The term “backward erosion” is usually used for piping-formations in uniformly graded soils (i.e., backward erosion piping, BEP), such as would occur in the erosion of dam foundations. Recently, to explain its role in causing sinkholes in dam bodies, the term global backward erosion (i.e., GBE) has been used. GBE is defined as a process assisted by gravity that can cause near-vertical pipes in a dam body that may surface at the dam’s crest in the form of sinkholes (ICOLD, 2013).

Suffusion, on the other hand, occurs inside the fixed bulk volume of a core soil or dam zone when internal instability makes it possible for the finer fraction of the gradation to be washed through the constrictions of its coarser fraction (ICOLD, 2013). However, rightly so, Douglas et al. (2016) suggested that the term internal instability should not only apply to suffusion but also to GBE, the other process for which there is an internal movement of particles within the soil matrix. Unless the finer fraction ( $F_f$ ) of its soil is  $F_f < \approx 35\%$ , a widely graded soil is probably not susceptible to suffusion (Wan, 2006; Rönnqvist, 2015; Douglas et al., 2016). Suffusion, as a process, is eliminated if  $F_f$  is excessive because the matrix-supported coarser particles will float in the finer fraction; however, such a soil can still be vulnerable to backward erosion.

From their study, Douglas et al. (2016) found that suffusion, when triggered, is a rapid process more or less independent of a downstream filter, while GBE, which exhibits more dependence on the adequacy of the downstream filter, progresses more slowly and may reactivate at a gradient increase. This reactivation is an important consideration for older dams, which may be apparently free of internal erosion, that are about to experience higher reservoir levels than they have previously. Both suffusion and GBE resulted in major erosion in the Douglas et al. (2016) tests, and they found that soils that self-filter sometimes developed very high local gradients, which was something also evidenced by the tests by Rönnqvist (2015).

## 3 DATA BASE OF SILT-SAND-GRAVEL GRADATIONS

Rönnqvist (2015) used a 300-mm-diameter seepage cell without added confining pressure to test 12 soils (table 1). The soils were composed of natural glacial till and mixes of this till with aggregates. The fines content,  $d_{\#200}$  (fraction with  $d < 0.075$  mm), was  $4 \leq d_{\#200} \leq 37\%$ , and the maximum particle size ( $D_{\max}$ ) was 30-45 mm. The average gradient in the tests was limited to 10. Douglas et al. (2016) conducted 37 tests on 22 silt-sand-gravel soils with  $0 < d_{\#200} \leq 36\%$  and  $D_{\max} = 19-75$  mm. The tests were performed in 450-mm seepage cells with the hydraulic gradient initially set at 1 and increased to 10, if necessary. They used no added confining pressure in the cell. Some tests were performed in a smaller 300-mm cell. There were no reported gradation data for  $d < 0.075$  mm from these tests.

Table 1 compiles the gradation data and test outcomes, and figure 3.1 shows the particle size distributions compared with the core soil gradations of damaged dams (from Sherard, 1979; Rönnqvist et al., 2014). Figure 3.1 shows that the tested soils were close in range with these dam core soils and that the range of core soils belonging to dams with an internal erosion incident was greater than that qualitatively proposed by Sherard (1979). Figure 3.2 provides detailed gradation plots of the test soils.

Based on their experimental data, Douglas et al. (2016) found that the majority of eroded particles had  $d < \sim 1$  mm, which would be “self-filtered” by the constrictions formed by the coarse-sand and fine-

gravel (i.e., the 1.18-4.75 mm fraction). By combining this with fine-medium-sand (0.075-1.18 mm), they found a correlation between non-plastic silt-sand-gravel soils and erodibility. The vulnerable gradations were those that had a steep coarser fraction and a flat, gap-graded finer fraction in their particle size distribution plots. Similarly, Rönnqvist (2015) found that “flat fine-tail” gradations were the ones that typically eroded, and these generally had a deficiency in sand content and a relatively small amount of fines.

Combining these experimental programmes provides 32 gradations, as described in table 1 and figure 3.2. Given the postulated erosion mechanisms from the tests (table 1), 12 of the Douglas et al. (2016) gradations were suffusive, five were afflicted by GBE, and three experienced very minor erosion (were practically stable). In terms of the Rönnqvist (2015) tests, four failed by suffusion, two by GBE, and the remaining six were stable and exhibited very minor erosion.

#### 4 DISCUSSION

The question can be raised of how accurate the evaluation of the internal erosion vulnerability of silt-sand-gravel soils (including glacial tills) can become. Such broadly graded soils carry with them several potential inherent deficiencies, e.g., susceptibility to segregation, which typically arises during handling. Some argue that it is the segregation to which we ought to pay attention (Ripley, 1986; Milligan, 2003). Nevertheless, there have been fruitful attempts to improve the assessment of internal erosion, e.g., by Wan (2006), Wan and Fell (2004), Douglas et al. (2016), and Rönnqvist (2015). Wan (2006) and Wan and Fell (2004) adapted the Burenkova (1993) method, which incorporates a plot of the ratios  $d_{90}/d_{60}$  and  $d_{90}/d_{15}$ , i.e., the slope of the coarser fraction in relation to the overall slope of the gradation; a steep coarser fraction in relation to a flat overall slope would make the soil suffusive. Douglas et al. (2016) advised, instead, to analyse the relation between the soil’s gravel and sand fractions, indicating similarly that low-sand and high-gravel soils are potentially suffusive. Using a different approach, the study by Rönnqvist proposed a shape-analysis of the slope of the gradation curve using the Kenney and Lau (1985, 1986) method to check whether there is insufficient finer fraction to fill the constrictions of the coarser fraction (i.e., internal instability).

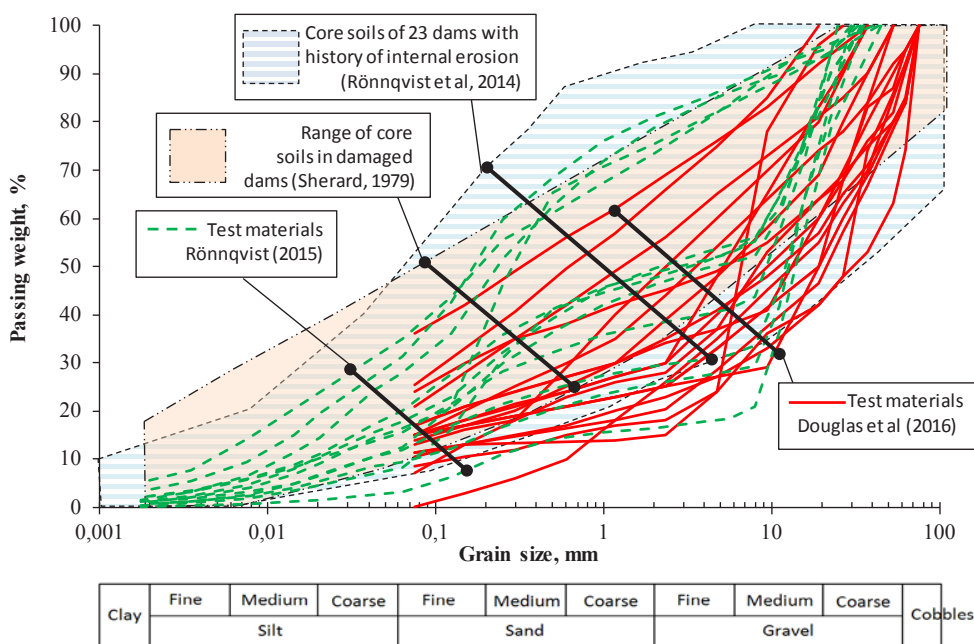


Figure 3.1. Rönnqvist (2015) (LTU) and Douglas et al. (2016) (UNSW) gradations compared to core soils in damaged dams (after Sherard, 1979. and Rönnqvist et al., 2014).

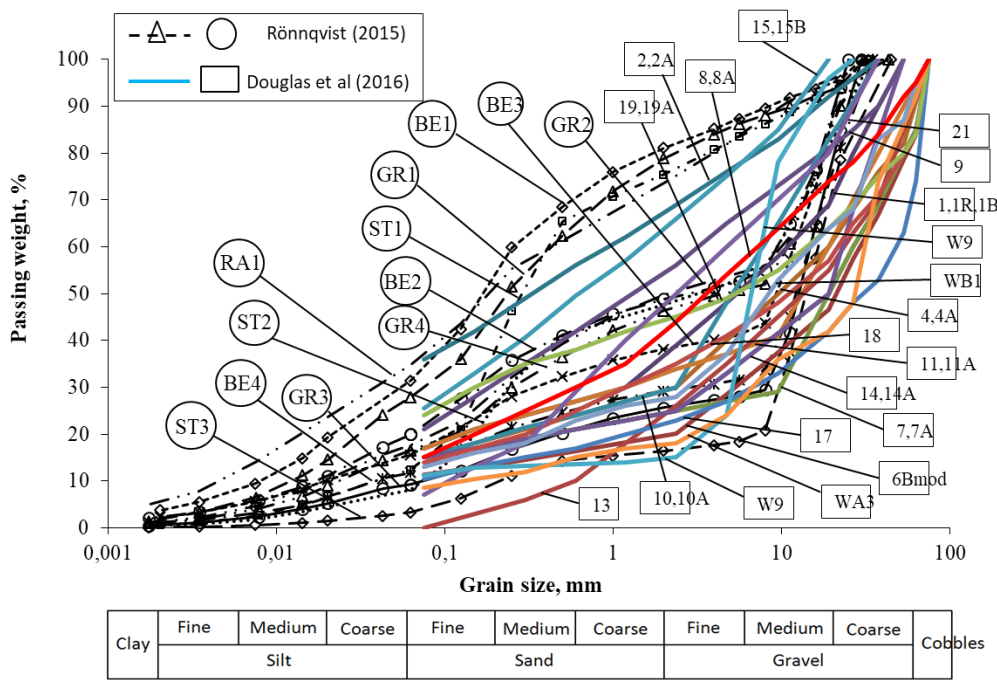


Figure 3.2. Rönnqvist (2015) (LTU) and Douglas et al. (2016) (UNSW) gradations.

Essentially, it is obvious that although they approached the problem differently, these studies together indicate that an insufficient amount of the important sand fraction in a broadly graded soil is a potential root cause of suffusion. Such an undesirable gradation would reduce the soil’s self-filtering ability, making its finer fraction vulnerable to erosion. Thus, to recap James Sherard (from 1987): “if a leak develops (...) (in a core with) an insufficient content of sand-sized particles (...) the finest soil particles can be carried out of the core, and the sand and gravel left behind is incapable of preventing progressive loss of fines from large volumes of the core” (after Nilsson and Norstedt, 2004).

Elaborating on the results from Rönnqvist (2015), Rönnqvist et al. (2017) proposed checking whether core soils composed of glacial till are vulnerable to suffusion by evaluating their fines and sand contents; if they are low on fines (approximately  $\leq 20\%$ ) and low on sand ( $\leq 25\%$ ), they are probably susceptible. This technique is used in the following analysis. The majority of the soils that underwent suffusion (solid black symbols) indeed have plotting positions that are within the “probably suffusive” region in figure 4.1. The GBE-afflicted soils exhibit greater intermixing, which is logical since internal instability is probably not GBE’s most important prerequisite, whereas the stable soils are all deemed “probably not susceptible” to suffusion based on the figure 4.1 plot. It has been shown that the Kenney and Lau (1985, 1986) method is conservative due to an included safety factor (Rönnqvist and Viklander, 2014). Their boundary of  $H/F=1$  (where  $H$  is the weight passing between  $d$  and  $4d$ , and  $F$  is the weight passing  $d$ ) tends to overpredict instability, even for granular material without fines (for which the method was formulated). Therefore, to adjust for this conservatism, a transition zone of  $0.68 \leq H/F < 1.0$  in the  $H:F$ -space was suggested (Rönnqvist et al., 2017). This methodology allows for a stricter assessment; however, the soils in table 1 plot in the  $H:F$ -space according to figure 4.2, which shows a considerable gap in the obviously suffusive soils (solid symbols). This gap indicates that the previous transition zone instead marks a region of *potential stability*, and gradually transitions towards unstable over the range  $0.45 \leq H/F < 0.68$  (*potentially unstable*) (figure 4.2). At a stability index of  $H/F < 0.45$ , a shape-analysis result that would clearly deem a soil as internally unstable represents the *suffusive* region of broadly graded silt-sand-gravel soils.

Let us consider the soils *W9* (UNSW), *ST3* (LTU), *BE4* (LTU) and *BE3* (LTU) (table 1). Using the Kenney and Lau (1985, 1986) method yields stability indices  $((H/F)_{\min})$  of 0.08; 0.15; 0.33; and 0.55, respectively (see the plotting positions in figure 4.2); thus, these are clearly unstable gradations, given that theoretical stability is achieved at  $H/F = 1.0$ . Forensic photos from their respective tests reveal that

the degree of severity of suffusion tends to vary correspondingly (figures 4.3 and 4.4), which suggests a correlation with the stability index (i.e.,  $H/F$ ). The two soils having the lowest  $(H/F)_{min}$ , i.e., *ST3* and *W9*, are shown in figure 4.3. The pre- and post-test photos reveal complete suffusion of the finer fraction of their top surfaces that exposed the primary fabric of the soils, i.e., the remaining coarser fraction. A very low hydraulic gradient was sufficient to initiate the erosion. The degree of suffusion generally decreased as the stability index increased, giving confidence in the possible transitions zones in the unstable H:F-space, as shown by the forensic photos of *BE4* and *BE3* (figures 4.4 and 4.5). For *BE4*, some finer fraction remained after the completion of the test (figure 4.4), and soil *BE3*, which had  $(H/F)_{min} = 0.55$ , clearly retained most of its finer fraction and imperviousness (figure 4.5) and suffered only minor erosion from suffusion (as determined by its headloss profiles and post-test sieving) (table 1). The soils in table 1 are generally non-plastic (or low-plasticity) soils, and the presence of measurable plasticity would likely increase the erosion resistance of the soils.

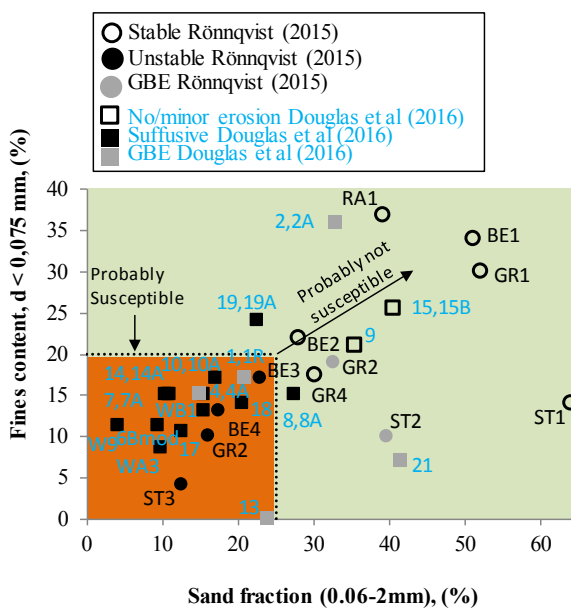


Figure 4.3. Fines versus sand content in silt-sand-gravel soils (after Rönqvist et al, 2017).

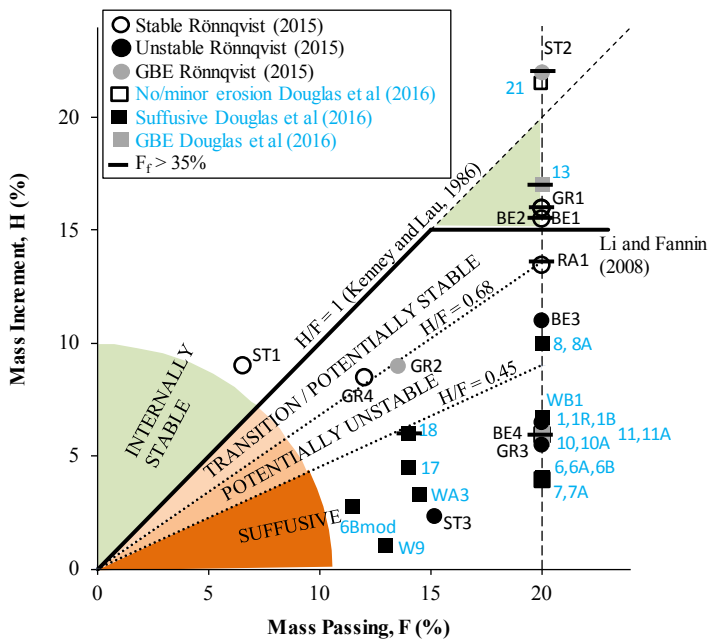


Figure 4.4. A method to evaluate suffusion of silt-sand-gravel soils (after Rönqvist et al., 2017).

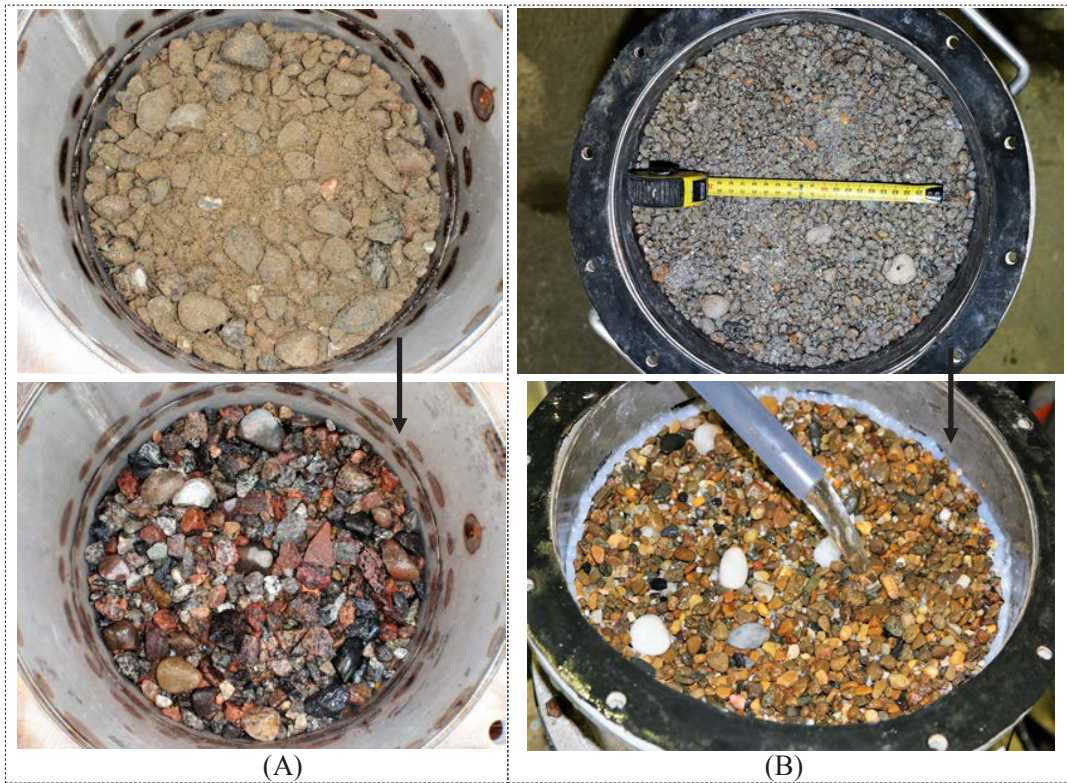


Figure 4.5. Forensic pre- (above) and post-test (below) photos of completely suffused soil (A) ST3 (LTU) and (B) W9 (UNSW, courtesy of Dr. Kurt Douglas, UNSW Sydney).

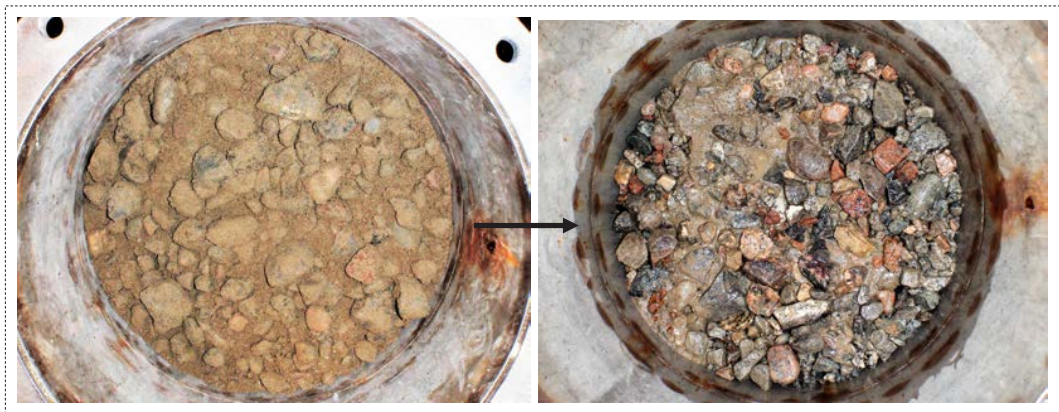


Figure 4.6. Forensic pre- (left) and post-test (right) photos of incompletely suffused soil BE4 (LTU).



Figure 4.7. Forensic pre- (left) and post-test (right) photos of slightly suffused soil BE3 (LTU).

## 5 CONCLUSIONS

This paper explores the findings of two recent laboratory studies of the suffusion of silt-sand-gravel soils conducted at UNSW and LTU. The author performed the tests at LTU. These studies tested a combined 32 soils, and the conclusion drawn is that an insufficient amount of sand fraction in a broadly graded, partly silty, soil is a possible predictor for suffusive behaviour. Several literature references point to the importance of the sand content which agrees with the findings herein. Detailed analysis indicates, furthermore, that the degree of severity from suffusion correlates to the stability index  $((H/F)_{\min})$ , the lower the stability index, the more severe erosion. For silt-sand-gravel soils transition zones in the H:F-space appear necessary to distinguish between internally stable and suffusive soils, and  $H/F < 0.45$  provides a possible boundary, below which this type of soil is suffusive. However, for important decisions, laboratory permeameter tests are recommended in order to specifically tailor this boundary for the intended soil. The author do not recommend the use of these boundaries for clean silt and gravel materials, but instead advocate guidelines as given in the source publication of Kenney and Lau.

## ACKNOWLEDGMENTS

Financial support for this paper was received from Energiforsk AB and RQV Teknik AB. Heartfelt thanks to Dr. Kurt Douglas, UNSW Sydney, for sharing the photos of his tests W9 and 7.

## NOTATIONS

CE	continuing erosion boundary (mm) (after Foster and Fell, 2001)
$d_x$	grain size for which x % is finer (mm)
$D_{\max}$	maximum particle size (mm)
EOS	equivalent opening size, $d_{15}/9$ (mm)
F	passing weight at d (%)
$F_f$	finer fraction (%), inflection on particle size distribution curve
Fines	amount finer than 0,075 mm (%).
GBE	global backward erosion
H	passing weight between d and 4d (%)
LTU	Luleå University of Technology (Sweden)
UNSW	University of New South Wales (Australia)

## REFERENCES

- Burenkova, V.V. (1993) Assessment of suffusion in non-cohesive and graded soils, *Proc. First International Conference "Geo-Filters" Filters in geotechnical engineering*, Brauns, Heibum, Schuler (eds), Rotterdam: Balkema, 357-360.
- Douglas, K., Fell, R., Peirson, B., and Studholme, H. (2016) Experimental investigation of global backward erosion and suffusion, *UNICIV report No. 465*, The University of New South Wales, May 2016.
- Foster, M.A. (1999) The probability of failure of embankment dams by internal erosion and piping, *PhD-thesis, The University of New South Wales*, May 1999.
- Foster, M., Fell, R. and Spannagle, M. (2000) The statistics of embankment dam failures and accidents, *Canadian Geotechnical Journal*, 37, 1000-1024.
- ICOLD (2013) Internal erosion of existing dams, levees and dykes, and their foundations, *Bulletin 164, Volume 1: internal erosion processes and engineering assessment*, Bridle, R. and Fell, R. (eds), International Commission on Large Dams.
- Kenney, T.C. and Lau, D. (1985) Internal stability of granular filters, *Canadian Geotechnical Journal*, 22(2), 215-225.

- Kenney, T.C. and Lau, D. (1986) Internal stability of granular filters: Reply, *Canadian Geotechnical Journal*, 23(3), 420-423.
- Leps, T.M. (1979) Sinkholes in dams of coarse broadly graded soils: Discussion, *Proc. 13th ICOLD Congress, New Dehli, India*, I:101-105.
- Li M, and Fannin R.J. (2008) Comparison of two criteria for internal stability of granular soil, *Canadian Geotechnical Journal*, 45, 1303-1309.
- Milligan, V. (2003) Some uncertainties in embankment dam engineering, *Journal of Geotechnical and Geoenvironmental Engineering*, 129 (9), 785-797.
- Nilsson, Å. and Norstedt, U. (2004) Reverse filters on the downstream slope to compensate for coarse graded filters in Swedish dams, *Proc. Canadian Dam Association 2004, Ottawa*.
- Ravaska O. (1997) Piping susceptibility of glacial till, *Proc. 19th ICOLD Congress, Florence, Q73*, 455-471.
- Ripley C.F. (1986) Internal Stability of Granular filters: Discussion, *Canadian Geotechnical Journal*, 23, 255-258.
- Rönnqvist, H. (2015) On the assessment of internal erosion of dam cores of glacial till, *PhD-thesis*, Luleå University of Technology, Luleå, Sweden.
- Rönnqvist, H., Viklander, P., and Knutsson, S. (2017) Experimental investigation of suffusion in dam core soils of glacial tills, *Geotechnical Testing Journal*, 40(3), 426-439.
- Rönnqvist, H. Fannin, R.J. and Viklander, P. (2014) On the use of empirical methods for assessment of filters in embankment dams, *Géotechnique Letters*, 4, 272-282.
- Rönnqvist, H. and Viklander, P. (2014) On the Kenney-Lau approach to internal stability evaluation of soils, *Geomaterials*, 4, 129-140.
- Sherard, J.L. (1979) Sinkholes in dams of coarse, broadly graded soils, *Proc. 13th ICOLD Congress, India*, 25-35.
- Skempton, A.W. and Brogan J.M. (1994) Experiments on piping in sandy gravels, *Géotechnique*, 44, 449-460.
- Wan, C.F. (2006) Experimental investigations of piping erosion and suffusion of soils in embankment dams and their foundations, *PhD-thesis*, The University of New South Wales, Sydney, Australia.
- Wan, C.F. and Fell, R. (2004) Experimental investigation of internal instability of soils in embankment dams and their foundation, *UNICIV report No. 429*, The University of New South Wales, Oct. 2004.

# Pipe depth measurement in small-scale backward erosion piping experiments

K. Vandenboer, V.M. van Beek & A. Bezuijen

*Ghent University, Deltares, Ghent University and Deltares*

**Abstract:** Backward erosion piping is an important failure mechanism for water-retaining structures, a phenomenon that results in the formation of shallow pipes at the interface of a sandy or silty foundation and a cohesive cover layer. Although the pipe depth reveals a lot of information on the backward erosion process, it has never been measured systematically. In this study we used a contactless laser triangulation sensor to measure the pipe depth during and after small-scale backward erosion experiments with a circular exit for three poorly graded sands with mean grain sizes varying from 0.155 mm to 0.544 mm. The pipes prove to be extremely shallow and the pipe depth close to the pipe tip is just large enough to let a particle through. As the pipe grows, the pipe depth increases due to scour and reallocation of grains, allowing for a higher flow rate and more grains to pass. Furthermore, the pipe often consists of a shallow part in the middle and deeper parts at the outside.

Keywords: Backward erosion piping, erosion, embankments, groundwater flow.

## 1 INTRODUCTION

### 1.1 Backward erosion piping

Backward erosion piping is an important failure mechanism for water-retaining structures founded on a sandy aquifer and covered by a cohesive blanket layer. A local disruption of the downstream top layer and sufficient head drop across the structure allows for erosion at that particular location (pipe initiation), resulting in the formation of shallow pipes in the sand layer (pipe progression). Eventually, the pipes form a direct connection between upstream and downstream, finally resulting in a (partial) collapse.

### 1.2 Current formulae

The safety factor regarding piping failure is often calculated according to Bligh's empirical rule (Bligh 1915), which is based on a large number of field failures and gives the maximum hydraulic load  $\Delta H_{cr}$  as a function of the soil type and length of the construction. More recently, various design formulae were developed, which either predict piping susceptibility by correlating them to similar field cases in the past (Glynn, et al. 2012; Vorogushyn, et al. 2009), have a theoretical basis (Benjasuppatananan and Meehan 2013; El Shamy and Aydin 2008; Ojha, et al. 2003; Schmertmann 2000), or a combined experimental-theoretical background (Schmertmann 2000; Sellmeijer, et al. 2011; Sellmeijer and Koenders 1991; Sellmeijer 1988; van Beek, et al. 2012).

### 1.2.1 Requirements for improvement of formula

None of the existing design formulae succeeds to correctly predict the piping susceptibility for a wide range of conditions. The large number of available models at present, with varying basic hypotheses indicates that the true incentive of backward erosion piping is not yet captured.

Up to now experimental studies have led to indispensable knowledge on key aspects of backward erosion piping either by analyzing the critical gradient or by studying the pipe formation in the sand bed: Hanses, et al. (1985), Miesel (1978) and van Beek, et al. (2011) identified the different phases involved and described the meandering character of the pipes. De Wit, et al. (1981) investigated the influence of the different downstream exit configurations on the critical gradient. Sellmeijer (1981) studied the erosion and fluidization in an outflow opening. Sellmeijer, et al. (2011) and van Beek, et al. (2010) considered a large number of sand types in order to identify the influence of relative density, uniformity, roundness, permeability and grain size on the susceptibility to backward erosion piping. Vandenboer, et al. (2013 and 2017) demonstrated that backward erosion piping should be treated as a three dimensional phenomenon rather than a two dimensional problem both in terms of groundwater flow and pipe development. van Beek, et al. (2014) studied the variation of pipe widths in relation to the grain size. Hanses, et al. (1985) and van Beek, et al. (2015) indicated progression is more likely to be driven by local detachment of the particles at the pipe tip, rather than erosion of particles at the pipe bottom.

An important parameter which has not yet been measured systematically is the depth of the pipe. However, the pipe depth is an important parameter in the research on backward erosion piping in several ways. Firstly, hydraulic analyses of water and sediment flow through the pipe and groundwater flow towards the pipe depend on the dimensions of the pipe and on the depth-to-width ratio of the pipe. Also, the variation of the pipe depth in time would indicate whether there is erosion at the pipe bottom (increasing depth) or not (constant depth). Moreover, implementation of incorrect estimations of the pipe depth and depth-to-width ratio in numerical simulations inevitably results in incorrect pore pressure distributions in the pipe and upstream of the pipe such that progress in understanding the piping process is again hindered.

This paper describes the measurement of the pipe depth in small-scale model tests for 3 different sands.

## 2 EXPERIMENTAL SETUP AND PROCEDURE

In laboratory conditions, the sandy aquifer is built in a pvc box, the cohesive water-retaining structure is replaced by an acrylate plate (see fig. 2.1) with a fixed circular opening representing a locally punctured top layer and the hydraulic gradient is applied by means of an upstream reservoir and a downstream overflow with adjustable head difference. The sand sample is prepared homogeneously at a relative density of more or less 80% in the box and has a total length of 0.4 m, a height of 0.1 m and a width of 0.3 m. The distance from upstream to the circular opening (seepage length) amounts 0.3 m. The hole type exit has a diameter of 5 mm and a height of 10 mm. A Perspex cylinder connects the hole type exit to the downstream reservoir.

A specific location in the setup can be described by its coordinates, see fig. 2.1a: the center of the hole type exit at the top of the sand bed is located at  $x = 0$  m,  $y = 0$  m,  $z = 0$  m. All other locations vary between  $x = -0.1$  m and  $x = 0.3$  m (upstream),  $y = -0.15$  m and  $y = 0.15$  m and  $z = 0$  m (top) and  $z = 0.1$  m (bottom).

The initial hydraulic head difference  $\Delta H$  of 0 cm is increased in steps of 0.5 cm every 5 minutes, as long as no erosion takes place. When the critical hydraulic head for initiation is exceeded, i.e. sand grains start to move and a pipe is formed, the hydraulic head is kept constant. If no erosion is observed for at least 5 minutes (equilibrium), the hydraulic head is increased again, usually resulting in progression of pipe growth. This process is repeated, until the 'critical hydraulic head for progression'  $\Delta H_{crit}$  is exceeded, i.e. no equilibrium state is achieved and the pipe grows until it reaches the upstream filter and the test is stopped.

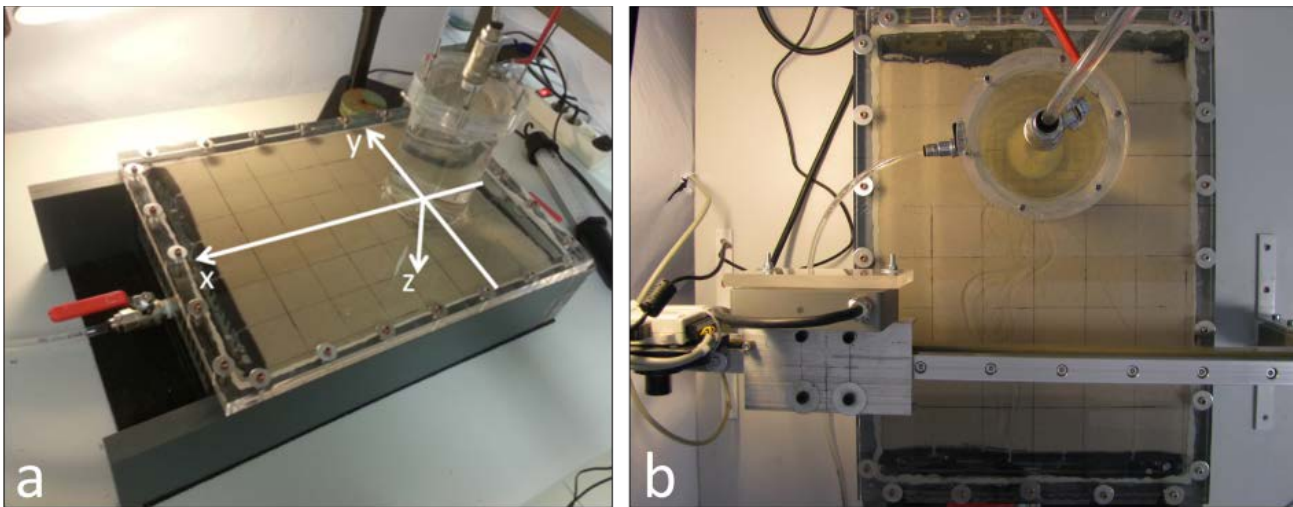


Figure 2.1. Experimental setup and pipe depth measurement device.

The pipe length is defined as the length of the projection of the pipe on the x-axis; the actual (meandering) pipe length is often longer. The eroded sand is deposited around the circular exit forming a crater. The flow rate is continuously measured by collecting the seepage water on a balance.

The replacement of the cohesive water-retaining structure by a transparent acrylate plate allows for measurement of the pipe depth through this cover. In this study a high-quality contactless laser triangulation sensor (resolution = 0.005 mm) is used which has been calibrated for its transition through the acrylate plate. By changing the position of the laser device, the pipe depth can be measured at different locations. Our setup is equipped with a one-dimensional linear guideway and position transducer in order to perform precise measurements in one direction (usually perpendicular to the pipe growth), see fig. 2.1b.

### 3 EXPERIMENTAL PROGRAM AND RESULTS

In this study, 3 different sand types were analyzed: ‘Mol sand M34’, ‘Mol sand M32’ and ‘Cobo sand’ (3 experiments for each sand type). These sand types are all poorly graded, and the mean grain size  $d_{50}$  varies from 0.155 mm to 0.544 mm. More characteristics can be found in table 3.1 Fig. 3.1 shows the critical head for progression  $\Delta H_{crit}$  for the three sand types.

Table 3.1. Sand type characteristics.

	M34	M32	Cobo
$d_{10}$ [mm]	0.128	0.172	0.248
$d_{30}$ [mm]	0.142	0.212	0.389
$d_{50}$ [mm]	0.155	0.251	0.544
$d_{60}$ [mm]	0.166	0.271	0.646
$d_{80}$ [mm]	0.209	0.311	1.680
$C_u$ [-]	1.29	1.58	2.61
$C_c$ [-]	0.94	0.96	0.95
$k$ [m/s] (at RD 80%)	1.03E-04	3.28E-04	6.17E-04

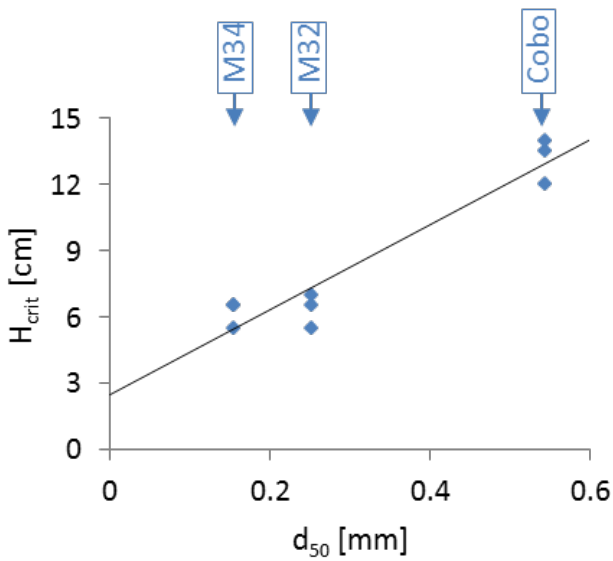


Figure 3.1. Critical hydraulic head for progression ( $\Delta H_{cr}$ ) as a function of mean grain size.

### 3.1 Online single-point measurements

During each experiment, the laser device continuously measures the pipe depth at a fixed location at  $x = 0.1$  m, where the device is placed at the location where the center of the pipe is expected to pass. In this way the pipe depth variation in time is monitored from the moment the pipe reaches a length of 100 mm until the experiment finishes. This technique is called the ‘online single-point measurement’.

Fig. 3.2a shows the top view of the pipe for one of the experiments on Mol sand M34. For this experiment, the online single point measurement is plotted in fig. 3.2b. The pipe reached a length of 100 mm after more or less 142 min, which is when the pipe depth at that location starts to increase. After 195 min, the pipe reaches the upstream filter and the experiment is ended. At that moment the pipe depth at  $x = 0.1$  m is 0.778 mm. A lot of disturbance is observed, which is attributable to the passage of sand grains through the pipe underneath the laser measurement device.

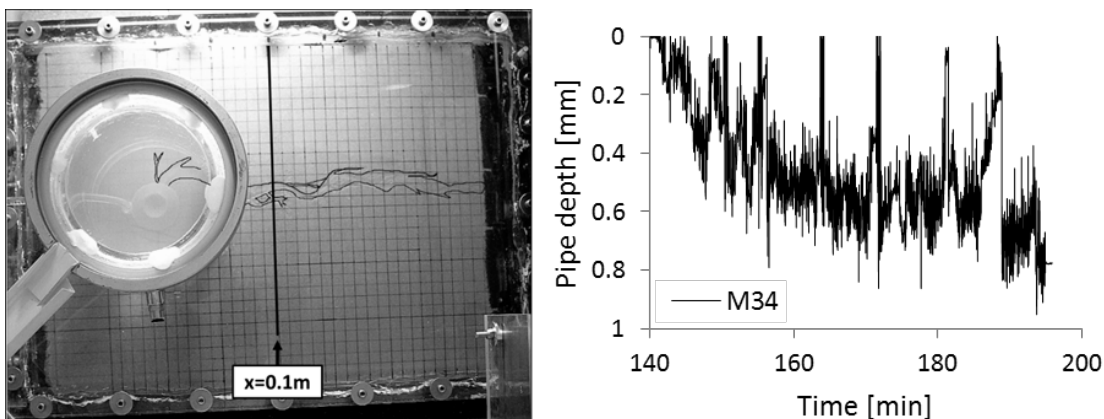


Figure 3.2. Photo at the end of an experiment on Mol sand M34 (a) and corresponding ‘online single point measurement’ at  $x=0.1$  m (b).

The device is originally placed at the location where the center of the pipe is expected to pass. Often the position of the main streamline in the pipe, changes during the process, e.g. due to meandering or branching of the pipe. As a result, the measurement device is not always located at the center of the pipe but occasionally measures the pipe depth at an edge of the pipe where the depth may be larger or smaller

than in the center. Moreover, the pipe depth at a location might decrease as sand grains are deposited in a previously formed pipe channel. In fig. 3.2b the pipe depth does decrease occasionally for a short period, but the position of the pipe does not change considerably (thanks to the rather straight pipe course in this experiment, see fig. 3.2a) so sand grains keep flowing at the position of the laser measurement device and the pipe depth keeps evolving. This is not always the case and as a result, a horizontal lapse may appear in the ‘online single point measurements’, meaning that there is no pipe depth development, nor passage of sand grains at that point anymore. When this was observed during the experiments and it was considered to be unlikely that the pipe would retake its former course, the position of the laser measurement device was changed to the new main stream of the pipe, still at  $x = 0.1$  m.

As the time scaling of the ‘online single point measurements’ is arbitrary for the different experiments, the pipe depth development (at  $x = 0.1$  m) is plotted as a function of the pipe length, averaged for each sand type, see fig. 3.3. Note that the pipe is only a few sand grains deep and is larger in absolute sense for sands with larger grain sizes (although the pipe depth is more or less equal for M32 and M34 in the first half of the graph). The pipe depth slightly increases with the pipe length: since water concentrates towards the pipe, the flow rate at a certain point increases continuously causing scour and thus deepening and widening of the pipe cross section as the pipe gets longer and the distance from the monitored location to the pipe tip increases with time. Note that fig. 3.3 shows measurements at one position in the pipe cross section and although it seems that for Cobo sand the pipe depth does not increase significantly, this finding does not necessarily apply for the entire cross section.

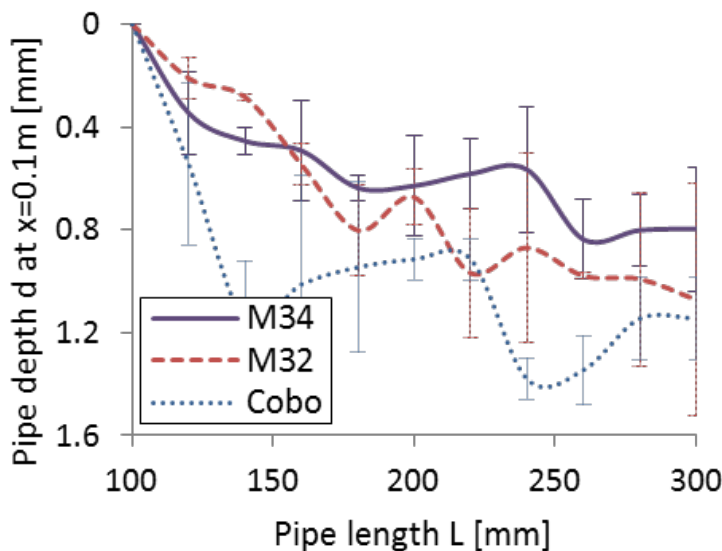


Figure 3.3. Online single point measurement at  $x=0.1$  m for different sand types as a function of the pipe length.

### 3.2 Full measurement after test

The second technique ‘full measurement after test’ studies the complete depth profile of the pipe at the end of each test. When the pipe reaches the upstream filter, all taps are closed so the piping process stops. At that moment, the cross section of the pipe is measured at several locations along its length by passing the laser measurement device over the cross sections while recording both the pipe depth and the  $y$ -coordinate. In this way the depth variation along both the pipe length and the pipe width are surveyed. It is noted that the forced end of the piping process by closing the taps causes floating sand grains in the pipe to drop immediately. As a result, the measured pipe depth will be slightly smaller than the actual pipe depth during erosion. Fig. 3.4 shows examples of measured cross sections along the  $x$ -axis for the pipe in fig. 3.2a (M34 sand). When examining for example the cross section at  $x = 0.1$  m, it is clear that the pipe is mainly located between  $y = 22$  mm and  $y = 45$  mm and consists of 2 deeper parts at the outsides and a shallow part in the middle. This is often observed, as meandering causes more scour at the

outside of a bend. In this case meandering evolved such that the outer bend at  $x = 0.1$  m was originally at one side and later at the other side. Note that the scales of the  $x$ - and  $y$ -axes are not the same: the pipe is extremely shallow with an average depth of 0.39 mm (2.5 times the average grain size) and a width of 22.5 mm. In fig. 3.5 these cross sections are combined to a 3D surface. Despite the observed scatter, the geometry and location of the pipe are clearly observable.

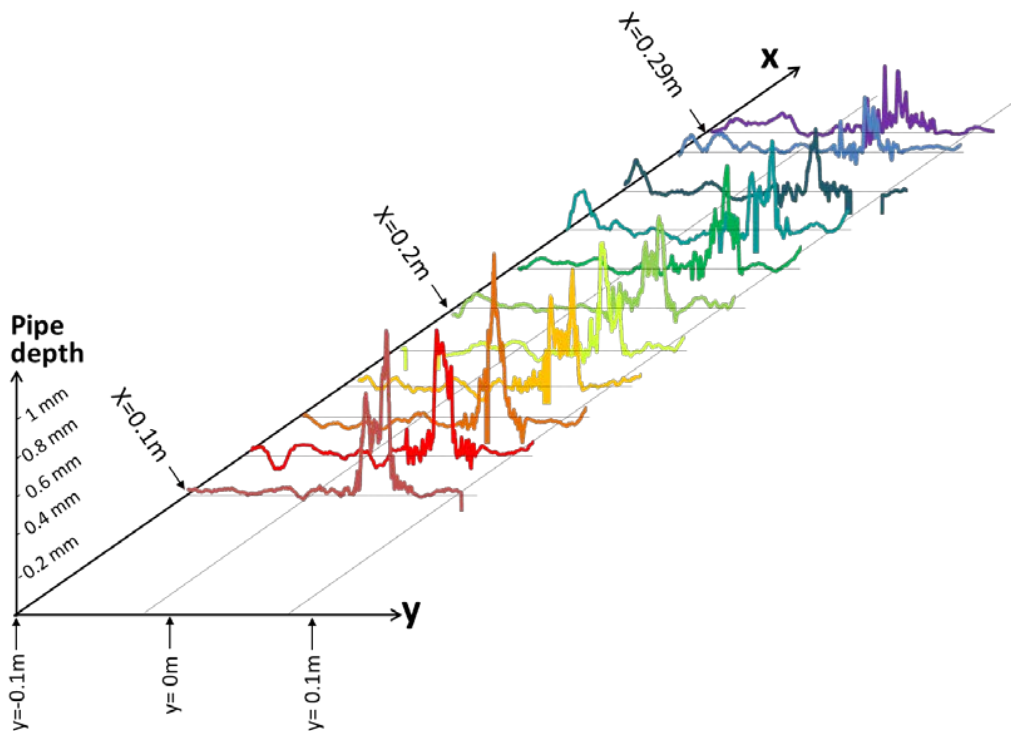


Figure 3.4. Pipe depth cross section measurements after test along  $x$  for M34 sand.

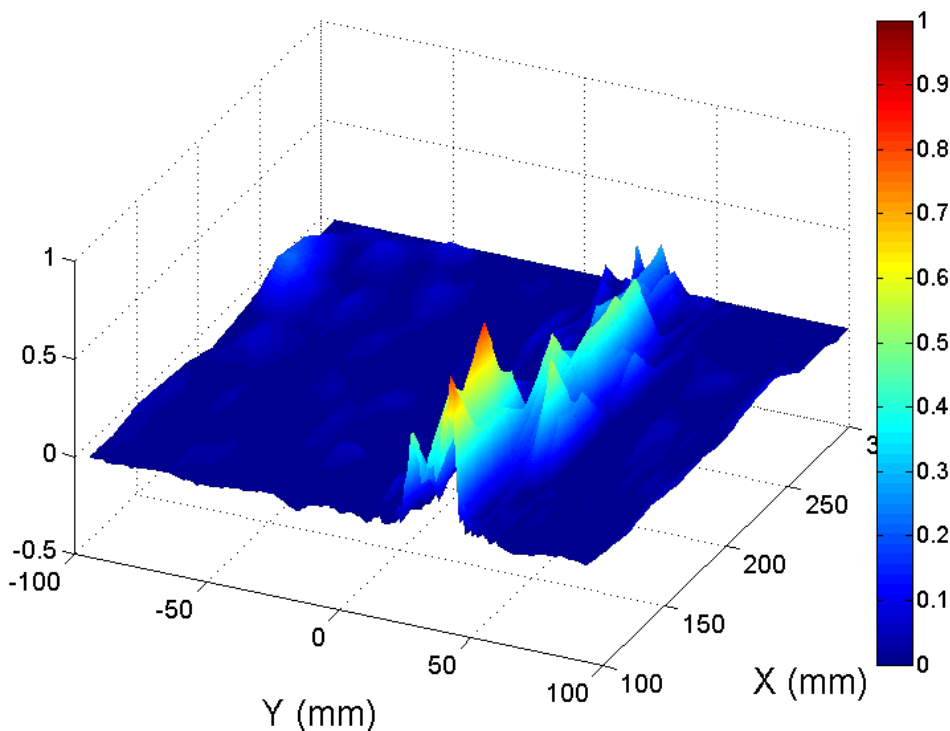


Figure 3.5. 3D surface of pipe depth cross section after test for M34 sand.

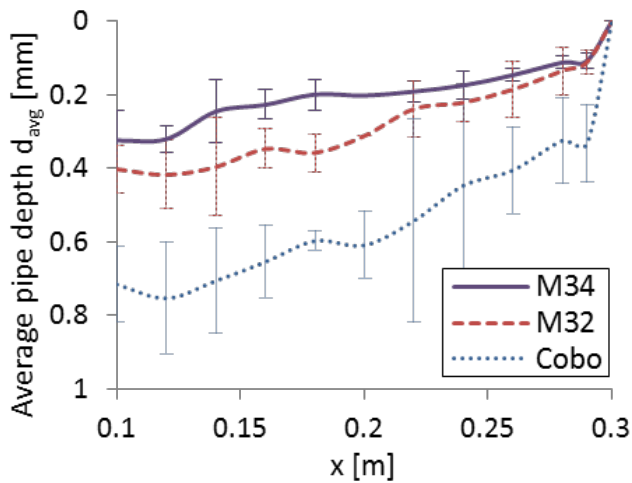


Figure 3.6. Full measurement of average pipe depth after test for each sand type.

In order to get a better idea of the evolution of pipe depth along the  $x$ -axis for the different sand types, the average pipe depth of each cross section  $d_{avg}$  is determined and averaged for all tests on the same sand type, see fig. 3.6. The pipe depth is larger for small  $x$ -values, as the pipe emerged early at that location and deepened in time, similar to fig. 3.3. Note that fig. 3.6 shows the average pipe depth of the cross section, implying that the pipe depth can be larger within the cross section (see fig. 3.4), which also explains that values smaller than 1 mm are observed close to  $x = 0.3$  m, while fig. 3.3 shows the pipe depth at one location (often in the deepest part of the pipe).

## 4 SUMMARY AND CONCLUSIONS

A series of small-scale backward erosion experiments on three poorly graded sands with mean grain sizes varying from 0.155 mm to 0.544 mm was performed for which the pipe depth during and after the tests was measured using a contactless laser triangulation sensor.

During each test, the pipe depth evolution was continuously measured at a laterally fixed position at 0.1 m upstream from the exit hole. As the position of the main streamline in the pipe changes during the process, the measurements are not necessarily at the center or at the deepest part of the pipe. The first measurements are recorded when the pipe reaches a length of 0.1 m. Initially, the pipe depth increases gradually or suddenly after which it continues to increase gently.

After each experiment, the taps are closed and the cross section of the pipe was measured at several locations, giving an impression of the overall pipe geometry. Due to the forced end of the experiment, floating sand grains drop immediately which implies that the measured pipe depth may be slightly smaller than the actual pipe depth during erosion. The pipe depth increases suddenly to a certain value near the pipe tip, and increases gradually with the distance from the pipe tip. The pipes are extremely shallow, smaller than 1 mm at a length of 0.3 m for the three examined sand types. Additionally, the width to depth ratio is very large (order of 50). Due to meandering of the pipe, the pipe depth increases at the outer bends, often leading to a maximum pipe depth at either one or both edges of the pipe cross section.

The obtained information about the pipe cross section, the pipe depth variations and the absolute values of the pipe depth give valuable input for numerical simulations and analytical studies and may lead to further understanding of the phenomenon backward erosion piping.

Furthermore, the pipes are hard to detect in practice under an existing water-retaining structure. However, monitoring techniques with the aim to detect backward erosion piping and prevent failure can be optimized when keeping these extremely small pipe depths in mind.

Further research is needed to examine whether the pipe depths are in the same range for other sands and at larger scales and to determine the influence of diverse boundary conditions.

## 5 REFERENCES

- Benjasuppatananan, S., and Meehaln, C.L. (2013). Analytical solutions for levee underseepage analysis: Straight and curved levee sections with an infinite blanket. *Geo-congress 2013*: 1129-1138.
- Bligh, W.G. (1915). Submerged weirs founded on sand. *Dams and weirs: an analytical and practical treatise on gravity dams and weirs; arch and buttress dams, submerged weirs; and barrages*, Chicago: 151-179.
- De Wit, J.M., Sellmeijer J.B., and Penning A. (1981). Laboratory testing on piping. *Tenth International Conference on Soil Mechanics and Foundation Engineering*. Stockholm Sweden: 517-520
- El Shamy, U., and Aydin F. (2008). Multiscale modeling of flood-induced piping in river levees. *Journal of Geotechnical and Geoenvironmental Engineering* 134(9):1385-1398.
- Glynn, E., Quinn M., and Kuszmaul J. (2012). Predicting piping potential along Middle mississippi river levees. *International conference on scour and erosion 2012, Paris, France*.
- Hanses, U., Müller-Kirchenbauer H., and Savidis S. (1985). Zur Mechanik der rückschreitenden Erosion unter Deichen und Dämmen. *Bautechnik, Berlin, Germany: Wilhelm Ernst & Sohn* 62(5):163-169.
- Miesel, D. (1978). Rückschreitende Erosion unter bindiger Deckschicht, *Deutsche Baugrundtagung, Berlin, Germany*
- Ojha, C.S.P., Singh V.P., and Adrian D.D. (2003) Determination of critical head in soil piping. *Journal of Hydraulic Engineering, ASCE*. 129(7):511-518.
- Schmertmann, J.H. (2000). The no-filter factor of safety against piping through sands. *Judgment and innovation at The Heritage and future of the geotechnical engineering profession, ASCE*,:68.
- Sellmeijer, H., de la Cruz, J.L., van Beek, V.M., Knoeff, H. (2011). Fine-tuning of the backward erosion piping model through small-scale, medium-scale and IJkdijk experiments. *European Journal of Environmental and Civil Engineering* 15(8):1139-1154.
- Sellmeijer, J.B., and Koenders M.A. (1991). A mathematical model for piping. *Applied Mathematical Modelling* 15(11-12):646-651.
- Sellmeijer, J.B. (1981). Piping due to flow towards ditches and holes. *Flow and Transport in Porous Media: proceedings of Euromech 143, Delft, the Netherlands*
- Sellmeijer, J.B. (1988). On the mechanism of piping under impervious structures, *PHD-thesis, TU Delft*.
- Van Beek, V.M., Essen, H.M., Vandenboer, K., Bezuijen, A. (2015). Developments in modelling of backward erosion piping. *Géotechnique* 65(9):740-754.
- Van Beek, V.M., Knoeff H., and Sellmeijer H. (2011). Observations on the process of backward erosion piping in small-, medium- and full-scale experiments. *European Journal of Environmental and Civil Engineering* 15(8):1115-1137.
- Van Beek, V.M., Knoeff, J.G., Rietdijk, J., Sellmeijer, J.B, Lopez de la Cruz, J. (2010). Influence of sand and scale on the piping process: experiments and multivariate analysis. *Physical modelling in geotechnics. L.S. Springman*, London: Taylor and Francis group, 1221-1226..
- Van Beek, V.M., Vandenboer K., and Bezuijen A. (2014). Influence of sand type on pipe development in small- and medium-scale experiments. *International conference on scour and erosion 2014. Perth, Australia*.
- Van Beek, V.M., Yao, Q., Van, M., Barends, F. (2012). Validation of Sellmeijer's model for backward erosion piping under dikes on multiple sand layers. *International conference on scour and erosion 2012, Paris, France*: 543-550.
- Vandenboer, K., van Beek V.M. and Bezuijen A. (2017). 3D character of backward erosion piping. *Géotechnique*, Advance online publication, doi:10.680/jgeot.16.P.091.
- Vandenboer, K., van Beek V.M., and Bezuijen A. (2013). 3D FEM simulation of groundwater flow during backward erosion piping. *5th international Young Geotechnical Engineers' Conference, Paris, France*: 301-304.
- Vorogushyn, S., Merz B., and Apel H. (2009). Development of dike fragility curves for piping and micro-instability breach mechanisms. *Natural Hazards and Earth System Sciences* 9(4):1383-1401.

## Physical measurements of the backward erosion piping process

B.A. Robbins

*U.S. Army Engineer Research and Development Center*

V.M. van Beek

*Deltares*

**Abstract:** A novel laboratory device is presented, in which the process of backward erosion piping is observed in cylindrical sand samples oriented horizontally. The cylindrical shape of the testing device constrained the location of the erosion path to the top of the sample, thereby allowing pore pressure measurements to be made in both the eroded pipe and the surrounding soil. Additionally, the pipe depth and width were measured. From the measurements, the local hydraulic gradient upstream of the pipe tip and the critical shear stress in the bottom of the eroded pipe were calculated. Results indicate that the local critical hydraulic gradient measured over a distance of 10 cm upstream of the pipe is not influenced by experiment scale. Further, the measurements suggest that the sediment transport in the eroded pipe can be adequately modelled using classic sediment transport theory for open channel flow.

Keywords: piping, backward erosion, seepage.

### 1 INTRODUCTION

Backward erosion piping (BEP) refers to a process by which sand is gradually eroded from the foundation of dams and levees. Erosion initiates at the downstream side of a structure where unfiltered seepage exits the foundation. The erosion then progresses upstream through sandy foundation material along the contact with a cohesive cover layer. The eroded materials are transported through the developing erosion channels towards the unfiltered seepage exit where they are deposited on the ground surface in a cone of sand (sand boil). If allowed to progress, the erosion channels may eventually connect to the river or reservoir upon which rapid enlargement of the erosion channels occur, possibly leading to catastrophic failure of the overlying embankment. For detailed descriptions of the process and physics of BEP, the interested reader is referred to Van Beek (2015).

BEP has been shown to account for approximately one-third of all internal erosion related failure modes (Richards and Reddy, 2007). Further, visible evidence of BEP activity is observed along levees during relatively frequent flood events (Turnbull and Mansur, 1961; USACE, 1956; ENW, 2010). As such, BEP has been the subject of numerous studies (Schmertmann, 2000; Sellmeijer, 1988; Townsend et al., 1981; Van Beek et al., 2011). Many of these studies were experimental in nature and attempted to measure the overall hydraulic conditions causing erosion to develop upstream. Typically, experiments of this nature are conducted in rectangular boxes in which a sand sample is subjected to unidirectional, horizontal flow. Erosion initiates at the downstream end of the sample and is allowed to progress along the sample boundary until it reaches the upstream end of the sample. Because of the rectangular shape of the sample, the erosion channels typically meander along the sample boundary seeking out the path of least resistance. In the case of the meandering channels, the location of the channel is not known *a priori* but rather varies from test to test. Therefore, it is typically not possible to make detailed measurements of the local hydraulic conditions near the developing erosion front. For this reason, the critical hydraulic gradient causing erosion is often characterized by the average hydraulic gradient across the sample. Using this average measurement to characterize the behavior requires that the measurements be adjusted

for geometry, scale, and boundary conditions to be applied to other conditions, such as the field (Schmertmann, 2000; Sellmeijer et al., 2011). In this study, a novel laboratory device is presented that permitted local measurements of the hydraulic aspects of the BEP process. From these measurements, insights are obtained regarding local hydraulic conditions causing pipe progression and flow conditions in the eroded pipes.

## 2 LABORATORY TESTING

In the following sections, the laboratory device, test procedures, and characteristics of the sand used for testing are briefly described. Detailed descriptions are available in Robbins et al. (2017).

### 2.1 Equipment

The laboratory equipment for the experiments presented in this paper consists of two acrylic cylinders fitted with pressure transducers along the top and bottom as shown in Figure 2.1. The two cylinders were identical in all regards except for diameter ( $D$ ). One cylinder had an internal diameter of 76.2 mm (Tube B), and the other cylinder had a diameter of 152.4 mm (Tube C). The two cylinder sizes were constructed to allow for the investigation of scale effects.

The cylinder is fixed to a rotating frame, such that the sand can be placed into the cylinder through water pluviation while in the vertical position. The cylinder is then rotated to the horizontal position for testing, causing the sand to form a natural slope at the downstream end of the tube. Eleven pressure transducers were located along the top and bottom of the sample at 0.1-m intervals. The head applied to both the upstream and downstream boundaries was regulated through constant head, overflow tanks. The downstream head tank was fixed, whereas the upstream head tank was raised through a winch and pulley system. In this manner, the upstream head could be controlled to the nearest millimeter. The pressure transducers were connected to a USB data acquisition module so that measurements could be recorded at one-second intervals. The flow rate was also recorded at one-second intervals by capturing the outflow in a bucket connected to a load cell with a resolution of 1 gram. In this manner, the outflow could be measured to the nearest mL/sec.

The cylindrical shape and the sloping sand bed resulted in the shortest seepage path (and highest gradients) occurring at the top (center) of the sample. Because of this, erosion would initiate at the top of the slope and progress backward along the sample directly beneath the pressure transducers. In this manner, detailed pressure measurements were recorded in the soil and eroded pipe during the process of BEP.

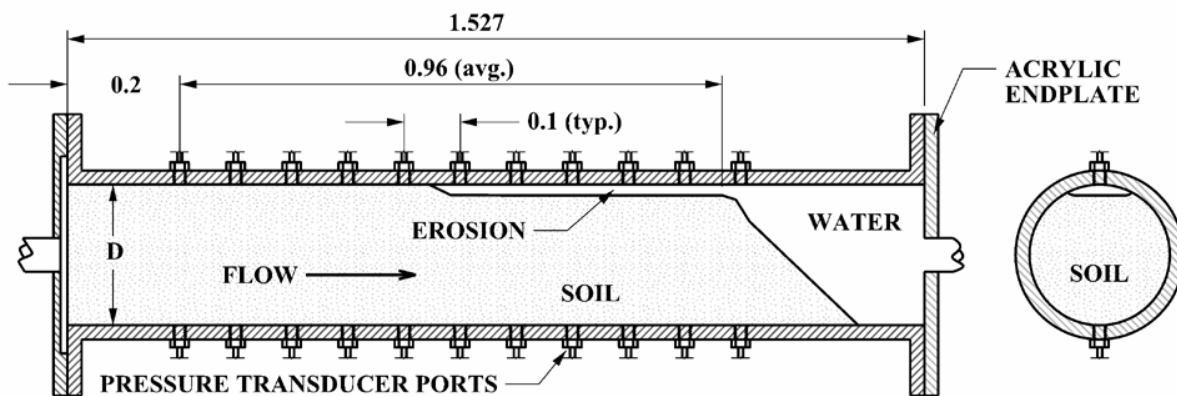


Figure 2.1. Schematic diagram of the laboratory testing device (units of meters).

## 2.2 Procedures

The following test procedures were followed for all tests conducted in this study.

1. The device was rotated to a vertical position for sample placement and saturated with deaired water.
2. The sand was water pluviated into the device from the top, tapping the sides of the cylinder with a rubber mallet during placement to achieve differing levels of densification.
3. After the sample was placed, the device was rotated to the horizontal position. The downstream slope would develop during rotation, coming to rest at the sand's natural angle of repose.
4. The upstream head tank was incrementally raised to increase the average gradient across the sample. The increments were selected to cause changes in average gradient varying from 0.01 to 0.05, with larger increments used during the beginning of the test. As critical conditions were approached, head increments resulting in gradient changes of 0.01 were used exclusively. In this manner, the hydraulic conditions at the onset of piping could be precisely measured.
5. Once piping initiated, the pipe was allowed to progress through the sample with pressure measurements and flow rate measurements being recorded at a frequency of 1 Hz. In some cases, the head was decreased once the pipe progressed halfway through the sample to stop the erosion. Once the erosion was stopped, the upstream head was gradually increased again until erosion was observed. This allowed the local hydraulic gradient near the head of the pipe to be measured at the onset of piping. When erosion reinitiated, it was allowed to progress the remainder of the way through the sample.
6. After the pipe progressed entirely through the sample, the pipe channel was allowed to enlarge until the sand in the bottom of the pipe came into equilibrium (as indicated by minimal grain movements). Measurements of the channel dimensions, pressure gradient, flow rate, and maximum flow velocity in the pipe (as indicated by colored dye streams) were obtained at the equilibrium state. These measurements were also recorded in some instances when the pipe was stopped part way through the sample.

## 2.3 Materials

A single sand was used for testing in both Tube B and Tube C. The sand, referred to as 40/70 sand, falls predominantly between the No. 40 and No. 70 U.S. sieve sizes. The sand characteristics are presented in Table 1. ASTM testing standards D4253 and D4254 were used to determine the maximum and minimum void ratios.

Table 1. Characteristics of 40/70 Sand

Property	Value
$d_{10}$ (mm)	0.227
$d_{30}$ (mm)	0.268
$d_{60}$ (mm)	0.322
$C_c$	0.98
$C_u$	1.42
$e_{min}$	0.56
$e_{max}$	0.80
Specific gravity	2.65

## 2.4 Test Results

A total of 11 tests were conducted: 7 tests in Tube B and 4 tests in Tube C. For each test, the average critical gradient across the sample for BEP initiation was recorded at the moment of pipe initiation. The critical average gradients obtained for all tests are shown in Figure 2.2. For all tests, a general decrease in

critical gradient with increasing void ratio is observed. This trend corresponds well with the results of previous studies (Van Beek et al., 2009; Weijers and Sellmeijer, 1993). Further, the tests conducted in Tube C exhibit lower average critical gradients than the tests in Tube B due to scale effects (Van Beek, 2015; Schmertmann, 2000). As the tube diameters are sufficiently different for scale effects to be exhibited, the experiment results can be examined at a local scale to determine if local hydraulic measurements are also subject to scale effects.

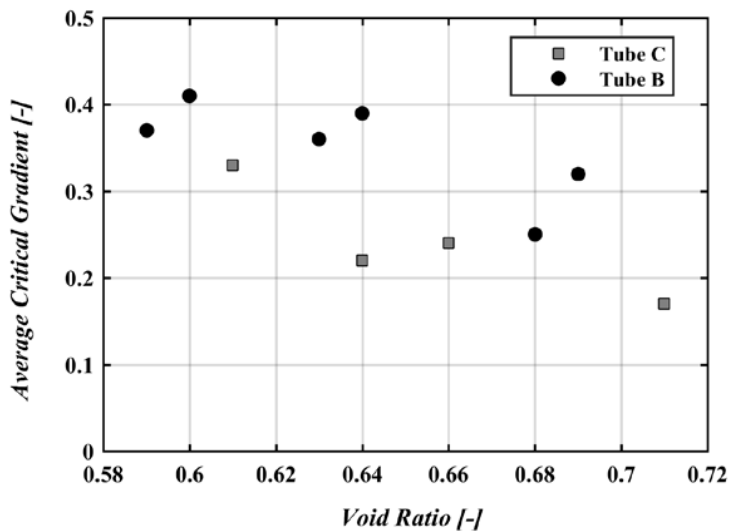


Figure 2.2. Average gradient measured at initiation of piping for all tests.

During each test, as the pipe passed the pressure transducers, the local horizontal gradient (over 10 cm) along the top of the sample was measured between each pair of pressure transducers. Additionally, the local vertical gradient (across the diameter of the cylinder) was measured across each pair of top/bottom transducers. Whenever the pipe reached a pressure transducer, the local horizontal gradient measured over the 10 cm immediately upstream of the pipe head obtained its maximum value. Likewise, the local vertical gradient measured at the location of the pipe head also reached its maximum value. Each time the pipe passed a pressure transducer, the magnitude of the maximum horizontal and vertical local gradients was noted. The measured values are shown in Figure 2.3. In most instances, the pipe was actively progressing as it passed the transducers and showed no signs of being near the critical conditions for progression. However, in a few instances (typically after the stopped pipe was restarted) the conditions were nearly at equilibrium and the pipe would stop progressing momentarily at the transducer location. The local gradients measured under these equilibrium conditions are distinguished in Figure 2.3.

Important observations that advance the understanding of BEP were made from the results of this testing. First, local measurements of gradient were substantially higher than the average gradients. This is indicative of the concentration in flow and high gradients that occur in the vicinity of the pipe head (Vandenboer et al., 2014). Secondly, it should be noted that the majority of the local gradient measurements were significantly larger than the critical, local gradient values measured near equilibrium. This can be explained by the fact that BEP is controlled by initiation in small experiments with sloped exits (Van Beek et al., 2014). That is, for this experiment configuration once BEP initiates, it will progress continuously through the sample due to the critical gradient for progression being far exceeded. This observation is confirmed by the generally high values of local horizontal gradient for the majority of the measurements. Lastly, the local critical gradients measured at the verge of equilibrium (Figure 2.3) are nearly identical in magnitude for both tube diameters and appear to be independent of the vertical gradient. This suggests that, when measured over a small enough distance, a scale-independent critical gradient can be measured. Further, it is solely the horizontal component of this local gradient that appears to control the progression of BEP.

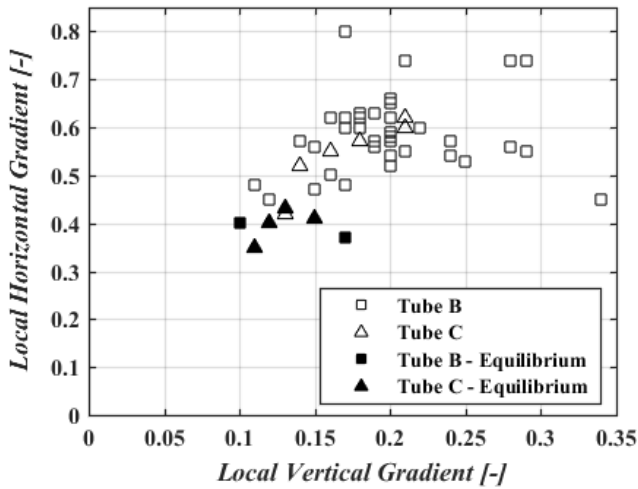


Figure 2.3. Local gradient measurements obtained during pipe progression.

### 3 PIPE CHANNEL EROSION

During each test, stable pipe channel configurations were obtained, in which the sand particles in the bottom of the pipe were in equilibrium. In some cases, stable pipe channels were obtained with the pipe penetrating through only a fraction of the sample. When stable pipe channel sections were obtained, the channel dimensions, pressure gradient, and maximum flow velocity were obtained as previously discussed. Approximating the pipe channel cross section as an ellipse, the channel wall shear stress,  $\tau_w$  ( $N/m^2$ ), can be computed from the measured quantities for laminar flow conditions (Van Beek et al, 2017) by

$$\tau_w = \sqrt{\rho_w g \frac{\partial \phi}{\partial x} v_{\max} 2\mu} \quad (1)$$

where  $\rho_w$  ( $kg/m^3$ ),  $g$  ( $m/s^2$ ),  $\partial \phi / \partial x$ ,  $v_{\max}$  ( $m/s$ ), and  $\mu$  ( $Ns/m^2$ ) represent the fluid density, acceleration of gravity, hydraulic gradient in the pipe channel, maximum flow velocity in the pipe channel, and dynamic fluid viscosity, respectively. In all experiments, the flow was observed to be laminar as indicated by the smooth dye streamlines (Figure 3.1). If the wall shear stress exceeds the critical shear stress for sediment transport, the wall of the erosion channel is eroded and the pipe deepens. The depth of the erosion channel is a fundamental aspect of numerical computations of coupled seepage-pipe hydraulics (Sellmeijer, 2006; Van Esch et al., 2013), and indirectly influences the local gradient at the pipe tip as well. Because of the importance of the pipe depth in BEP hydraulic computations, it is imperative that the critical shear stress be known precisely. Current practice in the Netherlands (TAW, 1999) predicts the critical shear stress,  $\tau_c$  ( $N/m^2$ ), in piping calculations using the approach proposed by White (1940) where

$$\tau_c = \eta \frac{\pi}{6} \gamma'_p d \tan \theta \quad (2)$$

with  $\eta$ ,  $\gamma'_p$  ( $N/m^3$ ),  $d$  ( $m$ ), and  $\theta$  (*degrees*), denoting White's constant, the submerged particle specific weight, the particle diameter, and the bedding angle of the sand particles, respectively. The values of White's constant and bedding angle have been prescribed through calibration of numerical models to large scale experiments (Lopez de la Cruz, Calle, and Schweckendiek, 2011). Relying on a fixed-parameter set based on model calibration brings into question the validity of the model under conditions

outside the calibration data set. A more generic approach for predicting the critical shear stress in BEP pipes was proposed by Hoffmans (2014) using the Shields curve as applied to open channel sediment transport problems. The Shields curve relates the dimensionless particle Reynolds number, given by

$$Re^* = \frac{\rho_w u^* d_{50}}{\mu} \text{ with } u^* = \sqrt{\frac{\tau_w}{\rho_w}} \quad (3)$$

to the Shields parameter given by

$$\Psi_c = \frac{\tau_c}{\gamma_p d} = f\left(\frac{\rho_w u^* d}{\mu}\right) \quad (4)$$

The general relationship between the particle Reynolds number and the Shields parameter has been determined experimentally for a variety of sediments and flow conditions (ASCE, 2008). Using this relationship, the flow conditions in the pipe can be related to the critical shear stress of the sediments in the bottom of the pipe to adjust BEP models to a broad variety of conditions.

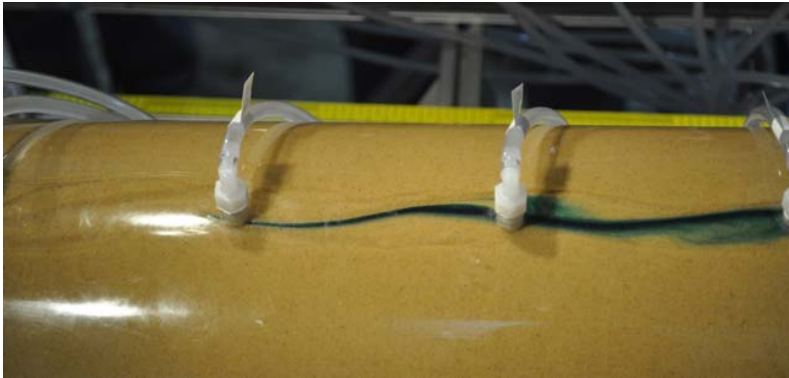


Figure 3.1. Stream lines indicative of laminar flow conditions in the developed pipes.

To examine the applicability of the Shields approach to BEP modeling, the erosion channel wall shear stress (shear stress exerted on the particles in the bottom of the pipe) was computed for all experiments in which the particles at the bottom of the eroded pipe appeared to be in equilibrium. Equilibrium was judged to be obtained when the pipe depth appeared to be constant and particle movement was relatively infrequent. The wall shear stress under these conditions was considered to be the critical shear stress of the sand particles, which relies on the observation by Govers (1987) that the transition from a stable to an unstable bed is sharply discernible in laminar flow as fluctuating shear stresses are absent. The wall shear stress for each experiment (both with the pipe penetrating partially and fully) was computed using Equation 1 with the measured pressure gradient and maximum velocity. The computed critical shear stress for the sand particles at the bottom of the BEP channels was compared to the Shields diagram (Cao, 2006) and various other data sets obtained in laminar flow conditions (Govers, 1987; Loiseleux et al. 2005; Mantz, 1977; C.M. White, 1940; S. White, 1970; Yalin and Karahan, 1979) as shown in Figure 3.2. Additionally, the Shields parameter corresponding to using White's approach with fixed parameters is shown on Figure 3.2 for comparison purposes. From the results, it is apparent that the Shields parameter estimated for the sediment in the BEP erosion channels corresponds well to both the data in the literature for laminar flow and the Shields curve. It is also interesting to note that the BEP data appears to be towards the upper end of the laminar flow regime, approaching the transition zone (near a particle Reynolds number of 10). For sands that are much coarser than those tested in this study, it is quite likely that the flow conditions will begin to become turbulent. This must be considered when applying the results of this study to BEP models.

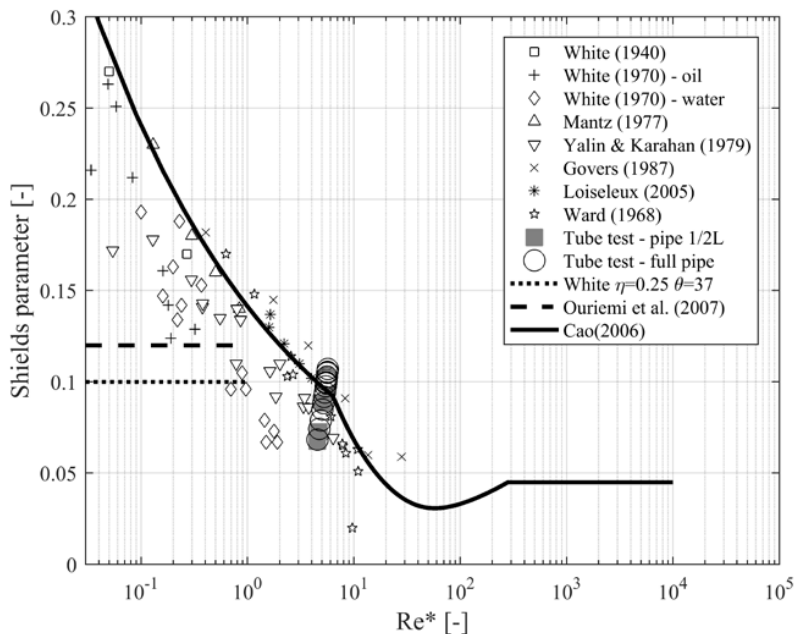


Figure 3.2. Shields parameter determined from laboratory experiments compared to data in the literature.

## 4 CONCLUSIONS

A cylindrical test device was constructed in which backward erosion piping (BEP) experiments could be conducted. The cylindrical sample shape ensured that the erosion path progressed along the center of the sample. Pore pressure transducers located along the top and bottom of the sample allowed the pressure gradients to be measured in the soil surrounding the pipe and in the pipe channel itself. From these measurements, it was found that the horizontal, hydraulic gradient measured over a distance of 10 cm in front of the advancing pipe was significantly higher than average hydraulic gradients across the entire sample. The local gradients were also, in the majority of cases, higher than the threshold gradient for progression. In instances where pipe progression was stopped, the local critical gradient in front of the advancing pipe was measured. It was found that the critical horizontal gradient 10 cm upstream of the pipe did not exhibit scale effects found in the average gradient measurements across the entire sample. Lastly, the gradient measurements obtained in the eroded pipe channels allowed the critical shear stress of the pipe sediments to be calculated. Results indicate that the incipient motion conditions in the pipe channel bottom align well with the Shields approach for predicting incipient motion. This validates the use of Shields diagram for BEP modeling providing a generic transport approach encompassing all conditions resulting in laminar flow. The combination of a local critical gradient in front of the pipe and the Shields approach for predicting incipient motion in the pipe allows for modeling of pipe progression.

Permission to publish was granted by Director, Geotechnical & Structures Laboratory.

## REFERENCES

- ASCE. (2008). *Sedimentation Engineering*. (M. Garcia, Ed.). American Society of Civil Engineers.
- Cao, Z., Pender G., & Meng, J. (2006). Explicit Formulation of the Shields Diagram for Incipient Motion of Sediment. *Journal of Hydraulic Engineering*, October 2006: 1097-1099.
- ENW (Expertisenetwerk Waterveiligheid) (2010) Piping – Realiteit of Rekenfout. Expertisenetwerk Waterveiligheid, see [http://www.enwinfo.nl/upload/Piping%20-%20Realiteit%20of%20Rekenfout%20\(72dpi\).pdf](http://www.enwinfo.nl/upload/Piping%20-%20Realiteit%20of%20Rekenfout%20(72dpi).pdf) (accessed 16-09-2013)
- Govers, G. (1987). Initiation of motion in overland flow. *Sedimentology*, 34(6), 1157–1164.

- <https://doi.org/10.1111/j.1365-3091.1987.tb00598.x>
- Hoffmans, G.J.C.M. (2014). An Overview of Piping Models. In *ICSE7* (p. 17). Perth, Australia.
- Loiseleux, T., Gondret, P., Rabaud, M., & Doppler, D. (2005). Onset of erosion and avalanche for an inclined granular bed sheared by a continuous laminar flow. *Physics of Fluids*, *17*(10). <https://doi.org/10.1063/1.2109747>
- Lopez de la Cruz, J., Calle, E., & Schweckendiek, T. (2011). Calibration of Piping Assessment Models in the Netherlands. In *International Symposium on Geotechnical Risk and Safety* (pp. 587–595). Munich, Germany. Retrieved from [http://vzb.baw.de/digitale\\_bib/geotech2011/PDF/5\\_Flood\\_Defence/5\\_04.pdf](http://vzb.baw.de/digitale_bib/geotech2011/PDF/5_Flood_Defence/5_04.pdf)
- Mantz, P.A. (1977). Incipient transport of fine grains and flakes by fluids - Extended Shields diagram. *J. Hydr. Div.*, *103*(HY6), 601–615.
- Richards, K.S., & Reddy, K.R. (2007). Critical appraisal of piping phenomena in earth dams. *Bulletin of Engineering Geology and the Environment*, *66*(4), 381–402. <https://doi.org/10.1007/s10064-007-0095-0>
- Robbins, B.A., van Beek, V.M., Lopez-Soto, J., Montalvo-Bartolomei, A., Murphy, J. (2017). A novel laboratory test for backward erosion piping. Manuscript submitted to publisher.
- Schmertmann, J.H. (2000). The No-Filter Factor of Safety Against Piping Through Sands. In F. Silva & E.J. Kavazanjian (Eds.), *Judgement and Innovation* (pp. 65–133). American Society of Civil Engineers.
- Sellmeijer, H., López, J., Cruz, D., van Beek, V.M. & Knoeff, H. (2011). Fine-tuning of the backward erosion piping model through small-scale, medium-scale and IJkdijk experiments. *European Journal of Environmental and Civil Engineering*, *15*(8), 1139–1154. <https://doi.org/10.3166/EJECE.15.1139-1154>
- Sellmeijer, J.B. (1988). *On the mechanism of piping under impervious structures*. Delft University of Technology.
- Sellmeijer, J.B. (2006). Numerical computation of seepage erosion below dams ( piping ). *International Conference on Scour and Erosion*.
- TAW. (1999). *Technical Report on Sand Boils ( Piping )*. Delft, The Netherlands.
- Townsend, F., Schmertmann, J.H., Logan, T.J., Pietrus, T.J., & Wong, Y.W. (1981). *An Analytical and Experimental Investigation of a Quantitative Theory for Piping in Sand*. Gainesville, FLorida.
- Turnbull, W.J., & Mansur, C.I. (1961). Investigation of underseepage- Mississippi River Levees. *ASCE Transactions*.
- USACE. (1956). Investigation of Underseepage, Mississippi River Levees, Alton to Gale, IL. Vicksburg, MS: Waterways Experiment Station.
- Van Beek, V., Bezuijen, A., Sellmeijer, J., & Barends, F.B.J. (2014). Initiation of backward erosion piping in uniform sands. *Géotechnique*, *64*(12), 927–941.
- Van Beek, V., Knoeff, H., & Sellmeijer, H. (2011). Observations on the process of backward erosion piping in small-, medium- and fullscale experiments. *European Journal of Environmental and Civil Engineering*, *15*(8), 1115–1137. <https://doi.org/10.3166/ejece.15.1115-1137>
- Van Beek, V.M. (2015). *Backward Erosion Piping: Initiation and Progression*. Technische Universiteit Delft. <https://doi.org/10.1007/s13398-014-0173-7.2>
- Van Beek, V.M., Luijendijk, M. S., Knoeff, J. G., & Barends, F. B. J. (2009). Influence of relative density on the piping process - Small- scale experiments.
- Van Beek, V.M., Robbins, B.A., Hoffmans, G., Bezuijen, A., van Rhijn, L. (2017). Use of incipient motion data for backward erosion piping modeling. Manuscript submitted to publisher.
- Van Esch, J.M., Teunissen, J.A.M., & Stolle, D. (2013). Modeling transient groundwater flow under dikes and dams for stability assesment. In *3rd International Symposium on Computational Geomechanics (ComGeo III)* (p. 9).
- Vandenboer, K., van Beek, V., & Bezuijen, A. (2014). 3D finite element method (FEM) simulation of groundwater flow during backward erosion piping. *Frontiers of Structural and Civil Engineering*, *8*(2), 160–166. <https://doi.org/10.1007/s11709-014-0257-7>
- Weijers, J., & Sellmeijer, J. (1993). A new model to deal with the piping mechanism. *Filters in Geotechnical and Hydraulic Engineering*, 349–355. Retrieved from <http://scholar.google.com/scholar?hl=en&btnG=Search&q=intitle:A+new+model+to+deal+with+the+piping+mechanism#0>
- White, C.M. (1940). The Equilibrium of Grains on the Bed of a Stream. *Proceedings of the Royal Society A: Mathematical, Physical and Engineering Sciences*, *174*(958), 322–338. <https://doi.org/10.1098/rspa.1940.0023>
- White, S. (1970). Plane bed thresholds of fine grained sediments. *Nature*, *228*, 152–153. Retrieved from

<http://adsabs.harvard.edu/abs/1970Natur.228..152W>

Yalin, M., & Karahan, E. (1979). Inception of sediment transport. *Journal of the Hydraulics Division*.  
Retrieved from <http://cedb.asce.org/cgi/WWWdisplay.cgi?5014975>

## Contribution for assessing filter efficiency in zoned dams

A. Benamar

*Normandie Univ, UNIHAVRE, CNRS, LOMC, 76600 Le Havre, France.*

S. Azirou & A. Tahakourt

*LGCA, Faculté de Technologie, Université de Bejaia, Algeria*

**Abstract:** Dam filters are mainly designed using filter criteria based on the grain size distribution. The main design criteria against which performance is assessed are a criterion for retention of fine particles. The characteristic size of finer fraction influences the size distribution of the filter pore and hence the retention capacity of flowing particles, and the permeability of the filter itself. This paper reports experimental results obtained on the soil-filter system behaviour subject to different hydraulic and geometrical conditions. Many core soils and filters were used. The objective of this study was to determine the effectiveness of the filter to protect the silt submitted to erosion under controlled water flow. Particles transport and filtration through each granular filter were analysed as regards to filter retention capacity and particles size selection. The plasticity of base soil influences greatly the filtration since slightly plastic soils are more erodible than plastic soils. The analysis of hydraulic conductivity in the filter is of a great concern and leads to understand the filtration process. A comparison of the efficiency of the filters is assessed toward the usual required criteria and the most appropriate for the dam filters. Matching experimental results with filter design criteria reveals that many of them are conservative. The filter porosity variation was assessed and correlated with clogging particles volume. The evolution of such parameter may be an indicator of likely filter clogging. A new approach of filter clogging was proposed by evaluating a damage index which is affected by various parameters such as the ratio  $D_{15}/d_{85}$  and the size of eroded particles. An approach linking the geometrical parameters (damage index) to the hydraulic conductivity leads to an estimation of the filter performance which provides an interesting and realistic criterion.

Keywords: erosion, filter, flow, plasticity, porosity.

## 1 INTRODUCTION

The concept of filtration in geotechnical engineering works describes the restriction of particles migration from a soil into or through a granular medium (filter). The presence of filters in hydraulic structures (dams and dykes) is essential for core protection against erosion. ICOLD recommendations (2015) provide methods to estimate the water level at which internal erosion will initiate and lead to failure in the four initiating mechanisms: concentrated leaks, suffusion, backward erosion and contact erosion. The study of particle transport process in protective filter was asked widely in civil engineering, in particular when designing zoned dams where the presence of filters is required. Filters are of a great importance for the permeability of embankment dams because of the necessity to ensure the transition between the base soil and the downstream mudstone fill. An adequately designed filter must retain loose soil particles eroded from base soil and therefore prevent piping, whereas it will be able to allow water seepage in order to avoid high internal pore pressures arising. The detachment of fine particles (from the base soil) and their subsequent transport throughout the filter pore network requires a sufficient pore opening. This pore space is conditioned by the particle size distribution (PSD) but also by the grain shape and their contact. The porosity influences the opening of the void space (Locke et al., 2001; Reboul et al., 2008). Many laboratory researches devoted to filtration criteria were developed for cohesionless soils, and resulted in empirical relationships based on grain size criteria (Vaughan et al., 1982; Foster et al.,

2001; USBR, 2011). Unstable filters prone to internal erosion may lead fines to be washed out, enlarging pore size and reducing filtration capability. Moffat et al. (2015) proposed a method to deduce an approached value of critical hydraulic gradient that triggers internal erosion in a cohesionless soil of known particle size distribution curve. The filter is assumed to be efficient when pore spaces between grains are enough small to capture some of larger base particles, which in turn allow retaining finer base particles (self-filtration). But this process will be not extended to finer particles in order to avoid filter clogging and high pore pressure rise. So, a residual permeability is required for preventing hydraulic structure damage. Filters, which are commonly used to provide stability and drainage in dams and dykes, are prone to long-term accumulation of fine micron-sized particles. When flowing through porous medium, the particles are brought into contact with the possible retention sites and may be trapped or carried away by the flow stream. This process leads to the reduction of the permeability, which in turn may lead to a severe decrease in the filter drainage capacity and a rise of uplift pressures in the core (Benamar, 2013). Clogging behavior was defined by Vaughan et al. (1982) as a slow blocking of the filter, occurring more with graded filters than with uniform ones. Reddi et al. (2000, 2005) reported that filters can be successful in preventing erosion of base soil, but they can face significant permeability reduction as a result of physical clogging caused by the accumulation of fine particles in pore voids. Other analyses are devoted to the time evolution of particles migration and attachment conditions within a filter as regards to different representative particles size ratio (Huang et al. 2014). In the present study, results from hole erosion and filtration tests, involving several base soils and filters, are presented and analyzed. A method based on porosity reduction and PSD of base soil, for estimating the filter efficiency, is presented. The model should help in the design and the quality control during filter construction. Moreover, important results are developed for predicting the filter performance and capacity retention of fine particles. The size distribution analysis of retained and recovered particles allowed an evaluation of filter opening.

## 2 MATERIALS AND TEST PROCEDURE

### 2.1 Materials

#### 2.1.1 Geotechnical parameters

In order to evaluate both erodibility of base soils and filters efficiency downstream the soil, three fine soils and four granular filters involving various characteristics are selected (Table. 1). Fig. 1 shows the grain-size distribution curves of the different soils used in the laboratory tests as base soils and downstream filters. According to Standard Soil classification System (ASTM D2487, 2011) the fine soils were classed as Lean Clays (Table. 2). Two base soils ( $CL_1$ ,  $CL_2$ ) have the same range of grain-size (0-120 $\mu$ m) while the third one ( $CL_3$ ) is coarser (0-361 $\mu$ m) (Fig. 2). The base soils  $CL_1$ ,  $CL_2$  and  $CL_3$  were collected respectively from Jossigny (France), Namur (Belgium) and Normandy (France). According to Sherard and Dunnigan (1985), these soils are classed in the Group 1 containing only particles passing No.200 sieve (85% finer than 75 $\mu$ m). From Table.1 which summarizes the main geotechnical characteristics of used base soils, the plasticity index (Atterberg Limits) indicates a very plastic clay for  $CL_1$  and a slightly plastic clay for both  $CL_2$  and  $CL_3$ . Additional geotechnical properties of the soils were measured in accordance with ASTM standards, including shear resistance (Vane Shear test).

The USBR (US Bureau of Reclamation) filter design has been extensively reported in literature and the resulted criteria have been used in various researches (Foster et al., 2001; Reddi et al., 2002; Delgado et al., 2012; Correia Dos Santos et al., 2014). The four granular filters are made of silica sand and selected by sieving selected according to USBR (2011) criteria (Fig. 1). The finer one (F0) provides grain size distribution ranging from 0.10 mm to 6.30 mm which is perfectly within the range of used criteria. But because this filter is prone to suffusion (internally unstable) under severe hydraulic load, fine particles (<400  $\mu$ m) are so removed from matrix for designing filter F1 whose granular size extend (WG, ASTM D2487) from 0.40 mm to 6.30 mm with angular grain shape (FHWA NHI-06-088). In order to investigate the grain shape effect on the filtration mechanism, a third filter F2 with rounded grain shape

(FHWA NHI-06-088) collected from Seine River (France) was selected with the same grain size distribution than filter F1 (angular grain shape). To go deeper in the research and to evaluate the impact of the ratio ( $D_{15}/d_{85}$ ) in filter behavior, a coarser filter F3 (WP, ASTM D2487) was selected, providing a different  $D_{15}$  than that of filter F1 (Table 3) and a grain-size distribution ranging from 0.63 to 6.30 mm (Fig. 1) with angular grain shape (FHWA NHI-06-088). The obtained values of the ratio  $D_{15}/d_{85}$  for different combinations soil-filter are larger than 6, indicating that the materials do not meet the usual criteria of filter design.

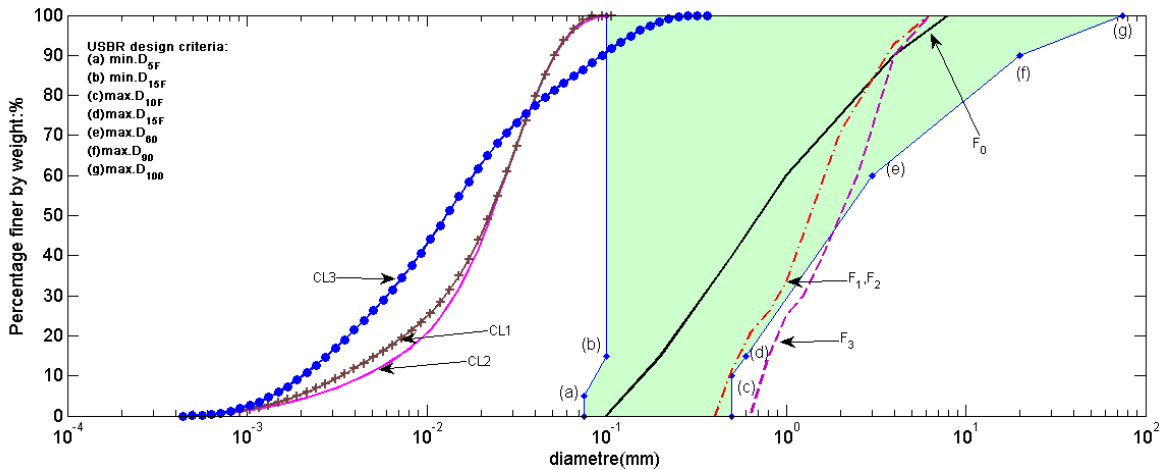


Figure 1. Particle size distribution of base soils and filters designed according to USBR criteria.

### 2.1.2 Soil dispersivity

It is reported that dispersive soil is more prone to suffusion and the dispersion phenomenon is recognized in the erosion investigation by the presence of a high turbidity in the water. The impact of the dispersion in the design of dam core sand granular filters is not broadly defined. Sherard et al. (1985) reported that there is not a significant difference between dispersive and non-dispersive clay. Delgado et al. (2012) conclude that the dispersivity affects the design of granular filters. Reiffsteck (2007) reported that final size of the hole in HET (Hole Erosion Test) provides the basic tool for classifying the dispersivity of the soil. In order to evaluate the susceptibility to dispersion of used base soils, the Crumb Test (ASTM D6572-00) was performed and provides an idea of what the suspension of a dispersive soil should look like after more than three hours. The results are displayed on Figs. 2a, 2b and 2c for  $CL_1$ ,  $CL_2$  and  $CL_3$  respectively; and some important differences are noticed in the dispersion behavior of the three soils. Pictures show that Jossigny lean clay ( $CL_1$ ) exhibits a cloud of suspension, usually spreading out in thin streaks on bottom of the beaker. So, this base soil was classified in Grade 3, according to ASTM D6572-00. The dispersivity is rather less apparent in Namur Lean Clay ( $CL_2$ ) where the fluid in the beaker is less opaque with a slight reaction. So, this soil was classified in Grade 2. The Normandy Lean Clay ( $CL_3$ ) behaves differently from other base soils, showing no reaction, crumbs may slake, but no sign of cloudiness caused by the suspension, and so this soil was then classified in Grade 1 (the less dispersive lean clay).

Table 1. Geotechnical parameters of used soils (ASTM D2487)

Lean Clay type	Atterberg limits			Undrained shear resistance (kPa)	$D_{15}/d_{85}$			
	WL (%)	Wp (%)	Plasticity Index (%)		F <sub>0</sub>	F <sub>1</sub>	F <sub>2</sub>	F <sub>3</sub>
CL <sub>1</sub> (Jossigny)	37	17	20 (very plastic)	4	4.4	11	11	13.8
CL <sub>2</sub> (Namur)	33	21	12 (slightly Plastic)	7	4.4	11	11	13.8
CL <sub>3</sub> (Normandy)	34	21	13 (slightly Plastic)	8	2.7	6.7	6.7	10.8

Table 1. Classification of different tested materials (ASTM D2487)

Soil Type	F <sub>c</sub> <sup>a</sup> (%)	G <sub>c</sub> <sup>b</sup> (%)	Dry density	Specific gravity	Coefficient		Soil classification (ASTM D2487, [3])
					Uniformity (C <sub>u</sub> <sup>c</sup> )	Curvature (C <sub>c</sub> <sup>d</sup> )	
F <sub>1</sub>	0	10	1.65	2.65	5	1.25	SP: Poorly graded sand
F <sub>2</sub>	0	10	1.65	2.65	5	1.25	SP: Poorly graded sand
F <sub>3</sub>	0	10	1.65	2.65	3.15	0.78	SP: Poorly graded sand
CL <sub>1</sub>	85	0	1.60	2.60	5.48	1.84	CL: lean clay
CL <sub>2</sub>	85	0	1.60	2.60	7.97	1.83	CL: lean clay
CL <sub>3</sub>	85	0	1.60	2.60	8.77	0.96	CL: lean clay

F<sub>c</sub><sup>a</sup>: fines content (mass fraction in percentage of particles finer than 75μm).

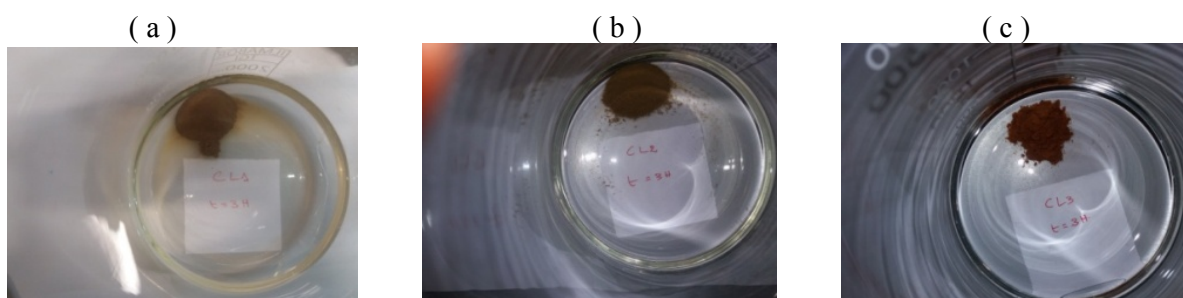
G<sub>c</sub><sup>b</sup>: gravel content (mass fraction in percentage of particles coarser than 4.75mm).

C<sub>u</sub><sup>c</sup>: uniformity coefficient ( $C_u = D_{60} / D_{10}$ )

C<sub>c</sub><sup>d</sup>: curvature coefficient ( $C_c = (D_{30})^2 / (D_{10} \times D_{60})$ )

Table 2. Grading parameters of used filters and base soils

	$d_{50b}$ (μm)	$d_{75b}$ (μm)	$d_{85b}$ (μm)	$d_{95b}$ (μm)	$D_{15F}$ (μm)	$D_{50F}$ (μm)
CL <sub>1</sub>	24.7	36	45.5	58	-	-
CL <sub>2</sub>	24.7	36	45.5	58	-	-
CL <sub>3</sub>	13.4	36	74	140	-	-
F <sub>1</sub> , F <sub>2</sub>	-	-	-	-	500	1700
F <sub>3</sub>	-	-	-	-	800	2000


 Figure 2. Visual results from the Crumb Test: (a) Jossigny (CL<sub>1</sub>), (b) Namur (CL<sub>2</sub>) and Normandy (CL<sub>3</sub>)

## 2.2 Experimental Setup

Specifically, the complete problem of particles detachment from base soil and their filtration by a downstream filter are addressed in this paper. The device used for erosion test in vertical flow conditions is quite similar to that described by Sherard et al. (1985) for No Erosion Filter (NEF) test. It is devoted to investigate the filtration of cohesive soils by granular filters with the presence of a crack. The so-called NEF test involves a permeameter (cell made of Plexiglas) which is 140 mm of diameter and 280 mm high (Fig. 2), connected to a water supply which provides a selected pressure in a range from 25 kPa to 75 kPa. The cell is equipped with a pressure gauge and the outlet is directed to a turbidity-meter and a flow-meter providing continuous records of measured values. The cell is mainly composed of four compartments: The filter layer (150 mm) packed with a target dry density of  $16.5 \text{ kN} / \text{m}^3$  on a glass beads (8 mm diameter) layer, the base soil sample of 25 mm thickness is compacted (to a target dry density of  $16 \text{ kN/m}^3$ ) on a steel plate. A 10 mm diameter pinhole was drilled through the base soil and the steel plate in order to introduce a concentrated flow through the hole. At the top of the cell a gravel layer is placed for spreading the inlet flow. The bottom layer of glass beads helps to compact the filter layer and also allows the flow discharge without retaining particles released from the filter.

A flow induced with a very low pressure is applied through the soil-filter system and once saturation reached, the water pressure is increased gradually by steps corresponding to selected pressure test values. Particle concentration is derived using a previous correlation between fines concentration in water and turbidity (NTU). The performance of the soil-filter combination is observed during a processing time close to 10 minutes under a constant hydraulic pressure.

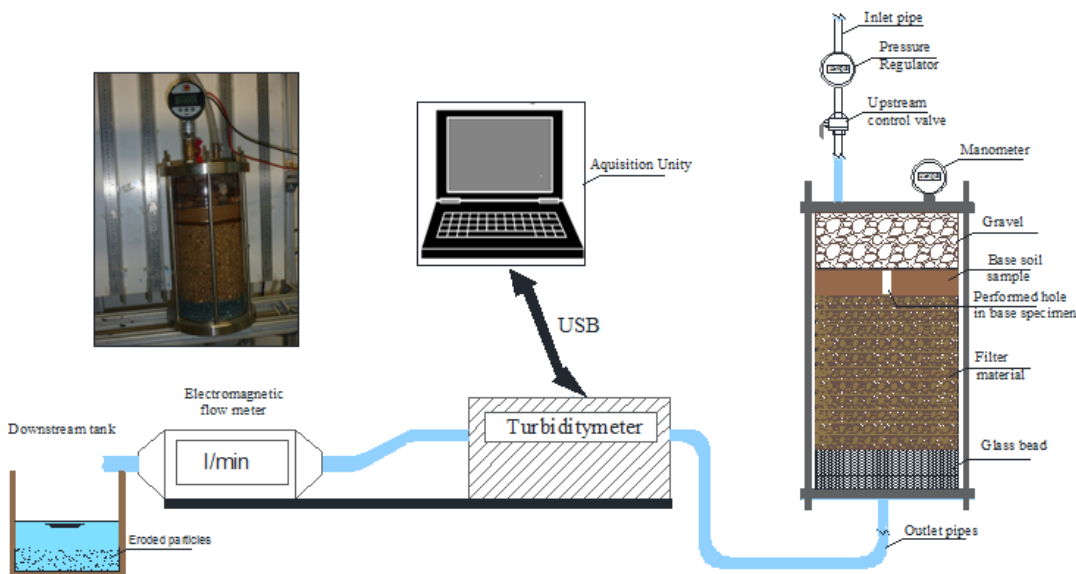


Figure 2. Schematic draw of the experimental set up

## 3 RESULTS AND COMMENTS

### 3.1 Base soil erodibility

The hole erosion test (without filter) performed on lean clays is devoted to investigate the erodibility of the soil and also to provide the boundary condition at the filter inlet for further test including a downstream filter. The test was carried out using three successive pressures (25, 50 and 75 kPa) and the eroded mass was measured after each pressure step. The results (Fig. 3) show that overall applied pressures the eroded mass increases; CL3 (Normandy lean clay) is the most resistant against erosion whereas CL2 (Namur lean clay) is the most prone to erosion. As regards to soil plasticity, Sherard et al.

(1985) reported that the base soil plasticity does not affect filtration, but Leonard's et al. (1991) concluded that for the investigated plasticity ( $13 < PI < 21$ ) the weathered clay shale with the lowest plasticity was the most susceptible to piping but plasticity had no apparent influence on the resistance to internal erosion. Recently, Delgado et al. (2012) reported that the base soil plasticity influences the boundary filter, but not as important as particle size distribution. In order to assess the effect of plasticity of tested base soils on their erodibility, the eroded mass after each applied step pressure is displayed (Fig. 4) as well as the pictures illustrating the enlargement of the hole after erosion test. The very plastic lean clay CL1 (PI=20), overall applied pressures, provides an eroded mass lower than that shown by the slightly plastic lean clay CL2 (PI=12), except for the pressure step of 25 kPa (starting test). Pictures of Fig. 3 illustrates this result. But CL3 even if less plastic exhibits a higher resistance against erosion than CL1. As regards to soil grading, CL3 shows a finer fraction of particles and wide gradation with coarsest particles, which lead to less detachability of the particles. As regards to dispersivity, the most dispersive soil (CL1) is not the most erodible, indicating that plasticity is not a key representative parameter for this kind of soils when investigating the susceptibility to internal erosion. The easy erosion obtained at the first pressure step can be explained by the saturation of the immediate ring close to the inner surface of the hole that makes the particles easily detachable, while following inner surface being not fully saturated is less prone to erosion.

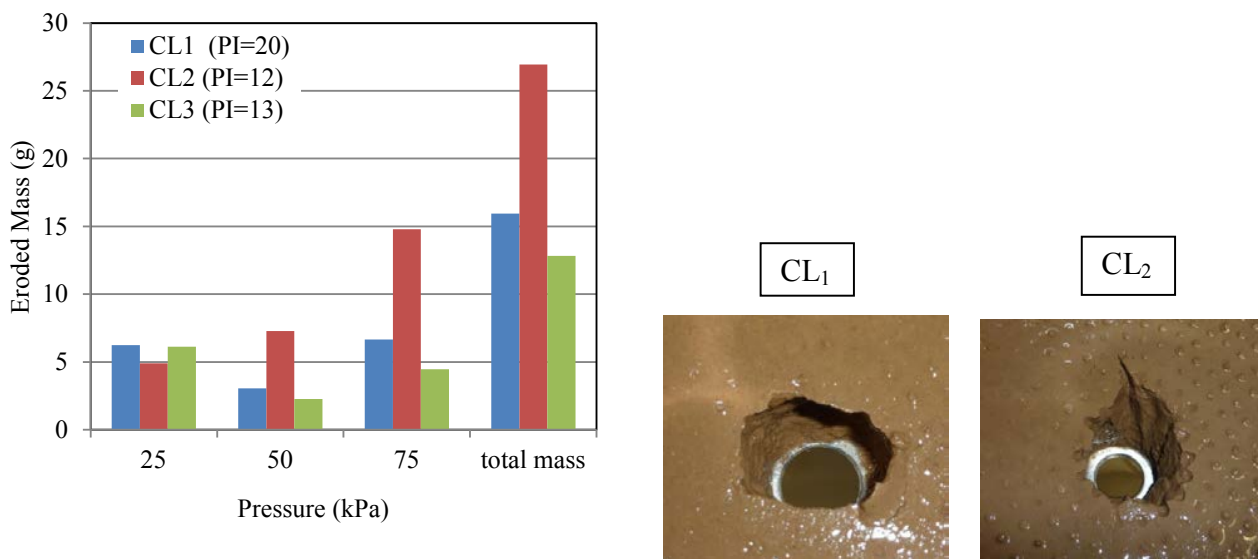


Figure 3. Soil erodibility versus applied pressure. Pictures of the hole enlargement after erosion for two soils.

### 3.2 Filter Retention

The filtration mechanism is easy to understand but difficult to quantify owing to the interaction between filter pore structure and particles to be filtered. Each porous medium has many pathways and there is uncertainty for determining the location where a particle settles. In order to address the efficiency of a filter, geometric (grading) and hydraulic requirements must be expressed through one parameter. Tien (2011) and El-Hedok et al. (1986) defined the filtration efficiency of a granular bed filter as the concentration ratio of the particle mass retained by the filter to the mass entering into the filter. Following this approach, we attempt to define the retention capacity of the filter as the mass ratio between filtered particles and injected ones. Since the hole erosion test without filtration (the sample placed in the same conditions as the case of the presence of filter) provides the eroded mass for each hydraulic load  $M_{in}$ , this latter becomes the injected mass when testing the filter (erosion-filtration test) in the same hydraulic conditions. The cumulated eroded dry mass  $M_e$  exiting from the filter is obtained

from the time integration of the product of particle concentration and flow rate, and can provide the retained mass  $M_r = M_{in} - M_e$ . The retention capacity  $R_r$  of the filter can be expressed by equation 1:

$$R_r(\%) = \left( \frac{M_r}{M_e + M_r} \right) \times 100 \quad (1)$$

The retention capacity is computed for many combinations of filter-base soil at each applied hydraulic load (Table.4). The results indicate that the retention capacity for different combinations increases with applied pressure. As assessed previously, the eroded mass from base soil broadly increases with increasing pressure. Since the amount of particles involved at the filter inlet increases with increasing pressure (Fig. 5), greater is the inlet soil mass through the filter, more the retention capacity is higher, leading to likely clogging. For filter  $F_1$  the comparison of the retention capacity obtained with different base soils indicates that the ultimate retention capacity is more important for  $CL_2$  (98.77 %) than for  $CL_1$  (93.64 %). This result is related to the more important erodibility of  $CL_2$  as discussed previously. As regards to the filtration of  $CL_2$  through filters  $F_1$  and  $F_3$  (98.77% and 86.23% of retention capacity respectively) the result can be related to the pore size distribution of the filter  $F_3$  which provides large void volume leading to a low particle retention. Despite its wide gradation with large particles base soil  $CL_3$  provides the lowest retention capacity in both filters  $F_1$  and  $F_3$ . However, when examining the grading of the two base soils  $CL_2$  and  $CL_3$ , one can note that  $CL_3$  contains more fines than  $CL_2$  (75% of fines), allowing less particle retention. If comparing the two filters with different grain shape (angular for  $F_1$  and rounded for  $F_2$ ), the retention capacity is obviously lower for both tested soils with the filter involving rounded grain shape (filter  $F_2$ ) which offers easy transfer of particles with few narrow flow paths. Despite the large voids involved in filter  $F_3$  the retention capacity with soil  $CL_3$  is higher than that of filter  $F_1$ . Since the capacity retention is evaluated from estimated inlet mass (assumed to be that obtained by hole erosion test), the combination of soil erosion with a downstream filter leads to an interface behavior which can change the filter boundary. In the case of filter  $F_1$  the likely increase of pressure at the soil-filter interface provides more erosion which tends to minimize the capacity retention as defined by equation 1. This result is corroborated by permeability measurements reported in further section. As regards to required rules of filter design, filter  $F_3$  tested with soil  $CL_3$  does not meet the no-erosion boundary condition ( $D_{15}/d_{85} < 9$ ) suggested by Foster and Fell (2001), whereas this criterion is met with filter  $F_1$  even if the capacity retention is also low.

Table 3. Retention capacity (%) of the different filters operating with different base soils

Filter	F <sub>1</sub>			F <sub>2</sub>		F <sub>3</sub>		
	CL <sub>1</sub>	CL <sub>2</sub>	CL <sub>3</sub>	CL <sub>1</sub>	CL <sub>2</sub>	CL <sub>2</sub>	CL <sub>3</sub>	
P(kPa)	25	93.44	96.09	32.71	81.21	91.16	71.77	35.86
	50	92.11	97.79	25.02	85.58	92.15	77.87	45.43
	75	93.64	98.77	44.08	90.66	95.35	86.23	62.26

### 3.3 Porosity reduction and particle size selection

The filtration is the process through which particles are trapped within filter pores, leading to porosity reduction. An indirect parameter allowing the evaluation of particle retention (filtration) is the hydraulic conductivity which can be directly measured. In order to evaluate the porosity reduction during filtration, the Kozeny correlation between hydraulic conductivity and filter porosity is used (Equation2).

$$k = k_0 \frac{n^3 (1 - n_0)^2}{n_0^3 (1 - n)^2} \quad (2)$$

With:

$k_0$ : the initial hydraulic conductivity of the filter, m/s;

$k$ : the measured hydraulic conductivity, m/s;

$n_0$ : the initial porosity of the filter;

$n$ : the porosity corresponding to the hydraulic conductivity  $k$ ;

Table 5 below shows computed results of the porosity variation for different filters from initial value  $n_0$  and final one  $n_f$ . The higher porosity reduction is obtained in the filter  $F_1$  with the base soil  $CL_3$  owing to the strong permeability reduction measured, despite the low retention capacity. This behavior can be attributed to the cake formation because of the relative large particles flowing through narrow constrictions. The porosity reduction in filter  $F_1$  is more important with  $CL_2$  than with  $CL_1$  and corroborated by the high retention capacity of  $CL_2$  soil as assessed previously. The soil  $CL_2$  tested with filter  $F_2$  shows a slightly higher porosity reduction compared to the filter  $F_1$  even if its retention capacity reveals lower value. Such results indicate that retention capacity is a global parameter measured while the hydraulic conductivity (and so the porosity reduction deduced) includes local values influencing strongly the parameter evolution along the filter. In addition, the retention capacity is a relative parameter depending on inlet particles mass.

Table 4. Porosity reduction from different filters tested with different base soils

Filters		F <sub>1</sub>			F <sub>2</sub>		F <sub>3</sub>	
		CL <sub>1</sub>	CL <sub>2</sub>	CL <sub>3</sub>	CL <sub>1</sub>	CL <sub>2</sub>	CL <sub>2</sub>	CL <sub>3</sub>
Base Soil	$n_0$	0.43	0.43	0.43	0.36	0.36	0.43	0.43
	$n_f$	0.36	0.32	0.22	0.30	0.26	0.36	0.36
Damage index	$\Delta n / n_0$	0.16	0.25	0.49	0.16	0.27	0.16	0.16

During filtration, particle trapping depends on the relative size distribution of flowing particles and filter constrictions. In order to evaluate the extent of filter pores filling during filtration, a damage index is deduced as the ratio of filled voids and the available voids within the filter. Filter  $F_1$  when operating with soil  $CL_3$  is the most impacted by particle deposition since the damage index reaches a high value close to 0.5. The analysis of particle size distribution of retained (infiltrated) mass allows the identification of size trapped particles and also those crossing the filter and passing through constrictions. Fig. 5 shows the PSD of trapped particles of base soils  $CL_2$  and  $CL_3$  when filtered by filter  $F_1$ . If comparing these distributions with initial ones, a gap is noticed and the curves are translated toward the coarser sizes. The gap is more pronounced for  $CL_2$  indicating a strong granular selection (the mean diameter being doubled). But this retention is a result of successive accumulation of different particles and self-filtration. So, small particles (3  $\mu\text{m}$ ) are retained owing to constriction reduction and narrow pore throats, but also coarser particles may escape at the beginning of filtration process (clean filter bed). The analysis of the results shows that slightly plastic base soil ( $CL_2$ ) produced the deposition of a large number of particles compared to the very plastic soil ( $CL_1$ ) which is less erodible but dispersive. The size selection is more important with soil  $CL_2$  for which large particles are retained by the filter, whereas as light size selection was operated on soil  $CL_3$ . The damage coefficient being more important with soil  $CL_3$ , the accumulation of particles involving various sizes leads to a greater impact on filter filling. The particle size distributions of two soils (Fig. 1) provide an explication of such result since soil  $CL_3$  present a wide size distribution including larger particles.

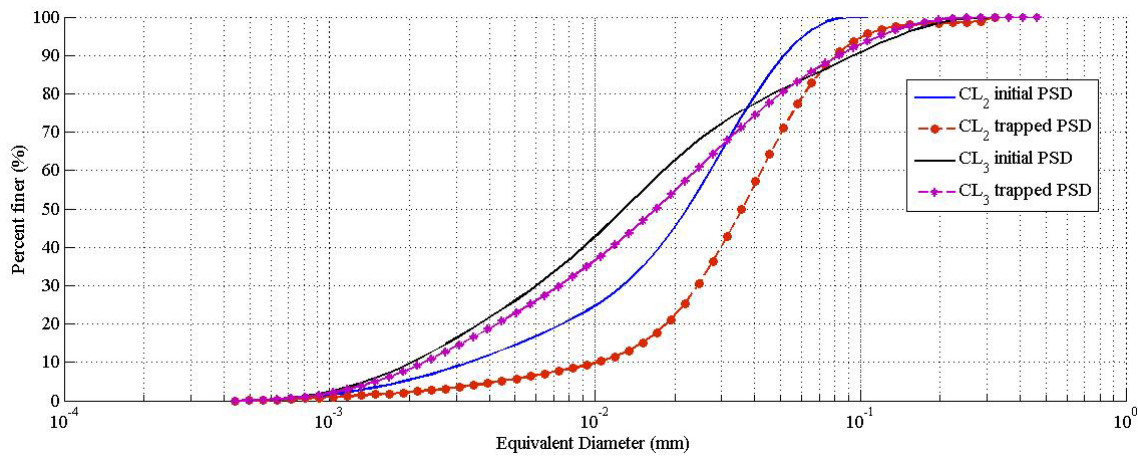


Figure 1. Particle Size Distributions of retained particles within filter  $F1$ .

## 4 CONCLUSIONS

An experimental study was performed in order to assess the filter design. Successive water pressures were applied through a combination of a base soil submitted to erosion and a downstream filter intended to protect it. Many filters and base soils have been selected to evaluate the damage caused by the cumulative trapped soil mass. The main purpose of these procedures is to assess the capability of a soil skeleton to retain moving particles transported by an internal fluid flow. The experimental results of this study allow concluding that:

- The analysis of the base soils erodibility (without downstream filter) indicates that plasticity is an important parameter in the consideration of erodibility rate of the base soil. The very plastic lean clay  $CL_1$  ( $PI=20$ ), overall applied pressures provides an eroded mass lower than that shown by the slightly plastic lean clay  $CL_2$  ( $PI=12$ ).
- The filter porosity reduction, due to particle retention, is deduced from the correlation with permeability measurements and a filter retention capacity was defined and measured at different hydraulic conditions including cumulative loading. The retention capacity, defined as the ratio of retained mass and inlet eroded mass, was found depending strongly on the grain size distribution and the erosion rate of base soil. The clogging occurrence in the filter was quantified and a geometrical parameter was defined as a damage index. Filter  $F_1$  when operating with soil  $CL_3$  is the most impacted by particle deposition since the damage index reaches a high value close to 0.5.
- The grading analysis of retained particles provides more quantitative data about the particle size selection. The results shows that slightly plastic base soil ( $CL_2$ ) produced the deposition of a large number of particles compared to the very plastic soil ( $CL_1$ ) which is less erodible but dispersive. The size selection is more important with soil  $CL_2$  for which large particles are retained by the filter, whereas as light size selection was operated on soil  $CL_3$ .

## REFERENCES

- ASTM D6572-00 (2000) *Standard Test Methods for Determining Dispersive Characteristics of Clayey Soils by the Crumb Test*. West Conshohocken, PA.
- ASTM D2487-11 (2011) *Standard Practice for Classification of Soils for Engineering Purposes (Unified Soil Classification System)*. West Conshohocken, PA.
- Benamar, A (2013), Clogging Issues Associated with Managed Aquifer Recharge Methods: Soil Clogging Phenomena In Vertical Flow. In: *IAH Commission on Managing Aquifer Recharge*, Australia, pp 77-83
- Correia Dos Santos, R N, Caldeira, M M S, Maranha Das Neves, E (2014), Experimental Study on Crack Filling by Upstream Fills in Dams. *Géotechnique* 65: 218-230.

- Delgado, R., Poyatos J.M., Osorio, F. (2012), Internal Erosion of Clayey Soils Protected by Granular Filters. *La Houille Blanche* 4-5: 42-47.
- El-Hedok, I., Whitmer, L., Brown, R.C. (2011), The Influence of Granular Flow Rate on the Performance of a Moving Bed Granular Filter. *Powder Technology* 214: 69-76.
- FHWA NHI-06-088 (2006) Federal Highway Administration US Department, Transportation. NHI I: 2-14
- Foster, M., Fell, R. (2001), Assessing Embankment Dam Filters that do not Satisfy Design Criteria. *J Geotech Geoenviron Eng* 127: 398-407.
- ICOLD (2015). Bulletin 164 Internal erosion of existing dams, levees and dikes, and their foundations, Volume 1: internal erosion processes and engineering assessment. [icold-cigb.org/bulletins](http://icold-cigb.org/bulletins).
- Leonards G., Huang A., Ramos J. (1991) Piping and Erosion Tests at Conner Run Dam. *J Geotech Eng* 108: 108-117.
- Locke M., Indraratna B., Adikari G. (2001) Time-Dependent Particle Transport through Granular Filters. *J Geotech Geoenviron Eng* 127: 521-528.
- Moffat R., Herrera P. (2015) Hydro-mechanical model for internal erosion and its relationship with the stress transmitted by the finer soil fraction. *ActaGeotech*10:643–650.
- Reboul, N. Vincens, E. Cambou, B. (2008). A statistical analysis of void size distribution in a simulated narrowly graded packing of spheres. *Granular Matter*, No. 10, 457–468.
- Reddi L.N., Xiao M., Malay G., Lee I.M. (2000) Permeability Reduction of Soil Filters Due to Physical Clogging. *J Geotech Geoenviron Eng* 126: 236-246.
- Reddi L.N., Park Y.J.L.A. (2002) Particle Transport Characteristics and Filtration of Granitic Residual Soils from the Korean Peninsula. *Can Geotech J* 39: 472-482.
- Reddi L.N., Xiao M., Hajra M.G., Lee I.M. (2005) Physical Clogging of Soil Filters Under Constant Flow Rate versus Constant Head. *Can Geotech J* 42: 804-811.
- Reiffsteck P. (2007) Evaluation of Erosion of Soil Used in Dykes and Earth Embankments which are subjected to Flood. In: Fell Fry (ed) *Internal Erosion Dam Foundations*. Taylor Francis Group. London.
- Sherard J.L., Dunnigan L.P. (1985) *Filter and Leakage Control in Embankment Dams*. Richard Volpe and William (ed). Kelly. California, pp 1-29.
- Tien Chi (1986) Effects of Particle Deposition on the Performance of Granular Filters. Fluid Filtration: Gas. In R Raber (ed), 1st edn. *American Society for Testing and Materials*. Philadelphia, pp 60-73.
- USBR (U.S Bureau of Reclamation) (2011) *Design Standard 13 Embankment Dams*, Chapter 5: Protective Filters. DS-13(5)-9: Phase 4.
- Vaughan P.R.M., Soares H.F. (1982) Design of Filters for Clay Cores of Dams. *J Geotech Eng Division* 108: 17-31.

## Development of a coaxial cell for porosity measurements during contact erosion experiments

T. Bittner, T. Bore, A. Scheuermann & M. Bajodek

*School of Civil Engineering, The University of Queensland, Australia*

K.J. Witt

*Bauhaus Universität Weimar, Germany*

**Abstract:** The rearrangement of soil particles during erosion, which is basically a transient mixing of base and filter particles, is accompanied by changes in porosity, leading to overall settlements which frequently can be severe for geotechnical structures such as levees. Therefore, not only the geometric and hydraulic boundary conditions, but also porosity changes are an important parameter that has to be observed during experiments. Classical approaches, like layer-wise analysis after the test, are usually not sufficient to allow any upscaling to technical dimensions. Furthermore, numerical approaches are under development allowing the computational modelling of hydro-mechanical problems in general. A decisive parameter governing both, hydraulic processes as well as the mechanical reaction, is the porosity. Former experiments have shown that Spatial TDR (Time Domain Reflectometry) is a promising technology for real time and spatial monitoring of porosity distributions. In order to use this measuring principle, an erosion experiment has to be designed and built to meet the requirements of this technique. The erosion cell itself serves additionally as the TDR-probe. Glass beads are used as an idealisation of a granular soil in order to minimise the effects of the grain angularity and different compositions of natural soils of varying sources, and thus allowing a high rate of repeatability. The data obtained in these experiments will help to get a better understanding about the progress of the erosion process and can be used for the calibration of numerical simulations.

Keywords: Contact erosion, porosity measurements, granular soils, Time Domain Reflectometry

### 1 INTRODUCTION

There are many geometric criteria regarding the onset of the internal erosion at the contact zone of two different soils, of which the best known is the one developed by Terzaghi (Fannin, 2008; Peck & Terzaghi, 1948). Additionally, hydraulic criteria were developed to meet the requirements of base/filter combinations that are beyond the specifications of the geometric criteria (Ziems 1969, Brauns et al. 1993). It has to be noted that all of this criteria are limited to the conditions under which they were developed, namely grain size distribution and the uniformity of the soils used or the boundary conditions of the equipment used (Sherard, Dunnigan, & Talbot, 1984). All these criteria have one important commonness: They are focussed on the onset, or, more precise, on the prevention of erosion, as this is an important part of geotechnical design (Schuler & Brauns, 1993). In some cases, a certain filtration length is accepted (Witt, 1993). But with that focus, the process beyond the onset of erosion is out of range.

In the case of geotechnical structures under construction which are under subject to hydraulic loading, it is the task of the engineer to develop a design which is safe against internal erosion. The difficulty is to meet this design requirements with the materials that are available.

With existing older structures or naturally built up soils, the situation is different. The geometrical design criteria are often not met in naturally layered soils and the numbers of failed earth-fill dams with poor or no control of erosion are considerable higher compared to those with a good control of erosion (Foster, Fell, & Spannagle, 2000).

As the initiation process within a structure is usually unnoticed, contact erosion can often only be detected after a certain progress, leading to changed flow characteristics or settlements that can pose a risk for the geotechnical structure. Therefore, it is mandatory to understand the mechanisms that induce and maintain the process of internal erosion. However, these mechanisms are not clearly understood (Bonelli, 2012).

The classical geometric and hydraulic filter criteria are more and more flanked by numerical models. The accuracy of these simulations is heavily dependent on the available data. Thus, experimental work is of great importance to get a better insight into the erosion process and to determine specific data required to calibrate numerical simulations.

An integrated approach of both, micro scale of the grains and pores and macro scale of the whole soil layers, is necessary to obtain a better insight. On the micro scale, recent studies showed that the porosity and the shapes and connections of the pores have a significant influence on the hydraulic conditions and the distribution of the flow velocity in the pores (Beguin, Philippe, & Faure, 2012; Bonelli, 2012; Harshani, Galindo-Torres, & Scheuermann, 2017). Thus, it is important to monitor the spatial distribution of the porosity and its alteration during the erosion process, as the hydraulic and mechanical properties are coupled and interdependent.

Different methods have been used for the determination of the porosity so far. A classical approach is the determination of the washed out fine fraction (Ke & Takahashi, 2014; Rochim, Marot, Sibille, & Thao Le, 2017). However, this method does not allow conclusions of the spatial distribution during a test. It is only possible to examine the soil sample layer-wise after the experiment or, as an extension, the monitoring of changes of the layer heights during the test (Ke & Takahashi, 2012). Depending on the experimental setup, conclusions of local changes of the porosity are feasible, but are limited to sections which can be monitored visually.

In order to determine porosity profiles of a sample before, during and after an erosion test, Sibille, Marot, and Sail (2015) utilised a gamma ray source and a scintillation counter. The drawback of this method, along with the hazard of radiation, is that the porosity can only be determined layer by layer.

Soil can be seen as a mixture of three different phases. An approach which takes advantage of the different dielectric permittivity of the solid, liquid and gaseous phases is based on high frequency electromagnetic methods such as TDR (Time Domain Reflectometry). The possibility to detect changes in one of the phases in a porous medium is premised on their dielectric contrast (Robinson, 2004). TDR has been successfully used to determine the water content and the density of soils (Drnevich, Ashmawy, Yu, & Sallam, 2005) and for the measurement of spatial porosity distribution along a rod probe (Scheuermann, Muehlhaus, Bittner, & Bieberstein, 2012).

In this paper, a newly developed experimental setup is introduced, which is designed to perform erosion tests in an optimised setting for electromagnetic measurement techniques. With this device, it is possible to determine the porosity profile along the soil sample in real time.

## 2 SPATIAL TDR

Considering soil as a porous media composed of solid, liquid and gaseous phases, it is obvious that the ratios of these fractions are subject to change during an erosion process or variations of the water content (drying, humidification). In various laboratory and field experiments, high frequency electromagnetic methods such as Time Domain Reflectometry (TDR) are currently used to assess water content and density. The measurement principle of TDR is based on the interactions of a high frequency electromagnetic field with the surrounding medium under test. The TDR-device, consisting of a pulse generator and an oscilloscope, emits a voltage step pulse via a coaxial cable into the probe built as a transmission line. At impedance discontinuities (e.g. the transition between cable and probe or sharp alterations of dimensions of the probe), the pulse is partly reflected. The remaining pulse travels further and is fully reflected at the end of the probe. The sum of the signals is shown by the TDR device's oscilloscope.

The first and second reflection in the TDR signal serve as an indicator for the beginning and the end of the probe. The travel time of the signal between the two reflections is dependent on the dielectric

permittivity of the medium under test and can be used easily to determine an average value of the porosity or water content by the tangent method (Huisman, Weerts, Heimovaara, & Bouten, 2002). A good approach for measuring moisture content and density using Time Domain Reflectometry (TDR) was developed in Siddiqui and Drnevich (1995) which was subsequently updated and further developed by Jung, Drnevich, and Abou Najm (2012).

However, there can be much more information found in a TDR signal than the travel time. Between the first and second main reflection, it contains a dielectric profile of the medium under test. The principle is to generate a permittivity profile out of the measured TDR signal. This is done by means of a simulation of the propagation of the TDR signal along the probe in the time domain using a numerical model (forward problem) based on the telegraph equations:

$$\left( L'(x)C'(x) \frac{\partial^2}{\partial t^2} + L'(x)G'(x) \frac{\partial}{\partial t} + \frac{1}{L'(x)} \frac{\partial L'(x)}{\partial x} \frac{\partial}{\partial x} - \frac{\partial^2}{\partial x^2} \right) V(x, t) = 0 \quad (1)$$

Both capacitance  $C'(x)$  and effective conductance  $G'(x)$  are influenced by the spatial distribution of the soils properties along the probe. The inductance  $L'(x)$  is not a function of the soil but of the transmission line (the probe) and can therefore be considered as a constant for a uniform geometry and a given probe.

For the simplified description of the wave propagation using the telegraph equations, some preconditions are to be met. This includes specific assumptions about the wave propagation itself as well as special requirements on the probe design. A more detailed description of probe design and wave propagation is given in (Huebner et al., 2005) and a comprehensive introduction of the inverse model in (Schlaeger, 2005).

TDR measurements can be made with one port in the reflection mode, which means the electromagnetic pulse can be fed only from one side into the probe, or with two ports in the transmission mode, where the measurements can be made from both ends of the probe. In the reflection mode, only the capacitance profile can be computed out of the TDR-signal, hence just one state parameter of the material under test can be detected, either the volumetric moisture content or the porosity. However, at fully saturated conditions, the volumetric water content can directly converted into changes in porosity (Scheuermann, 2012).

The setup presented here is limited to the reflection mode due to design reasons and the measurements are thus limited to porosity changes. As the erosion experiments are made on fully saturated samples in order to eliminate the permeability fluctuations of entrapped air, this means no restriction for the experimental setup. In this respect the use of glass beads with uniform dielectric permittivity as an idealisation of natural granular soils is further beneficial.

### 3 EXPERIMENTAL SETUP

#### 3.1 General setup

The general setup equals a constant head permeability test with an upwards directed flow and can be seen schematically in Figure 3.1. The hydraulic boundary conditions are defined by the potential, which is defined by an adjustable overflow upstream and a fixed overflow downstream of the column. The water circulation system consist of a 100 litre water reservoir, a submerged pump, a valve for the control of the flow rate, the adjustable constant head overflow tank upstream of the erosion cell, the erosion cell with the downstream overflow and finally a flow meter. A detailed description of the coaxial erosion cell and its development is given in section 4. In order to reduce the flow resistance at high flow rates and to avoid head losses, all connecting hoses have an inner diameter of 32 mm. Therefore, the flow meter is placed downstream of the erosion cell, as it acts as a constriction. The setup has been used previously for fluidisation experiments and has been changed to meet the requirements of the erosion test setup presented here (Bittner, Bore, Wagner, Karlovsek, & Scheuermann, 2016).

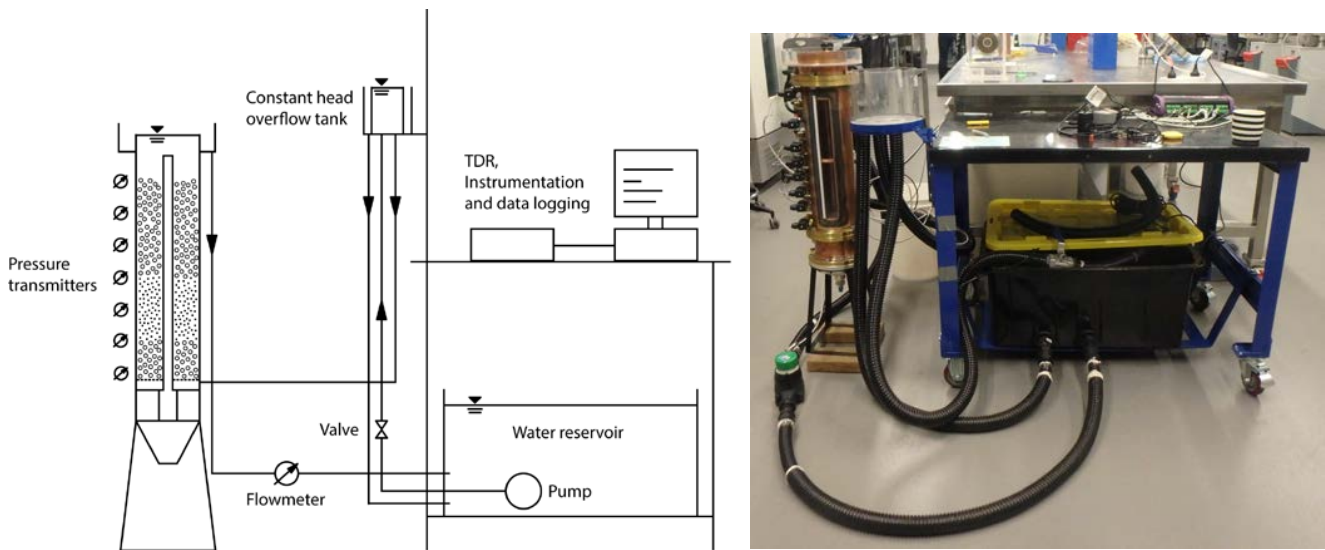


Figure 3.1. Schematic and photograph of the experimental setup with the coaxial erosion cell.

The vertical distribution of the hydraulic potential is measured with 14 pressure transmitters WIKA A-10. According to the data sheet of the manufacturer, they have an accuracy of 0.5 %. They are installed vertically in a distance of 25 mm to 50 mm in the side wall of the cell. The hydraulic gradient can be calculated out of the vertical distance and the difference of the hydraulic head. The flow rate is measured with a displacement flowmeter ManuFlo MES20-S-T. According to the data sheet, the accuracy is 1.5 % and the repeatability 0.3 %. The measurements of the hydraulic potential and the flow rate are automatically recorded every 10 s by a Data Taker Geologger DT85. With these two hydraulic parameters, a comprehensive analysis of the hydraulic behaviour of the soil during the erosion process can be made.

### 3.2 Materials

In the experimental setup presented here, beads of soda-lime glass are used as an idealisation of granular material instead of natural sand and gravel. With a density comparable to quartz based soil grains, glass beads offer the advantage of being free of influences like grain angularity and density variations which are typical for soils of different sources. Therefore, glass beads are a common replacement for erosion tests (Scheuermann et al., 2012; Sibille et al., 2015; Tomlinson & Vaid, 2000). The properties of the glass beads used in the tests presented here can be found in Table 1. The two fine fractions serve as base materials, the coarse fractions are used as filter.

Table 1. Properties of the glass beads used in the experiments

Diameter/Tolerance	Roundness	Colour	Grain density	Application
0.3 – 0.425 mm	≥ 70 %	Clear	25 kN/m <sup>3</sup>	Base II
0.425 – 0.6 mm	≥ 70 %	Red	25 kN/m <sup>3</sup>	Base I
2.0 mm ± 0.2 mm	90 %	Blue	25 kN/m <sup>3</sup>	Subbase filter
6.0 mm ± 0.3 mm	≥ 90 %	Clear	25 kN/m <sup>3</sup>	Filter D
8.0 mm ± 0.4 mm	≥ 90 %	Clear	25 kN/m <sup>3</sup>	Filter A

## **4 COAXIAL EROSION CELL**

### **4.1 Design**

In former experiments, a five-rod probe with a quasi-coaxial arrangement was inserted into an erosion cell (Scheuermann et al., 2012). As a drawback of this device, the distribution of the electromagnetic field is not fixed to the boundaries of the cell.

To avoid this issue, the cell itself acts now as a probe for the electromagnetic measurements by using its metallic walls as a conductor for the electromagnetic field. Coaxial arrangements have been used for the dielectric characterisation of liquids (Kaatze & Feldman, 2005) and soils (Wagner et al., 2013). The soil samples are either prefabricated or prepared directly in the cell.

The novelty of the coaxial erosion cell presented here is that the main intention is to observe the spatial and temporal changes of the density condition of the material under test in the cell during the measurements. The force that induces these changes is the water flow, hence the cell has to be optimised for the electromagnetic measurements as well as for the required hydraulic boundary conditions.

Depending on the largest particle of the material under test, the dimension of the probe has to be designed accordingly to the Representative Elementary Volume (REV) (Robert, 1998). The useable frequency bandwidth is coupled with the dimensions of the cell. The larger the cell, the lower is the upper frequency. This is leading to a compromise in the design of the cell between the required dimensions and the achievable frequency range.

The cell is made of commercially available rigid line components produced by the company Spinner GmbH. The great advantage is that the cell is comparatively cost effective to assemble in a workshop. Especially readily available conical transitions between the cell and a cable as a connection to the TDR device can be used. The drawback is that only a limited range of dimensions is at choice. The cell can be seen in Figure 3.1.b on the left side of the table and in Figure 5.1 filled with glass beads during an experiment.

In order to control the initiation and the progress of the erosion process, an inspection window with a height of 420 mm and a width of 40 mm is mounted in the outer wall of the cell.

### **4.2 Calibration**

The inversion procedure will provide the apparent permittivity profile from the TDR waveform. The final step is the computation of the porosity profile. Two methods can be used here. The first consists of a specific material calibration. Previous measurement of apparent permittivity with known porosities were performed in order to derive an empirical equation. This can be done with tests of different glass beads mixtures with known porosities. Mixtures of different sizes are leading to low porosities (Scheuermann, 2012). High porosities can be achieved by fluidisation (Bittner et al., 2016). Alternatively, mixing rules (Sihvola, 1999) can be used for materials with known dielectric properties like glass beads and water to get a function of dielectric permittivity and porosity. The Bruggeman-Hanai-Sen (BHS) model has proven its applicability for saturated glass beads (Jung et al., 2012; Sen, Scala, & Cohen, 1981).

In this study, the BHS model is used, as the dielectric properties of the media under test are known. A material specific calibration should be taken into account, if particles of different shapes or dielectric permittivity are used, e.g. natural soils.

## **5 EROSION EXPERIMENTS**

### **5.1 Experimental procedure**

With the base and filter materials listed in Table 1, four base/filter combinations are possible, as the 2 mm beads are exclusively used as a subbase filter to keep the base material in place. In the preliminary

tests, three combinations were tested, Base I and Filter A as well as Base II in combination with Filter A and D. All combinations are geometrically unstable.

### 5.1.1 Hydraulic boundary conditions

An upwards directed flow was applied in all tests. Two different schemes of the hydraulic potential as a boundary condition were used. In the first scheme, the hydraulic potential was increased stepwise for 1 cm every 10 minutes until base and filter were fully mixed.

In the second scheme, the increase of the potential is coupled to the response of the erosion process. Until the erosion process has started, which was marked by the first movements of the base particles, the hydraulic potential was increased 1 cm every 5 minutes. After the onset of particle movement, the potential was kept constant until no further progress of the erosion process was noticeable. Then, the potential was again increased by 1 cm and so on until a complete mixing of the base particles with the filter was achieved.

### 5.1.2 Preparation

The glass beads were inserted layer-wise into the cell. Each layer consisted of beads of the same size, in other words, there were no mixtures of beads of different diameters during the setup. All beads were trickled dry into the cell which resulted in porosities between 0.36 and 0.40, regardless of the beads' diameter. The porosity of each layer was determined by means of the volume, calculated out of the layer height, and the dry mass.

Saturation of the fine base material was achieved through a concurrent increase of the water level during the setup. The water level was controlled in way that the top layer of the base particles was moist, but no free water surface was present. The capillary forces ensured a complete saturation, while entrained air was able to escape from the pores. This procedure turned out to work better than the previously used one, where the beads were trickled into the already water-filled column (Bittner et al., 2016).

## 5.2 Initial results

### 5.2.1 Hydraulic measurements

A good impression about the behaviour and the progress of the erosion process can be seen in the typical results of the preliminary experiments. For the illustration, the combination of Base II and Filter A according to Table 1 and the hydraulic boundary conditions of the second scheme was chosen. The setup of the experiments and the development of the erosion process can be seen in Figure 5.1. The initial height of the base was 8.5 cm and of the filter 17.5 cm.

It was assumed that the less permeable layers of the base material, consisting of comparatively small particles, and the developing mixture zone, characterised by a low porosity through mixing of particles of different sizes, rule the progress of erosion. This is confirmed by the records of the hydraulic potential along the cell (Figure 5.2). A degradation of the potential was found mainly in the named layers. After the onset of erosion, the gradient in the base layer remained nearly constant, whereas the further increased potential was degraded mainly in the developing mixture zone. It is apparent that the discharge remained nearly constant due to the decreasing permeability of the extending mixture zone. In other words, the extension of the mixture zone regulates the erosion process. In this special case, this leads to a kind of self-healing process for a given hydraulic head, which comes with the cost of having settlements of the filter.

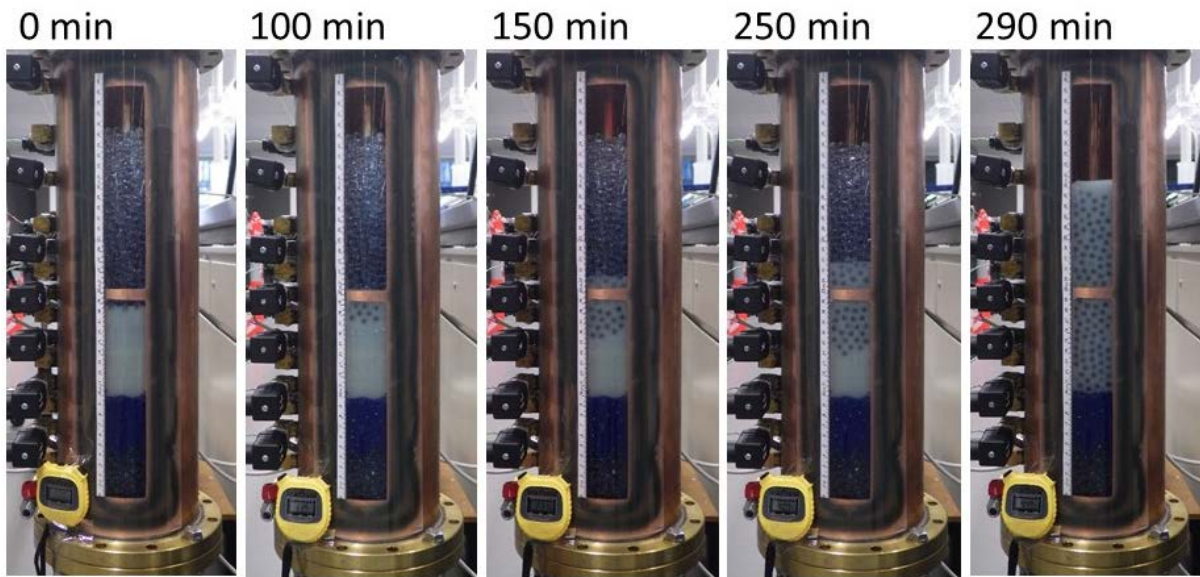


Figure 5.1. Development of the erosion process at different time steps. Note the settlements of the filter and the formation of the mixture zone.

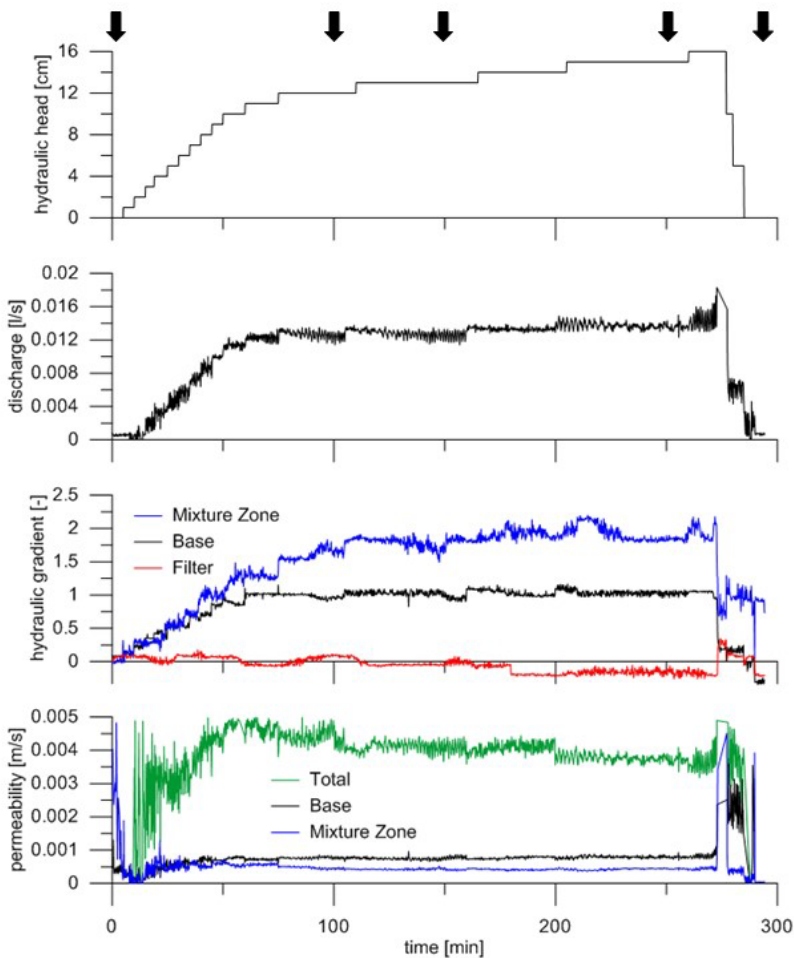


Figure 5.2. Hydraulic parameters. The arrows are showing the time matching to the pictures in Figure 5.1. Note that the peak values of discharge and permeability are cut off between minute 273 and 277, as they are out of the range of the graphs.

### 5.2.2 Porosity measurements

A comparison of the porosity profiles at different time steps can be seen in Figure 5.3. Before the onset of erosion, the porosity is nearly uniform over the full length of the column, as all layers consist of monodisperse glass beads. After the onset, the formation and elevation of a mixture zone can be seen, which is characterised by a lower porosity due to the mixing of different sized beads. The porosity of the mixture zone as a control of the TDR measurements was estimated by means of the visible changes in the layer heights monitored through the inspection window, which might be not the same for the overall area of the column. The fractions of base and filter above and below the mixture zone were regarded as unaffected by the mixing. That might not be the case for the filter, which experienced settlements. This leads to slightly lower porosities for the mixture zone than measured, as can be seen in Figure 5.3.

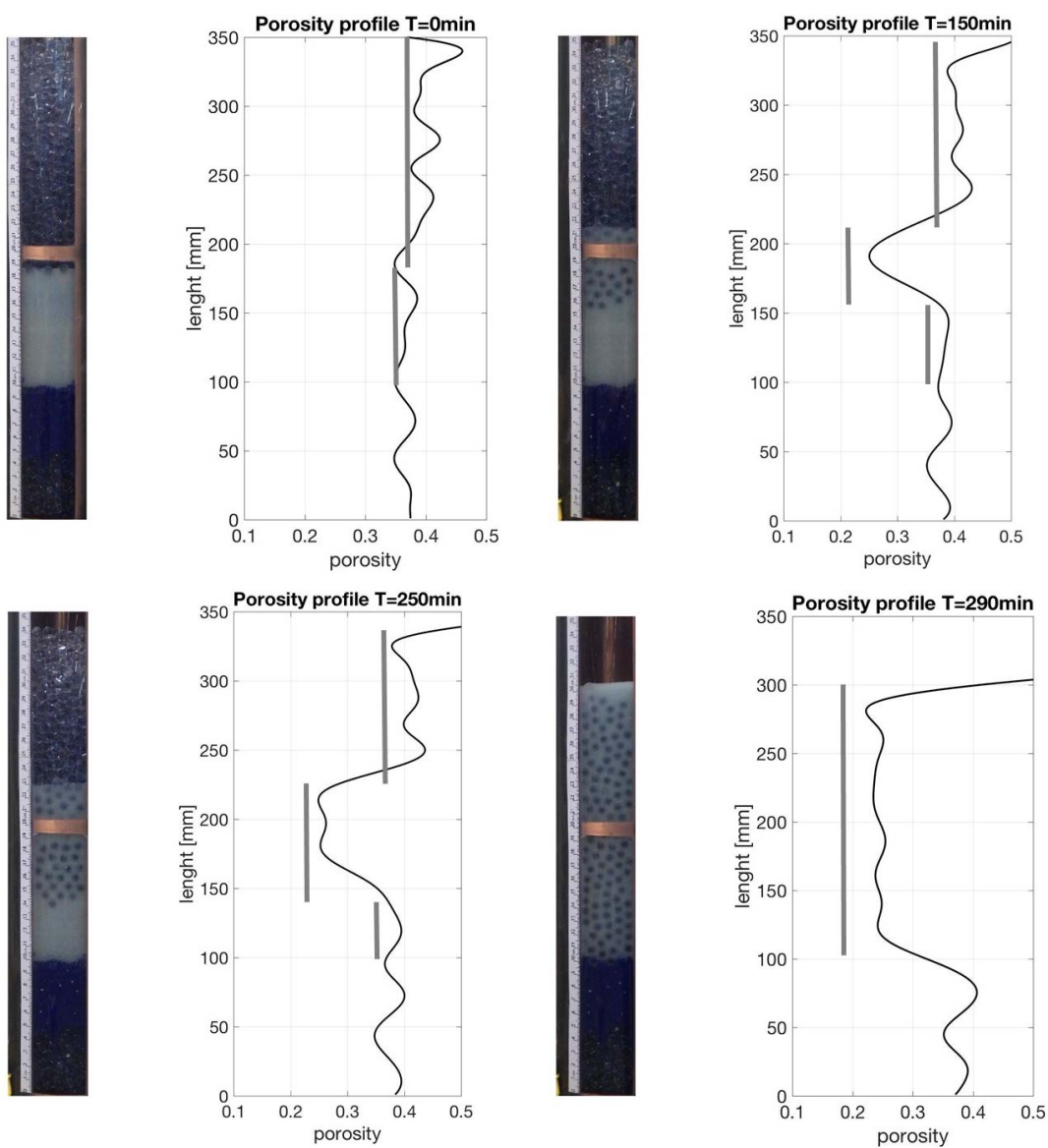


Figure 5.3. Comparison of the development of the mixture zone in the cell and the porosities determined by the layer heights with the porosity obtained with Spatial TDR. Note that both the boundaries of the mixture zone as well as the alterations in the overall height can be detected in the porosity profile with a resolution of approx. 2cm.

## 6 CONCLUSIONS AND OUTLOOK

A new type of cell for erosion experiments was developed which enables real-time measurements of the spatial porosity distributions by means of Spatial TDR, and preliminary experiments were carried out.

The contact zone of base and filter and the mixture zone are the determining factor for the onset and the progress of contact erosion. In the case of an upwards directed flow, a kind of self-healing behaviour can be noticed if settlements can be tolerated.

The work on the inversion of the TDR-signals is in progress. First results are showing the alterations in the porosity profile according to the progress of the erosion process and the formation of a mixture zone.

Due to the early stage, there is a need for repeated measurements in order to validate the data obtained so far. Special attention will be paid to the interface of base and filter. Additionally, further experiments are planned with added superimposed loads. This will allow studying the development of the base/filter combinations under extended boundary conditions.

## 7 ACKNOWLEDGEMENTS

This work was funded by the Discovery Project (DPI120102188), Hydraulic erosion of granular structures: Experiments and computational simulations, funded by the Australian Research Council and supported by a Queensland Science Fellowship awarded to A. Scheuermann.

The Professorship Geotechnics at the Bauhaus University Weimar supports this work by providing the opportunity of the use of a large scale erosion cell for future experiments.

## REFERENCES

- Beguin, R., Philippe, P., & Faure, Y.-H. (2012). Pore-scale flow measurements at the interface between a sandy layer and a model porous medium: Application to statistical modeling of contact erosion. *Journal of Hydraulic Engineering*, 139(1), 1-11.
- Bittner, T., Bore, T., Wagner, N., Karlovsek, J., & Scheuermann, A. (2016). Experimental investigation of the dielectric properties of soil under hydraulic loading. *Measurement Science and Technology*.
- Bonelli, S. (2012). *Erosion of geomaterials*: John Wiley & Sons.
- Drnevich, V. P., Ashmawy, A. K., Yu, X., & Sallam, A. M. (2005). Time domain reflectometry for water content and density of soils: study of soil-dependent calibration constants. *Canadian Geotechnical Journal*, 42(4), 1053-1065. doi: 10.1139/t05-047
- Fannin, J. (2008). Karl Terzaghi: from theory to practice in geotechnical filter design. *Journal of geotechnical and geoenvironmental engineering*, 134(3), 267-276.
- Foster, M., Fell, R., & Spannagle, M. (2000). The statistics of embankment dam failures and accidents. *Canadian Geotechnical Journal*, 37(5), 1000-1024.
- Harshani, H., Galindo-Torres, S., & Scheuermann, A. (2017). Pore scale measurements for onset of contact erosion. *Journal of Computers and Geotechnics*, submitted.
- Huebner, C., Schlaeger, S., Becker, R., Scheuermann, A., Brandelik, A., Schaedel, W., & Schuhmann, R. (2005). Advanced measurement methods in time domain reflectometry for soil moisture determination. *Electromagnetic Aquametry* (pp. 317-347): Springer.
- Huisman, J., Weerts, A., Heimovaara, T., & Bouten, W. (2002). Comparison of travel time analysis and inverse modeling for soil water content determination with time domain reflectometry. *Water resources research*, 38(6).
- Jung, S., Drnevich, V. P., & Abou Najm, M. R. (2012). New methodology for density and water content by time domain reflectometry. *Journal of geotechnical and geoenvironmental engineering*, 139(5), 659-670.
- Kaatze, U., & Feldman, Y. (2005). Broadband dielectric spectrometry of liquids and biosystems. *Measurement Science and Technology*, 17(2), R17.
- Ke, L., & Takahashi, A. (2012). Strength reduction of cohesionless soil due to internal erosion induced by one-dimensional upward seepage flow. *Soils and Foundations*, 52(4), 698-711.

- Ke, L., & Takahashi, A. (2014). Triaxial erosion test for evaluation of mechanical consequences of internal erosion. *Geotechnical Testing Journal*, 37(2), 1-18.
- Peck, R. B., & Terzaghi, K. (1948). Soil mechanics in engineering practice.
- Robert, A. (1998). Dielectric permittivity of concrete between 50 MHz and 1 GHz and GPR measurements for building materials evaluation. *Journal of Applied Geophysics*, 40(1), 89-94.
- Robinson, D. (2004). Measurement of the solid dielectric permittivity of clay minerals and granular samples using a time domain reflectometry immersion method. *Vadose Zone Journal*, 3(2), 705-713.
- Rochim, A., Marot, D., Sibille, L., & Thao Le, V. (2017). Effects of Hydraulic Loading History on Suffusion Susceptibility of Cohesionless Soils. *Journal of geotechnical and geoenvironmental engineering*, 04017025.
- Scheuermann, A. (2012). Determination of porosity distributions of water saturated granular media using Spatial Time Domain Reflectometry (Spatial TDR). *Geotechnical Testing Journal*, 35(3), 441-450.
- Scheuermann, A., Muehlhaus, H.-B., Bittner, T., & Bieberstein, A. (2012). Measurement of porosity distributions during erosion experiments using spatial time domain reflectometry (spatial tdr). Paper presented at the 6th *International Conference on Scour and Erosion (ICSE-6)*.
- Schlaeger, S. (2005). A fast TDR-inversion technique for the reconstruction of spatial soil moisture content. *Hydrology and Earth system sciences discussions*, 9(5), 481-492.
- Schuler, U., & Brauns, J. (1993). Behaviour of coarse and well-graded filters. *Filters in Geotechnical and Hydraulic Engineering*, 3-18.
- Sen, P., Scala, C., & Cohen, M. (1981). A self-similar model for sedimentary rocks with application to the dielectric constant of fused glass beads. *Geophysics*, 46(5), 781-795.
- Sherard, J.L., Dunnigan, L.P., & Talbot, J.R. (1984). Basic properties of sand and gravel filters. *Journal of Geotechnical Engineering*, 110(6), 684-700.
- Sibille, L., Marot, D., & Sail, Y. (2015). A description of internal erosion by suffusion and induced settlements on cohesionless granular matter. *Acta Geotechnica*, 10(6), 735-748.
- Siddiqui, S.I., & Drnevich, V.P. (1995). Use of Time Domain Reflectometry for Determination of Water Content and Density of Soil.
- Sihvola, A.H. (1999). *Electromagnetic mixing formulas and applications*: Iet.
- Tomlinson, S.S., & Vaid, Y. (2000). Seepage forces and confining pressure effects on piping erosion. *Canadian Geotechnical Journal*, 37(1), 1-13.
- Wagner, N., Bore, T., Robinet, J.C., Coelho, D., Taillade, F., & Delepine-Lesoille, S. (2013). Dielectric relaxation behavior of Callovo-Oxfordian clay rock: A hydraulic-mechanical-electromagnetic coupling approach. *Journal of Geophysical Research: Solid Earth*, 118(9), 4729-4744.
- Witt, K. (1993). Reliability study of granular filters. *Filters in Geotechnical and Hydraulic Engineering*, 35-42.

## Erosion behaviour of gap-graded soils due to upward flow

R. Correia dos Santos & L. Caldeira

*Laboratório Nacional de Engenharia Civil*

E. Maranhã das Neves

*Instituto Superior Técnico*

**Abstract:** A laboratory study aiming at the evaluation of the suffusion behaviour of coarse gap-graded soils is presented. Six granular gap-graded soils missing the medium-to-coarse sand fraction have been examined. Four soils have no fines, one has 5% of non-plastic fines, and one has 5% of clayey fines (with plasticity index of about 14%). The use of available methods to assess internal stability of soils suggests that the majority of the selected soils are susceptible to suffusion. Testing has been carried out in the Upward Flow (UF) seepage test. A cylindrical seepage cell is used to impose vertical flow, from the bottom to the top, along a soil specimen with 200 mm-diameter and 150 mm-thick. During an UF test, the hydraulic gradient in the specimen is slowly increased in steps. The observation of the erosion behaviour at the top surface of specimen, together with the evolution of the discharge flow rate, allows determining the hydraulic gradients causing initiation of erosion on top of the specimen and development of suffusion in the soil. Some tests have been conducted with a low friction sheet placed in the inner surface of the test cell, to evaluate the influence of the cell wall roughness in the soil erosion behaviour. A 'sand boiling' phenomenon has been observed in soils exhibiting suffusion, resulting in the deposition of the finer particles at the specimen surface. Laboratory testing on soils with no fines clearly shows that the higher the fine sand content the higher the amount of material deposited on the specimen top, but the gradients associated to initiation of suffusion and development of 'sand boiling' also increase. Whenever high hydraulic gradients are not likely to occur, the gap-graded soil with 5% of plastic fines should be more resistant to initiation and development of suffusion than the gap-graded soil with 5% of clayey fines.

Keywords: Internal erosion, suffusion, gap-graded soils, upward seepage tests, internal stability

### 1 INTRODUCTION

Gap-graded soils are usually very susceptible to suffusion. Suffusion occurs when the fine particles are removed through the constrictions between the larger particles by seepage flow, leaving behind an intact matrix of coarser particles. The scope of this study is to experimentally evaluate the susceptibility to suffusion of gap-graded soils, missing the medium-to-coarse sand fraction, likely present in the foundation of embankment dams and dikes. Six soil mixtures are tested. In particular, 4 gap-graded soils with no fines formed by blending different proportions of sand and gravel, and 2 gap-graded soils with 5% of fines formed by adding to soil mixture also non-plastic fines or clayey fines.

Upward Flow seepage tests have been performed to study the hydraulic gradients causing initiation and development of suffusion, and to evaluate the evolution of permeability with the progress of the erosion process. The test cell is has a cylindrical mould, and the direction of water flow is vertical from the bottom upward. Hydraulic gradient across a test specimen is steadily increased by raising slowly in steps the level of a water supply tank. In initial tests, an aluminium ring has been placed on the top of the specimen, to avoid parasitic flow paths between the mould and the soil. To evaluate the influence of the upper aluminium ring, and of the roughness of the inner surface of the mould, additional tests have been conducted on one soil. In particular, these additional tests have been performed without the upper ring, and, in some, the inner surface of the mould was lined with a Teflon® sheet.

The gradients at which erosion started and developed are presented, and the critical soil parameters influencing those gradients are indicated.

## 2 MATERIALS AND METHODS

### 2.1 Tested soils

Figure 2.1 shows the grain-size distribution curves of the six gap-graded soils tested. Table 1 shows the main properties of the six soils tested. As example, Figure 2.2 shows one of the soils tested, prior and after being mixed thoroughly with an amount of water to achieve a water content of about 7%.

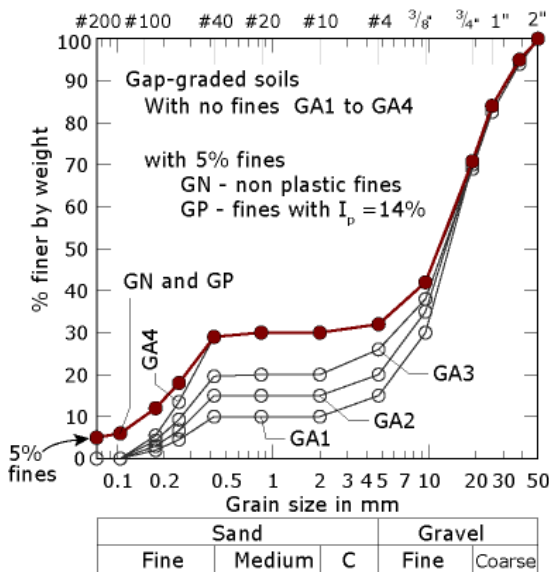


Figure 2.1. Grain-size distribution curves of gap-graded soils (Correia dos Santos, 2014).

Figure 2.2. Aspect of soil GN: soil fractions (up), and soil mixed with water (down) (Correia dos Santos, 2014).

Table 1. Main properties of gap-graded soils tested

soils	Soil fractions			Plasticity		Coefficients		Soil classification ASTM D2487	ASTM D854 <i>G</i>	Standard density tests ASTM D4254 and ASTM D4253	
	<i>pf</i> <sub>200</sub> %	<i>pc</i> <sub>4</sub> %	<i>p</i> <sub>sand</sub> %	<i>w</i> <sub>L</sub> %	<i>PI</i> %	<i>C</i> <sub>u</sub>	<i>C</i> <sub>c</sub>			$\gamma_{d,min}$ kN/m <sup>3</sup>	$\gamma_{d,max}$ kN/m <sup>3</sup>
GA1	0	85	10	–	–	8.6	2.6	GW	2.72	15.2	18.1
GA2	0	80	15	–	–	59	14	GP	2.72	16.6	18.7
GA3	0	74	20	–	–	66	10	GP	2.72	17.3	19.6
GA4	0	68	30	–	–	69	0.4	GP	2.72	17.6	20.0
GN	5	68	25	NP	NP	90	0.3	GP-GM	2.72	17.7	20.2
GP	5	68	25	38	14	90	0.3	GP-GC	2.72	17.6	20.1

*pf*<sub>200</sub> = Mass fraction, in percentage, of soil particle finer than 0.075 mm (No. 200 sieve). *pc*<sub>4</sub> = Mass fraction, in percentage, of soil particles coarser than 4.75 mm (No. 4 sieve). *p*<sub>sand</sub> = % of fine sand. *G* = Specific gravity,  $\gamma_{d,min}$  e  $\gamma_{d,max}$  = minimum and maximum dry unit weight, respectively.

Soils GA1, GA2, GA3 and GA4 are gap-graded soils with no fines, and no medium sand size particles. They are formed by blending fine sand (silica) with a soil fraction coarser than No. 10 sieve (schist). Soils GA1, GA2, GA3 and GA4 are soil mixtures containing a content of fine sand, respectively, 10, 15, 20 and 30%. Soil fraction coarser than the No. 10 sieve is made mainly of fine to coarse gravel, with some coarse sand. Soils GN and GP are gap-graded soils with low fines content. These are obtained by mixing fine sand (silica), gravel (schist) and 5% of non-plastic or plastic fines, resulting in soils GN or GP, respectively.

## 2.2 Experimental setup

Figure 2.3 (a) shows a picture of the device used in the tests performed in this study. The test apparatus used is similar to those developed by Skempton and Brogan (1994) and by Wan and Fell (2004), which perform tests on samples with 300 mm diameter and 250 mm thick. The main differences of the developed cell are the smaller size of the cylindrical mould (200 mm–internal diameter) and the thinner test specimen (about 150 mm–thick). The test cell is composed mainly by a mould and a base, both of stainless steel.

In this test, the direction of water flow is vertical from the bottom upward. During the test, the top surface of the soil specimen is accessible to allow the visual observation of the erosion process. Hydraulic gradient across a test specimen is steadily increased with upward seepage. This is performed by raising slowly in steps the level of a water supply tank, which is connected at the bottom of the cell.

In order to evaluate the influence of the presence of the upper aluminium ring, and of the roughness of the inner surface of the mould, in the soil erosion behaviour, additional tests have been conducted on soil GA4. This soil was selected because it showed strong signs of internal instability for considerably higher gradients than the other gap-graded soils without fines. In particular, all these tests have been performed without the upper ring, and, in some, the inner surface of the mould was lined with a Teflon® sheet (PTFE – Polytetrafluoroethylene) (as shown in Figure 2.3 (b)). To avoid the passage of water between the mould and the Teflon® sheet the bottom and upper extremities were sealed using silicone.

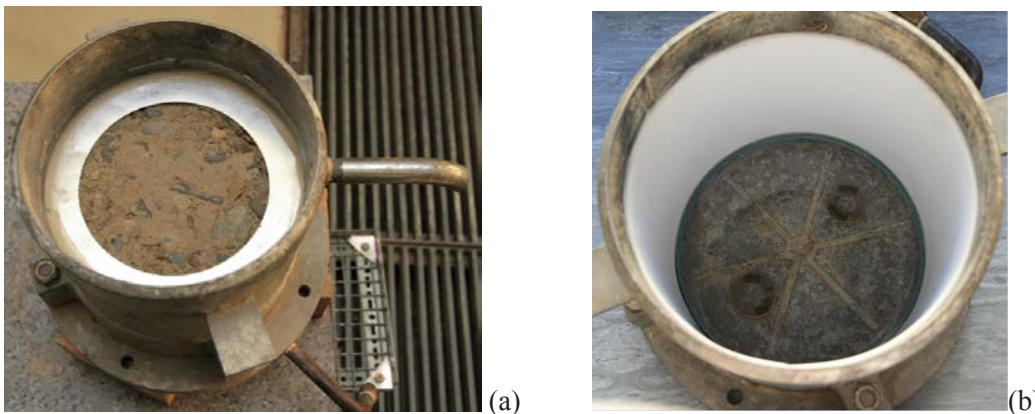


Figure 2.3. (a) Test cell with compacted specimen, (b) device with the inner surface of the mould lined with a Teflon® sheet

An overflow pipe placed at the top of seepage cell allows the estimation of the flow rate through the system, by measuring the volume of effluent collected within a specified period. In general, the flow rate was measured a few minutes after raising the water level in the inlet tank, when the discharge flow appears to be relatively steady, and immediately before the next total head increment.

## 2.3 Compaction characteristics

Table 2 presents the effective compaction characteristics of the specimens tested.

The specimens were compacted manually in three layers of about 50mm–thick using a standard Proctor compaction hammer. The dry density was controlled by selecting the total mass of dry soil to be compacted in each 50mm-thick layer. For each layer, a known amount of water was added to the previously selected mass. Then, the soil was mixed thoroughly and placed in a closed bag during at least 24 hours prior to compaction.

Specimens of soils with no fines were prepared with a water content of about 3.5%. Specimens of soils with 5% of fines were prepared at their standard optimum water content,  $w_{opt}$ . Specimens of gap-graded soils with 5% of fines were compacted at near 95% of the maximum dry unit weight of standard Proctor compaction tests. The ratio between the actual bulk density and the reference one obtained from density tests,  $D_r$ , is about 100%.

Table 2. Effective compaction characteristics of specimens tested

UF test	$w$ (%)	$\gamma_d$ (kN/m <sup>3</sup> )	Void ratio, $e$	Porosity, $n$ (%)	Relative density, $D_r$ (%) <sup>(1)</sup>	Compaction degree $\gamma_d/\gamma_{d,max}$ (%) <sup>(2)</sup>
<i>Tests on specimens compacted against the stainless steel mould and wherein the upper ring has been used</i>						
GA1	3.5	18.5	0.44	30.8	111	-
GA2	3.5	18.9	0.41	29.1	109	-
GA3	3.5	19.7	0.35	25.7	108	-
GA4	3.5	20.0	0.33	24.5	101	-
GN	6.9	20.2	0.32	24.2	100	95
GP	6.9	20.1	0.32	24.5	101	96
<i>Test on soil GA4 compacted against the stainless steel mould and without the upper ring</i>						
GA4.1	3.5	20.1	0.32	24.0	106	-
<i>Tests on soil GA4 compacted against the Teflon® sheet and without the upper ring</i>						
GA4.2	3.5	20.5	0.30	23.1	116	-
GA4.3	3.5	17.7	0.50	33.3	5	-

(1) Ratio between the actual bulk density and the reference one calculated using results from maximum and minimum density tests.

(2) In relation to the maximum dry unit weight given by standard Proctor compaction tests.

Specimens of gap-graded soils with no fines were prepared with the aim of being also compacted at relative densities,  $D_r$ , of 100%. However, for soils GA1, GA2 and GA3 the application of a compaction effort similar to the one used on soils GN and GP, resulted in layers somewhat thinner than 50 mm and, therefore, in relative densities slightly larger than 100%.

The specimens of the special tests GA4.1 and GA4.2 have been prepared also aiming a relative density of 100%, but ended up having higher densities,  $D_r = 106$  and 116%, respectively. The specimen of test GA4.3 has been intentionally prepared to a very low relative density ( $D_r = 5\%$ ), to evaluate the influence of the density of the specimen in the erosion behaviour of soil GA4.

### 3 INTERNAL STABILITY OF SOILS FROM AVAILABLE METHODS

The assessment of the susceptibility to internal instability of the gap-graded soils selected was performed accordingly with the predictive methods of Kenny and Lau (1985, 1986) and Burenkova (1993), and with the probabilistic method of Wan and Fell (2004, 2008). Detailed results of these analyses are presented in Correia dos Santos (2014). The results of those analyses show that all selected gap-graded soils are considered internally unstable by the Kenney and Lau method. The other methods suggest that soil GA1 is the only gap-graded material considered as internally stable.

## 4 RESULTS AND ANALYSIS

### 4.1 Presentation of test results

Typical plots of the results of a test are shown in Figure 4.1 and Figure 4.2. These plots are of the test GA4. In particular, Figure 4.1 shows the evolution of the measured flow rate,  $Q$ , as the hydraulic gradient,  $i = \Delta H/L$ , is steadily increased.  $\Delta H$  is the applied head loss, adjusted by raising the water level in the inlet tank, and  $L$  is the initial height of the sample. This plot also shows the maximum discharge capacity,  $Q_{max}$ , of the hydraulic system for the corresponding applied  $\Delta H$ , which was assessed prior of carrying out the tests. Figure 4.2 shows the variation of the average discharge velocity,  $v = Q/A$ , and the coefficient of permeability of the soil,  $k$ , with respect to  $i$ .  $k$  is an average value on the area of the sample, and is calculated considering the Darcy's law.  $A$  is the area of the cylindrical seepage cell. The value of  $k$  should remain practically constant as long as the position of soil particles remains unaltered. Figure 4.3 and Figure 4.4 summarize the results of tests performed with the upper ring, in terms, respectively, of the discharge velocity,  $v$ , and of the "apparent permeability",  $k$ , in relation to the applied gradient,  $i$ .

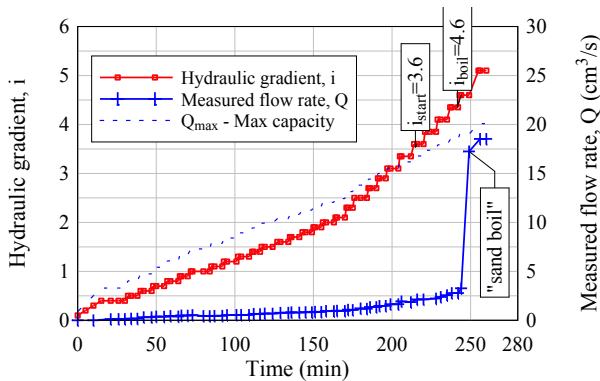


Figure 4.1 – Test on GA4. Evolution of discharge flow rate as the hydraulic gradient is steadily increased.

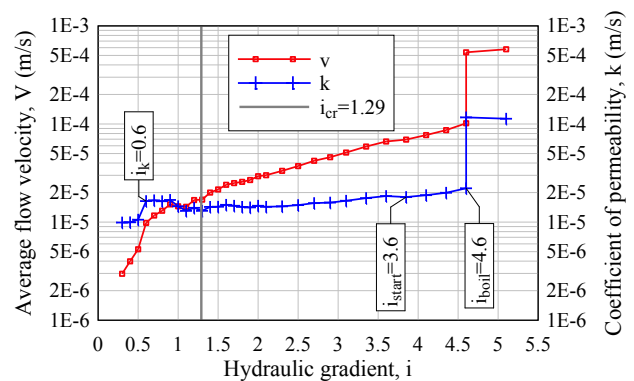


Figure 4.2 – Test on GA4. Velocity and coefficient of permeability versus applied hydraulic gradient.

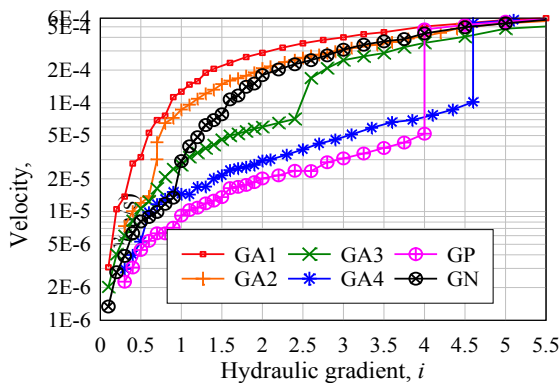


Figure 4.3 – Discharge velocity *versus* applied hydraulic gradient, in tests with the upper ring.

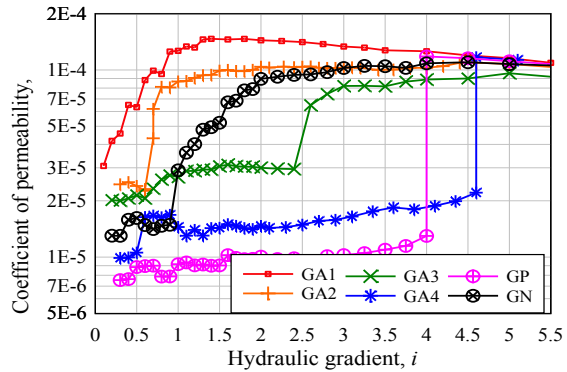


Figure 4.4 – Coefficient of permeability *versus* applied hydraulic gradient, in tests with the upper ring.

Figure 4.5 compares  $v$  and  $k$  against  $i$  in tests on soil GA4, in which the specimen has been compacted to relatively similar relative densities ( $D_r$  from 101 to 116%). This figure is useful when comparing the results of the tests using different boundary conditions. Figure 4.6 compares  $v$  and  $k$  against  $i$  in the two tests on soil GA4, in which the specimen has been compacted against the mould lined with a Teflon<sup>®</sup> sheet. This figure is useful to evaluate the influence of the relative density of the specimen in the soil erosion behaviour.

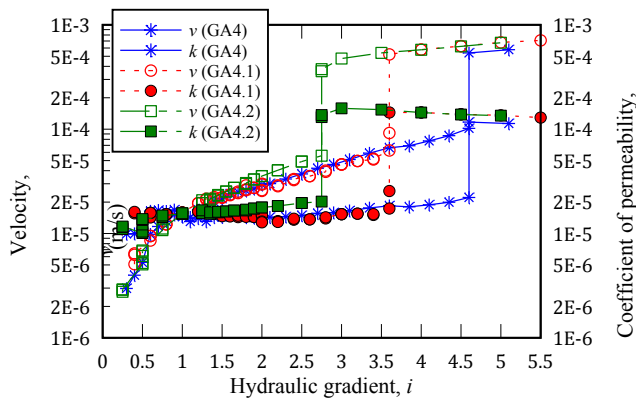


Figure 4.5. Velocity and permeability vs the applied gradient, in tests on soil GA4 with  $D_r > 100\%$ : comparison of tests with different boundary conditions.

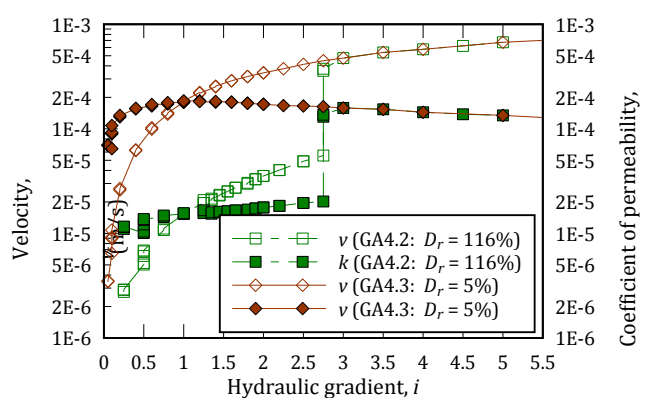


Figure 4.6. Velocity and permeability vs the applied gradient, in tests on soil GA4 using the Teflon<sup>®</sup> sheet: comparison of tests on specimens with different  $D_r$ .

## 4.2 Time lapse photos of tests

Figure 4.7 and Figure 4.8 show a series of photos for each test carried out with and without the upper ring, respectively. In particular, these photos show the top surface of specimens prior to soil submersion, and during and at the end of the tests.

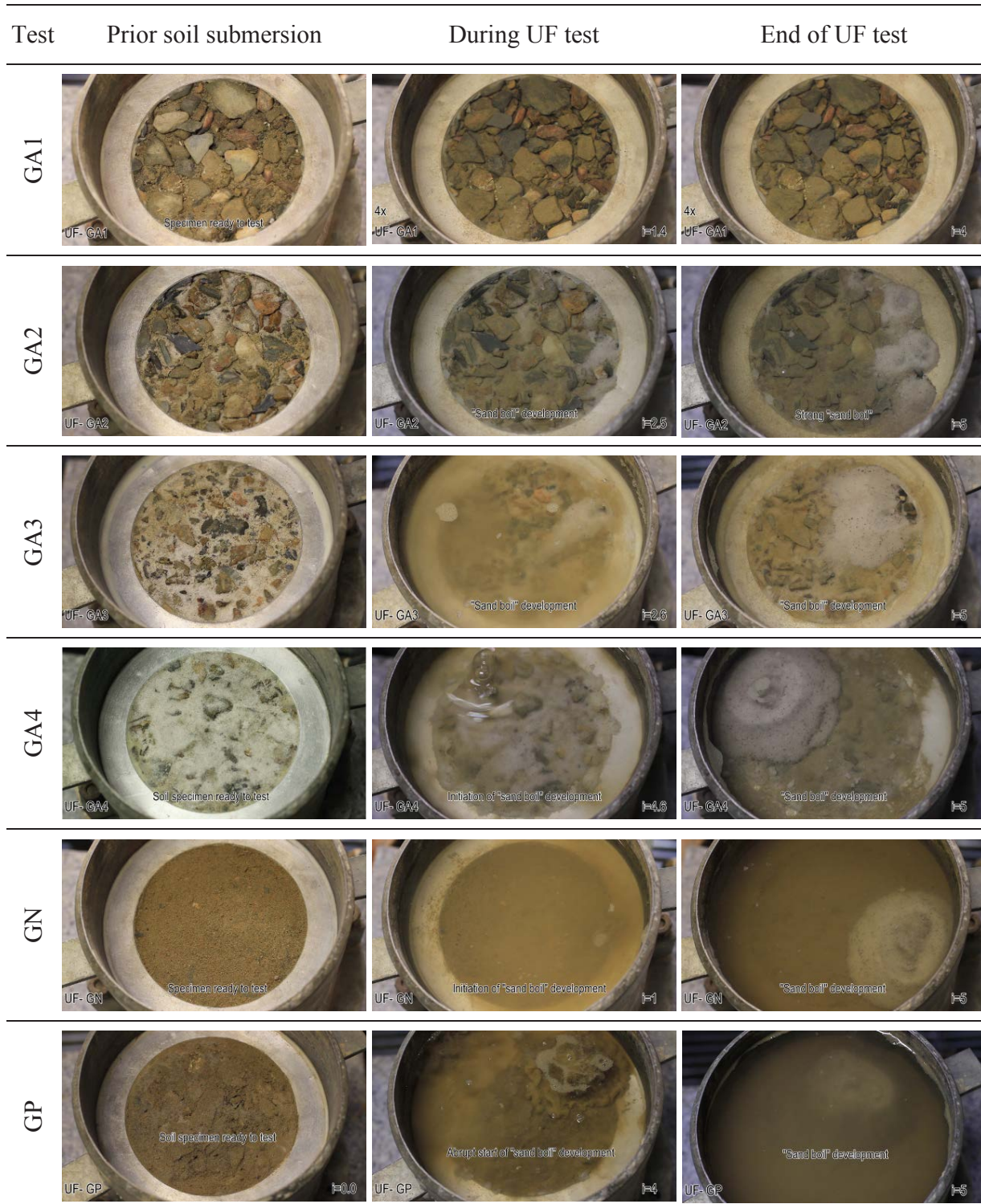


Figure 4.7. Photos of tests *with* the upper ring: after compaction of specimens, and during and at the end of test.

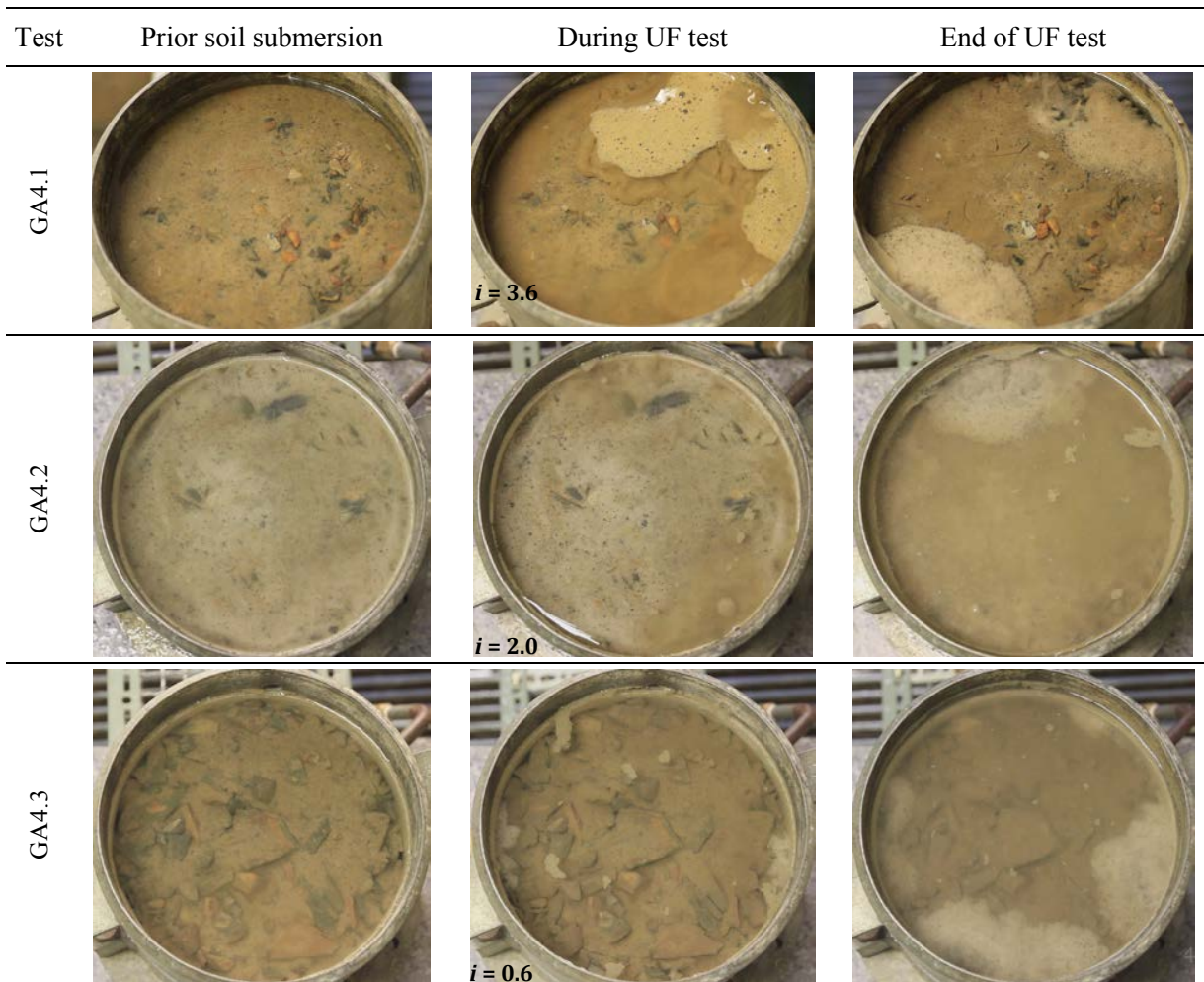


Figure 4.8. Photos of tests on soil GA4 *without* the upper ring: after compaction, during and at the end of tests.

Plots shows that soil GA1 is the only where evident signs of internal instability have not been observed visually for the level of hydraulic gradients applied. The discharge flow velocities in that test are the highest recorded, among the tests on specimens compacted to relative densities higher than 100%. Thus, one could be led to conclude that a limiting flow condition could have been reached, due to limited size of the inlet pipe of the test apparatus. However, the discharge velocities in the test on soil GA4 compacted to  $D_r = 6\%$  (test GA4.3) are much alike as those recorded in the test on soil GA1, and yet notable signs of erosion have been observed in that specimen and for very low hydraulic gradients. Soil GA1 and soil GA4 are the selected gap-graded soil mixtures, respectively, with the lowest and the highest content of the fraction most likely to be susceptible to erosion. This proves that the fine sand content in the samples is likely an important parameter in their suffusive behaviour.

All other specimens showed relevant signs of selective erosion of fine sand, and on soils GN and GP, of fines. The presence of ‘sand boils’ on the top surface of the specimens suggests selective erosion of fine sand particles. Extreme cloudiness of discharge water indicates the occurrence of selective erosion of fines.

### 4.3 Hydraulic gradients at which suffusion occurs

Table 3 summarizes the results of tests performed on the selected gap-graded soils. These include the information about the number and relative size of the ‘sand boil(s)’ formed in the top of the specimens in tests showing signs of suffusion, the critical hydraulic gradient,  $i_{cr}$ , and the observed gradients ( $i_k$ ,  $i_{start}$  and  $i_{boil}$ ).

Table 3. Summary of results from tests on gap-graded soils.

UF test	Test specimen characteristics			Formation of 'sand boil(s)'	$i_{cr}$	Estimated gradients		
	$\gamma_d$ (kN/m <sup>3</sup> )	$D_r$ (%)	$n$			$i_k$	$i_{start}$	$i_{boil}$
<i>Tests with upper ring and stainless steel mould</i>								
GA1	18.5	111	0.31	None	1.19	0.2	NA	NA
GA2	18.9	109	0.29	Yes (multiple but small)	1.22	0.7	1.2	1.5
GA3	19.8	108	0.26	Yes (one medium)	1.27	0.7	1.7	2.6
GA4	20.0	101	0.26	Yes (one large suddenly)	1.29	0.6	3.6	4.6
GN	20.2	100	0.24	Yes (one large)	1.30	0.4	0.9	1.0
GP	20.1	101	0.25	Yes (one large suddenly)	1.30	0.5	2.0	4.0
<i>Special tests without the upper ring</i>								
GA4.1	20.1	106	0.24	Yes (two large)	1.30	0.6	3.6	3.6
GA4.2	20.5	116	0.23	Yes (one large suddenly)	1.31	0.5	1.8	2.75
GA4.3	17.7	105	0.33	Yes (multiple but smaller)	1.14	0.1	0.4	0.8

In the majority of the tests carried out on the gap-graded soils, three different levels of vertical hydraulic gradients were observed, which are labelled as  $i_k$ ,  $i_{start}$  and  $i_{boil}$ .

The first gradient,  $i_k$ , is associated with the onset of the movement of soil particles inside the test specimen, resulting in a progressive slow increase of the coefficient of permeability of the soil. This stage corresponds to an internal adjustment of the finer fraction more susceptible to suffusion, but there are no observable signs of erosion on the top surface of the test specimen.  $i_k$  is defined by the point in the curve  $i \sim k$  showing the start of a trend for progressive slow increase of  $k$ . The second gradient,  $i_{start}$ , corresponds to the start of erosion of fine particles indicated by the cloudiness of the flow, in soils with fines, or by the visual observation of the movement of particles on the top surface of the specimen. This stage does not necessarily occur together with a sudden increase of the discharge flow rate. The third gradient,  $i_{boil}$ , is associated to more severe erosion indicated by violent agitation of fine sand particles ('sand boiling' condition), which results in many cases in a sudden increase in the discharge flow rate. In some tests it may be perceptible as an increase of the total volume of the specimen.

#### 4.4 Experimental results versus critical hydraulic gradient

Critical gradient,  $i_{cr}$ , of tested specimens ranges between 1.19 and 1.30.  $i_{cr}$  is lower, for a given  $e$ , the coarser the specimen. In all tests,  $i_k$  is considerably lower than the theoretical critical gradient,  $i_{cr}$ . It appears that all tested soil specimens began to exhibit some particle transport at relatively low gradients. In particular, in tests GA1 and GA4.3 (soil GA4 in very loose condition),  $i_k$  is the gradient practically just after the first increase of the water level of the inlet tank.  $i_k$  is practically similar for all the other soils with no fines tested, ranging from 0.5 to 0.7. The specimens in the tests on specimens GA1 and GA4.3 have the highest porosities tested, and therefore the lower hydraulic critical gradients. The finer particles of those specimens should have moved more freely through the constrictions of the coarse particles, which form the primary fabric (i.e., the basic skeleton), than in the other tests. It is noted that, the low amount of the finer fraction (fine sand) in soil GA1 susceptible to suffusion justifies the absence of observable signs of erosion at top surface of the specimen. For this reason,  $i_{start}$  and  $i_{boil}$  were not set for this test specimen.

$i_{start}$  is higher than the critical gradient,  $i_{cr}$ , with exception of the tests on GN and GA4.3. That is likely due to limited diameter of the seepage cell, which allows the development of friction effects on the periphery of the test specimen. In addition, the aluminium ring fixed to the seepage cell, on top surface of the specimen, should allow arch effects on soil, increasing its resistance to erosion. In the particular test on GP (with clayey fines), inter-particle electrochemical forces are likely to act together with gravity forces against the uplift seepage forces. For soils with no fines, the difference between  $i_{start}$  and  $i_{cr}$  shows a tendency to increase with the  $i_{cr}$  value.

The value of  $i_{start}$ , lower than  $i_{cr}$ , in specimen GN, is because the minerals of non-plastic fines are more easily transported by water than the silica ones, revealed by the considerable water cloudiness immediately after immersion of the specimen.

In test GA4.3,  $i_{start} < i_{cr}$  most likely due to the very high soil porosity, which should have led to the formation of concentrated flow paths of high velocity through the finer fraction composed by the fine sand. The parasitic flow paths have been observed mainly between the specimen and the lateral surface of the mould. The results of these two tests support the observations made by Skempton and Brogan (1994). They noticed that suffusive behaviour might initiate at hydraulic gradients lower than  $i_{cr}$ .

Gradient  $i_{start}$  in test GA4.1 (mould with stainless steel surface) is much smaller than in GA4.2 (mould with Teflon® surface). This suggests that the less the roughness of the lateral inner surface of the mould the lower should be  $i_{start}$ . The tests on soil GA4 suggest that the upper ring should not have much influence on  $i_{start}$ , given that GA4 and GA4.1 have equal gradients for the start of erosion.

Gradient  $i_{boil}$  is substantially higher than the critical gradient,  $i_{cr}$ , with exception again of test specimens on soils GN (with non-plastic fines) and GA4.3 ( $D_r = 5\%$ ). In test on soil GN, boiling condition occurred shortly after the first signs of erosion, for a hydraulic gradient lower than  $i_{cr}$ .

For soils with no fines performed with the upper ring, the difference between  $i_{boil}$  and  $i_{start}$  shows a tendency to increase with the  $i_{cr}$  value. However, when comparing the tests GA4 and GA4.1, becomes obvious that the upper ring has led to a much higher  $i_{boil}$ . In the tests showing a considerable volume increase, which are those wherein one large ‘sand soil’ is formed suddenly, the upper ring should act against the upward movement of particles.  $i_{boil}$  should increase with the roughness of the inner lateral surface of the mould, just has been observed for  $i_{start}$ .

#### 4.5 Influence of fines, sand and gravel contents and plasticity on suffusion behaviour

Figure 4.9 shows plots of  $i_k$ ,  $i_{start}$  and  $i_{boil}$  against the gravel content,  $pc4$ , of soil specimens tested. To have the same basis of comparison, only the tests performed with the upper ring are presented. The upper ring in the UF test, represent a significant hurdle to the seepage flow along the upstream soil, forcing the streamlines to converge to the centre of the specimen.

For the specimens on soils with no fines, plots show an obvious trend that  $i_{start}$  and  $i_{boil}$  are higher the lower the gravel content of the soil. Soils GN and GP, with 5% of fines, have the same gravel content than GA4. However, they showed lower  $i_{start}$  and  $i_{boil}$  values than in test on GA4. The erosion of fines was observed for a smaller gradient than that necessary to cause visible movement of sand particles on top of specimen of GA4. The hydraulic gradients causing erosion are substantially higher in soil GP (with clayey fines) than in soil GN (with non-plastic fines). This is mainly because, in the former, there are additional inter-particle electrochemical forces acting against the uplift seepage forces.

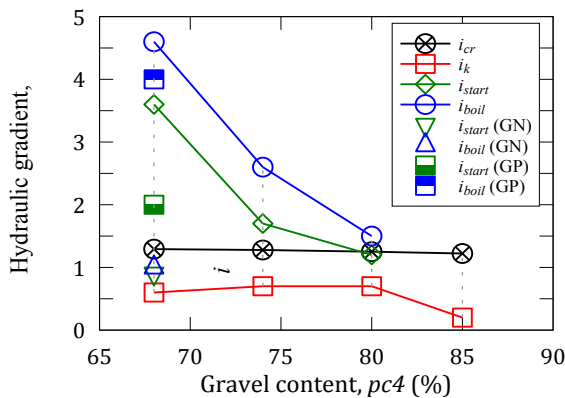


Figure 4.9. Hydraulic gradients  $i_k$ ,  $i_{start}$  and  $i_{boil}$  against the gravel content,  $pc4$ , in tests using the upper ring.

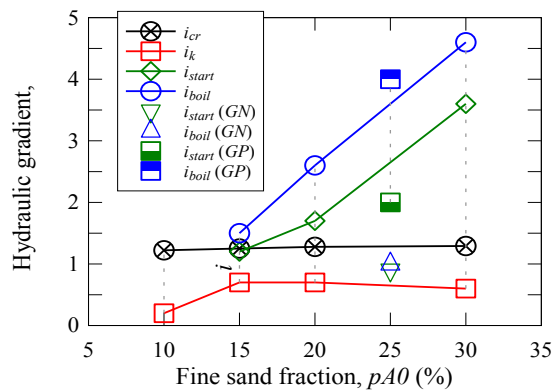


Figure 4.10. Hydraulic gradients  $i_k$ ,  $i_{start}$  and  $i_{boil}$  against the percentage of fine sand fraction in soil mixtures, in tests using the upper ring.

The influence of the content of fine sand (soil A0) in the soil mixtures,  $pA0$ , on the gradients  $i_k$ ,  $i_{start}$  and  $i_{boil}$  is revealed in Figure 4.10. Once again, only tests using the upper ring are plotted. Excluding test on GN (with non-plastic fines), plots show an obvious trend that  $i_{start}$  and  $i_{boil}$  are higher the higher the  $pA0$ . Considering just the tests of soils with no fines, this trend for  $i_{boil}$  is practically linear.

Photos shown in Figure 4.7 also reveal the influence of  $pA0$  in the erosion behaviour of the soils. The size of the resulting 'sand boil' is strongly dependant on the percentage of fine sand (soil A0) in soil mixture. It appears that the amount of sand in the 'sand boil' formed at the top surface of specimen is larger the higher the  $pA0$ .

## 5 CONCLUSIONS

This paper presents an experimental study using a cylindrical permeameter to evaluate the behaviour of six gap-graded soils in terms of their susceptibility to suffusion. Samples were subjected to upward vertical flow, with gradual increments of the gradient, up to a maximum gradient of about 6.

No signs of erosion were observed in the top of the specimen in the test carried out with the gap-graded soil with no fines and lower percentage of fine sand (10%). This conclusion seems to be in line with the methods of Burenkova (1993) and Wan and Fell (2004, 2008), which attribute to that material an internally stable behaviour. In the test carried out on the soils with fine sand of 15, 20, 25 or 30%, up to three levels of notable hydraulic gradients were identified. The first level corresponds to the initial change in the permeability of soil,  $i_k$ . The second level corresponds to the initial observation of particle movement on the top of the specimen,  $i_{start}$ . The third level corresponds to the onset of a "boiling condition" visible on top of the specimen,  $i_{boil}$ .

In all tests,  $i_k$  is considerably lower than the theoretical critical gradient,  $i_{cr}$ . It appears that all tested soil specimens began to exhibit some particle transport at relatively low gradients.  $i_{start}$  is higher than the critical gradient,  $i_{cr}$ , with exception tests on specimen with non-plastic fines and with lower relative density ( $D_r = 5\%$ ). That is likely due to the development of friction effects on the periphery of the test specimen. In the test on specimen with clayey fines, inter-particle electrochemical forces are likely to act together with gravity forces against the uplift seepage forces. The test on soil with non-plastic fines showed  $i_{start}$  in lower than  $i_{cr}$ , likely because the minerals of non-plastic fines are more easily transported by water than the silica ones. Sample with lower  $D_r$  showed erosion for gradient lower than the critical, most likely due to the very high soil porosity, which should have led to the formation of concentrated flow paths of high velocity through the finer fraction composed by the fine sand.  $i_{start}$  in test using mould with stainless steel surface is much smaller than in test using the mould with Teflon®. This suggests that the lower the roughness of the lateral inner surface of the mould the lower should be  $i_{start}$ .  $i_{boil}$  is substantially higher than the critical gradient,  $i_{cr}$ , with exception again of test specimens on soils with non-plastic fines and with lower relative density.

The results of tests show that the percentage of fine sand, the fines and the type of fines are the critical parameter in the suffusive behaviour of the gap-graded soils tested. Excluding test on soil with non-plastic fines, results show an obvious trend that  $i_{start}$  and  $i_{boil}$  are higher the higher the fine sand content. The higher the fine sand content the higher the amount of material deposited on the specimen top, but the gradients associated to initiation of suffusion and development of 'sand boiling' also increase. For normal gradients in dams, the gap-graded soil with 5% of plastic fines should be more resistant to initiation and development of suffusion than the gap-graded soil with 5% of clayey fines.

## REFERENCES

- Burenkova, V. V. (1993). Assessment of suffusion in non-cohesive and graded soils. In *Filters in geotechnical and hydraulic engineering*. Heibaum, and Schuler (eds), Balkema.
- Correia dos Santos, R. (2014). *Experimental investigation on limitation of the progression of internal erosion in zoned dams*. PhD Thesis, Instituto Superior Técnico, Universidade de Lisboa, Lisbon, Portugal, pp. 315.
- Kenney, T.C. & Lau, D. (1985). Internal stability of granular filters. *Canadian Geotechnical Journal* 22:215-225.
- Kenney, T.C. & Lau, D. (1986). Internal stability of granular filters: Reply. *C. Geotechnical Journal* 23:420-423.

- Skempton, A.W. & Brogan, J.M. (1994). Experiments on piping in sandy gravels. *Géotechnique* 44(3):449-460.
- Wan, C.F. & Fell, R. (2004). Experimental investigation of internal instability of soils in embankment dams and their foundations. Report UNICIV No. R-429, Sydney, Australia.
- Wan, C.F. & Fell, R. (2008). Assessing the potential of internal instability and suffusion in embankment dams and their foundations. *Journal of Geotechnical and Geoenvironmental Engineering* 134(3):401-407.

# Historical information and advanced tools for flood protection and structures management

S. Aielli, S. Parodi, S. Pavan & A. Rosso

*AIPO – Interregional Agency for the river Po*

**Abstract:** The river Po is the main river of Italy, and crosses the entire North Italy from the Western Alps to the Adriatic sea. Its middle-lower course is characterized by an imposing levees' system, which origins go back to the XVI Century, and which size has been continuously increased until nowadays. As it often occurs, when dealing with earth dykes, this system is subject to seepage phenomena, that can lead to embankments piping if not properly managed. In particular, during last flood events (years 1994 and 2000), about 130 sand boils have been detected, surveyed and controlled. The first organized list of filtration phenomena has been built in 2004 by the River Po Basin Authority (AdBPo), and published in a document named "Catasto delle arginature maestre del fiume Po" (i.e. "Real estate registry of main embankments of the river Po") After the last large flood event of November 2014, AIPO (the Interregional Agency for the River Po, i.e. the public body responsible for levee construction and maintenance), together with AdBPo, felt the necessity to update and integrate this registry, adding specific information about the hydraulic condition (flood height and duration) associated to new sand boils activation or old sand boils reactivation. This paper describes how the collection of historical data, together with most recent information, even from the 2016 flood event, allowed the creation of an information database (DB), with a simple but efficient structure ready to be updated with data from future events. Monographic data sheets containing basic information for understanding every filtration phenomena can be obtained by querying this DB. Main contents are: identification number of the filtration phenomena and/or of the surveyed sand boil; exact location of the phenomena given by geographical coordinates and support maps; time of activation (when known); critical flood height, estimated accounting for maximum flood height without activation and minimum recorded flood height with activation; any other available information (e.g. size curve of the transported material, soil characteristics, stratigraphy of the subsurface, etc.). At the conclusion of this work, the aim is to demonstrate that the proper organization of all these information, together with the interpretation of the interactions among hydraulic factors and local soil characteristics, can help the deep phenomena's understanding, and make the DB a useful tool for levees' hazard analysis, allowing a modern and efficient management of earth embankments and other flood protection structures.

Keywords: levees, sand-boils, filtration, flood management, data management

## 1 INTRODUCTION

River Po is the main Italian river both for the length of the main course, approximately 660 km, and for the discharge, fed along its course by 141 tributaries. The hydrographic basin area covers over 71,000 square kilometers, a quarter of the entire national territory, embracing 3,200 municipalities in six regions: Piedmont, Valle d'Aosta, Lombardy, Veneto, Liguria, Emilia-Romagna, and the Autonomous Province of Trento (see Figure 1.1).

The significance of river Po is not mainly related to its size, which is small in comparison to the major European rivers, but to the strong anthropization of the territory across which it flows. The population density of the area, the manufacturing activities, the infrastructure and water resources use make the Po basin an exceptionally diverse area and a focal point for the Italian national economy.

Since ancient times, the populations living along the river Po have tried to limit the hazard due to river flooding, to control its course and claim land surfaces for agricultural activities, urban settlements and production areas. Large artificial levees have been built during centuries along the Po and many of its tributaries to prevent flooding of the adjoining countryside. Figure 1.2 shows an example of the earth embankment evolution over the last fifty years in a cross-section of the delta area, but this situation is typical for the entire reach. Furthermore, many artificial flood control storage areas along tributaries have been built in more recent times. At present, the Po river levees' system extends about 900 km along its main course and 150 km along the arms of its delta.

Flood risk is managed by two main public bodies: the Po river Basin Authority (AdBPo), which has a planning role, and defines the general setting of flood protection works based on the reference flood event (i.e. the flood with 200 years of returning period); the Interregional Agency for the river Po (AIPo), which can be defined as the operating arm of AdBPo, and has the responsibility for flood protection works executive design, construction and maintenance. Besides the management of flood control storage areas, the levees maintenance and surveying are the most important activities of AIPo.

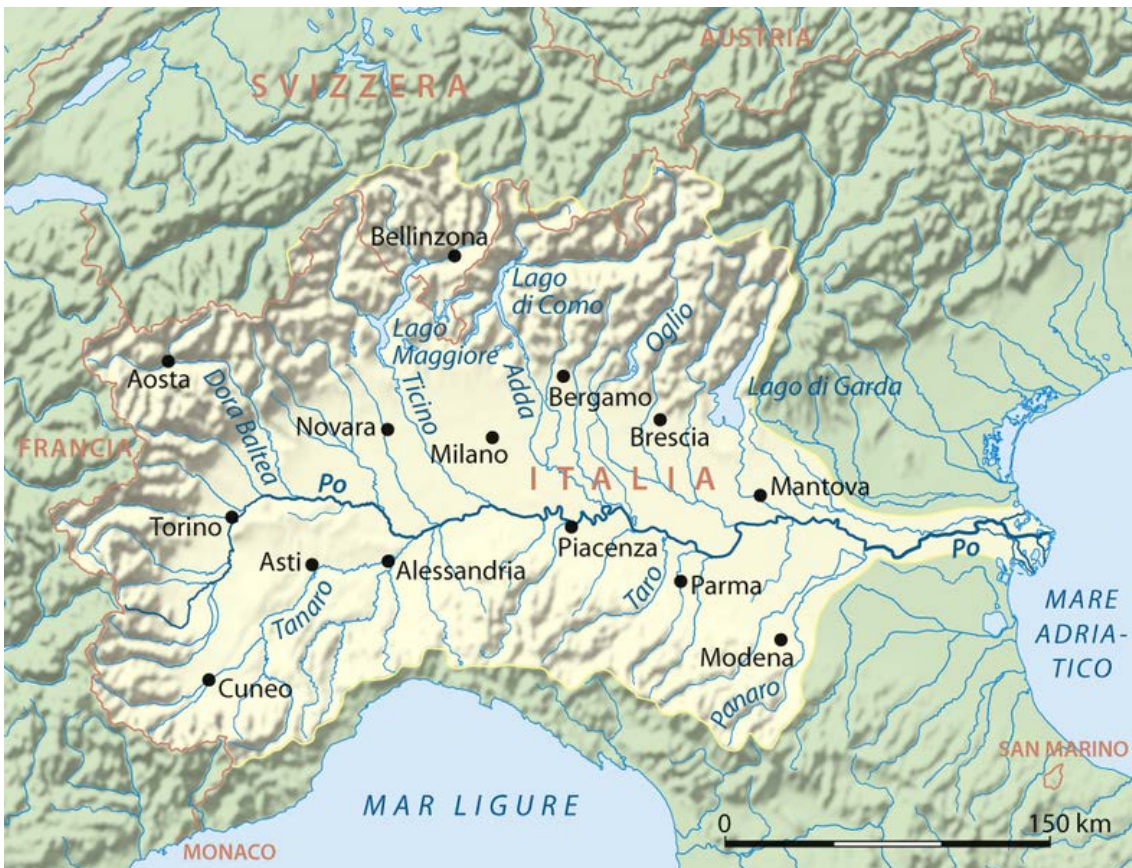


Figure 1.1. Po river basin

After the significant floods of 1994 and 2000, that together with the flood of 1951 represent the full-fledged highest levels ever recorded, the entire river Po embankments' system has been raised and enlarged, leading to a significant mitigation of overtopping risk.

Moreover, a broad study about the geotechnical stability state (Gottardi et al., 2013) demonstrated that the Po river embankments, with current geometries, generally do not reveal vulnerability towards stability failure, even under seismic conditions. On the other hand, the same study confirmed that backward-erosion piping risk remains at high level. The levees of the river Po are in fact historically subject to backward-erosion piping, with high numbers of surveyed phenomena and variable distributions over time. With Garcia et al. (2017), a deeper knowledge of the phenomenon has begun, and

the need to reorganize historical and recent data on surveyed sand-boils emerged in the start-up phase of this work.

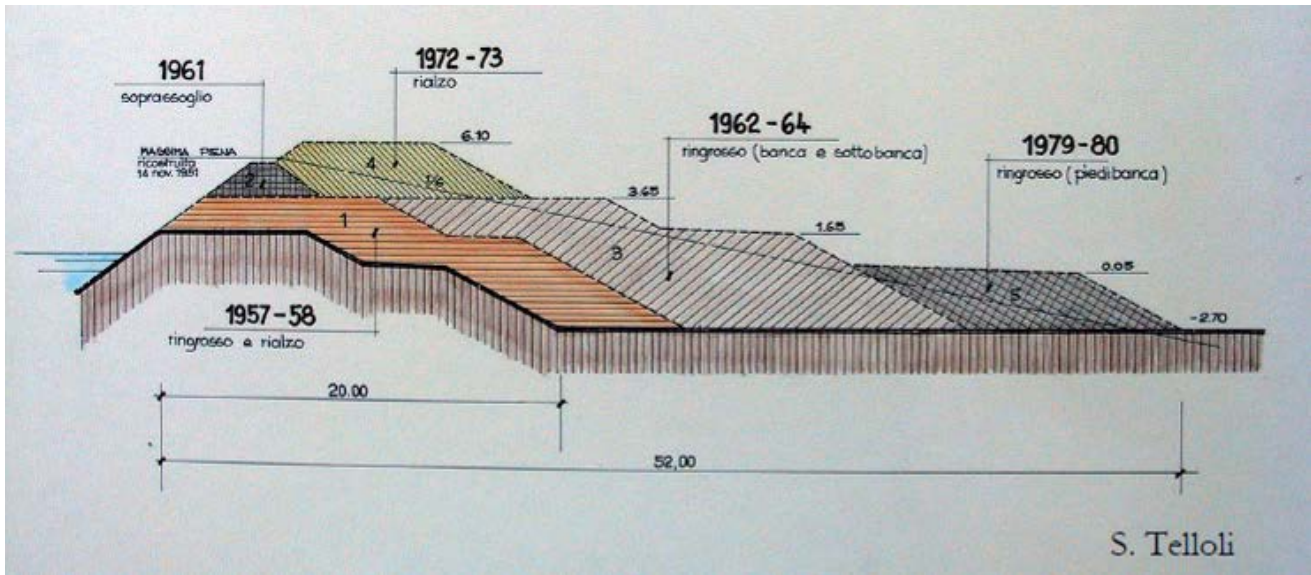


Figure 1.2. Example of Po levees evolution during last 50 years.

## 2 SAND BOILS

During flood events, many sand boils can appear along the dry side of levees, at variable distance from the toe. They are usually managed under a well-structured protocol between various public bodies that constitute the complex system of Italian Civil Protection. To avoid the risks connected to sand boil evolution, provisional little embankments with sand bags or different material are usually put at work to create a ring around the boil, inducing the creation of a small water reservoir (Figure 2.1).

In this way, the hydraulic load due to the flood stage inside the river is balanced by the weight of the small reservoir water column, thus diminishing the filtration velocity. Sand bags walls are then upraised until this velocity gets lower than the critical velocity for soil material movement and sand stops coming out, letting just clear water spring.

The River Po Basin Authority (AdBPo) in its census of historical river Po breaches (2014) enumerated 31 breaches caused by piping phenomena, in the period from 1812 till 1951 (last levee failure started by piping registered along the Po river).



Figure 2.1. Sand boil near Ferrara (2014 November flood event)

## 2.1 The flood protection works real estate registry

The first organized list of filtration phenomena (e.g. sand boils, seepage) has been built in 2004 by AdBPo, and published in a document named "Catasto delle arginature maestre del fiume Po" (i.e. "Real estate registry of main embankments of the river Po"). This document contains information about the levees system, and classifies systematically the main features of hydraulic works (see Figure 2.2).

Information that can be found in this document is:

- Levee geometry (elevation tables and cross sections sketches);
- Main reference flood water levels (200 years return period discharge profile, historical floods recorded profiles, etc.);
- Presence of cut-off walls (concrete made or plastic);
- Filtration areas;
- # 77 *fontanazzi* (the Italian word for sand boils) surveyed

Sand boils are registered with a unique identification number, all along Po main course, until the Po di Goro inlet (beginning of the delta area).

This register is a complete work, showing a picture of the system status after the floods of 1994 and 2000. Then, consequently to the last large flood event of November 2014, AIPo, together with AdBPo, felt the necessity to update and integrate this registry, adding specific information about the hydraulic condition (flood height and duration) associated to new sand boils activation or existing sand boils reactivation. Meanwhile, cataloguing work has been extended to the delta area, taking out a total number of 130 sand boils.

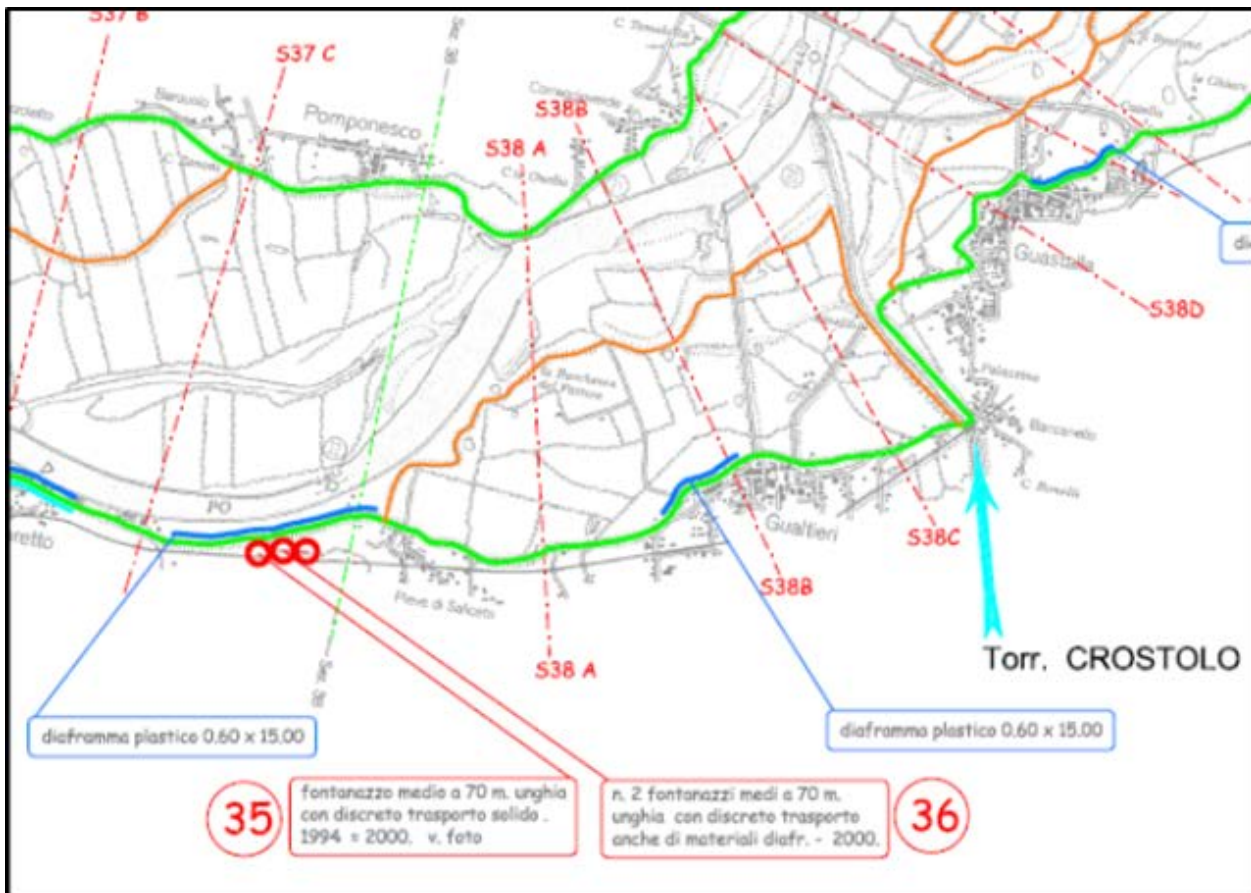


Figure 2.2. Extract from the “real estate registry of main embankments of the river Po”

### 3 DATA BASE

In order to systematize an important number of data initially uneven, this work considered the construction of a DataBase (DB), to allow the analysis and comparison of the considered parameters. At the beginning, the development of the DB had the target to create a shared tool between AIPo’s coworkers in each territorial office. The DB was created with MS Access® 2010, a software available for every worker of the Agency (but all data are available for exportation in other free software).

The first issue about data that arose, regarded the parameters to be taken into account and to be inserted into the DB. Another issue regarded the best way for data processing. The decision was that one of the most important features of the DB would have been a simple but efficient architecture, ready to be updated with data from future events. So the priority has been the design of few tables, strictly connected to each other, and to monographic data sheets that can be obtained by querying the DB, containing basic information for the understanding of every filtration phenomena.

Main contents are:

- Identification number of the filtration phenomena and/or of the surveyed sand boil
- Exact location of the phenomena given by geographical coordinates and support maps
- Time of activation (when known)
- Critical flood height, estimated accounting for maximum flood height without activation and minimum recorded flood height with activation.
- Any other available information (e.g. size curve of the transported material, soil characteristics, stratigraphy of the subsurface, etc.)

Hydraulic conditions of different flood events are registered through AIPo’s hydrometric gauges network, which includes 18 stations along river Po, mainly installed after the flood of 1994. Data from 1994’s flood event come from a direct field survey made by employees of the Agency.

Water elevation data are available both in relative and in absolute value (meters above sea level). They can easily be linked to topographic data, from which the elevation of the ground in correspondence of the sand boil can be guessed. The most important topographic field survey has been carried out in 2005 (“Rilievo del fiume Po da confluenza Ticino al mare”), and produced a number of cross sections (average distance 1500 m from one another). In addition to that, a Digital Terrain Model has been produced in 2015 from aerial survey, including a wide band of land also outside levees, precisely intended to be used to know the exact altitude of critical filtration areas.

Another matter to be addressed was the reconstruction of the flood wave shape and elevation just close to each sand boil. Water elevation is in fact exactly known only where it is measured by gauges. The problem was solved by a short software script for flood wave interpolation in space and time, in order to reproduce the fairly exact propagation of water levels from one measuring station to the next. Also these data are available inside the DB and rapidly accessible.

Once ready, the DB has been fed with all information available in the AdBPo real estate registry of 2005. Then this cadaster was update and integrate, adding specific information about the hydraulic condition (flood height and duration) associated to new sand boils activation or existing sand boils reactivation, following flood events of 2014 and 2016. The same information is also organized into a shape file, which attribute table corresponds exactly to the DB main table.

The DB gathers for each sand boil all available information, such as geographic coordinates, with link to Google Maps to obtain a quick geolocalization, cartographic data, link to related files (hydrographs, sieve analysis, pictures and files useful for a better description of phenomena) sand boil behavior during floods and the main physical features (see an example of the contents in Figure 3.1).

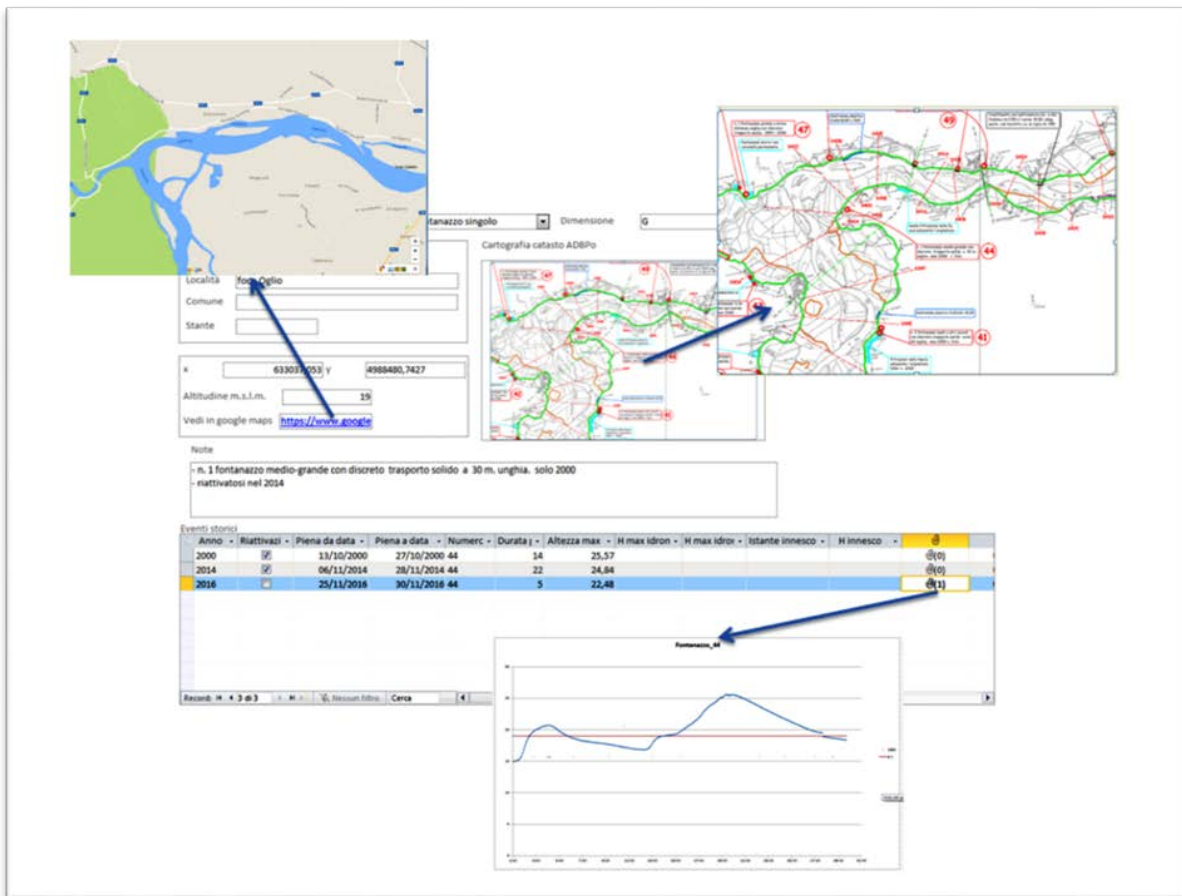


Figure 3.1. Window extract from DB

Finally, a report can be created, which will have the form of a monograph with the description of every single sand boil.

During a flood event it is possible to query the DB and evaluate in real time the risk of reactivation by comparing historical data with flood height estimated by the AIPo's flood early warning system (described in the following paragraph). The DB is an important resource, with a homogenous structure, easily accessible and shareable. The next step will be the implementation of a DB with a Geodatabase (GDB). The main features of geodatabase are to join "geo" (spatial data) with "database" (data repository), to create a central repository of the data to manage spatial data. In this way it will be possible to save GIS data in a central server and use the GDB at Desktop, Server or Mobile solutions.

The proper organization of all these information, together with the interpretation of the interactions among hydraulic factors and local soil characteristics, can help the deep phenomena's understanding, and make the DB a useful tool for levees' hazard analysis, allowing a modern and efficient management of embankment and other flood protection structures.

#### **4 FLOOD ALERT TRESHOLDS AND EARLY WARNING SYSTEM**

As explained in the previous paragraphs, the Interregional Agency for the River Po has the primary role in the operations that have to be undertaken during a flood event, besides coordinating all other Civil Protection actors.

Different operations are logically related to different alert thresholds of water levels exceeded. To allow an efficient organization, a succession of thresholds has been set all along the river Po, in correspondence of the main gauging stations. Figure 4.1 shows as an example of the threshold scheme at Pontelagoscuro cross section. Level 1, represented by the yellow line, identifies the limit between the main flow channel and the overbanks. Below this stage, the entire Po discharge flows inside the main channel and no specific action is required. Level 2, represented by the orange line, is set as the average elevation at which flood protection works begins to be touched by the water, i.e. to the toe of levees. Between Level 1 and 2 the river flows above the overbanks, the alert threshold is called "Ordinary", and the Civil Protection systems starts its operative action by intensifying the flood propagation monitoring through remote gauging stations. AIPo activates the on-call service and ensure the availability of its staff. Level 3, the red line, is set at minimum 1 m and maximum 1.5 m above Level 2, depending on the Po river reach and on its peculiarity. Nevertheless, above this level levees are all affected by the ongoing flood. Between Level 2 and Level 3 the alert threshold is defined "Moderate": AIPo begins the "flood service", which implies the direct surveys of embankments and all connected hydraulic works, usually with the help of Civil Protection voluntaries. Above Level 3, the alert threshold becomes "High": activities are the same of previous step, but intensified.

At the "Moderate" and "High" stages, a consistent portion of levees height is touched by the flood, and water level is surely above countryside level. This is understandably the condition which can start filtration phenomena.

The organization of emergency activities during flood, and the preparedness to the exceeding of alert thresholds is helped by a flood early warning system, based on hydrologic and hydraulic models. The forecast are synthetized on a risk bulletin which is shared by AIPo to all public bodies possibly involved in the management of the flood event. This system allows the Civil Protection structure to know in advance the expected water levels and the critical issues connected.

The DB that has been developed will be connected to alert thresholds and to the early warning system, in order to have indications in advance about the possible reactivation of filtration phenomena and favor the coordination of actions against sand boils, such as being ready with sand bags and proper number of people in place.



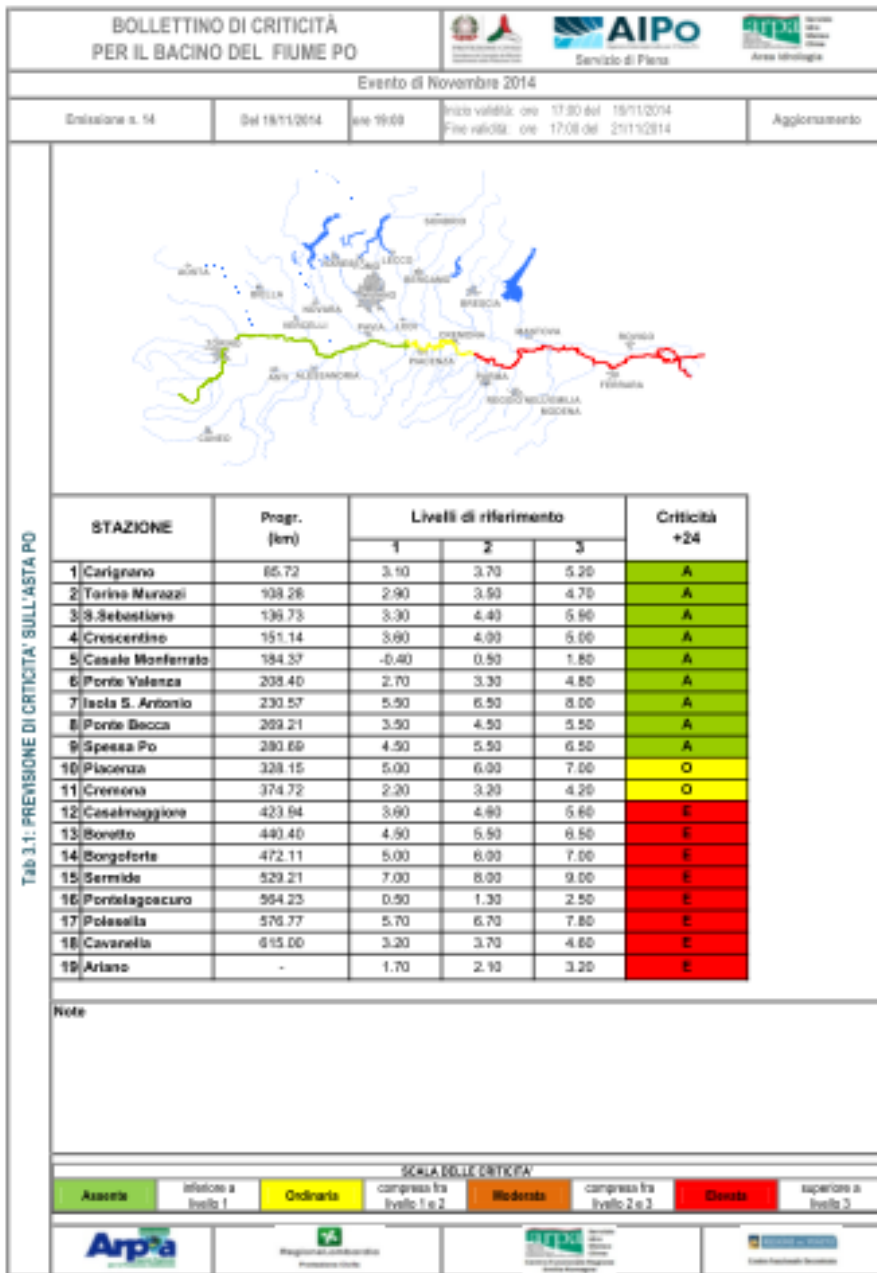


Figure 4.2. Example of flood alert bulletin shared by AIPo with Civil Protection structures. The probability of threshold trespassing is simply noticeable by colors in the table and along river course.

## 5 CONCLUSIONS

The organization and interconnection of a large size of data about sand boils allows the forecast of the possible reactivation of these phenomena, creating a relationship between their behavior and the flood water elevation.

In particular, the identification of maximum water levels occurred without reactivation and, on the other hand, of minimum water levels which gave start to the filtration phenomena, permits to recognize the activation interval. The closer are the two limit values, the more precise will be the definition of the activation interval.

The use of early warning flood forecast models will then complete the framework, giving the possibility to put in work in advance all necessary precautionary measures against piping hazard originated by filtration phenomena and in particular from sand boils evolution.

## REFERENCES

- Autorità di Bacino del fiume Po, (2005). *Catasto arginature maestre del fiume Po*.
- Autorità di Bacino del fiume Po, (2014). *Fiume Po da Torino a mare. Censimento delle rotte storiche*.
- Gottardi G., Marchi M., and Tonni L., (2013). *Verifiche sismiche degli argini in sponda destra del fiume Po nel tratto compreso tra Ro (FE) e Boretto (RE) (Progetto SISMAPO) - Attività 11a: Verifiche di stabilità in condizioni statiche*. Rapporto finale, Università di Bologna.
- García Martínez M.F., Bezuijen A., Gottardi G., Marchi M., Tonni L., Rosso A., (2017) *Numerical simulation of the groundwater flow leading to sand boil reactivation in the Po River* . 25th Meeting of European Working Group on Internal Erosion.

# Numerical simulation of the groundwater flow leading to sand boil reactivation in the Po River

M.F. García Martínez, M. Marchi, L. Tonni & G. Gottardi

DICAM, University of Bologna, Bologna, Italy

A. Bezuijen

Department of Civil Engineering, Gent University, Gent, Belgium  
Deltares, Delft, Netherlands

A. Rosso

Agenzia Interregionale per il fiume Po, Parma, Italy

**Abstract:** The reliability of river embankments is essential for flood risk management. The Po River, which flows through the North of Italy, is safeguarded over half of its length by major river embankments. Performance assessment of such water-retaining structures has become a major concern following some significant flood events in the past. Among the possible initiating causes of failure, backward erosion piping turns out to be particularly threatening in the middle-lower stretch of the river. In particular, the November 2014 high-water event triggered the formation or reactivation of a few important sand boils. The paper presents a preliminary 3D finite element model of the groundwater flow through a selected cross section of the Po river, located in the Province of Reggio Emilia, which experienced a reactivation of piping phenomena after the 2014 event. The numerical model, based on a detailed geotechnical characterization obtained from in situ tests, was calibrated on the basis of the 2014 high-water event measurements and verified for a subsequent event that took place in November 2016, though without any relevant sand boil reactivation. Results are discussed with the aim of providing some insight into the mechanism under study.

Keywords: groundwater flow, backward erosion piping, sand boil , Po River

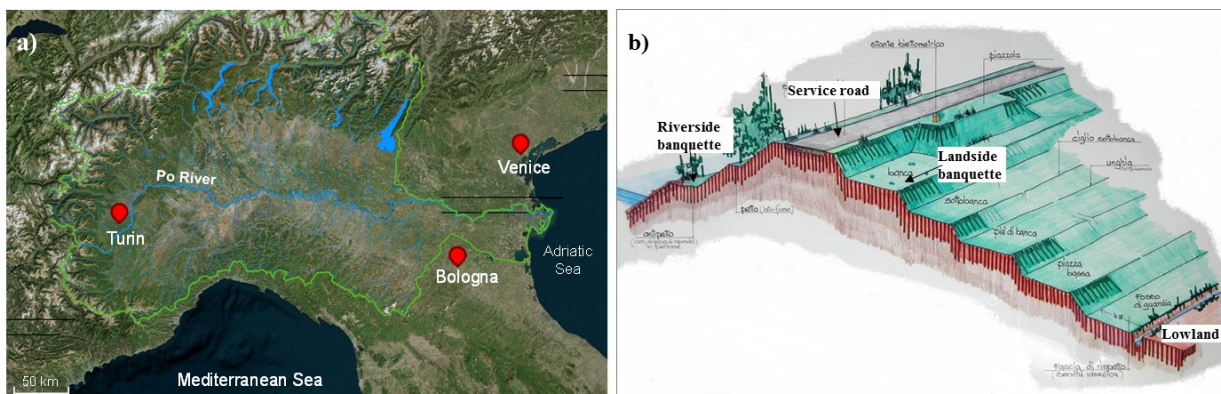


Figure 1. a) View of the Po basin ; b) Drawing of the evolution of the main embankment in the Rovigo Municipality, middle-lower portion (courtesy of AiPo).

## 1 INTRODUCTION

The Po River flows through the North of Italy from West to East (Figure 1a) and is the longest watercourse in the country. It is typically safeguarded by water-retaining structures existing since the 16<sup>th</sup> century. Following some significant past events, flood prevention has become a crucial concern and current river embankments (Figure 1b) have been progressively improved by enlargement of their cross section, increase of their height or enhancement of their mechanical properties. This has decreased the frequency of failure occurrence. Furthermore, such flood protection systems have been extended upstream and towards the main tributaries, thus leading to higher water levels reached during heavy rainfall events.

The Po plain is very densely populated and has a high concentration of extensive agricultural and industrial activities, hence the human and economic damages induced by a river embankment failure would be very high. The stability of such structures is therefore essential for local communities.

As can be observed in Figure 2, backward erosion piping, which involves the development of shallow channels in the sandy aquifer right below the embankment, has proven to be, after overtopping, one of the most important failure mechanisms during the last two centuries. The 2014 major high-water event has been the most relevant in the last decades. It occurred in the mid of November (from 16<sup>th</sup> to 22<sup>nd</sup>), preceded by two more moderate flood waves, and it was particularly threatening in the middle-lower stretch of the river, triggering the formation or reactivation of a few important sand boils (García Martínez et al., 2016).

The relevance of backward erosion piping phenomenon in the Po river embankments has led to new investigations and studies (promoted and coordinated by the Interregional Agency for the Po River, AiPo) being carried out in order to early detect and prevent it. In particular, a new database of the most critical areas is currently under construction. Furthermore, it is intended to develop a methodology for the definition of an alarm threshold that would correlate the river level evolution to the initiation of the phenomenon, which would be a sort of early warning system.

The term backward erosion is designated here to the mechanism by which shallow pipes are formed at the interface of the sandy aquifer and an impermeable layer, which overlies it and acts as a roof to the pipes, preventing their collapse (Bonelli, 2013). This is a typical configuration of Po river embankment sections.

The process starts when a sufficient hydraulic head difference exists across the embankment that leads to a concentration of flow lines toward a downstream unfiltered open exit, which is often due to local cracks in the impervious layer. Such concentration of groundwater flow near the exit cause higher flow velocities near it. This can lead to the formation of sand boils. When the water flow is sufficient to carry sand particles from the aquifer outside the boiling zone, deposition occurs forming what is commonly

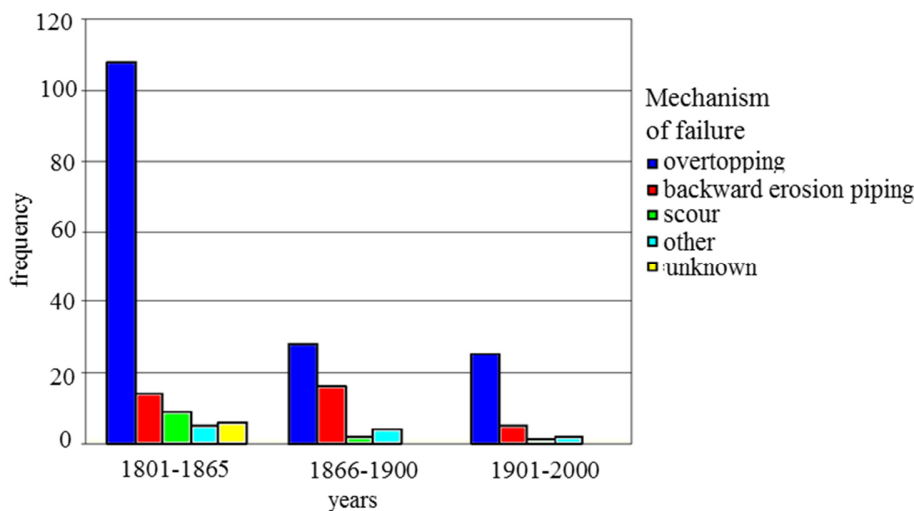


Figure 2. Number of Po river embankment failures, divided into mechanisms of collapse, during the last two centuries (modified from Autorità di bacino del fiume Po, 2005).



Figure 3. Ringed sand volcano near Boretto (Courtesy of AiPo).

known as “sand volcano” (*fontanazzi* in Italian). At this point, shallow pipes might start to develop in the aquifer (van Beek, 2015).

Sand volcanoes are often observed on the land side of Po river embankment sections during high-water events. A countermeasure that is typically implemented is ringing them with sand sacks in order to reduce hydraulic gradients and stop sand transport. Figure 3 shows a ringed sand volcano during the 2014 high-water event near Boretto, in the Province of Reggio Emilia.

In particular, this paper describes the reactivation of a sand boil (Fig. 3) along a river embankment cross section in the Province of Reggio Emilia. Detailed stratigraphic profile and geotechnical characterization of the river embankment foundation system have been based on in situ testing. Then, a preliminary 3D finite element model is presented, aimed at reproducing the groundwater flow which led to sand boil reactivation. The model has been calibrated on the basis of the 2014 high-water event measurements and then verified for a subsequent event that took place in November 2016, during which sand boil reactivation did not occur.

## 2 THE CASE STUDY

In the case of study presented in this paper, a cross section located in the province of Reggio Emilia and affected by a recently reactivated sand boil has been analysed. In particular, the last reactivation occurred during the November 2014 high-water event, when sand transport was observed in the morning of the 15<sup>th</sup>.

### 2.1 Geotechnical characterization

The geotechnical properties of the subsoil have been defined according to the information provided by a number of situ tests carried out along the selected cross-section. In particular, a set of three piezocone tests (CPTU), located in the floodplain area, on the bank crest and at the toe of the bank, respectively, has been used. Such tests were carried out within a major project funded by the Italian Government for assessing the seismic stability of about 90 km of Po river embankments in the middle-lower stretch (Merli et al., 2014; Gottardi et al., 2015). Boreholes and laboratory tests were also part of the large database collected within such comprehensive investigation programme.

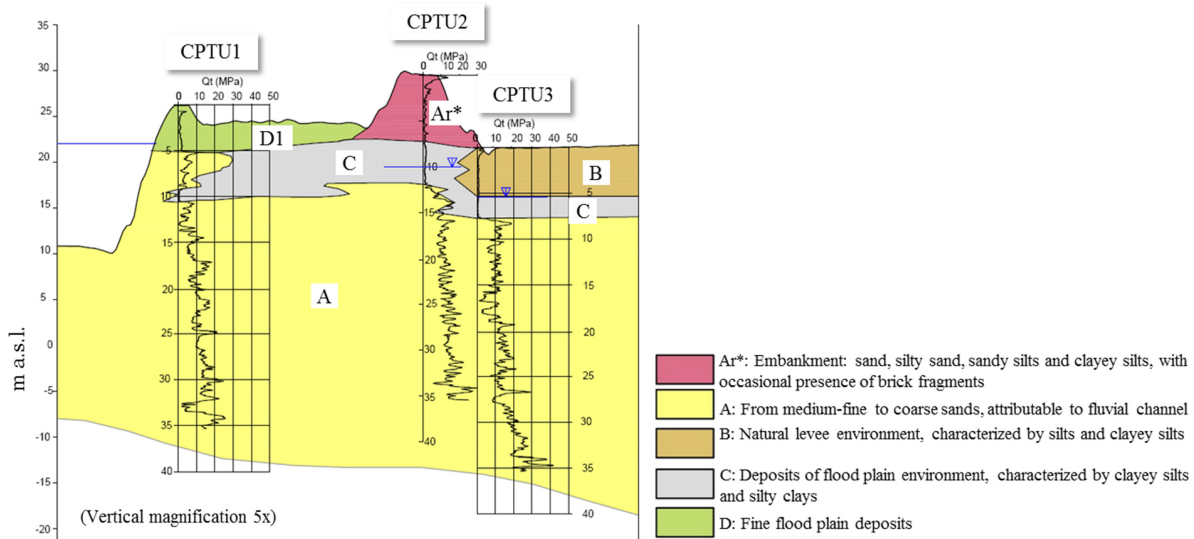


Figure 4. Stratigraphic cross-section in the Province of Reggio Emilia, with location of CPTU tests.

Figure 4 shows the embankment cross section with the location of CPTU tests. A detailed stratigraphic profile has been derived using the classification framework proposed by Robertson (2009), aimed at identifying the *in situ* Soil Behaviour Type (SBT). As an example, results from the application of the method to data from CPTU3 are shown in Figure 5 together with the corrected cone resistance  $q_t$  and pore water pressure  $u$  profiles. The following well-defined stratigraphic units have been identified using the SBT approach:

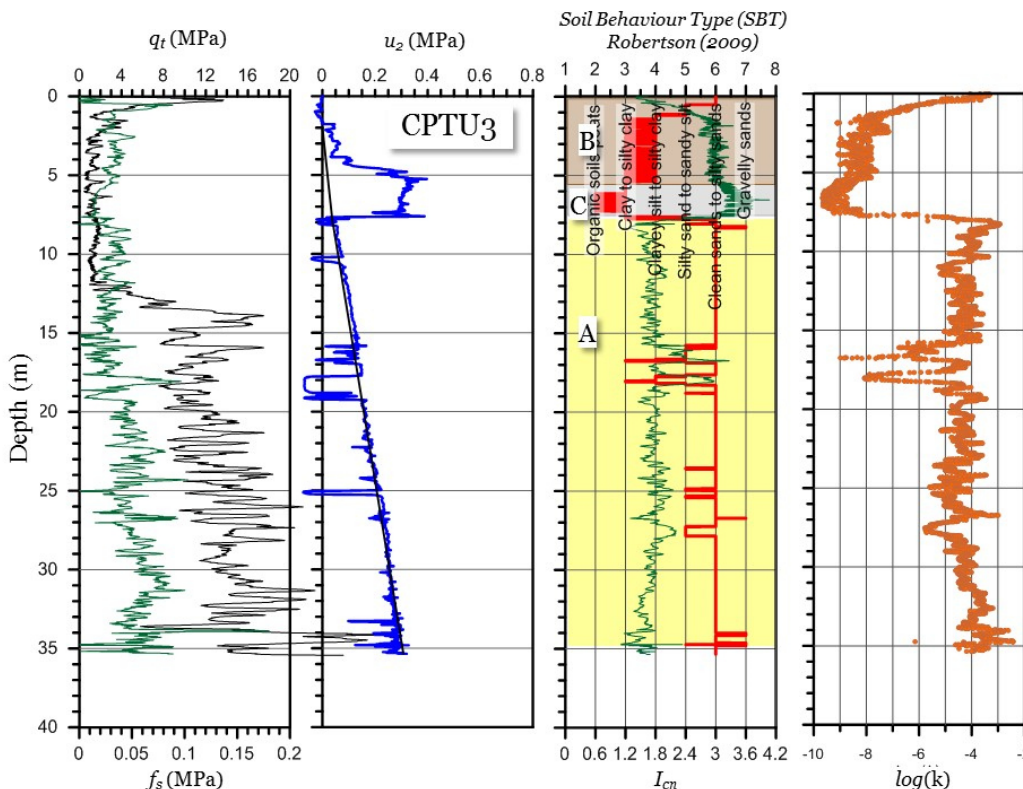


Figure 5. CPTU3 log profiles, classification results and profile of the computed coefficient of permeability in terms of  $\log(k)$ .

- Unit Ar, which forms the major embankment and is made up of soils extracted from nearby borrow pits, consisting of an alternation of sands, silty sands, sandy silts and clayey silts (SBT zones 3, 4 and 5);
- Unit D, fine flood plain deposits, consisting of an alternation of clayey silts to sandy silts;
- Unit C, predominantly clays and silty clays (SBT zone 3), with occasional presence of peat and organic soils (SBT zone 2);
- Unit B, alternation of silts and clayey silts (SBT zones 3 and 4);
- Unit A, predominantly sands and silty sands (SBT zone 6).

As a result, the analysis of CPTU measurements provides evidence of a foundation soil consisting of a clay to clayey silt layer, 7-8 m thick, overlying a sandy unit of about 30 m thick, thus confirming that the stratigraphic arrangement is compatible with the typical configuration required for the initiation of backward erosion piping.

In this study, relevant soil parameters have been estimated using some well-known CPTU-based correlations. In particular, soil permeability profiles have been derived using the relationship proposed by Robertson (2010):

$$\begin{aligned}
 1.0 < I_c < 3.27 \quad k &= 10^{(0.952-3.04I_c)} \quad (m/s) \\
 3.27 < I_c < 4.0 \quad k &= 10^{(-4.52-1.37I_c)} \quad (m/s)
 \end{aligned}
 \tag{1}$$

in which  $I_c$  is the Soil Behaviour Type index (Robertson, 2009). The hydraulic conductivity (in terms of  $\log k$ ) profile deduced from CPTU3 is also plotted in Figure 5. As can be observed,  $k$  of the aquifer (unit A) is in order of magnitude of  $10^{-5} \div 10^{-4}$  m/s.

## 2.2 The numerical model

The numerical simulation of the groundwater flow leading to the reactivation of a sand boil along the selected cross section has been carried out using the finite element code PLAXIS 3D.

The cross-section geometry has been established using data from topographic surveys, whereas the proposed stratigraphic arrangement relies on the CPTU-based classification results and soil unit identification commented above. As evident from Figure 4, it has been assumed that the sandy unit (referred to as Unit A) extends up to the left boundary of the model, hence such highly permeable layer is present beneath the river bed. Figure 6 shows the finite element mesh eventually adopted, composed 62938 tetrahedral 10-noded elements.

It is worth observing that, in this preliminary attempt to model the reactivation of a sand boil, a vertical cylindrical region (named pipe, hereafter) has been created in the downstream impermeable layer, in correspondence to the real location of the sand boil, being the idea to simulate a “hole type” exit configuration. Furthermore, a semi-spherical region at the base of the cylinder has been considered, aimed at facilitating the flow and make the calculated pressure in the aquifer more realistic. Further field investigations would be required in order to confirm the correctness and effectiveness of such preliminary geometric assumption.

An elastic-perfectly plastic constitutive formulation, based on the Mohr-Coulomb failure criterion, has been adopted for the different soil units, using the available CPTU data for calibration of the soil shear strength.

To model the groundwater flow, an uncoupled analysis has been performed. The initial steady-state condition for the groundwater flow analysis has been generated by considering the average river level over the days preceding the November 2014 high-water event in combination with piezometer readings collected previously (Severi and Biavati, 2013), providing information about water table levels in the land side. Then, the period from 05/11/2014 to 25/11/2014 (Figure 7) has been selected for the transient groundwater flow analysis.

Particular attention has been paid to boundary conditions, and different approaches have been taken into account and compared in some preliminary analyses. The permeable aquifer, overlain by impermeable top layers, results in a semi-confined aquifer with a long leakage length of approximately 1400 m (see also

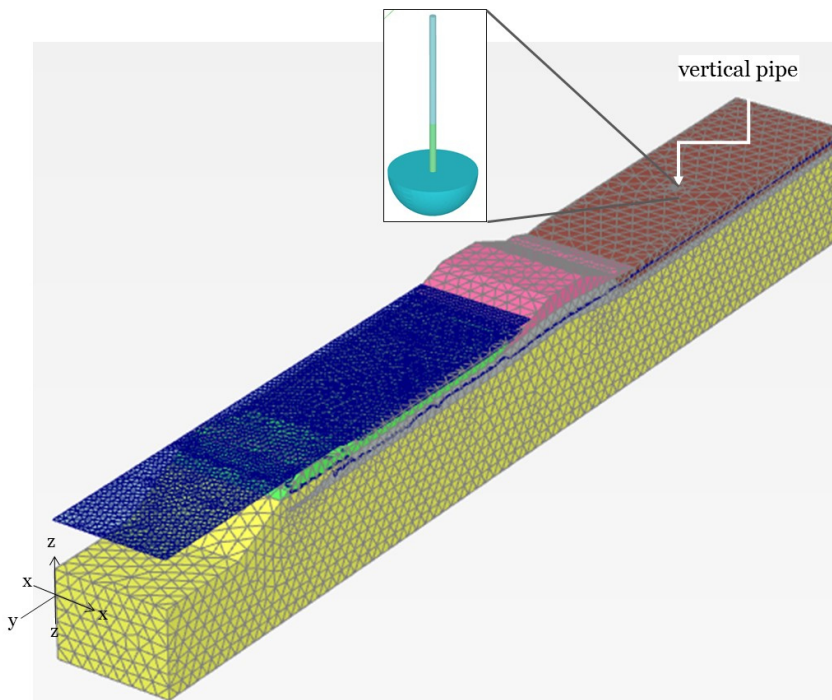


Figure 6. Discretized model of the river embankment, with indication of the soil layering and detail of the vertical pipe.

Bezuijen, 2017) with pressure fluctuations that are still noticeable at a considerable distance from the embankment and the river. The modelling of such a long part of the aquifer using a 3D approach would result in an extremely time consuming analysis. However, assuming a constant piezometric head at the right-hand side of the model (at  $y_{max}$ ) or a no flow boundary condition will underestimate or overestimate the piezometric head at the vertical pipe respectively. The plot reported in Figure 7 shows the hydraulic boundary conditions (BC) eventually assumed in the numerical model. While the river level fluctuations, as monitored during the whole period of high-water event, has been directly assigned along the riverside model boundary, hydraulic boundary conditions at the right-hand side of the model, referred to the aquifer piezometric level ( $y_{max}$ ), have been derived from parallel 2D numerical analyses, performed by considering a model long enough to result in a constant hydraulic head with time at the landward side.

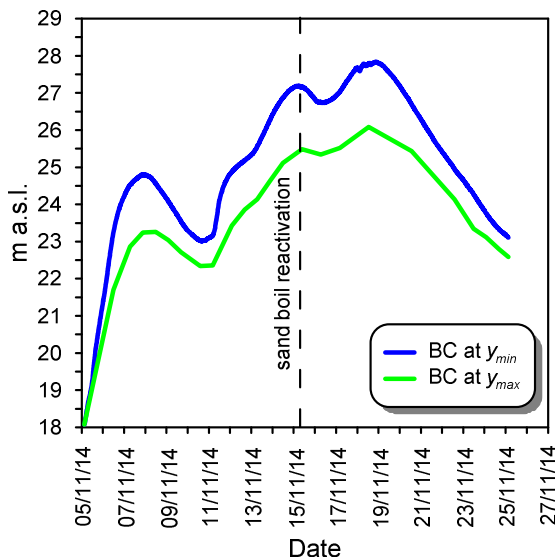


Figure 7. Hydraulic loads evolution within the period of simulation.

The model has been calibrated based upon the USACE (1956) criteria, by which it is accepted that sand boils might occur at an upward gradient through the top stratum of 0.5. Furthermore, sand boils will be observed when the flow velocity in the vertical pipe exceeds the falling velocity of the grains in the sand-water mixture (van Beek, 2015), obtained herein by the application of the Richardson and Zaki (1954) semi-empirical equation:

$$v_z \geq w_t(1-c)^n \tag{2}$$

in which  $c$  is the volumetric concentration,  $n$  is an empirical determined exponent dependent on the particle Reynolds number, ranging approximately between 4.65 and 2.4, and  $w_t$  is the settling velocity for small spherical particles according to Stokes law:

$$w_t = \frac{\rho_s - \rho_w}{1800\eta} d^2 \tag{3}$$

where  $\rho_s$  is the density of the single grain,  $\rho_w$  is the water density,  $\eta$  kinematic viscosity of the water and  $d$  is the grain diameter. Then, assuming for this case of study a uniform initial concentration of 0.55 (or 0.45 of porosity),  $n$  equal to 4,  $\rho_s$  equal to 2.65 g/cm<sup>3</sup>,  $\eta = 1.33 \cdot 10^{-5}$  g·s/cm<sup>2</sup> (T = 10° C) and, according to some available grain size distribution curves,  $d = d_{50} = 0.22$  mm, it turns out that  $v_z \geq 1.4$  mm/s. Although parameters assumed are based on the known range of possible real values, predictive accuracy should be improved with further calibrations such as particle size distribution of sediments within the vertical pipe or discontinuity.

From the above-mentioned, and in the absence of any further information, the model has been calibrated to match  $i \geq 0.5$  e  $v_z \geq 1.4$  mm/s. Sensitivity analyses have shown that the parameters which have a major influence on the results are the coefficient of permeability of the aquifer and of the vertical pipe, the diameter of the pipe, the presence of a high permeability region at the interface between the pipe and the aquifer and the model width.

At this preliminary stage of development, two aspects of the model have been calibrated: the hydraulic conductivity of the vertical pipe as well as its diameter. On the other hand, the permeability of the aquifer has been determined using Eq. (1), the diameter of the semi-spherical region at the pipe base has been set to 4 m and the width of the model used is equal to 40 m.

Figure 8 shows the results of the model calculations, in terms of average vertical gradient along the pipe ( $\Delta h/L_{pipe}$ ) and average vertical flow velocity ( $v_z$ , in mm/s) at the time the sand boil reactivated, for pipe permeability ( $k_{pipe}$ ) varying linearly with the permeability of the aquifer. The permeability of the semi-

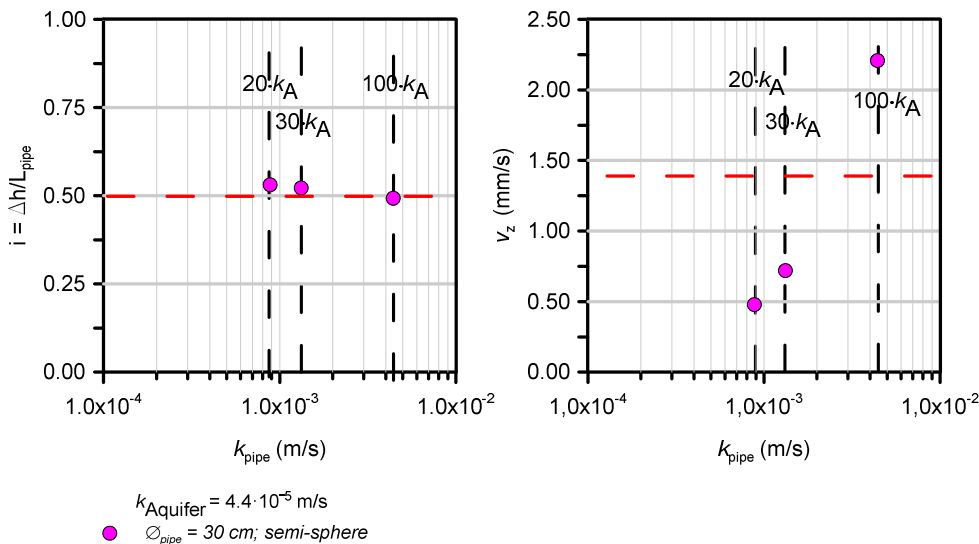


Figure 8. Predicted average vertical gradient along the pipe and average vertical flow velocity.

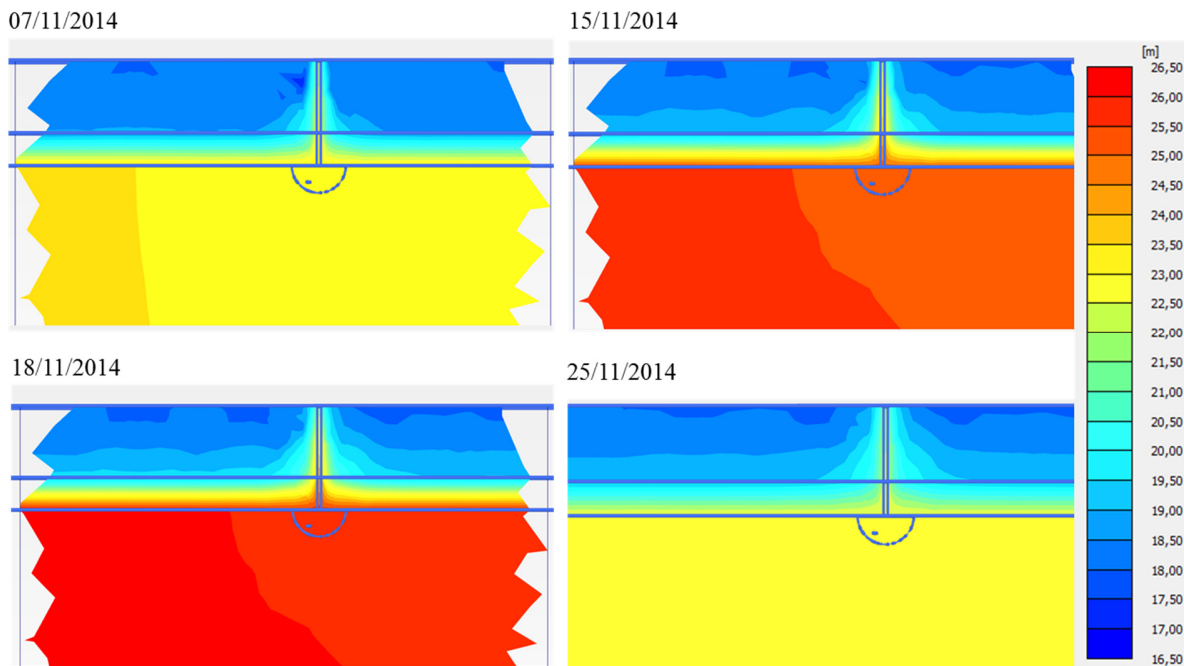


Figure 9. Countour plots of groundwater head in the y-z plane at different stages of the simulation.

spherical cluster was set equal to  $k_{pipe}$ . As can be clearly observed, the gradient decreases and velocity increases when  $k_{pipe}$  is increased, being  $v_z$  much more sensitive. Final calibrated parameters are  $\varnothing$  30 cm (for the pipe) and  $k_{pipe} = 100 \cdot k_{aquifer} = 4.4 \cdot 10^{-3}$  m/s. It is worth remarking that greater diameters of the pipe were found not to fulfil the criteria adopted for the sand boil reactivation, also taking into account that such values would be rather unrealistic. Further observations and detailed investigations, not currently available, would certainly help in confirming the reliability of the outcomes from calibration analyses.

Figure 9 shows the contour plots of groundwater head, in the y-z plane passing through the pipe, computed with PLAXIS 3D at three different stages. Finally, the calibrated model has been verified for the November 2016 high-water event, in which the sand boil did not reactivate. Indeed, both hydraulic gradient and vertical flow velocity at the peak flow were significantly smaller than those obtained for the 2014 event.

### 3 CONCLUSIONS

This paper has proposed a numerical study aimed at providing a better insight into the groundwater conditions leading to the reactivation of sand boils at the toe of river embankments. The analysis has been carried out with reference to a specific segment of the Po river embankments, located in the province of Reggio Emilia (Northern Italy), which has experienced recurrent piping phenomena over the last two decades, the latest having occurred during the 2014 major high-water event.

According to the available in-situ testing data, the resulting stratigraphic arrangement of the foundation subsoil has turned out to be fully consistent with soil layering configurations typically affected by backward erosion piping. The geotechnical parameters of the different soil units, including permeability, have been carefully determined from piezocone tests, although a certain spatial variability and thus heterogeneity are very likely to affect the whole river embankment system and could be taken into account in a more advanced interpretation model.

In order to simulate properly the reactivation of a sand boil, the presence of a pre-existing outflow exit has been included in the discretized FE model as a vertical pipe. Its dimension, as well as its hydraulic conductivity, have been determined by back-analysis, taking into account some well-recognized criteria found in the literature (e.g. USACE) for sand boil reactivation.

The preliminary sensitivity analyses have allowed identifying the parameters having a major influence on the model performance. In particular, the crucial role played by both the diameter and the coefficient of permeability of the vertical pipe suggests the need for further investigations and more detailed information on the geometry and the granular soil characteristics of such volume.

On the other hand, the proposed numerical model seems to simulate properly the response of the embankment, as observed in the last high-water events. Indeed, the numerical results, while confirming the occurrence of a sand boil after the 2014 event, have correctly shown that the river water level evolution monitored in November 2016 would not lead to a sand boil reactivation.

## REFERENCES

- Autorità di bacino del fiume Po (2005). Progetto strategico per il miglioramento delle condizioni di sicurezza idraulica dei territori di pianura lungo l'asta medio-inferiore del fiume Po. *Technical report (in Italian)*.
- Bezuijen, A. (2017). The influence of the leakage length on the initiation of backward erosion piping. Proc. 25th EWG-IE, Delft.
- Bonelli, S. (2013). *Erosion in Geomechanics Applied to Dams and Levees*. Wiley, Hoboken.
- García Martínez, M.F., Gragnano, C.G., Gottardi, G., Marchi, M., Tonni, L. and Rosso, A. (2016). Analysis of Underseepage Phenomena of River Po Embankments. *Procedia Engineering*, 158, 338-343.
- Gottardi, G., Marchi, M. and Tonni, L. (2015). Static stability of Po river banks on a wide area. Geotechnical Engineering for Infrastructure and Development. *Proc. of the XVI European Conf. on Soil Mechanics and Geotechnical Engineering*, 4, 1675-1680.
- Merli, C., Colombo, A., Riani, C., Rosso A., Martelli, L., Rosselli, S., Severi, P., Biavati, G., De Andrea, S., Fossati, D., Gottardi, G., Tonni, L., Marchi, M., García Martínez, M.F., Fioravante, V., Giretti, D., Madiari, C., Vannucchi, G., Gargini, E., Pergalani, F. and Compagnoni, M. (2015). Seismic stability analyses of the Po River Banks. *Engineering Geology for Society and Territory*, 2, 877-880.
- Richardson, J.F. and Zaki, W.N. (1954). Sedimentation and fluidisation: part 1. *Trans. Inst. Chem. Eng.*, 32, 35-53.
- Robertson, P.K. (2009). Interpretation of cone penetration tests – a unified approach. *Can. Geotech. J.*, 46(11), 1337-1355.
- Severi, P. and Biavati, G. (2013). Definizione del modello geologico e idrogeologico della zona arginale del fiume Po in destra idrografica da Boretto (RE) a Ro (FE). *Internal report*. Regione Emilia-Romagna, Servizio Geologico Sismico e dei Suoli.
- USACE (1956). Investigation of underseepage and its control – Lower Mississippi river Levees. *Technical memorandum No. 3-424*, Volume 1, Waterways Experiment Station, Vicksburg, Mississippi.
- van Beek, V.M. (2015). *Backward erosion piping: initiation and progression*, PhD thesis, TU Delft, The Netherlands.

# The influence of the leakage length on the initiation of backward erosion piping

A. Bezuijen

*Ghent University, Ghent, Belgium / Deltares, Delft, the Netherlands*

**Abstract:** The earliest relation describing the risk of backward erosion piping, from Bligh in 1915, calculates an overall gradient over the dike. This gradient should be lower than a certain value depending on the material of the dike foundation for the dike to be safe. Later developments rationalize this number, showing the influence of grain size, permeability, density and added the influence of the thickness of the aquifer. However, the principle remains the same. The actual overall gradient is compared to a critical gradient.

This contribution will show, using analytical groundwater flow calculations that for the beginning of backward erosion piping, not only the overall gradient but also the leakage length of the semi-confined aquifer, usually present at the landward side of the dike, is of importance. This leakage length determines the piezometric head on the landward side of the dike. This is not very new, since this is also used in the ‘blanket theory’ developed and used in the USA, but a slightly different approach results in some new conclusions.

It will also be shown that the influence of the leakage length on the pipe progression and in ultimo on the breach of the dike is less. This means that with a long leakage length the difference in overall head between pipe initiation and breakthrough is larger than for the situation with a shorter leakage length.

Keywords: Backward erosion piping, leakage length, example calculation,

## 1 INTRODUCTION

The earliest relation describing the risk of backward erosion piping, from Bligh in 1915, calculates an overall gradient over the dike. This gradient should be lower than a certain value depending on the material of the dike foundation for the dike to be safe. Later developments (Lane 1935, Sellmeijer 1998, Schmertmann, 2000) rationalized this number, showing the influence of grain size, permeability, density and added the influence of the thickness of the aquifer. However, the principle remains the same. The actual overall gradient is compared to a critical gradient.

There is one exception, the “Blanket Theory” used in the USA (USACE, 2000). This theory is not based on a critical gradient over the dike but calculates the piezometric head in an aquifer at the landside of the dike and compares this with an allowed piezometric head at that position.

Not all piping events are adjacent to the dike. In some cases, they occur at some distance of the dike, see Figure 1. Therefore, it is of interest to investigate the flow in the aquifer not only underneath the dike but also at some distance of the dike.

This contribution uses analytical groundwater flow calculations to calculate the beginning of backward erosion piping and how the piezometric head distribution changes when the pipes become longer. The situation shown in Figure 1 will be used throughout this paper as an example.



Figure 1. Piping along the Po river. Apart from the 'fresh' sand boil on the left part of the picture two older sand boils can be seen (sand boils indicated with arrows).

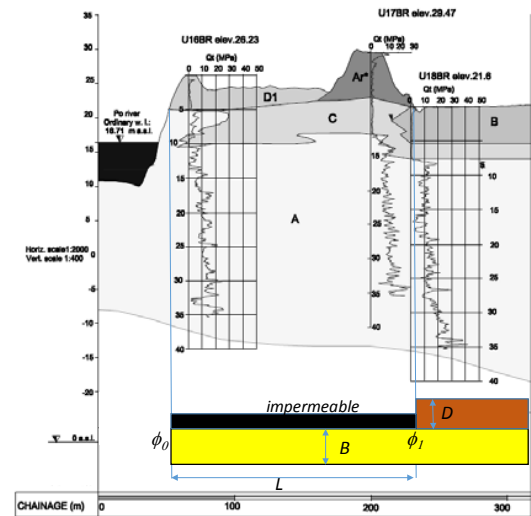


Figure 2: Typical cross-section in that area and schematization used. The letters in the upper part represent the different soil types; the letters *B*, *D* and *L* in the schematization refer to the thickness and length of the layers.

## 2 SITUATION STUDIED

In this paper the situation studied is shown in Figure 1 and Figure 2. A sandy aquifer with a relative high permeability is overlain by a low permeability dike and low permeability layer(s) at the landward side. The water level in the river is in direct contact with the aquifer. This situation is quite common along rivers. The example shown in the figure is from the river Po in Italy, but comparable situations occur in the Netherlands (Van Beek, 2015), along the Mississippi in USA (USACE, 1956) and in China (Yao et al., 2009, Cao, 1994). Without any pipes, the dike can be seen as impermeable and the layers at the landward side that overlay the aquifer as low permeability layers, making that part of the aquifer a semi-confined aquifer. When the water level in the river rises, this will directly lead to an increase in the piezometric head in the semi-confined aquifer, see Figure 3.

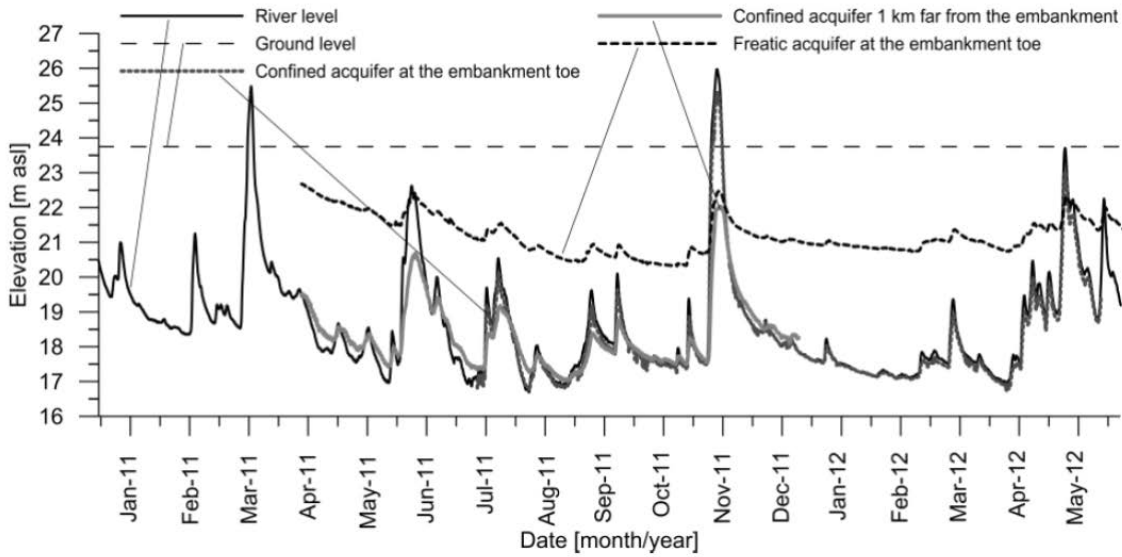


Figure 3. Measured piezometric head at different locations for the cross-section shown in Figure 2. The permeability of the different layers are for this situation shown in Table 1. See Gracia et al. (2017) for more information how the soil data are obtained.

Table 1. Parameters of the soil layers shown in Figure 2 (cross-section, upper part).

layer	permeability (m/s)	thickness (m)
A	3.21E-05	30
B	1.08E-08	5
C	1.25E-09	2

### 3 CALCULATIONS

#### 3.1 Schematisation for groundwater flow calculation without piping erosion

The aquifer is schematized to two blocks to calculate the groundwater flow in the sand layer (and thus the piezometric head). At the riverside of the dike and underneath the dike it is assumed that there is only flow through the sand layer and that the foreland and dike are impermeable over a length. This assumption is reasonable because of the relatively thick layer with soil type C in that area. Furthermore, on the riverside of the dike there will be no water outflow during a high water situation because this area will be overflowed by water. The land side of the dike is schematized as a semi-confined aquifer.

Assuming that the flow is predominantly horizontal in the sand layer (yellow in Figure 2) and vertical in the less permeable clay layers (brown in Figure 2). The flow in the sand layer underneath the dike can be written as:

$$Q = k(\phi_0 - \phi_1) \frac{B}{L} \quad (1)$$

Where  $Q$  is the discharge per unit length ( $\text{m}^2/\text{s}$ ),  $k$  the permeability (m/s),  $\phi_0$  the piezometric head at the river (m),  $\phi_1$  the piezometric head in the sandy aquifer at the landside toe of the levee (m),  $L$  the length of the aquifer at the riverside and underneath the embankment (m) and  $B$  the thickness of the aquifer (m).

According to the theory of the semi-confined aquifer, the piezometric head in such an aquifer can be written as:

$$\phi = \phi_1 \cdot \exp\left(-\frac{x}{\lambda}\right) \quad (2)$$

Where  $x$  is the distance from the toe of the embankment (m) and  $\lambda$  the leakage length of the semi-confined aquifer (m). In this formula, it is assumed that the piezometric head far from the dike is zero m. When, as in this case, the impermeable layer is composed out of 2 layers, the leakage length can be written as:

$$\lambda = \sqrt{kB \left( \frac{D_1}{k'_1} + \frac{D_2}{k'_2} \right)} \quad (3)$$

Where:  $D_1$  the thickness of the first impermeable layer (m),  $D_2$  the thickness of the second impermeable layer (m),  $k'_1$  the permeability of the first impermeable layer (m/s) and  $k'_2$  the permeability of the second impermeable layer (m/s). Derivation of Equation (2) to  $x$  results in the gradient as a function of  $x$  and with Darcy law that leads to the following relation for  $Q$  in the aquifer at the toe of the embankment:

$$Q = k\phi_1 \frac{B}{\lambda} \quad (4)$$

This should be the same value of  $Q$  as defined in Equation (1) and this leads to:

$$\phi_1 = \frac{1}{1 + \frac{L}{\lambda}} \phi_0 \quad (5)$$

An interesting result of this equation is that the relation between the piezometric head at the river and in the aquifer at the toe of the embankment does not depend directly on the permeability of the aquifer nor the thickness as such. It depends on the combination of parameters as defined in the leakage length and the length of the impermeable part on the riverside and underneath the river. With the data given in Table 1 and Equation (3) it can be determined that the leakage length in this case is 1400 m, much longer than  $L$  (approximately 180 m). This means that according to Equation (5) the piezometric head in the aquifer at the toe of the embankment is only a bit lower than the piezometric head at the river (the amplitude of  $\phi_1$  is 0.88 time the amplitude  $\phi_0$ ), which is in agreement with Figure 3. The horizontal gradient is relatively limited due to the long leakage length. Taking the derivative of Equation (1) to  $x$  results in a maximum average gradient in the sand of  $\phi_1/\lambda$ . The maximum water level difference that can occur, according to Figure 2, is around 6 m above the reference height, or the dike will overtop, thus  $\phi_1=6$  m, with  $L=1400$ m. This means that the gradient is at maximum 0.0043, an order of magnitude less than the horizontal gradient necessary for piping according to Bligh (1915). Therefore, in this case sand boils do not occur because of the horizontal gradients but because of high vertical gradients over the semi-impermeable upper layers that caused also vertical gradients in the sand layer close to a weak spot. The loading (the piezometric head) will only decrease slowly with the distance from the toe of the embankment. If there is a weak spot in the cover layers at some meters of the embankment this will fail first. This explains why sand boils can occur at some distance of the toe of the river dike.

The derived equations are comparable as in the 'Blanket Theory' as used by USACE in the United States (USACE, 2000). Only there the semi-confined aquifer has a finite length, leading to a somewhat more complicated formula, but the principle is the same.

### 3.2 Groundwater flow calculation with piping erosion

Assume now that piping erosion occurs. Since the calculation described above is a 2-D calculation, the groundwater flow due to piping erosion can only be included if we assume that piping holes occur at a regular distance along the dike, so that there will be  $n_g$  holes per meter dike. In this analytical calculation, it is difficult to calculate the influence of real pipes, but it is possible to include erosion holes that have a shape as shown in Figure 4. Although Figure 4 is a 2-D picture, the assumed erosion hole is a half sphere. When there is a piezometric head difference  $\phi$  between the sand far away from the hole and the erosion hole itself. The flow to the erosion hole can be written as.

$$Q = 2\pi k\phi R \quad (6)$$

The total flow underneath the dike (Equation (1)) must be equal to the flow in the semi-confined aquifer (Equation (4)) plus the flow through the erosion holes (Equation (6)):

$$k(\phi_0 - \phi_1) \frac{B}{L} = k\phi_1 \frac{B}{\lambda} + n_g 2\pi k\phi_1 R \quad (7)$$

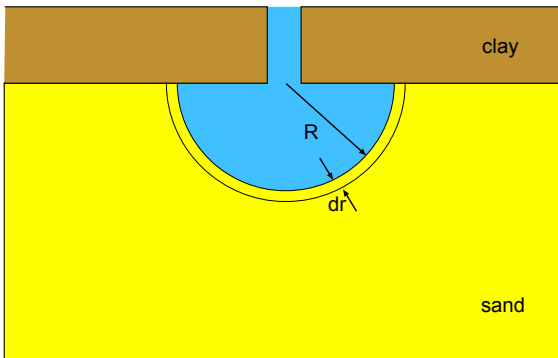


Figure 4. Sketch spherical erosion hole.

Here it is assumed that the erosion holes are present at the toe of the dike. The factor  $n_g$  (1/m) comes in because it is assumed that there are  $n_g$  holes per meter dike. Equation (7) can be written as:

$$\phi_1 = \frac{1}{1 + \frac{L}{\lambda} + 2\pi n_g R \frac{L}{B}} \phi_0 \quad (8)$$

Again, the result depends on the leakage length.

Assume that there is an erosion hole every 50 m (which seems reasonable looking at Figure 1 and Figure 7). For the situation that erosion just starts, a reasonable value for R seems to be 0.1 m (a bit larger than the average pipe diameter when erosion starts). For this situation the last term in the denominator of Equation (8) is 0.075 (parameters from the case Boretta studied in this paper, the length of the fore shore and toe of the dike,  $L=180$  m, the thickness of the sand layer,  $B=30$  m, other parameters mentioned in Table 1). This means that the influence of the erosion hole on  $\phi_1$  is only small, since the 0.075 is small compared to one, which is also in the denominator of equation (8). However, if significant erosion occurs under the dike and  $R=10$  m than the value of this last term is 7.5 and it is the dominant term that determines  $\phi_1$ . Such a large erosion 'hole' will not be circular anymore, but in this calculation it is schematized to a circular hole with the same outflow. In this way, this simple calculation explains that there is in this case a large difference between 'initiation' and 'progression'. As soon as erosion starts,

the piezometric head in the aquifer reduces at the toe of the embankment and this will slow down further erosion due to vertical flow while the horizontal gradient is still too low to initiate erosion. For a short leakage length, this will not be the case and if erosion starts (this will start later because  $\phi_l$  is less), it will be caused by the horizontal gradient and there will be no mechanism to stop the erosion. This corresponds with the results of physical model tests. A slope type exit (which corresponds with  $\lambda = 0$  m needs a higher difference in piezometric head to start backward erosion piping than a hole type exit,  $\lambda = \infty$  m), but erosion continues for the slope type exit. This means that when backward erosion piping occurs in the situation with a short leakage length, this is much more dangerous, because risk of ongoing erosion is greater.

### 3.3 Initiation and progression

Up to now, the start of a sand boil is investigated, thus the initiation of piping. Therefore, the gradient at the sand pipe interface is important. However, failure of the levee will only occur when an ongoing pipe can form underneath the levee, thus progression. For such an ongoing pipe not only the gradient at the boundary between the pipe and the sand is important, but also the overall gradient over the pipe. When this gradient is too small, grains loosened at the tip or along the pipe will settle, clog the pipe and stop the erosion. The following calculation gives an order of magnitude of the gradient needed. Assume that the depth of the erosion pipe is much less than its width. Furthermore, assume that the depth of the erosion pipe is only a small number of grains. This is shown to be the case by Van Beek et al. (2015), see also below. For such a situation the relation between pressure drop over the tube and the shear stress on the boundaries can be written as (see also Figure 5):

$$\Delta p \cdot h = 2\tau \cdot l \quad (9)$$

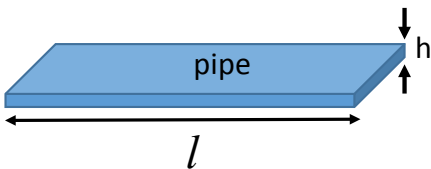


Figure 5. Sketch of schematized pipe used in calculations.

With  $\Delta p$  the pressure difference over the pipe,  $\tau$  the shear stress along the walls of the pipe,  $l$  the length of the pipe and  $h$  the height. Using the relation for the dimensionless Shields shear stress:

$$\tau^* = \frac{\tau}{(\rho_g - \rho_w)gd} \quad (10)$$

With  $\rho_g$  is the density of the grains,  $\rho_w$  the density of water,  $g$  the acceleration of gravity and  $d$  the diameter of the grains. Using equation (9) and (10), it is possible to come to a rather simple relation for the minimum gradient necessary ( $i_{min}$ ) in the pipe to prevent sedimentation:

$$i_{min} = 2\tau^* \cdot \Delta \frac{d}{h} \quad (11)$$

According to the original Shields theory,  $\tau^*$  determined the start of erosion and it is likely that the value of  $\tau^*$  is even lower for sedimentation that would mean that  $d/h$  can be even less, but this is only valid when all erosion is from the tip.

It can be argued that the usefulness of this equation is limited because when  $h$ , the thickness of the pipe increases then  $i_{min}$  decreases. However, as mentioned before, experiments have shown that the thickness of the pipes is only a few grains, see also Figure 6, based on the experiments of Van Beek et al. (2015).

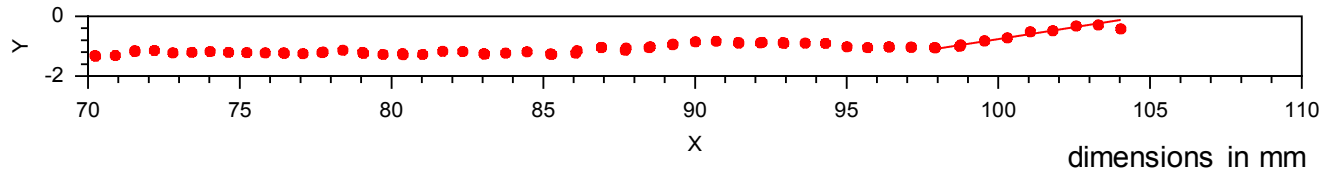


Figure 6. Measured depth of an erosion pipe at the pipe tip in graph with the same horizontal and vertical scale and on this scale the dots represent grains of 380µm sand.

The value of Shields parameter varies with the grainsize and the type of flow, based on calculations by Van Beek (2015) a value of 0.1 is chosen, valid for medium sand and laminar flow.

Using a value for  $h$  of 11 grains (thus  $d/h=11$ ), the minimum value for the gradient as calculated with this formula is quite similar to the value found by Bligh (1915).

The calculation shown here, can only be used to indicate the order of magnitude, since the value of Shields parameter is never determined in such a narrow slit as an erosion pipe, but the calculation indicates that sedimentation of sand in an existing erosion pipe is likely for hydraulic gradients in the pipe lower than the overall critical gradient over the levee as determined by Bligh. Usually the gradient in the pipe is even less than the average gradient over the levee. However, measurements have shown that for small pipes these gradients can be comparable (Van Beek, 2015).

The leakage length, as shown in the previous sections, therefore determines the occurrence of sand boils (initiation). However, ongoing erosion (progression) is only possible if the overall horizontal gradient over the levee reaches values in the order of 0.055. If such a gradient is not reached, there will be sedimentation in the pipe.

#### 4 MITIGATING MEASURES?

It is possible that in the situation of this example no mitigating measures are necessary. Assume that there is such an amount of erosion that the last term in the denominator of equation (8) is by far the largest term in the denominator. In that case  $\phi_l$  will be close to zero, thus the drop in piezometric head over the foreshore and the levee will be 6 m at maximum. The horizontal gradient is then much larger than calculated in Section 3.1. It is now 6/180 or 1/30= 0.033 and it was 0.0043, but still according to Bligh this would be a stable dike with a reasonable safety margin. That means that for this dike section failure due to overtopping is more likely than failure due to a breach caused by piping. Bligh is nowadays not the most sophisticated model, but it is still used to predict the order of magnitude. Calculations with more sophisticated models, as Sellmeijer (1988), were difficult because some parameters from this model were not known. However, even with pessimistic assumptions ( $d_{70}=100$  mm) a factor of safety of 2 was reached against ongoing piping leading to a breach.

This leads to an interesting conclusion: In a location where sand boils as large as trucks are found, see Figure 7, it may be not necessary to install mitigating measures to avoid a dike breach.

Still it is likely that the landowners do not like to have such sand boils in their 'backyard'. In that case, the calculations from the previous sections can be used to design a mitigating measure for the initiation of backward erosion piping. In this case pressure relieve wells may be an option. Pressure relieve wells are chosen because the more traditional measures will not work. A berm is not very effective since, due to the large leakage length, still sand boils will occur. A screen is difficult to install because of the thickness of the impermeable layers and the thickness of the sand layer. A short screen will help to prevent a breach, but will not prevent sand boil and it was discussed that in the present situation a breach is not likely to happen. A pressure relieve well is effective due to the long  $L$ .

Therefore, a relatively limited flow is sufficient to reduce the piezometric head on the landward site. Equation (7) and (8) can be used to design the pressure relieve wells. Assume the wells are of the half circular shape as shown in Figure 4, but now the blue is not water, but a filter with a much (10 times) higher permeability than the sand. The actual shape can be different. Finite element calculations can be used to see whether a filter with a different shape is as efficient at the half spherical shape.

The ratio between the piezometric head in the river and the piezometric head at the toe of the dike can be calculated with Equation (8). It should be realized that the piezometric head of passive pressure relieve wells (wells without a pumping system) cannot be lower than the ground surface, thus 23.75 m in Figure 3, which was assumed to be the piezometric head 0 m level in the calculations. Active pressure relieve wells, with a pumping system, are more effective but there is always a risk that the pumps will not work at the critical moment. Assume a pressure relieve system that realizes a piezometric head at  $\phi_l$  that is only 0.3 the piezometric head at  $\phi_0$ . Due to the passive system this means that if the water level in the river rises 2 m above ground level, as occurred around 11 November 2011 see Figure 3, thus until 25.75 m, the piezometric head at  $\phi_l$  is 24.35 m. Without pressure relieve wells,  $\phi_l$  would be 25.52 m. The reduction in piezometric head can be realized for the parameters of this example with wells every 25 m with an effective diameter of 1.5 m. These wells will result in extra water on the land behind the dike. This extra water is equal to the last term of Equation (7). In this example and with a water level in the river that is 2 m above the ground level at the toe of the embankment this will result in a discharge of 0.3 m<sup>3</sup>/hour/m, which is quite reasonable and can be pumped away easily. Maintenance of such a system is quite important. It has to be verified regularly that the filter is still sufficient permeable.



Figure 7. Sand Boils near the river Po, Boretto, Italy, 2003. (Picture Google Earth, 2003)

## 5 CONCLUSIONS

This example shows clearly that simply knowledge about the horizontal gradient over the dike is not sufficient to predict whether sand boils will occur. In case of the presence of an unconfined aquifer at the landward site of the river, a calculation method as presented by the USACE, blanket theory is more suitable.

The leakage factor and geometry are important parameters to evaluate whether sand boils will occur. The influence of these parameters and the influence of the discharge to the sand boils can be estimated by the formulas presented in this paper.

In the situation as dealt with in this paper, a relatively long impermeable fore shore and a long leakage length, there is a significant difference between the river water level necessary to start sand boils and the level that will lead to breaching of the dike. In this example, it appears that failure due to overtopping is more likely than failure due to piping although the large visible sand boils suggest otherwise.

## REFERENCES

- Bligh, W.G. (1915) Submerged weirs founded on sand. *Dams and weirs: an analytical and practical treatise on gravity dams and weirs; arch and buttress dams, submerged weirs; and barrages*. pp. 151-179. Chicago.
- Cao D. (1994). Countermeasures for seepage erosion of Yangtze River main dikes. *Yangtze River* 25(1): 25-30.
- Gracia Martínez M.F., Marchi M., Tonni L., Gottardi G., Bezuijen A. (2017) Numerical simulation of the groundwater flow leading to sand boil reactivation in the Po River, Proc. 25th EWG-IE, Delft.
- Lane, E.W. (1935). Security from under-seepage masonry dams on earth foundations. *Transactions American Society of Civil Engineers* 100(1): 929-966.
- Schmertmann, J.H. (2000) The no-filter factor of safety against piping through sands. *ASCE. Judgment and innovation at The Heritage and future of the geotechnical engineering profession*:68.
- Sellmeijer, J.B. (1988) *On the mechanism of piping under impervious structures*, PHD-thesis, TU Delft.
- Van Beek, V.M. (2015) *Backward erosion piping, initiation and progression*, PHD-thesis, TU Delft. ISBN 978-94-6259-940-6, <http://repository.tudelft.nl/>
- USACE (1956). *Investigation of underseepage and its control - Lower Mississippi river Levees*. Technical memorandum No. 3-424, Volume 1, Waterways Experiment Station, Vicksburg, Mississippi.
- USACE (2000). *Design and Construction of Levees*. *U.S. Army Corps of Engineers, Manual* No. 1110-2-1913, Washington, DC.
- Yao, Q., Xie, J., Sun, D., Zhao, J. (2009). *Data collection of dike breach cases of China*. Sino-Dutch Cooperation Project Report. China Institute of Water Resources and Hydropower Research.

# Evaluation of Dutch backward erosion piping models and a future perspective

V.M. van Beek & G.J.C.M. Hoffmans

*Deltares*

**Abstract:** The prediction of backward erosion piping is important for safety assessment of dikes in the Netherlands, where subsurface conditions are prone to this erosion mechanism. In the current assessment methodology, the adapted Sellmeijer rule is in use. In combination with the national safety philosophy and uncertainty in input parameters, this model results in high failure probabilities. This paper evaluates the Sellmeijer model and the recently developed Shields-Darcy model alongside recent developments in research on modelling of backward erosion piping, leading to a future perspective.

**Keywords:** Backward erosion piping, Shields-Darcy model, Sellmeijer model, groundwater flow, incipient motion.

## 1 INTRODUCTION

Backward erosion piping is a failure mechanism for dams and dikes whereby particles are transported from granular layers under the action of water flow, leaving a shallow hollow space (a pipe), which progressively develops in the opposite direction of water flow. Given enough time and sufficient hydraulic loads, the process will eventually lead to undermining and breach of the water-retaining structure.

The process typically occurs in granular and relatively uniform layers covered by a cohesive layer that forms a roof to the pipe. This situation is often found in deltaic and fluvial areas. Given an unfiltered exit to the surface and a sufficient head drop across the structure, transported sand accumulates in a ring around the downstream defect, forming a sand boil. Sand boils are often observed during high waters, for example along some of the main rivers in the Netherlands, United States, Italy and China.

In the Netherlands, a few dike failures are attributed to backward erosion piping (Vrijling et al., 2010). More recent case histories are known in the United States, such as Kaskaskia Island and Bois Brule (Navin, 2016). The excessive number of sand boils observed during high water in relation to the relatively small number of failure cases is one of the indicators that optimized prediction of failure should be related to the prediction of the development of the pipe towards the upstream side rather than to the prediction of initial sand boil formation. Experiments at a small and medium scale confirm that sand boils can form at lower water levels than required for pipes to progress towards the upstream side, eventually leading to failure (Van Beek et al., 2015).

Safety assessment in the Netherlands for backward erosion piping consists of a multi-staged approach. The first step (elementary assessment) consists of a set of simple rules to judge the possibility of backward erosion piping for a certain dike section. Dikes that fail this elementary assessment are subjected to a detailed assessment, in which the failure probability is determined for the processes of uplift of the cover layer, transport of particles through a defect (heave) and the progression of the pipe. The uplift calculation is based on the comparison of water pressures in the aquifer and the overlying weight of the blanket layer. For the vertical transport of particles through the defect a critical vertical gradient of 0.3 across the blanket layer is used. The probability for pipe progression is calculated using the Sellmeijer rule (Sellmeijer et al., 2011). The final step in the safety assessment consists of a tailor-

made analysis using more detailed data or software, for example DGFlow (Van Esch et al., 2013) in which the Sellmeijer model is implemented.

Due to several changes in the backward erosion safety assessment in the recent years, such as the inclusion of the length effect (investigated by Kanning (2012)), the transition from dikes regulated by the probability of a flood level to a probability of flooding per section of each dike ring (Vrijling et al., 2011b), the abandoning of Bligh's rule (Bligh, 1910) and an adjustment in the Sellmeijer rule (Sellmeijer et al., 2011), more dike sections fail the new (detailed) assessment. Therefore, a need exists for more advanced piping prediction. This challenge is faced by several research groups around the world. In the past years new insights have been developed, both in experimental and numerical aspects. Parallel to the various laboratory and numerical efforts to understand and simulate the backward erosion process, Hoffmans (2014) has developed a method for prediction of pipe progression, the Shields-Darcy (SD) model.

This paper presents the similarities and differences of the two currently available Dutch backward erosion piping models (the Sellmeijer model and the SD model) alongside with new insights into backward erosion piping, leading to a future perspective of backward erosion modeling.

## 2 EVALUATION OF DUTCH BACKWARD EROSION PIPING MODELS

The Sellmeijer model and the SD model have many similarities. Both models attempt to predict the critical head at which the pipe progresses towards the upstream side by analyzing the groundwater flow towards the pipe, the flow through the pipe, and erosion criteria for onset of particle motion.

### 2.1 Groundwater flow

It is clear that groundwater flow is the driving force for the occurrence of backward erosion piping. In the early days of piping prediction (Bligh, 1910; Lane (1935), many people already stressed the importance of modelling groundwater flow (Harza, 1935, Terzaghi in response to Lane (1935)). It has been demonstrated by various researchers that the effect of scale (represented by seepage length or aquifer depth) on the overall critical gradient can be explained by groundwater flow (Sellmeijer et al., 1989, De Wit, 1984, Van Beek et al., 2014). The critical gradient decreases with increase of scale, which is related to the larger area available for flow.

Initially the Sellmeijer model was developed with analytical equations for 2D groundwater flow towards the pipe (Sellmeijer, 1988) for an infinitely deep aquifer. The limited application of such a model was soon realized, resulting in a mathematical formulation of groundwater flow towards the pipe in homogeneous and isotropic aquifers with finite depth (Sellmeijer et al., 1989). The Sellmeijer model was implemented in the 2D groundwater finite element model MSEEP, in which the pipe was modelled as a boundary condition with the head at the boundary based on equations for pipe flow and limit state equilibrium of particles (Sellmeijer, 2006). In this way numerical calculations could be used for determining the flow towards the pipe, allowing for more complex (multi-layer and anisotropic) subsurface configurations. The rule currently used in the safety assessment (Sellmeijer et al., 2011) is a curve-fit based on thousands of piping calculations in MSEEP. Recently the model has been implemented in DGFlow, a more refined FEM allowing for transient flow (Van Esch et al., 2013), using one-dimensional line elements.

The SD model (Hoffmans, 2014) approximates the 2D groundwater flow towards the pipe for a homogeneous and isotropic sand layer. The groundwater flow is schematized by defining two zones (see Figure 1): Zone A with thickness  $D_{ref}$  close to the pipe (where there is a dip in the hydraulic gradient) and Zone B at greater depth (where the hydraulic head is assumed not to be affected by the flow towards the pipe). It is assumed that the flow through Zone B does not affect the piping mechanism at all.

The thicknesses of zone A and B are not defined directly, but the concept of divided flows is used in the derivation of equations. The derived thickness of Zone A is discussed in section 2.4. Next to this, it is assumed that the flow upstream of the pipe is horizontal, and thus that the gradient upstream of the pipe is constant. In the influence zone of the pipe (in Zone A, below the pipe), the flow towards the pipe is calculated, assuming a linear head drop in the pipe for reasons of simplicity. It is assumed that all of the



## 2.2 Pipe flow

Both the Sellmeijer model and SD model use equations for laminar and incompressible flow in the pipe to assess the load on the particles in the pipe. Sellmeijer continues the 2D approach applied for groundwater flow and assumes pipes of infinite width. For this situation Sellmeijer (1988) solved the Navier-Stokes equations, resulting in the Hagen-Poiseuille equation for parallel plates:

$$\rho g \frac{d\varphi}{dx} a^3 = 12q\mu \quad (2)$$

in which  $a$  is the pipe height. Hoffmans (2014) uses an equation for circular pipes with the hydraulic radius, applicable for different shapes, for which the equation holds:

$$\pi\rho g S_{pipe} NR^4 = \frac{1}{2} \mu Q \quad (3)$$

in which  $R$  is the hydraulic radius of the pipe. The total flow is multiplied by  $N$ , representing the number of pipes. The load acting on the particles on the pipe bottom is represented by the wall shear stress, defined as below for infinitely wide pipes (approach Sellmeijer) and pipes with hydraulic radius  $R$  (SD-model) respectively:

$$\tau_w = \frac{a}{2} \rho g \frac{d\varphi}{dx} \quad (4)$$

and

$$\tau_w = R \rho g S_{pipe} \quad (5)$$

The pipe shape is relevant in connecting the flow and head loss in the pipe to a shear stress. Measurements in experiments (Hanses, 1985 and Van Beek et al., 2015) indicate that the pipe is relatively shallow compared to its depth. Ratios of width and depth were analysed by Van Beek (2015) and were found to be in the order of 7-13 for two analysed different sand types, i.e. such that the assumption of the equation for parallel plates is justified. The consequences of using equations with a hydraulic radius rather than with a flat wide pipe is not investigated here, but the parallel plates seem a more obvious choice in future considerations.

The assumption of laminar flow is most likely valid for fine to medium sands (Robbins and Van Beek, 2017), but may not be suited for all sand types encountered. More research is required to investigate the effect of wall turbulence and turbulent flow in the pipe on backward erosion piping.

## 2.3 Erosion criteria

To determine whether a pipe can or cannot progress, erosion criteria need to be defined. Hanses (1985) defined two types of erosion relevant for pipe progression: erosion at the pipe tip, causing the pipe to lengthen and referred to as primary erosion, and erosion of the pipe walls and bottom, deepening and widening the pipe, referred to as secondary erosion.

Both the Sellmeijer model and the SD model rely on secondary erosion only, and thus base the pipe progression on the critical conditions in the pipe. In the Sellmeijer model the pipe is assumed to be in equilibrium when the particles at the pipe bottom are in equilibrium at every location in the pipe. When this equilibrium is exceeded, the pipe is assumed to lengthen.

In the previous section the shear stress exerted by the water on the particles is described for the situation of an infinitely wide pipe. The limit-state equilibrium is defined in the Sellmeijer model by defining a critical shear stress according to White (1940), who considered the equilibrium of forces on the particles in relation to the distribution of the load over a group of particles:

$$\tau_c = \eta \frac{\pi}{6} \gamma'_p d \tan \theta \quad (6)$$

In which  $\eta$  is the coefficient of White and  $\theta$  is the bedding angle (rolling resistance in top layer of grains). In White's approach the coefficient  $\eta$  was originally combined with another coefficient  $\alpha$ , the former describing the ratio of the area of the grains over which the shear stress is divided to the total area considered, the latter being an experimental coefficient to account for the action of forces above the gravity of the grain. The combined coefficient of  $\alpha\eta$  was later simplified by Sellmeijer to  $\eta$ . Based on the flume experiments on two sand types in which White studied the incipience of motion in laminar flow, Sellmeijer defined a constant and conservative (compared to the values suggested by White) value of 0.25 for the coefficient of White. The bedding angle, also derived by White in two experiments, was used later as a calibration parameter in large scale backward erosion piping experiments (described later on in the section on calibration) and applied as a constant in the current assessment rule. The particle diameter,  $d$ , was not described in detail by White, but Sellmeijer (1988) assumed that the representative particle size should be between  $d_{65}$  and  $d_{75}$  since fine particles are more easily transferred than larger particles, and larger particles need to be transported as well. In later publications the  $d_{70}$  was chosen as the representative grain diameter (TAW, 1999, Sellmeijer et al., 2011).

In the SD model the pipe lengthens, widens and deepens when the average gradient in the pipe exceeds a critical value ( $S_{\text{pipe}} > S_{\text{pipe,c}}$ ). The progression is therefore determined by the equilibrium of particles in the pipe (secondary erosion), rather than by a criterion for loosening and detaching the intact sand bed upfront of the pipe (primary erosion). Hoffmans (2014) was the first to apply the Shields diagram (1936) for incipient motion to backward erosion piping. In this approach the threshold of particle movement is governed by balancing the driving force and the resistance force, similarly to the approach by White, but by lumping the unknown coefficients into one parameter, the critical Shields parameter:

$$\tau_c = \Psi_c \gamma'_p d_{50} \quad (7)$$

The Shields parameter is determined using many flume experiments, both in turbulent and laminar flow, and was found to be a function of the Reynolds shear number. Due to the pressure fluctuations typical for turbulent flow, particles move easier in turbulent flow than in laminar flow. Since the flow in the pipes is assumed to be laminar, Hoffmans (2014) proposed a relation for estimating the critical shear stress, based on the laminar flow flume experiments by Govers (1987), Pilotti and Menduni (2001) and Loiseleux et al. (2005), in the range of  $0.1 \text{ mm} < d_{50} < 0.5 \text{ mm}$ :

$$\Psi_c = 0.2(D_*)^{-1/3} \text{ for } 2 \leq D_* \leq 15 \quad (8)$$

in which  $D_*$  is the dimensionless particle number:

$$D_* = d_{50} \left( \frac{\Delta g}{\nu^2} \right)^{1/3} \quad (9)$$

Although the critical Shields parameters were determined based on the  $d_{50}$  (equation 7), Hoffmans and Van Rijn (2017) proposed to use the  $d_{15}$  instead of the  $d_{50}$  to account for grading in the sand, since according to the load and strength probability distributions proposed by Grass (1970), the finer particles will move first for sands with  $d_{90}/d_{10}$  under 4:

$$\tau_{c,k} = \Psi_c \gamma'_p d_{15} \quad (10)$$

The approach by Grass was developed for turbulent flow and it is yet unclear whether it is also applicable to laminar flow. The use of a median particle diameter could be advocated based on the observations by

Govers (1987), who found that in laminar flow particles tend to move as a grain carpet, giving a sharply discernible critical state for incipient motion, due to the lack of fluctuating shear stresses typical for turbulent flow.

For graded sands with  $d_{90}/d_{10} > 4$ , the finer particles are not representative for describing the initiation of motion as they could be locked between the coarser ones (Van Rijn, 2014). In such cases it is recommended to use  $d_{50}$ , or an upper limit, for example  $d_{70}$ . It is noted that equation 9 was not altered with respect to the representative grain size.

Recent research suggests (Robbins and Van Beek, 2017) that the Shields approach, applied with  $d_{50}$  as representative diameter, is reasonable for the prediction of the gradient in the pipe. The use of a constant bedding angle in the approach by White causes an overestimation of the critical gradient, unless this is corrected for in other parameters (as is done in the adapted rule in Sellmeijer et al., 2011). More research is required to understand the incipient motion of particles for the specific conditions of shallow pipes in sands of variable density.

Recent developments focus not only on criteria for secondary erosion, but also on criteria for primary erosion. Several authors agree that a local scale-independent criterion exists that causes the progression of the pipe (Hanses, 1985, Van Beek et al., 2015, Robbins et al., t.b.p., Rotunno et al., 2017). An important aspect is that this is a *local* phenomenon: the velocities and gradient upstream of the pipe locally rise due to the concentration of flow. This was well illustrated by De Wit (1984) using Figure 2, which shows the head drop below an impervious structure, with identical local gradients near the exit, but varying average gradients for two scales. A similar figure could be drawn for the situation with a pipe. Even when a criterion for primary erosion would control the progression, secondary erosion affects the head loss in the pipe and therefore indirectly influences the local gradient upstream of the pipe.

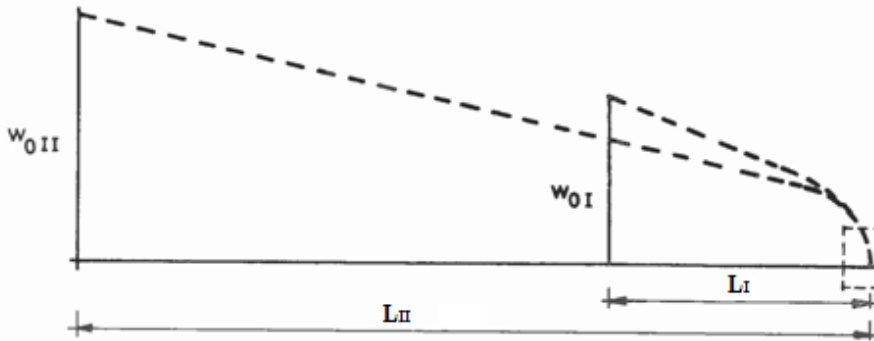


Figure 2: Head distribution in critical conditions (critical head drop denoted by  $w_0$ ) in two identical set ups, but with different seepage lengths. Identical local gradients, but varying overall gradients below impervious structures of different sizes (adapted after De Wit, 1984)

## 2.4 Synthesis

Originally the Sellmeijer model combined the analytical equations for groundwater flow to the equations for pipe flow and particle equilibrium to find an ‘equilibrium head’ for each pipe length. Later (Sellmeijer, 2006) numerical groundwater calculations were conducted to solve the specific boundary conditions and to find the equilibrium head at different pipe lengths. The maximum equilibrium head found in this way is denoted as the critical head. The specific boundary condition which is solved is obtained by combining equations 2, 4 and 6, eliminating the pipe height, and reads:

$$Q \left( \frac{d\varphi}{dx} \right)^2 = \frac{\gamma_w}{12\mu} \left( \frac{\pi \gamma_p'}{3 \gamma_w} d\eta \tan \theta \right)^3 \quad (11)$$

By curve-fitting and comparison with a very large number of numerical calculations in MSEEP a relation was obtained between the critical head and the material properties, for a standard dike geometry which agrees very well with the numerical results and which reads (Sellmeijer et al., 2011):

$$F_R = \eta \frac{\gamma'_p}{\gamma_w} \tan \theta$$

$$\frac{H_c}{L} = F_R F_S F_G \quad F_S = \frac{d_{70}}{\sqrt[3]{\kappa L}} \quad (12)$$

$$F_G = 0.91 \left( \frac{D}{L} \right) \left( \frac{D}{L} \right)^{0.28} - 1$$

The SD model is synthesized starting with the simplified equation for groundwater flow (equation 1, variables illustrated in figure 3).

$$\frac{H_c}{L} = S_{pipe,c} + \left( 1 - \frac{\ell_c}{L} \right) (S_{sand,c} - S_{pipe,c}) \quad (13)$$

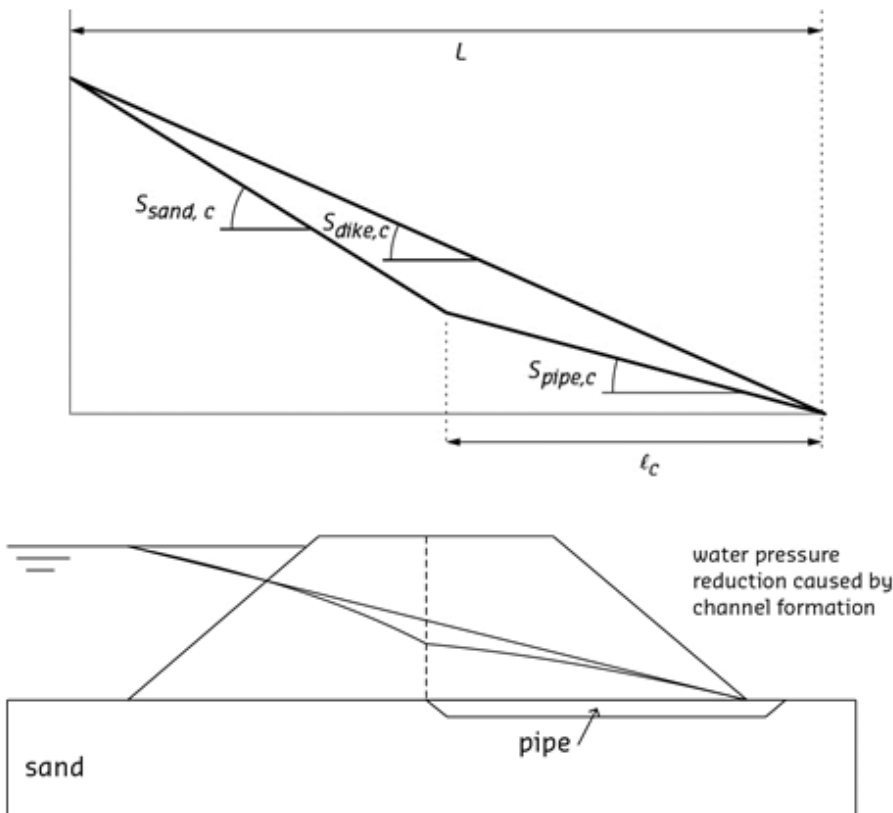


Figure 3: Schematization of critical hydraulic gradients

To obtain the critical gradient across the dike, three unknowns need to be determined, which are the critical average gradient upstream of the pipe  $S_{sand,c}$ , the critical pipe length  $\ell_c$  and the critical pipe gradient  $S_{pipe,c}$  (at which the particles are in limit-state equilibrium). Using the continuity equation in

zone A (thus assuming that the flow through zone A is equal to the total flow through the pipe), the critical hydraulic gradient in the sand can be given by:

$$S_{sand,c} = S_{pipe,c} \frac{\Omega_{s,A,c}}{\Omega_{p,c}} \quad (14)$$

In this equation the ‘resistance of the sand  $\Omega_{s,A,c}$ ’ is unknown. Therefore a ‘virtual discharge’  $dQ^*$  is introduced in zone B. The total flow through zone B, including the virtual discharge

$$Q_2^* = Q_2 + dQ^* \quad (15)$$

is assumed to be equal to  $\frac{S_{pipe}}{\Omega_s}$ . Using this equation, it can be derived that (for further explanation see Hoffmans, unpublished):

Hoffmans, unpublished):

$$\Omega_{s,A,c} = \Omega_s + \Omega_{p,c} \quad \text{with } \Omega_s = (BDK)^{-1} \quad (16)$$

When this equation is combined with equation 14, the resulting equation for  $S_{sand,c}$  is:

$$S_{sand,c} = \left(1 + \frac{\Omega_s}{\Omega_{p,c}}\right) S_{pipe,c} = S_{pipe,c} + Q_{p,m,c} \Omega_s = S_{pipe,c} + \frac{q_{p,m,c}}{DK} \quad (17)$$

Hence, the critical hydraulic dike gradient may be written as (see also Eq. 1):

$$\frac{H_c}{L} = S_{pipe,c} + \left(1 - \frac{\ell_c}{L}\right) \frac{q_{p,m,c}}{DK} \quad (18)$$

Noteworthy, but not required for the further analysis of the critical gradient is that the thickness of zone A can now be written based on the continuity equation ( $Q_{1,A} = Q_{p,m}$ ) as:

$$D_{ref} = \frac{Q_{p,m}}{BKS_{sand}} = \frac{q_{p,m}}{KS_{sand}} \quad (19)$$

or with Equation 15:

$$D_{ref} = D \left(1 - \frac{S_{pipe}}{S_{sand}}\right) \quad (20)$$

The average gradient in the pipe, which is an unknown in equation 18 is based on the equilibrium of particles (Equation 5 and 10):

$$S_{pipe,c} = \frac{\Psi_{lam,c} (\rho_s / \rho - 1) d_{15}}{R_c} \quad (21)$$

Since the hydraulic radius is unknown Eq. 21 is rewritten by using equation 5 and the definition of the Reynolds number:

$$S_{pipe,c} = \frac{\sqrt{g} (\Psi_{lam,c} (\rho_s / \rho - 1) d_{15})^{3/2}}{v \sqrt{\alpha_{Re,\ell}}} \quad (22)$$

where the calibration parameter  $\alpha_{Re,\ell}$  is assumed to be a constant (Hoffmans and Van Rijn, 2017) and includes the variation in pipe height from upstream to downstream (through  $C_{\ell,c} = \frac{\ell_{p,h,c}}{\ell_{p,m,c}}$ ) and the Reynolds number at the downstream side of the pipes.

$$\alpha_{Re,\ell} = \frac{1}{2} (1 + C_{\ell,c})^2 Re_{m,c} \quad (23)$$

The normalized critical pipe length is determined using Equation 24, which was based on the assumption that the critical pipe length depends on the shape of the aquifer (D/L) and the pipe gradient, using computational results of the Sellmeijer model. The factor  $\alpha_f$  is a calibration factor:

$$\frac{\ell_c}{L} \approx \exp \left( - \left( \frac{\alpha_f D}{L} \right)^2 S_{pipe,c} \right) \quad (24)$$

The total flow through the pipe,  $q_{p,m,c}$  can be rewritten using the Reynolds number in the pipe at the downstream side ( $q_{p,m,c} = 2 Re_{m,c} v$ ). The Reynolds number ( $Re_{m,c}$ ) is not known, but is estimated based on the mean grain size and a calibration parameter  $\ell_{Re}$ :

$$2 Re_{m,c} \approx \frac{d_{50}}{\ell_{Re}} \quad (25)$$

This is justified as follows. The flow through the pipe and its shape depend on the flow towards the pipe. Consequently, the critical pipe dimensions (through  $C_{\ell,c}$  giving the ratio of the pipe diameter at the exit point and the middle of the seepage path) are related to the relation between pipe resistance and sand resistance ( $C_{G,v} = \Omega_p / \Omega_{s,A}$ ). If these assumptions are taken into account and applying equation 5 then (see also Hoffmans (unpublished) for a justification):

$$\frac{2(1 + C_{G,v}) C_{\ell,c}^4}{1 + C_{\ell,c}} = 1 \quad (26)$$

If the vertical groundwater can easily flow into the pipes (thus if  $C_{G,v} \rightarrow \infty$  or if  $K$  is large) then the pipes are cone-shaped ( $C_{\ell,c} \rightarrow 0$ ). If the vertical inflow is negligible (thus if  $C_{G,v} \rightarrow 0$  or if  $K$  is small) then the pipe geometry does not alter ( $C_{\ell,c} \rightarrow 1$ ). Using the Kozeny-Carman equation ( $K \propto d^2$ ) the following approximation can be made (for  $0_{|d=0.5 \text{ mm}} < C_{\ell,c} < 0.7_{|d=0.2 \text{ mm}}$ ).

$$\frac{1 + C_{\ell,c}}{d^{-1/2}} \approx \text{constant} \quad (27)$$

Since the summation of the vertical inflow increases from the entry points to the exit point the flow velocities and Reynolds numbers in the pipes increase. On the landside the critical Reynolds number is at maximum and is written as:

$$\text{Re}_{m,c} = \frac{4 \text{Re}_c}{(1 + C_{\ell,c})^2} \quad (28)$$

Hence,

$$2 \text{Re}_{m,c} \nu \approx \frac{d_{50} \nu}{\ell_{\text{Re}}} \quad (29)$$

Note that according to the SD-model thick sand layers (say  $D/L > 0.5$ ) are very unstable since the critical pipe length equals approximately nil. In such cases, the critical Shields parameter must be lowered from ‘general transport’ to ‘no erosion’ which results in a smaller allowable dike gradient.

## 2.5 Calibration

Both the Sellmeijer model and the SD model were calibrated to laboratory experiments. Sellmeijer’s model was calibrated in different research periods. Shortly after the development of the initial rule (Sellmeijer et al., 1989), large scale experiments were conducted in the DeltaFlume (Silvis, 1991), using only one sand type. The bedding angle was calibrated to these experiments and based on expert judgment a value of 41 degrees was selected in combination with White’s coefficient of 0.25 for prediction of piping in practice (TAW, 1999). After the numerical implementation of the Sellmeijer model in 2006, a bedding angle of 37 degrees was selected based on the same calibration (Sellmeijer, 2006). At the time it was initially presented, it was already realized that especially for coarse grained material the rule did not match well with experimental results (Weijers and Sellmeijer, 1993). A renewed calibration was conducted in 2011, after a series of small-, medium- and full-scale experiments (Van Beek et al., 2011). A multi-variate analysis was conducted on the results of small-scale experiments only, relating material properties like hydraulic conductivity, grain size ( $d_{70}$ ), uniformity coefficient and roundness to the critical head. From this analysis it was concluded that the effect of roundness was limited (although the tested selection of natural sands did not show a lot of variation in roundness), and the effect of grain size was smaller compared to the original Sellmeijer rule. Lacking a theoretical explanation, the rule was adjusted using the empirical factors obtained from the multi-variate analysis, while retaining the fitted bedding angle from the previous calibration. The empirical fitting leads to the clear disadvantage for the model of not being applicable outside the tested range of sand types.

The SD model counts three unknowns: a length scale parameter ( $l_{\text{Re}}$ ), a groundwater coefficient ( $\alpha_f$ ) and a Reynolds coefficient ( $\alpha_{\text{Re},l}$ ). All available laboratory experiments (leaving out duplicates) from Dutch literature were used to calibrate and validate these three parameters.

Calibration of models with field or laboratory data is often inevitable. However, when extrapolating outside the calibration range, it is of importance to verify that the calibration parameters are really constants under all circumstances. The bedding angle, used as a calibration parameter in the Sellmeijer model is essentially not a constant, and results in overestimation of the critical shear stress for coarser sands (Van Beek et al., 2015), which required a correction through empirical factors. The length scale and geometric pipe coefficients in the SD model are a function of several parameters including the Reynolds number in the pipe, in turn dependent on the velocity and particle depth in the pipe. The consequence of keeping these two parameters constant for all circumstances is not investigated here, although the fit proves to be good for experiments at small and medium scale and Hoffmans and Van Rijn (2017) have verified these constants at different scales.

## 2.6 Validation

After adaptation of the Sellmeijer rule with the empirical factors based on the small-scale experiments, the result was calibrated with the medium- and full-scale experiments (Sellmeijer et al., 2011). It was

$$\text{Re}_{m,c} = \frac{4 \text{Re}_c}{(1 + C_{\ell,c})^2} \quad (28)$$

Hence,

$$2 \text{Re}_{m,c} \nu \approx \frac{d_{50} \nu}{\ell_{\text{Re}}} \quad (29)$$

Note that according to the SD-model thick sand layers (say  $D/L > 0.5$ ) are very unstable since the critical pipe length equals approximately nil. In such cases, the critical Shields parameter must be lowered from ‘general transport’ to ‘no erosion’ which results in a smaller allowable dike gradient.

## 2.5 Calibration

Both the Sellmeijer model and the SD model were calibrated to laboratory experiments. Sellmeijer’s model was calibrated in different research periods. Shortly after the development of the initial rule (Sellmeijer et al., 1989), large scale experiments were conducted in the DeltaFlume (Silvis, 1991), using only one sand type. The bedding angle was calibrated to these experiments and based on expert judgment a value of 41 degrees was selected in combination with White’s coefficient of 0.25 for prediction of piping in practice (TAW, 1999). After the numerical implementation of the Sellmeijer model in 2006, a bedding angle of 37 degrees was selected based on the same calibration (Sellmeijer, 2006). At the time it was initially presented, it was already realized that especially for coarse grained material the rule did not match well with experimental results (Weijers and Sellmeijer, 1993). A renewed calibration was conducted in 2011, after a series of small-, medium- and full-scale experiments (Van Beek et al., 2011). A multi-variate analysis was conducted on the results of small-scale experiments only, relating material properties like hydraulic conductivity, grain size ( $d_{70}$ ), uniformity coefficient and roundness to the critical head. From this analysis it was concluded that the effect of roundness was limited (although the tested selection of natural sands did not show a lot of variation in roundness), and the effect of grain size was smaller compared to the original Sellmeijer rule. Lacking a theoretical explanation, the rule was adjusted using the empirical factors obtained from the multi-variate analysis, while retaining the fitted bedding angle from the previous calibration. The empirical fitting leads to the clear disadvantage for the model of not being applicable outside the tested range of sand types.

The SD model counts three unknowns: a length scale parameter ( $l_{\text{Re}}$ ), a groundwater coefficient ( $\alpha_f$ ) and a Reynolds coefficient ( $\alpha_{\text{Re},l}$ ). All available laboratory experiments (leaving out duplicates) from Dutch literature were used to calibrate and validate these three parameters.

Calibration of models with field or laboratory data is often inevitable. However, when extrapolating outside the calibration range, it is of importance to verify that the calibration parameters are really constants under all circumstances. The bedding angle, used as a calibration parameter in the Sellmeijer model is essentially not a constant, and results in overestimation of the critical shear stress for coarser sands (Van Beek et al., 2015), which required a correction through empirical factors. The length scale and geometric pipe coefficients in the SD model are a function of several parameters including the Reynolds number in the pipe, in turn dependent on the velocity and particle depth in the pipe. The consequence of keeping these two parameters constant for all circumstances is not investigated here, although the fit proves to be good for experiments at small and medium scale and Hoffmans and Van Rijn (2017) have verified these constants at different scales.

## 2.6 Validation

After adaptation of the Sellmeijer rule with the empirical factors based on the small-scale experiments, the result was calibrated with the medium- and full-scale experiments (Sellmeijer et al., 2011). It was

found that the adapted rule performed better than the original rule, especially for coarser sand, for which the original rule was found to be unsafe.

The SD model was validated using basically the same set of experiments as for the calibration, by applying the duplicates of the tests. Next to this, the SD model is verified by using three Delta-flume experiments and three IJkdijk tests, for which the model predicts well. Finally the results of the SD model were compared to three field cases, one Chinese dike (failed dike) and two Dutch dikes (heavy sand boils). It should be realized that the input parameters of these field cases are rough estimates, and are therefore not very suitable for the precise validation of models. Next to this, many aspects that are known to affect the occurrence of piping are not yet included in the models, such as heterogeneity of the subsurface and 3D-flow, which also complicates the validation of models with field cases. Field cases can be used to compare general trends, but are not well suited for validation on an individual basis.

One general trend that is essential for the extrapolation to the field is the effect of scale on the critical gradient. Figure 4 shows the scale effect in different models resulting from increase of length, while retaining D/L ratio and sand characteristics (fine sand). It is noted here that due to the constant D/L ratio, the same trends can be found when using the aquifer thickness as reference scale. Figure 5 shows a similar graph with experimental and field data. Although obviously more parameters that influence the critical gradient are not plotted, causing scatter, a general decrease with increase of scale can be observed.

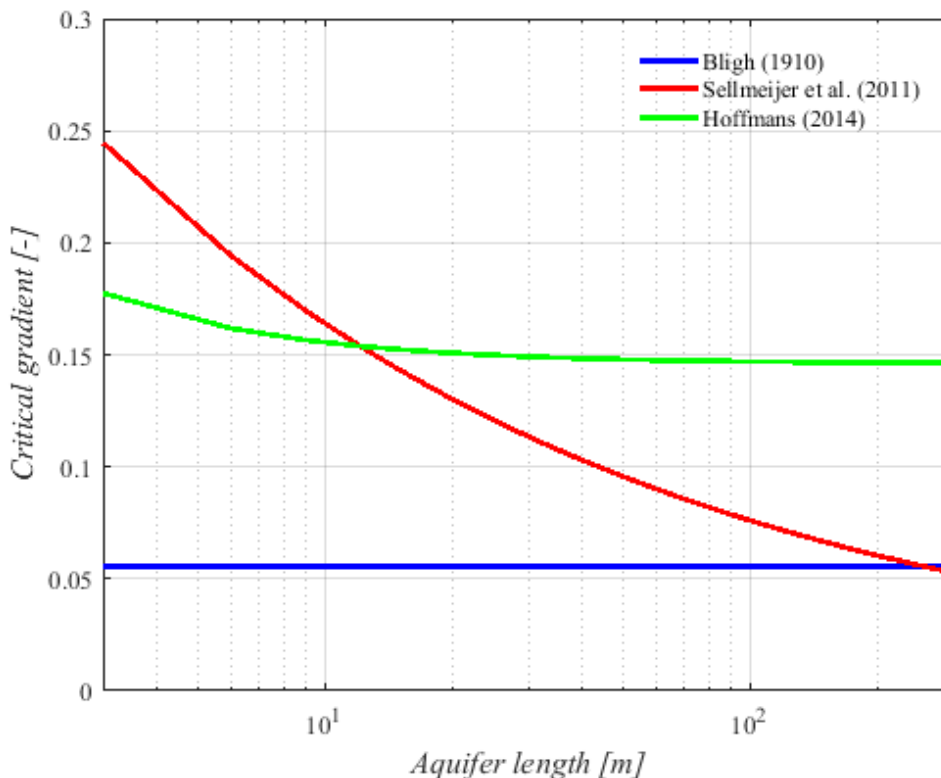


Figure 4. Illustration of the scale effect (represented by L) in different models, given a constant D/L ratio of 1/3 and constant material properties (fine sand)

Comparison of the graphs shows that a decrease of critical gradient with increase of scale is expected, but that the degree by which critical gradient decreases with scale significantly varies for the different models. The scale effects are much more limited in the SD model (and even absent once a certain aquifer depth is exceeded), compared to the Sellmeijer model, which converges to the rule of Bligh for the chosen configuration. It is noted that the recommendation for the SD model to move from 'general transport' to 'no erosion' is not followed for these cases since the D/L ratio is much smaller than 1. A possible cause for the difference in outcome is the inclusion of groundwater flow in deeper layers in the

Sellmeijer model, as opposed to the SD layer, in which it is assumed that flow through deeper layers does not affect the piping process. Next to this, the groundwater flow is simplified for the SD model, whereas it was numerically calculated for the Sellmeijer model (using MSEEP).

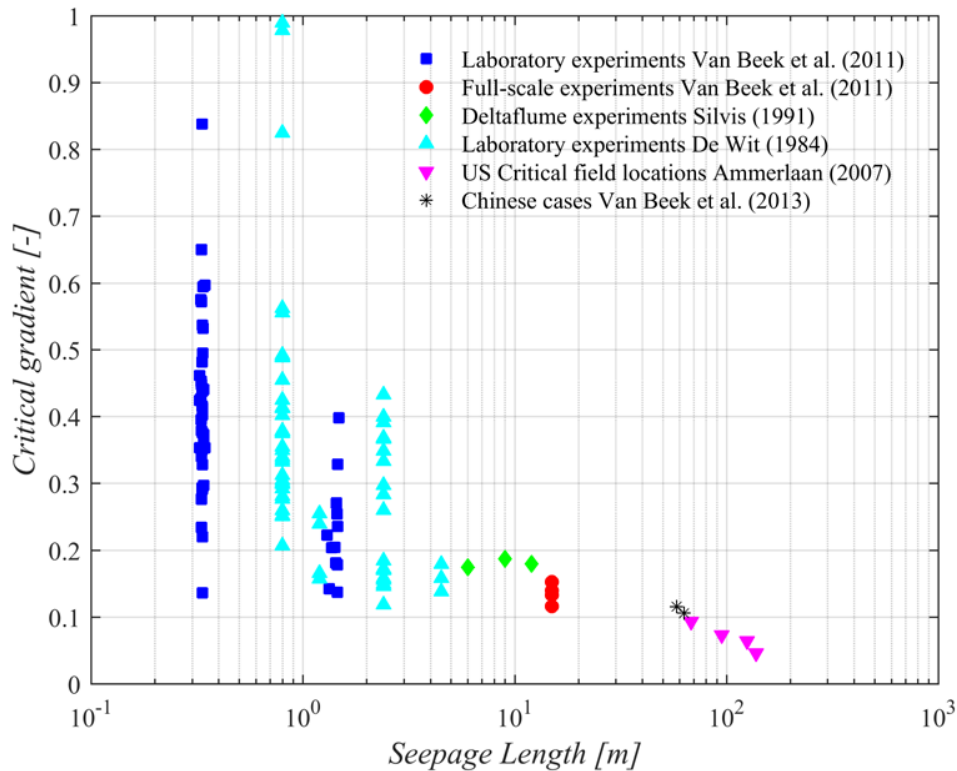


Figure 5. Illustration of the scale effect (as represented by  $L$ ) in laboratory experiments and field data

### 3 A FUTURE PERSPECTIVE ON BACKWARD EROSION PIPING MODELLING

In the last years, a significant amount of research has been conducted to better understand the occurrence of backward erosion piping. The models discussed here, the Sellmeijer model and SD model both simplify reality. Since a model is always a simplification of reality, this is essentially not an issue. However, if effects are excluded or simplified that turn out to be of major importance to the outcome of the model, the model may become impractical or even incorrect. For example, recent research shows that the assumption of 2D flow may lead to unsafe predictions, whereas heterogeneity may lead to additional strength. Calibration with field cases may overcome this issue, as can be seen in the model of Lane (1935), which has a limited theoretical basis, but is generally considered as a safe method for design against backward erosion piping for structures with a vertical component in the seepage path, due to the numerous cases on which it relies. For backward erosion piping without vertical structures this is more difficult, since only a few failure cases are available and the relevant parameters are difficult to determine accurately. Sand boils indicate a susceptibility to piping, but are known to occur at lower water levels than the critical head and therefore do not give an indication of the critical head. Given the limited number of field cases, much depends on the extrapolation from laboratory results to the field, which requires a full understanding of the physical processes involved and the characteristics in the field. Once the physical processes are fully understood, a simplification of reality is still often requested and can be safe when conservative choices are made for schematization. An accumulation of conservative choices however, e.g. homogeneous subsurface, steady-state groundwater flow calculations, conservative input

parameters, will result in a safe outcome, but this can also be impractical in the field due to the lack of distinction.

At this point several steps still need to be taken for reliable prediction of piping in practice, consisting of better characterization of the field situation, in terms of heterogeneity and groundwater flow, the collection of observations, a better understanding of the mechanism in various (heterogeneous) soil types, including the development of criteria for pipe lengthening, widening and deepening, and the modeling of the mechanism. Based on the current state of the art of backward erosion modelling, this will, among other things, involve 3D modeling of the process, including the expected variability of the sand layer, and validation with full-scale field tests. Calculation rules based on simplified schematizations may still be useful in an early stage of a safety assessment, if the physical processes are well enough understood to extrapolate to the field.

Considering this, aspects of the Sellmeijer model and SD model will likely still be found in the future developments, such as the Shields approach (not only in laminar but also in turbulent conditions) for prediction of the head loss in the pipe, the pipe flow through shallow and wide pipes and the groundwater flow towards the pipe (numerically calculated, allowing for complex configurations).

## 4 CONCLUSIONS AND RECOMMENDATIONS

This paper evaluates two Dutch backward erosion piping models, the Sellmeijer model and the SD model. The models are rather similar, since both rely on erosion criteria which are driven by 2D groundwater flow and laminar flow through the pipe. Although the models are similar, the outcomes of the models are very different, especially for prototype conditions.

The SD model simplifies the groundwater flow, by assuming zones in the subsurface where the head drop changes linearly. In the Sellmeijer model the flow towards the pipe is calculated numerically in MSEEP. Recent investigations (Vandenboer et al. (2014a and 2014b), Van Beek et al. (2015),) indicate the importance of 3D groundwater flow calculations. Models calibrated with experiments with 2D exits and limited width may overestimate the critical gradient, leading to an unsafe result.

Erosion criteria control the progression of the pipe. The Sellmeijer model relies on erosion in the pipe only, using a particle equilibrium based on the approach by White (1940), with a constant value for the bedding angle calibrated in large-scale experiments, whereas in the SD model the more widely accepted Shields approach is applied. Recent experiments indicate the existence and relevance of a local, scale-independent critical gradient upstream of the pipe, which is currently not included in the models.

Both models have several calibration parameters, although the used set of experiments for calibration differs. The SD model was calibrated with an extensive set of laboratory experiments and validated with the duplicate experiments of this set, whereas the Sellmeijer model was calibrated with one series of small-scale experiments and validated with medium- and full-scale experiments. The SD model was verified with six large scale experiments and compared with some field cases. Here it is noted that field cases can be used for validation of general trends, but single cases cannot be easily used for validation of models. Extrapolation of the models to the field therefore remains challenging. Based on available experiments and cases it can be concluded that considerable scale effects exists.

The two models as discussed have been calibrated and validated with tests on a small, medium and a large scale. They both yield satisfactory results for the experiments that have been investigated. However, for prototype conditions large differences occur, which are likely related to the manner of groundwater flow calculation. In addition, important aspects like 3D flow, heterogeneity and time dependency are currently not included in the assessment rules, although the Sellmeijer model implemented in DGFlow (Van Esch et al., 2013) already offers far more possibilities than the rules. Future developments should aim for an improved piping model, which include aspects of both models, such as the Shields approach for prediction of the head loss in the pipe, the pipe flow through shallow and wide pipes and the numerical calculation of groundwater flow towards the pipe, combined with new insights on a local, scale-independent criterion for progression at the pipe tip. In addition better subsurface characterization and collection of field observations are essential for model validation and safety assessment.

## LIST OF NOTATIONS

$B$	width of the dike (m)
$C_{G,v}$	vertical seepage transmissivity (-)
$C_\ell$	geometry factor of pipe (-)
$d$	particle diameter (m)
$d_i$	particle diameter for which $i\%$ of the sediment particles is finer than $d_i$ (m)
$D$	thickness of the sand layer (m)
$D_{ref}$	(= $D_{eff}$ ) thickness of zone A (below the pipes) (m)
$D^*$	[= $d_{50}(\Delta g/v^2)^{1/5}$ ] dimensionless particle diameter related to $d_{50}$ (-)
$g$	acceleration due to gravity ( $m/s^2$ )
$H$	local head (m)
$H_1$	river level (m)
$H_2$	water level in the ditch or surface level (m)
$H_\ell$	hydraulic head where erosion in the pipe starts (m)
$K$	hydraulic conductivity of sand layer (m/s)
$\ell$	length of pipe (m)
$\ell_{Re}$	(= $18 \cdot 10^{-6}$ m) length scale (m)
$L$	seepage length (m)
$q$	discharge per unit width, outflow ( $m^2/s$ )
$Q$	discharge ( $m^3/s$ )
$Q_1$	(= $Q_{1,A} + Q_{1,B}$ ) discharge in sand layer at the inflow section (riverside) ( $m^3/s$ )
$Q_2$	discharge in sand layer at outflow section (landside) ( $m^3/s$ )
$RD$	packing density (-)
$RD_m$	(= 0.725; default value) packing density (-)
$Re$	Reynolds pipe number (-)
$Re_m$	Reynolds pipe number on the landside (at $x = 0$ ) (-)
$R$	hydraulic radius (m)
$S$	average hydraulic gradient (-)
$S_{dike}$	average hydraulic dike gradient (-)
$S_{pipe}$	hydraulic pipe gradient (mean hydraulic gradient in the pipes) (-)
$S_{sand}$	hydraulic sand gradient (mean hydraulic gradient upstream of the pipes) (-)
$S_{vert}$	hydraulic vertical gradient (in zone A) (-)
$\alpha_f$	(= 5) groundwater coefficient (-)
$\alpha_{Re,\ell}$	(= 6) geometric pipe coefficient (-)
$\gamma'_p$	under water particle weight ( $N/m^3$ )
$\Delta$	(= $\rho_s/\rho_w - 1$ ) relative particle density (-)
$\eta$	White coefficient (-)
$\kappa$	(= $K/v/g$ ) intrinsic permeability ( $m^2$ )
$\nu$	kinematic viscosity ( $m^2/s$ )
$\rho$	density of water ( $kg/m^3$ )
$\rho_s$	density of particles ( $kg/m^3$ )
$\tau_c$	critical mean wall shear stress ( $N/m^2$ )
$\tau_{c,k}$	critical characteristic wall shear stress ( $N/m^2$ )
$\tau_w$	mean wall shear stress ( $N/m^2$ )
$\Psi$	Shields parameter (-)
$\Omega$	resistance of conductor (ohms)
$\Omega_p$	pipe or overall pipe resistance ( $s/m^3$ )
$\Omega_{p,h}$	horizontal pipe resistance ( $s/m^3$ )

$\Omega_s$	horizontal seepage resistance (s/m <sup>3</sup> )
$\Omega_{s,A}$	horizontal seepage resistance in zone A (s/m <sup>3</sup> )
$\Omega_{s,B}$	horizontal seepage resistance in zone B (s/m <sup>3</sup> )
$\Omega_{s,h}$	horizontal seepage resistance in zone A (s/m <sup>3</sup> )
$\Omega_{s,v}$	vertical seepage resistance in zone A (s/m <sup>3</sup> )

### Subscripts

$c$	critical
$\ell_{lam}$	laminar

### REFERENCES

- Ammerlaan, P.R.M. (2007). *Levees and levee evaluation – The Dutch and US practice compared*. Msc. Thesis, TU Delft.
- Bligh, W.G. (1910). Dams Barrages and Weirs on Porous Foundations. *Engineering News* 64(26): 708-710.
- De Wit, J.M. (1984) *Onderzoek zandmeevoerende wellen Rapportage Modelproeven*. Grondmechanica Delft report CO-220887/10.
- Ding, L., Yao, Q., Sun D., Liu, C. (2007). Experimental studies on piping development in three-stratum dike foundations. *Water Resources and Hydropower Engineering*, 38(2): 19-22.
- Govers, G. (1987). Initiation of motion in overland flow. *Sedimentology* 34:1157-1164.
- Grass, A.J., 1970. Initial instability of fine bed sand, Hydraulic Division, *Proc. of ASCE*, Vol. 96, HY3, pp. 619-632.
- Hanses, U. (1985). *Zur Mechanik der Entwicklung von Erosionskanälen in geschichtetem Untergrund unter Stauanlagen*. Dissertation Grundbauinstitut der Technischen Universität Berlin, Germany.
- Harza, L.F. (1935). Uplift and seepage under dams on sand. *Transactions American Society of Civil Engineers* 100: 1353-1406
- Hoffmans, G.J.C.M., 2014. An overview of piping models. Keynote Lecture. *Proc. of Int. Symp. of Scour and Erosion*. Perth, Australia.
- Hoffmans, G.J.C.M., Van Rijn, L.C. (2017). Hydraulic approach for predicting piping in dikes. *Journal of Hydraulic Research*, ISSN 0022-1686 print/ISSN 1814-2079 online: <http://www.tandfonline.com>
- Hoffmans, G.J.C.M. (unpublished). *Shields-Darcy model. Alternative piping model?* – available upon request.
- Kanning, W. (2012). *The Weakest Link – Length Effects for Piping*. Phd thesis, Delft University of Technology, Delft, The Netherlands.
- Lane, E.W. (1935). Security from under-seepage masonry dams on earth foundations. *Transactions American Society of Civil Engineers* 100:1235-1351.
- Loiseleux, T., Gondret, P., Rabaud, M., Doppler D. (2005). Onset of erosion and avalanche for an inclined granular bed sheared by a continuous laminar flow. *Physics of fluids* 17(103304): 1-9.
- Müller-Kirchenbauer, H. (1978). Zum Zeitlichen Verlauf der Rückschreitenden Erosion in Geschichtetem Untergrund unter Dämmen und Stauanlagen, Beitrag zum *Talsperrensposium*, München.
- Navin, M. (2016). Kaskaskia Island and Bois Brule Levee Breaches during the 1993 Mississippi River Flood. *International Symposium on the Mechanics of Internal Erosion for Dams and Levees*.
- Pilotti, M. and Menduni, G., 2001. Beginning of sediment transport of incoherent grains in shallow shear flows. *Journal of Hydraulic Research*, Vol. 39, No. 2, p. 115-124.
- Robbins, B.A. (2016). Numerical modeling of backward erosion piping. *Applied Numerical Modeling in Geomechanics*, eds Gómez, Detournay, Hart and Nelson (eds.). p. 551-558.
- Robbins, B.A., Van Beek, V.M., López – Soto, J.F., Montalvo-Bartolomei, A.M., Murphy, J. (to be published). A novel laboratory test for backward erosion piping. *International Journal of Physical Modelling in Geotechnics*.
- Robbins, B.A. and Van Beek, V.M. (2017). Physical measurements of the backward erosion piping process. *Proceedings 25th meeting European Working Group on Internal Erosion*.
- Rotunno, A.F., Callari, C., Froiio, F. (2017). Computational Modeling of Backward Erosion Piping. *Models, Simulation, and Experimental Issues in Structural Mechanics*, Springer Series in Solid and Structural Mechanics 8, M. Frémond et al. (eds.), Springer International Publishing DOI 10.1007/978-3-319-48884-4\_12.

- Sellmeijer, J.B. (2006). Numerical computation of seepage erosion below dams (piping). In *Proceedings Third International Conference on Scour and Erosion*, 596-601, CURNET, Gouda, The Netherlands.
- Sellmeijer, J.B. (1988). *On the mechanism of piping under impervious structures*. Doctoral dissertation, TU Delft, The Netherlands.
- Sellmeijer, J.B., Calle, E.O.F., Sip, J.W. (1989). Influence of aquifer thickness on piping below dikes and dams. In *Proceedings of International symposium on analytical evaluation of dam related safety problems*, 357-366.
- Sellmeijer J.B., Lopéz de la Cruz J., Van Beek V.M., Knoeff J.G. (2011). Fine-tuning of the piping model through small-scale, medium-scale and IJkdijk experiments. *European Journal of Environmental and Civil Engineering* 15(8): 1139-1154.
- Shields, A. (1936). *Anwendung der Ahnlichkeitsmechanik und Turbulenzforschung auf die Geschiebebewegung*. Mitteilungen der Preußischen Versuchsanstalt für Wasserbau und Schiffbau, heft 26, Berlin.
- Silvis, F. (1991). *Verificatie Piping Model: Proeven in de Deltagoot*. Grondmechanica Delft, Delft, The Netherlands.
- TAW (1999). *Technisch rapport Zandmeevoerende wellen*. Technische Adviescommissie voor de Waterkeringen, Delft, The Netherlands.
- Van Beek, V.M., Knoeff, J.G., Sellmeijer, J.B. (2011). Observations on the process of backward piping by underseepage in cohesionless soils in small-, medium- and full-scale experiments. *European Journal of Environmental and Civil Engineering* 15(8): 1115-1137.
- Van Beek, V.M., Bezuijen A., Sellmeijer, J.B., Barends F.B.J. (2014). Initiation of backward erosion piping in uniform sands, *Géotechnique* 64(12): 927-941.
- Van Beek, V.M., Van Essen, H.M., Vandenboer, K., Bezuijen, A. (2015). Developments in modelling of backward erosion piping. *Géotechnique* 65(9): 740-754.
- Van Beek, V. M., Yao, Q.L., Van, M.A., 2013. Backward Erosion piping model verification using cases in China and the Netherlands, Paper No. 3.29a, *7th Int. Conf. on Case Histories in Geotechnical Engineering and Symposium in Honor of Clyde Baker*.
- Van Beek, V., Yao Q., Van M., Barends F. (2012). Validation of Sellmeijer's model for backward piping under dikes on multiple sand layers, *Proceedings of 6th International Conference on Scour and Erosion*, pp. 543-550.
- Van Esch, J.M., Sellmeijer, J.B., Stolle, D. (2013). Modeling transient groundwater flow and piping under dikes and dams. *Proceedings COMGEO III*, Krakow, Poland, International Centre for Computational Engineering.
- Van Rijn, L.C., 2014. *Review of Piping Processes and Models*, Report prepared for Deltares. [www.leovanrijn-sediment.com](http://www.leovanrijn-sediment.com).
- Vandenboer, K., Van Beek, V., Bezuijen, A. (2014a). 3D finite element method (FEM) simulation of groundwater flow during backward erosion piping. *Front. Struct. Civ. Eng.* 8(2): 160 – 166.
- Vandenboer, K, Bezuijen, A, Van Beek, VM (2014b). 3D character of backward erosion piping: Small-scale experiments. In Scour and Erosion (Cheng, Draper and An (Eds)), *Scour and Erosion*, p. 81-86, Taylor & Francis Group, London.
- Vrijling, J.K., Kok, M., Calle, E.O.F., Epema, W.G., Van der Meer, M.T., Van den Berg, P., Schweckendiek, T. (2010). Piping - *Realiteit of Rekenfout?* Technical report, Dutch Expertise Network on Flood Protection (ENW).
- Vrijling, JK; Schweckendiek, T; Kanning, W. (2011b). Safety standards of flood defenses. *Proceedings of the 3rd International Symposium on Geotechnical Safety and Risk*, ISGSR 2011. ed. N Vogt; B Schuppener; D Straub; G Brau. p. 67-84.
- Weijers, J.B.A. and Sellmeijer, J.B. (1993). A new model to deal with the piping mechanism. In *Filters in Geotechnical and Hydraulic Engineering* (Brauns, Schuler and Heibaum (eds)) 349-355, Balkema, Rotterdam, the Netherlands.
- White, C.M. (1940). The equilibrium of grains on the bed of a stream. *Proceedings Royal Society*, no. 174A, p. 322-338.

# Stress-strain behavior of soils having undergone different amounts of internal erosion

S. Li & A.R. Russell

*Centre for Infrastructure Engineering and Safety, School of Civil and Environmental Engineering, The University of New South Wales, Sydney, NSW 2052, Australia*

D. Muir Wood

*School of Science and Engineering, University of Dundee, UK*

**Abstract:** Results of an experimental investigation are reported, conducted to study the stress-strain behavior of a soil having undergone different amounts of internal erosion. The soil used is gap-graded and cohesionless comprising silt, sand and gravel. Internal erosion tests and subsequent triaxial tests are performed in a specially designed apparatus having modified perforated end platens and a drainage system that permitted the erosion to occur. A constant water head tank is used to drive the erosion and an effluent collection system is used to observe the eroded material. Different amounts of erosion, which progressively narrow the soil grading while maintaining a constant confining stresses, are caused by passing water through compacted soil samples inside the triaxial apparatus in an upward or downward direction. Flow rate through, settlement and volume change of the samples are monitored during the erosion. After erosion, drained compression tests are conducted. Another drained compression test is also conducted on a sample that has not eroded for comparison. It is observed that drained peak deviator stresses progressively reduce and the volumetric deformation of samples become less dilative with increasing amounts of erosion.

Keywords: Internal erosion; gap-graded cohesionless soil; stress-strain behaviour; mechanical effects.

## 1 INTRODUCTION

Internal erosion is caused by water seeping through soils and progressively washing out particles. It is a particular concern for cohesionless soils in dam cores, filters and transition layers and silt/sand soils in dam and levee foundations. Internal erosion of the soils forming water retaining structures may occur and lead to expensive maintenance costs or, in extreme cases, total collapse. Around 50% of dam failures and dysfunctions are caused by internal erosion (Foster et al., 2000).

Recent studies have set out to investigate the mechanical influence of internal erosion on soil. Some have developed new triaxial erosion testing systems to measure the stress-strain behaviour of soils which have undergone erosion, focusing on the strength and volumetric change, initial fines content and hydraulic conductivity of the test soils (eg, Chang and Zhang, 2011; Xiao and Shwiyhat, 2012; Chang et al., 2014; Ke and Takahashi, 2012, 2014a, 2015; Sato and Kuwano, 2015; Ouyang and Takahashi, 2015). The internal erosion in these tests was allowed to occur until the effluent became clear, signifying the end of erosion. Thus the amount of erosion is not a controlled variable in those tests. Others have studied the mechanical consequences of particle removal using numerical methods, but they are not concerned with the process of coupled flow and particle removal (eg, Wood et al., 2010; Scholtès et al., 2010). In this study, a series of triaxial tests are conducted to study the stress-strain behaviour of soil samples having undergone different amounts of internal erosion. The focus is to examine the erosion characteristics in terms of flow rate and cumulative eroded soil mass, as well as the evolution of mechanical behaviour caused by the erosion.

## 2 TESTING APPARATUS

To study the initiation, rate of progression and consequences of internal erosion, a triaxial apparatus, modified to enable erosion, is used. The apparatus consists of a triaxial compression testing system, a drainage system enabling water to seep through samples and cause erosion, a constant head water tank to drive the seepage, and system to collect the water once it has seeped through the soil. The system is broadly similar to others (eg, Chang and Zhang, 2011; Xiao and Shwiyhat, 2012; Chang et al., 2014; Ke and Takahashi, 2012, 2014a, 2015; Sato and Kuwano, 2015; Ouyang and Takahashi, 2015). A schematic illustration is shown in Figure 2.1.

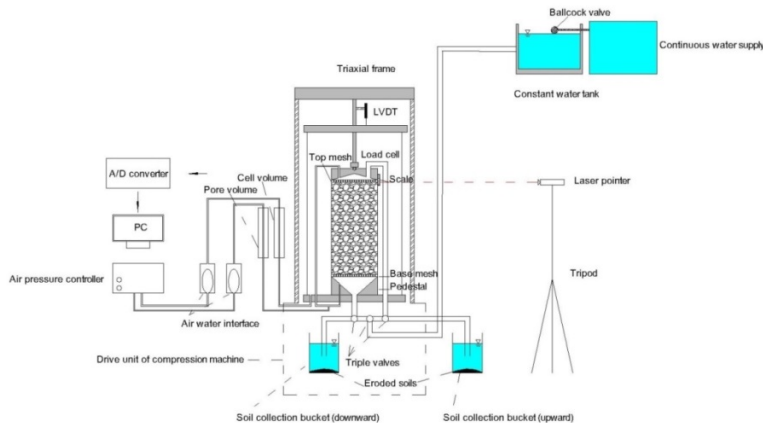


Figure 2.1. Schematic diagram of the internal erosion triaxial testing system.

### 2.1 Triaxial system

The triaxial testing apparatus, used to test cylindrical samples 200 mm in diameter and 400 mm in height, is displacement-controlled. A motorized load frame applies axial load to samples, in which the motor speed can provide a predetermined constant rate of displacement, and the resulting axial load can be measured by a submersible load cell at selected intervals of time. A drive unit, with a multispeed gearbox giving displacement speeds down to 0.0001 mm/min, is employed. The axial displacement of the sample during shearing is measured using a linear variable differential transducer (LVDT) with a precision of 0.0001 mm. Testing data are automatically logged at regular time intervals through a program with an interactive visual interface.

### 2.2 Drainage system

The base pedestal and top-cap contain funnel-shaped voids to enable seepage water containing soil particles to exit a sample through its ends and pass into a collection system. Perforated stainless steel discs cover each funnel-shaped void and provide and act as rigid base and top sample boundaries. The perforations are circular, 5 mm in diameter, and make a grid pattern with a center-to-center spacing of 8 mm. The 5 mm perforation size is sufficiently large to prevent clogging by fine particles. They are sufficiently small to prevent coarse particles from passing thus preventing collapse of a sample. The largest eroded particle is less than (and usually much less than) 15% of the maximum particle size (Wan, 2006), being 13 mm in this study. All flow channels and fittings have an internal diameter of 7.5 mm.

Seepage water can be introduced and passed through samples in both upward and downward directions to cause particle removal under a range of confining stresses and hydraulic gradients prior to shearing. Passing water through two directions enables a more homogeneous sample to be achieved prior to triaxial testing than possible by Bendahmane et al. (2008), Chang and Zhang (2011) and Ke and Takahashi (2012). In these researches, equipment permitted only the one directional passage of water causing significant variations in particle size distributions along the sample lengths.

### 2.3 Constant water head and effluent collection system

The seepage water is supplied via a constant head tank. The constant head tank comprises a watertight barrel fitted with an inlet ballcock valve, by which continuous water supply can be achieved. In the tests conducted here the water tank is located 3.2 m above the base of the sample, with the water exiting the sample being collected in containers level with the base, causing an average hydraulic gradient  $i=8$  to be imposed across the sample. Higher or lower hydraulic gradients can be achieved by raising or lowering the constant head tank.

Once internal erosion is initiated, and particles begin to wash out from the sample, the flow rate and the mass of eroded soil are determined. The collected water is allowed to stand for a period of time so that suspended soil particles settle out from the water.

Axial deformation of a sample during erosion is measured by reading the vertical separation of the laser mark generated by a fixed laser pointer in front of triaxial cell.

## 3 TEST SOIL PREPARATION

### 3.1 Soil material

The soil for this study is a mixture of three base materials comprising silt, sand and gravel-sized particles in different proportions. The three base materials are referred to as silica 60G, 5 mm basalt and 10 mm basalt. The particle size distribution of each is shown in Figure 3.1. They are mixed in the proportions 0.26:0.10:0.64 to produce a gap-graded soil for testing, having a gravel content of 58.2%, with a full particle size distribution also shown in Figure 3.1. This particular gap-graded soil is selected to ensure that erosion will occur, noting that soils having gravel contents of around 60% (or larger) are internally unstable (Wan, 2006). Other physical properties of the test soil are summarized in Table 1. The erodibility of the soil mixture is evaluated as internal unstable according to several particle size distribution-based criteria (U.S. Army Corps of Engineers, 1953; Istomina, 1957; Lubochkov, 1965; Kenney and Lau, 1985, 1986; Burenkova, 1993; Wan and Fell, 2008), as shown in Table 2.

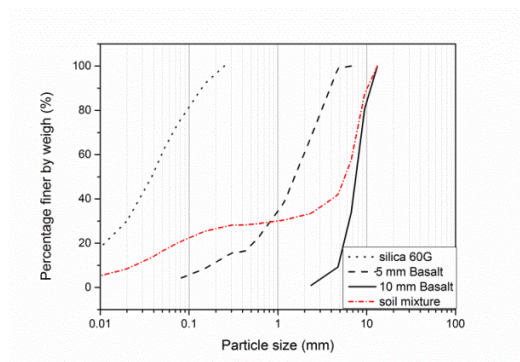


Figure 3.1. Particle size distribution of soils.

Table 1. Physical properties of the gap-graded test soil

Physical property	Value	Physical property	Value
$d_{90}$	10.1	$h' = d_{90}/d_{60}$	1.5
$d_{60}$	6.9	$h'' = d_{90}/d_{15}$	232
Mean particle size $d_{50}$ , mm	5.7	Specific gravity, $G_s$	2.73
$d_{30}$	0.97	Minimum dry density, $g/cm^3$	1.79
$d_{15}$	0.04	Maximum dry density, $g/cm^3$	2.49
Effective particle size $d_{10}$ , mm	0.02	USCS (ASTM D2487-11)	GM
Uniformity coefficient $C_u$ , mm	284.6	Particle description	sub-angular
Curvature coefficient $C_c$	5.6	$h' = d_{90}/d_{60}$	1.5

$d_x$  denotes the particle size finer than which the soil mass by percentage is  $x\%$

### 3.2 Sample formation

Moist tamping is used to form the samples as it leads to minimal particle segregation. Several thin soil layers are tamped, layer by layer, to form a sample. The modified 'undercompaction' method of Vo and Russell (2013) is employed to achieve samples with uniform density. The method is similar to that of Bradshaw and Baxter (2006). The compaction energy applied to each layer of soil in forming the sample is controlled in order to achieve a uniform density throughout the sample. An electric Kango percussion hammer fitted with a round steel pad with a diameter of 195 mm is used to apply compaction energy. The relationships between compacting duration and dry density for a single layer, having a moisture content of 7.3%, are obtained as shown in Figure 3.2.

Table 2. The evaluation of the mixture's erodibility

Physical property	Value	Physical property	Value
$d_{90}$	10.1	$h' = d_{90}/d_{60}$	1.5
$d_{60}$	6.9	$h'' = d_{90}/d_{15}$	232
Mean particle size $d_{50}$ , mm	5.7	Specific gravity, $G_s$	2.73
$d_{30}$	0.97	Minimum dry density, $g/cm^3$	1.79
$d_{15}$	0.04	Maximum dry density, $g/cm^3$	2.49
Effective particle size $d_{10}$ , mm	0.02	USCS (ASTM D2487-11)	GM
Uniformity coefficient $C_u$ , mm	284.6	Particle description	sub-angular
Curvature coefficient $C_c$	5.6	$h' = d_{90}/d_{60}$	1.5

U=unstable; P=probability of internal instability.

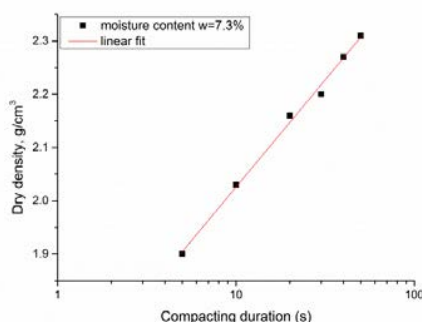


Figure 3.2. Compacting durations versus dry density of soil.

According to Skempton (1986) and Fell and Wan (2003), cohesionless soils compacted to a relative density greater than 65% have a low likelihood of internal erosion. In this study, all the samples are prepared targeting a density of  $2.08 \text{ g/cm}^3$  when the moisture content is 7.3%, which corresponds to a relative density of 50%. The corresponding compacting duration for a single layer to reach the target is 14.5 s. Compaction trials on a layered soil showed that, when the top layer was subjected to 14.5 seconds of compaction, the top layer absorbed 75% of compaction energy, the second layer absorbed 20% of the compaction energy and the bottom layer absorbed 5% of the compaction energy. It follows, using the Vo and Russell (2013) technique, that the compaction times for each layer of a six layered sample are 14.5, 14.5, 14.5, 14.3, 14.0, 20.0s, (from bottom to top) will produce a sample with a dry density of  $2.08 \text{ g/cm}^3$  throughout. The uniformity of the density of a sample was checked by measuring the thickness of each layer. The maximum, minimum and average ratios between actual density and target density are 1.08, 0.99 and 1.03, respectively,

## 4 TEST PROCEDURES

The purpose of this experimental investigation is to study the erosion characteristics of a gap-graded silt-sand-gravel mixture and its mechanical response following different amounts of internal erosion.

### 4.1 Saturation, consolidation and erosion

A sample is placed in the triaxial cell and then saturated to achieve a B-value of at least 0.95. It is then consolidated under an isotropic confining stress of 50 kPa. An erosion test is then performed.

A hydraulic gradient of  $i=8$  is sufficient to cause fine particles to migrate and the samples to erode internally. A confining pressure of 80 kPa is applied during erosion. As the constant head tank imposes a pore water pressure of about 30 kPa where it enters a sample, and the water pressure is 0 kPa where it exits the sample, a gradient of effective stress exists across the sample as erosion occurs, with maximum and minimum values of about 80 kPa and 50 kPa.

Three different samples are subjected to three different amounts of erosion by passing through 15, 45 or 90 litres of water. The time required for the collected effluent to reach certain volumes is recorded. The seepage direction is reversed after every 15 liters of seepage, causing the effective stress gradients to be reversed also.

The changes in volume of the samples during erosion are determined using the cell volume changes, and the axial settlements are measured using the laser pointer.

Once the required volume of water had passed through each sample the confining pressure is raised to 260 kPa and the pore pressure is raised to 210 kPa, imposing a uniform and isotropic effective stress of 50 kPa on each sample, immediately prior to conducting a drained triaxial compression test.

### 4.2 Drained triaxial compression tests

Drained triaxial compression tests are conducted at a strain rate of 0.2 mm/min on the samples subjected to different amounts of internal erosion as well as a sample which had not been subjected to internal erosion. This strain rate was determined to be sufficiently slow for drained conditions to prevail. The confining and pore pressures are maintained constant at 260 kPa and 210 kPa, respectively. The axial displacement and axial load are automatically recorded every 20 seconds and photographs of the pore volume and cell volume burettes are captured using a high definition camera every 60 seconds.

## 5 RESULTS AND DISCUSSION

### 5.1 Internal erosion results

The flow rate is used here as an indicator of the progress of internal erosion. Richards and Reddy (2009) suggest that hydraulic velocity is a better indicator than flow rate for cohesionless soils. However, since

the true cross-sectional area of seepage flow in a sample is not measured here, it was not possible to determine the hydraulic velocity in a reliable way.

The variations of flow rate and volumetric strain with time for the sample subjected to 90 liters of seepage are shown in Figure 5.1. The flow rate generally increases with time until a certain time is reached, beyond which it becomes stable. The increasing flow rate suggests that fine particles are being removed creating additional void space. At a certain time, once a large amount of fine particles have been removed, stable flow channels have formed within the sample and a stable flow rate is observed. The soil sample reduced in volume at all times, albeit it by very small amounts, and the reduction is most pronounced during the initial stages when particle removal is most prevalent.

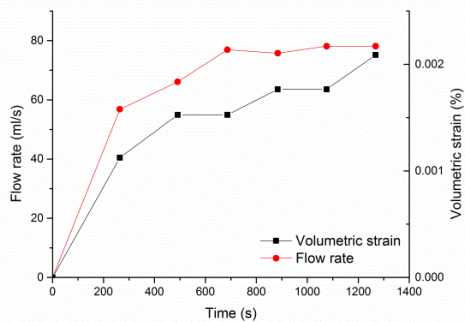


Figure 5.1. Flow rate and volumetric strain with time.

## 5.2 Post-erosion particle size distributions

After erosion and the subsequent triaxial test each sample is quartered using four layers of equal thickness. The particle size distribution of each is determined and those for the sample subjected to 90 liters of seepage are shown in Figure 5.4. The bottom quarter erodes the most while the top quarter erodes the least. The second and third quarters experience the same amount of erosion. Although the variation in post-erosion grading at top and bottom layers cannot really be eliminated because of gravity and the physical structure of gap-graded soil, the post-erosion grading at middle part of sample shows an uniform erosion.

## 5.3 Drained compression test

Drained tests are conducted on samples subjected to 15, 45 and 90 litres of seepage, along with a sample which had not been subjected to erosion. A repeat test on a sample subjected to 45 liters seepage was also conducted. Figure 5.4 plots the stress-strain curves together with the volumetric strain curves. Table 3 presents the friction angles and the dilation angles of each sample at peak and large strains. These friction angles are obtained by assuming zero cohesion.

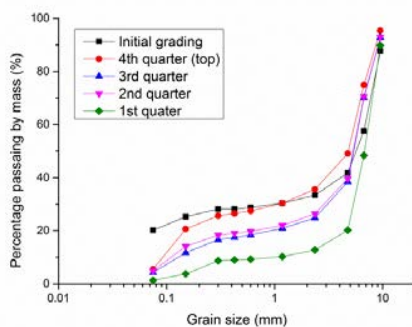
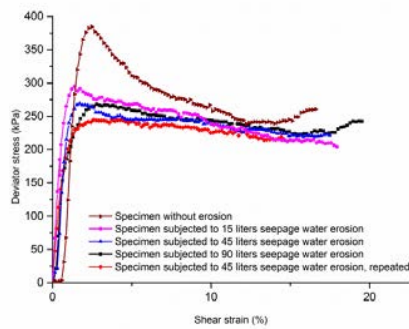
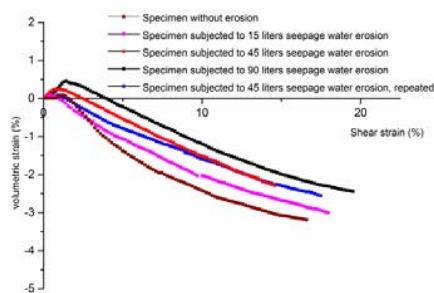


Figure 5.4. Post-erosion particle size distribution.



(a) Stress-strain relationships.



(b) Volumetric strain and shear strain relationships.

Figure 5.5. Drained compression tests on samples subjected to different amount of erosion.

The drained peak strength of the eroded samples is significantly lower than that of the sample which had not experienced erosion, in agreement with Wood et al. (2010), Ke and Takahashi (2014) and Chang et al. (2014).

The peak deviator stress tends to decrease as the volume of seepage water and erosion increase. The rate at which the strength decrease occurs tends to slow down as the volume of seepage water increases. This is consistent with the slow-down of the rate of eroded soil mass accumulation.

The large-strain shear strengths exhibited a different trend. The sample which experienced the most erosion (from 90 litres of seepage) has a larger strength than those which experienced lesser erosion (from 15 and 45 litres of seepage). At large strains, where the initial (post-erosion) sample density is not expected to affect the large strain strength, the increasing coarseness of particle size distribution following erosion may be the cause for the strength increase. This trend is consistent with findings by Chang et al. (2014). However, the increasing coarseness of the particle size distributions of the eroded samples does not explain why they had lesser constant volume strengths than the sample which had not experienced erosion. Further data is needed to explore and confirm this aspect of behavior and understand its causes.

As can be seen in Figure 5.2(b) the volumetric deformations of samples became less contractive at small shear strains with increasing amounts of erosion. Also, at large shear strains the samples subjected to erosion exhibited a reduced tendency for dilation compared to the sample which had not experienced erosion. The erosion caused the samples to become looser and thus tend to be more contractive at large shear strains, in agreement with Scholtes et al. (2010) and Chang and Zhang (2011). From Table 3, the friction angles and the dilation angles at peak are greater than each of them at large strain. And generally, the friction angle and dilation angle at peak slightly reduces as erosion proceeds, while the differences in friction angles at large strain is minor. For eroded soils, the differences in dilation angles at large strain are not much.

Table 3. The change in friction angle of samples subjected to different amounts of erosion

Amount of erosion (litres)	Percentage of lost fine particles occupies total mass	Peak friction angle (°)	Large strain friction angle(°)	Dilation angle at peak (°)	Dilation angle at large strain (°)
0	0	50.1	43.8	25.1	2.3
15	4.6%	47	43	20.8	5.7
45	7.1%	46.7	43.5	10.2	6.3
90	7.7%	46.3	43.8	13.5	5.7

#### 4. CONCLUSIONS

An experimental investigation was conducted to study the erosion progression and the post-erosion stress-strain behavior of a gap-graded silt-sand-gravel mixture. During erosion the flow rate gradually increased prior to attaining a constant value. In the drained triaxial compression tests it was observed that the peak deviator stresses progressively reduced with increasing amounts of erosion, due to the samples becoming progressively looser with increasing amounts of erosion. The samples became less dilative with increasing amounts of erosion, again due to the samples becoming progressively looser with increasing amounts of erosion. For the eroded samples the large strain shear strengths tended to increase with the amount of erosion, probably caused by the increasing coarseness of the particle size distributions. In contrast, the eroded samples had lesser constant volume strengths than the sample which had not experienced erosion. Microstructural investigation like x-ray CT test is needed to explore and confirm the mechanism of the macro-behavior and understand its causes.

#### REFERENCES

- Bendahmane, F., Marot, D., and Alexis, A. (2008). "Experimental parametric study of suffusion and backward erosion," *Journal of Geotechnical and Geoenvironmental Engineering*, 134(1), 57-67.
- Bradshaw, A.S., and Baxter, C.D.P. (2007). "Sample preparation of silts for liquefaction testing," *Geotechnical Testing Journal*, 30(4), 324-332.
- Burenkova, V.V. (1993). Assessment of suffusion in non-cohesive and graded soils. Filters in geotechnical and hydraulic engineering. Balkema, Rotterdam, 357-360.
- Chang, D.S. and Zhang, L.M. (2011). "A Stress-controlled Erosion Apparatus for Studying Internal Erosion in Soils," *Geotechnical Testing Journal*, 34(6), 579-589.
- Chang, D., Zhang, L., & Cheuk, J. (2014). *Mechanical consequences of internal soil erosion*. HKIE Transactions, 21(4), 198-208.
- Fell, R., Wan, C.F., Cyganiewicz, J., and Foster, M. (2003). "Time for development of internal erosion and piping in embankment dams," *Journal of geotechnical and geoenvironmental engineering*, 129(4), 307-314.
- Foster, M., Fell, R. and Spannagle, M. (2000). "The statistics of embankment dam failures and accidents. Can," *Geotech. J.*, 37:1000-1024.
- Istomina, V.S., (1957). Filtration Stability of Soils, Gostroizdat, Moscow.
- Ke, L. and Takahashi, A.(2014) "Triaxial Erosion Test for Evaluation of Mechanical Consequences of Internal Erosion," *Geotechnical Testing Journal*, 37(2), 347-364.
- Ke, L., and Takahashi, A. (2012). "Strength reduction of cohesionless soil due to internal erosion induced by one-dimensional upward seepage flow," *Soils and Foundations*, 52(4), 698-711.
- Ke, L., and Takahashi, A. (2015). "Drained monotonic responses of suffusional cohesionless soils," *Journal of Geotechnical and Geoenvironmental Engineering*, 141(8), 04015033.
- Kenney, T.C., and Lau, D. (1985). "Internal stability of granular filters," *Canadian geotechnical journal*, 22(2), 215-225.

- Kenney, T.C., and Lau, D. (1986). "Internal stability of granular filters: Reply," *Canadian Geotechnical Journal*, 23(3), 420-423.
- Ladd, R.S. (1978) "Preparing test specimens using undercompaction," *Geotechnical Testing Journal*, 1(1), 16-23.
- Lubochkov, E.A. (1965). "Graphical and analytical methods for the determination of internal stability of filters consisting of non cohesive soil," *Izvestia, vniig*, 78, 255-280.
- Ouyang, M., and Takahashi, A. (2015). "Influence of initial fines content on fabric of soils subjected to internal erosion," *Canadian Geotechnical Journal*, 53(2), 299-313.
- Richards, K.S., and Reddy, K.R. (2009). "True triaxial piping test apparatus for evaluation of piping potential in earth structures," *Geotechnical Testing Journal*, 33(1), 1-13.
- Sato, M., and Kuwano, R. (2015). "Influence of location of subsurface structures on development of underground cavities induced by internal erosion", *Soils and Foundations*, 55(4), 829-840.
- Scholtès, L., Hicher, P.Y., and Sibille, L. (2010). "Multiscale approaches to describe mechanical responses induced by particle removal in granular materials," *Comptes Rendus Mécanique*, 338(10-11), 627-638.
- U.S. Army Corps of Engineers, (1953). "Filter Experiments and Design Criteria," Technical Memorandum No. 3-360, Waterways Experiment Station, Vicksburg, MS.
- Vo, T., and Russell, A.R. (2013). "Unsaturated soil interacting with a rotating model wall" *International Journal of Physical Modelling in Geotechnics*, 13(2), 63-78.
- Wan, C.F., and Fell, R. (2008). "Assessing the potential of internal instability and suffusion in embankment dams and their foundations," *Journal of Geotechnical and Geoenvironmental Engineering*, 134(3), 401-407.
- Wan, C.F. (2006). *Experimental investigations of piping erosion and suffusion of soils in embankment dams and their foundations. PhD thesis*. The University of New South Wales, Sydney, Australia.
- Wood, D.M., Maeda, K., and Nukudani, E. (2010). "Modelling mechanical consequences of erosion," *Geotechnique*, 60(6), 447-457.
- Xiao, M., and Shwiyhat, N. (2012). "Experimental investigation of the effects of suffusion on physical and geomechanic characteristics of sandy soils," *Geotechnical Testing Journal*, Vol. 35, No. 6, 2012, pp. 890-900.

# Large triaxial device for suffusion erodibility and mechanical behavior characterization of coarse soils

D. Marot, F. Bendahmane, R. Andrianatrehina & R. Gelet

*University of Nantes, Institute GeM, UMR CNRS, 58 rue Michel Ange, Saint-Nazaire, France*

**Abstract:** Suffusion, one of the main internal erosion processes, selectively erodes the fine particles which move through the voids formed by the coarser particles. In the literature, the mechanical consequences of suffusion on soil were investigated by several researchers. However, no general conclusion can be drawn because the already published results appear to be opposite. The objective of this study is to investigate these consequences. A large triaxial erodimeter was developed in order to perform suffusion tests and triaxial tests on coarse soils which are often encountered in French dikes. For the suffusion characterisation, the proposed interpretative method is based on the energy expended by the seepage flow and the cumulative loss of dry mass. The results of triaxial tests on non-eroded and eroded specimens show the significant effect of an achieved suffusion process on the mechanical strength of soils.

Keywords: dam and dike safety, suffusion, erodimeter, water seepage energy, mechanical strength.

## 1 INTRODUCTION

Suffusion is a selective erosion of fine particles under the effect of seepage flow within the matrix of coarser particles. This complex phenomenon is a combination of three processes: detachment, transport and possible filtration of the finer fraction. It can induce a change in particle size distribution, porosity and hydraulic conductivity of the material.

Fell and Fry (2013) proposed three criteria which have to be satisfied for suffusion to occur: 1) geometric criterion, the size of fine particles must be smaller than the size of the voids between the coarser particles, which compose the matrix of the soil; 2) stress criterion, the fine particles do not cram the space between the coarser particles and are carrying a small part of the effective stresses; 3) hydraulic criterion, the velocity of flow through the soil matrix must be high enough to move the loose fine soil particles through the constrictions between the larger soil particles.

The grain size distribution has a key influence on the two first criteria, so that in the past few decades, the research on soil gradation has gathered much attention in order to characterize the potential of suffusion. Fell and Fry (2007) concluded that soils having a grain-size distribution curve either discontinuous or upwardly concave are likely to suffer from suffusion. Proposals of various geometric assessment methods exist in the literature, mostly based on the particle size distribution (Kenney and Lau, 1985; Wan and Fell, 2008; Chang and Zhang, 2013a; among others). With the purpose to take also into account the influence of the relative density, Indraratna et al. (2015) proposed a criterion based on constriction size distribution.

The third criterion is related to the action of the fluid phase with respect to the seepage loading required to detach and transport the fine particles. Skempton and Brogan (1994) proposed to relate the onset of suffusion with an increase of hydraulic conductivity and to characterize the corresponding hydraulic loading by the hydraulic gradient, termed as the critical hydraulic gradient. However, the filtration of some detached particles can induce a clogging process within the soil accompanied with a decrease of the hydraulic conductivity (Reddi et al. 2000; Bendahmane et al. 2008; Marot et al. 2009;

Nguyen et al. 2012). In consequence, Marot et al. (2016) considered the simultaneous variation of the difference of the hydraulic head and of the flow rate to evaluate the hydraulic loading. This simultaneous variation is best represented by the total power expended by the seepage flow:

$$P_{\text{flow}} = Q \gamma_w \Delta h \quad (1)$$

where  $Q$  is the fluid flow rate,  $\gamma_w$  is the unit weight of water and  $\Delta h$  is the drop of hydraulic head.

Marot et al. (2011) expressed the erosion resistance index by:

$$I_\alpha = -\log \left( \frac{m_{\text{dry}}}{E_{\text{flow}}} \right) \quad (2)$$

where  $E_{\text{flow}}$  is the expended energy, computed by time integration of the instantaneous flow power, and  $m_{\text{dry}}$  is the cumulative eroded dry mass. From this energy based method, and thanks to twenty-three tests performed with a triaxial erodimeter, six categories of suffusion soil sensibility were proposed: from highly resistant to highly erodible (Marot et al., 2016).

Based on this energy approach, previous studies show that suffusion susceptibility can be evaluated with accuracy for different hydraulic loading histories (Rochim et al., 2017) and for different specimen sizes (Zhong et al., submitted).

However, the mechanical consequences of suffusion on soil remain an open question and the conclusions of several investigations already published appear to be opposite. In a modified triaxial apparatus, Chang and Zhang (2013b) performed drained monotonic compression tests at different stress states on a gap-graded cohesionless soil (i.e. gap-graded soil is defined by a broad gradation in which an intermediate range of size is missing). They concluded that after the loss of a significant amount of fine particles in the soil, the original dilative stress-strain behavior becomes a contractive one and the peak stress decreases. In the same way, Ke and Takahashi (2015) tested three gap-graded mixtures, composed of two sands, and showed that the soil strength decreases after suffusion.

We can also mention the DEM analyses realized by Scholtès et al. (2010) and Muir Wood et al. (2010), which pointed out that the soil shear strength may decrease once some fine particles are removed. Moreover based on a micromechanical model, Hicher (2013) predicted that internal erosion of soils may trigger a diffuse failure in earthen structures.

On the contrary, Sterpi (2003) tested samples of well-graded silty sand and concluded that the partial or total removal of the fine particles produces an increase of stiffness and shear strength. However it is worth stressing that for this study, the drained triaxial compression tests were performed on non-eroded specimens, i.e. homogeneous specimens were reconstituted with a fine percentage which should represent the post suffusion gradation.

Those opposite conclusions may be due to the type of gradation: gap-graded for the first mentioned studies and well-graded in the case of the last one. But another reason might be related to the heterogeneities triggered by the suffusion process, which cannot be appropriately represented by a *reconstituted* specimen, even with the same gradation as that of a post-suffusion-specimen. Since all internal erosion processes, including suffusion, may increase the risk of failure of earth structures, it appears necessary to develop further investigation on this topic.

The ASTM Standard (D2850 2003) specifies the specimen size for triaxial test and the largest particle diameter shall be smaller than one sixth the specimen diameter. It is worth stressing that soils of several dikes in France can be relatively coarse, so the triaxial apparatus must permit to test specimen with appropriate size.

## 2 EXPERIMENTAL CAMPAIGN

### 2.1 Main characteristics of the testing device

With the objective to investigate the mechanical consequences induced by an achieved suffusion process, a dedicated triaxial apparatus was developed. This device allows independent control of multi-staged

hydraulic gradient and stress state (see Figure 1). Moreover the developed apparatus comprises a large triaxial cell which allows to test specimens up to 200 mm in diameter and 500 mm in height. This specificity targets materials endowed with a relatively large maximum grain size which is typical for several dikes in France.

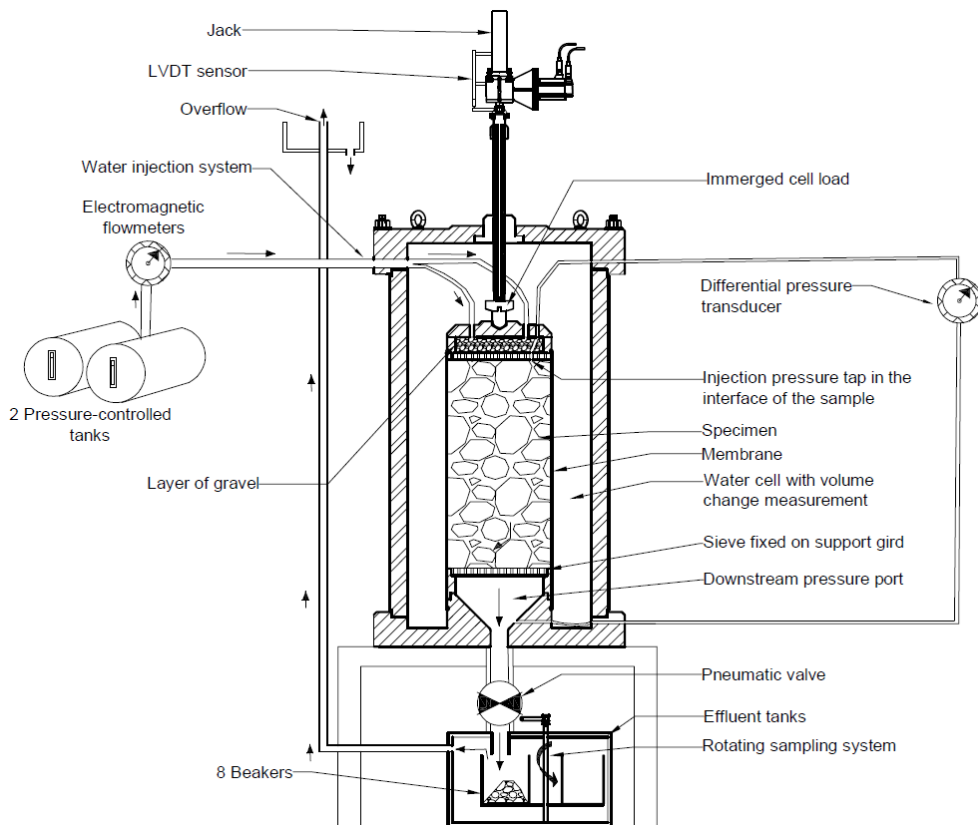


Figure 1. Schematic diagram of the large triaxial erodimeter.

For the hydraulic loading, the fluid circulates into the top cap which contains a layer of gravel to diffuse the hydraulic loading uniformly on the top surface of the specimen. The cell base has a funnel-shaped draining system, specially designed to avoid clogging. The draining system is connected to a collecting system which is composed of an effluent tank containing a rotating support with eight beakers to catch the eroded particles during the test. All specimens are placed on a 1.2 mm pore opening size which is fixed on a 10 mm mesh screen. One of the two electromagnetic flowmeters is selected according to the injected flow range. The hydraulically controlled system is composed of a pressure controller connected to two 200 L tanks, used alternatively to continuously apply the targeted hydraulic loading. The differential pore water pressure across the specimen is measured using a differential pressure transducer connected to the top cap and base pedestal of the triaxial erodimeter.

For the mechanical loading, an electric jack and a reaction frame compose the axial loading system. An immersed load cell measures the axial force on the loading rod. The piston displacement and thus the specimen axial strain are measured by a Linear Variable Differential Transducer (LVDT) sensor.

Device control and data acquisition are driven and recorded by a single servo drive plugged into a computer and a LabVIEW software developed by the authors.

## 2.2 Testing materials

The suffusion susceptibility and the mechanical consequences of suffusion were evaluated for three specimens of well graded coarse soils (named specimens 5.2-5.7, 6.2-6.7 and 11.2-11.7) all coming from the same French dike. The name of each specimen is related to its depth location within the dike. A laser

diffraction particle-size analyzer was used to measure the grain-size distribution of these three specimens (see Figure 2), with demineralized water and without deflocculation agent.

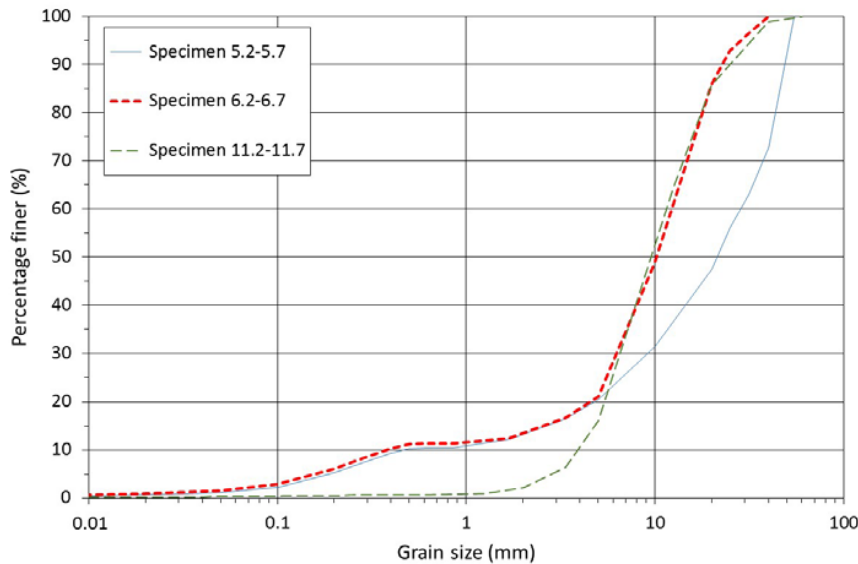


Figure 2. Grain size distribution of tested soils.

According to grain size based criteria proposed by Kenney and Lau (1985) and Indraratna et al. (2015), both gap graded soils 5.2-5.7 and 6.2-6.7 are, indeed internally unstable (see Table 1). However, as the percentage of fine  $P$  is smaller than 10%, and as the gap ratio,  $G_r$  is smaller than 3, Chang and Zhang (2013)'s method assess these two soils as internally stable. According to Wan and Fell (2008), the method that they proposed seems not to be applicable for gap-graded soils and soils with a mass of fine fraction lower than 15 %. Then this method is only relevant for the widely graded soil 11.2-11.7 which is classified as internally stable. This soil is also classified stable by Kenney and Lau (1985)'s criterion and Chang and Zhang (2013)'s criterion because the ratio  $H/F$  is higher than 1 for the whole fine fraction. On the contrary, this soil is unstable according to Indraratna et al. (2015)'s criterion.

Table 1 Properties of Tested Gradations

Properties	Tested gradations		
	5.2-5.7	6.2-6.7	11.2-11.7
$P$ (%)	1.45	1.87	0.31
$G_r$	1.42	1.42	WG
$C_c$	6.32	8.83	1.07
$C_u$	59.52	34.33	2.98
$d_{15}/d_{85}$	0.06	0.14	0.24
$(H/F)_{\min}$	0.26	0.14	0.36
$D (H/F)_{\min}$ (mm)	0.47	0.48	15.00
$D_{c35}^c/d_{85,SA}^f$	103.98	102.85	145.74
Kenney and Lau's criterion	U	U	S
Wan and Fell's criterion	/	/	S
Chang and Zhang's criterion	S	S	S
Indraratna's criterion	U	U	U

Note:  $P$  = percentage of particle smaller than 0.063mm;  $G_r = d_{\max}/d_{\min}$  ( $d_{\max}$  and  $d_{\min}$ : maximal and minimal particle sizes characterizing the gap in the grading curve);  $C_c$  = coefficient of curvature

$C_u$  = uniformity coefficient;  $d_{15}$  and  $d_{85}$  are the sieve sizes for which 15% and 85% respectively of the weighed soil is finer;  $F$  and  $H$  are the mass percentages of the grains with a size, lower than a given particle diameter  $d$  and between  $d$  and  $4d$  respectively;  $D (H/F)_{\min}$  is the corresponding diameter with the minimum value of ratio  $H/F$ ;  $D_{c35}^c$  is the controlling constriction for coarser fraction from constriction size distribution by surface area technique;  $d_{85,SA}^f$  is the representative size for finer fraction by surface area technique; WG = widely graded soil; U = unstable; S = stable; / = method not relevant for considered soil.

### 2.3 Testing program

The saturation and consolidation procedures follow the methodology described in Bendahmane et al. (2008). For each soil specimen, the experimental procedure comprises two tests. First a monotonic compression triaxial test is performed under drained conditions, in order to evaluate the mechanical strength of the intact soil. The second test aims to evaluate the mechanical strength of the soil post-suffusion and is composed of three successive steps:

- 1) It starts by applying the same mechanical loading path as test on intact soil until the deviatoric stress reaches the value of geostatic stress which was applied in situ on the considered sample.
- 2) At this stress state, a full suffusion test is performed by applying a downward seepage flow under multi-staged hydraulic gradient.
- 3) The third step consists in increasing the deviatoric stress until the specimen fails.

## 3 TEST RESULTS AND DISCUSSION

### 3.1 Hydraulic conductivity and rate of erosion

Figure 3 shows the time evolution of the hydraulic gradient that was applied during the suffusion tests and Figure 4 shows the corresponding evolutions of the hydraulic conductivity.

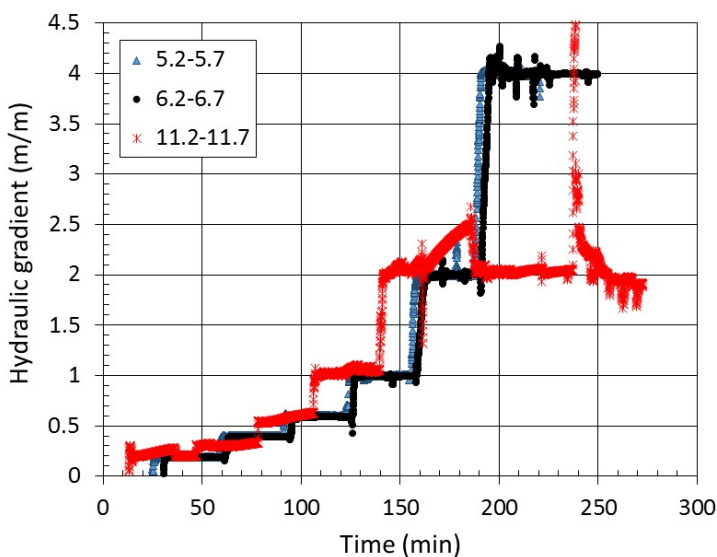


Figure 3. Time series of the applied hydraulic gradient.

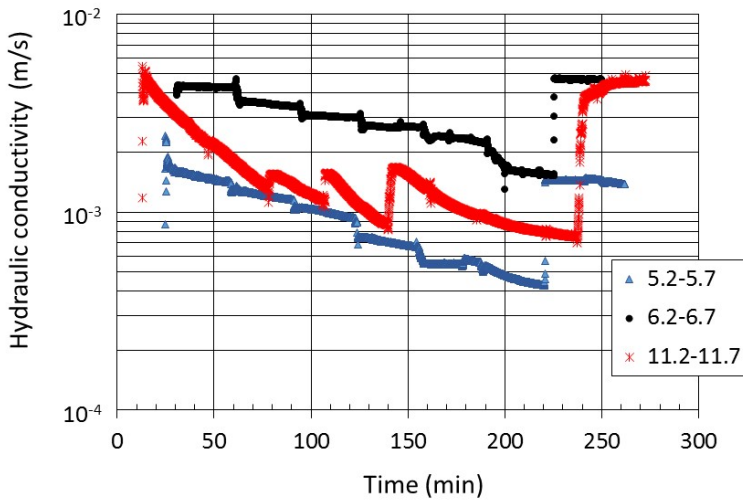


Figure 4. Time series of the recorded hydraulic conductivity.

The comparison of the time evolutions of the hydraulic conductivity with the erosion rate per unit cross section can provide further information to improve the understanding of the suffusion process. The erosion rate per unit cross section is expressed by equation (3) and the time evolution of corresponding values is shown by Figure 5:

$$\dot{m} = \frac{m(\Delta t)}{S \Delta t} \tag{3}$$

where  $m$  is the eroded dry mass during the elapsed time  $\Delta t$  and  $S$  is the specimen cross section.

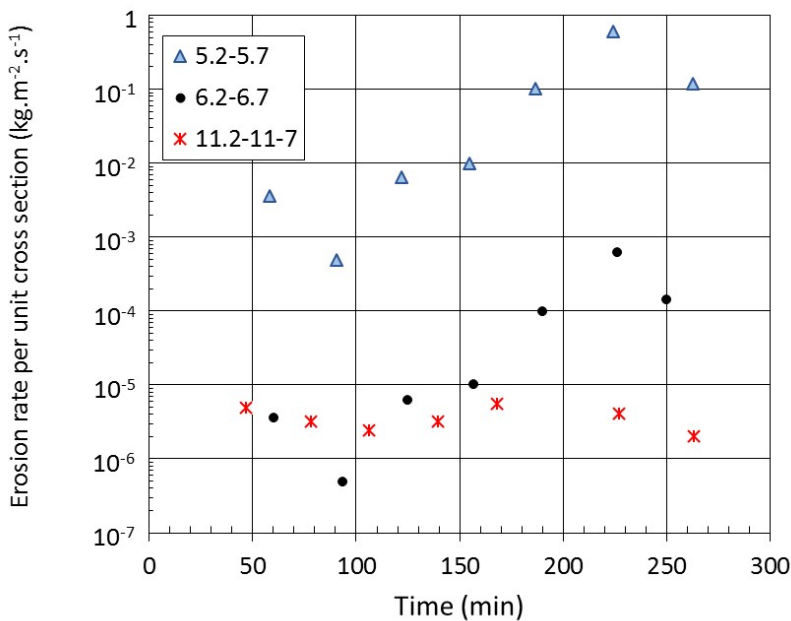


Figure 5. Time series of the erosion rate per unit cross section. For each test, the seven points correspond to the cumulative eroded dry mass issued from the seven beakers contained in the rotating sampling system (see Figure 1).

For tested soils, the hydraulic conductivity first decreases (see Fig. 4). However, at the beginning of each hydraulic gradient stage, when the applied hydraulic gradient is increased, it worth stressing that the hydraulic conductivity sharply increases. This sudden hydraulic conductivity increase is immediately followed by a slow decrease of hydraulic conductivity. A sudden increase in hydraulic conductivity can be also measured when the applied hydraulic gradient reaches 4, but a rough increase of the erosion rate occurs simultaneously. These simultaneous increases suggest that a clogging firstly restricting the water flow can be blown away by a sudden increase of the hydraulic loading. Finally hydraulic conductivity tends to stabilize while the erosion rate decreases.

### 3.2 Post-suffusion-test particle size distribution of specimens

Figure 6 shows the initial gradation and the post-suffusion gradation of the specimen 6.2-6.7, divided into three layers.

It can be noted that the loss of fine particles is slightly higher in the upstream part of the specimen in comparison with the middle part of the specimen. This result is in agreement with results of Ke and Takahashi (2012). The transport of detached particles from upstream to downstream parts can partly offset the loss of particles in the downstream part.

Moreover, these results confirm that suffusion is a complex combination of three processes: detachment, transport and possible filtration of the finer fraction. In consequence, even with the same average gradation as that of a post-suffusion-specimen, an homogeneous *reconstituted* specimen cannot represent an eroded specimen.

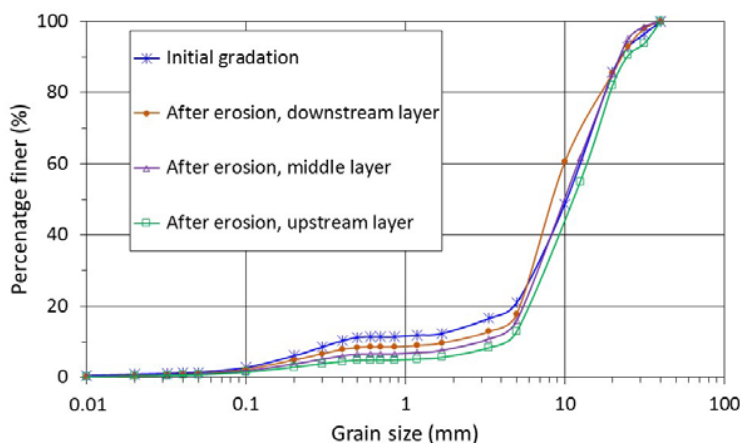


Figure 6. Initial gradation and post suffusion gradations of specimen 6.2-6.7.

### 3.3 Suffusion susceptibility characterization

The suffusion susceptibility is evaluated by the energy based method which characterizes independently the hydraulic loading and the induced erosion. The hydraulic loading is represented by the total energy expended by the seepage flow ( $E_{\text{flow}}$ ) which is computed until the simultaneous stabilization of the hydraulic conductivity and the decrease of the erosion rate. The occurrence of these two criteria represents the end of the suffusion process. For the same duration, the total eroded dry mass is measured to characterize the corresponding soil response. The erosion resistance index is then computed by equation (2). The corresponding values of  $I_{\alpha}$  for specimens 5.2-5.7, 6.2-6.7 and 11.2-11.7 are 4.3, 4.9 and 6.2 respectively. Therefore specimens 5.2-5.7 and 6.2-6.7 are moderately resistant whereas specimen 11.2-11.7 is highly resistant according to the suffusion susceptibility classification (Marot et al. 2016).

### 3.4 Influence of suffusion on the mechanical strength

Figure 7 shows the deviatoric stress versus the axial strain for the non-eroded specimen 6.2-6.7 and for the test on the same soil with a suffusion step (see Section 2.3).

It is worth noting that the suffusion process induces, in the case of this specimen, a decrease of the peak deviatoric stress, from 256 kPa to 208 kPa, which corresponds to a relative variation of 19%.

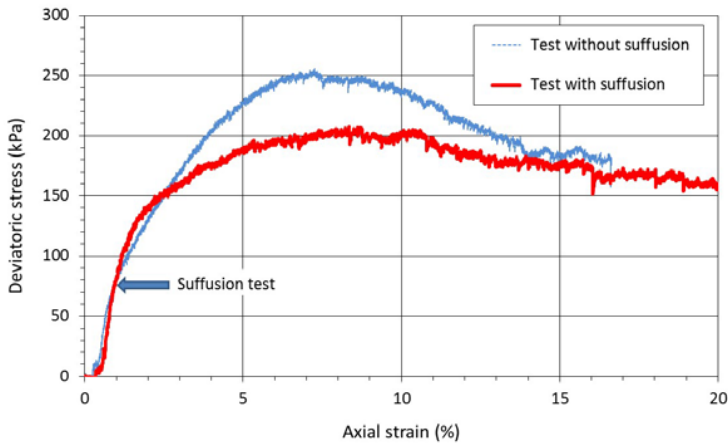


Figure 7. Deviatoric stress vs axial strain for specimen 6.2-6.7, with and without a full suffusion process.

Figure 8 shows the relative variation of each peak deviatoric stress versus the erosion resistance index for the three tested specimens.

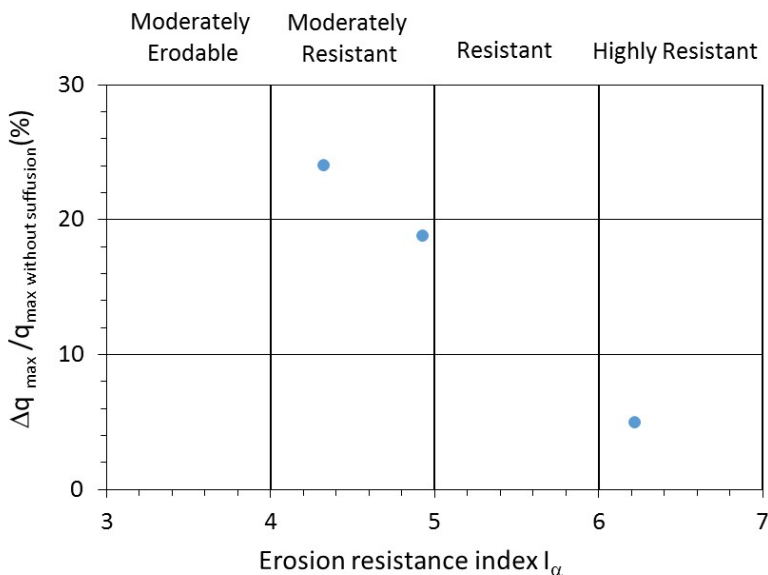


Figure 8. Relative variation of the peak deviatoric stress versus the erosion resistance index.

These first results highlight the decrease of the mechanical strength induced by a full suffusion process. Moreover, this decrease is more severe for the most erodible soils.

Since these results were obtained for moderately resistant and highly resistant soils, further investigations on other soils are needed to validate this trend.

## 4 CONCLUSION

In this study, a newly developed triaxial apparatus is used in order to investigate the mechanical consequences of a full suffusion process on coarse soils. The tested specimens consist of well graded coarse soils coming from a French dike. A series of monotonic compression triaxial tests is carried out on non-eroded soils and on post-suffusion soils. Suffusion tests are performed under multi-staged hydraulic gradient conditions. The interpretative method links the cumulative loss of dry mass to the energy dissipated by the fluid flow. At the end of the suffusion test, which corresponds to the invariability of the hydraulic conductivity and to the decrease of the erosion rate, the energy-based method permits to determine the suffusion susceptibility. For these soil specimens, the results show that an achieved suffusion process induces a decrease of peak deviatoric stress.

## ACKNOWLEDGEMENTS

The authors thank EDF for providing financial support for this work.

## REFERENCES

- ASTM Geotechnical Engineering Standards. (2003). Standard Test Method for Unconsolidated-Undrained Triaxial Compression Test on Cohesive Soils. *D 2850*
- Bendahmane, F., Marot, D. and Alexis, A. (2008). Experimental parametric Study of Suffusion and Backward Erosion. *J. Geotech. Geoenviron. Eng.*, **134**(1), 57-67.
- Chang, D.S. and Zhang, L.M. (2013a). Extended internal stability criteria for soils under seepage. *Soils Found.*, **53**(4), 569-583.
- Chang, D.S. and Zhang, L.M. (2013b). Critical hydraulic gradients of internal erosion under complex stress states. *Journal of Geotechnical and Geoenvironmental Engineering* **139**(9): 1454-1467
- Fell, R. and Fry, J. J. (2007). *Internal erosion of dams and their foundations*, Taylor & Francis, London.
- Fell, R. and Fry, J.J. (2013). *Erosion in geomechanics applied to dams and levees*, S. Bonelli Ed., ISTE—Wiley, London, 1–99.
- Hicher P.-Y. (2013). Modelling the impact of particle removal on granular material behavior. *Géotechnique* **63**(2): 118–128
- Indraratna, B., Israr J. and Rujikiatkamjorn, C. (2015). Geometrical method for evaluating the internal instability of granular filters based on constriction size distribution. *J. Geotech. Geoenviron. Eng.*, **141**(10), 04015045.
- Ke, L. and Takahashi, A. (2012). Strength reduction of cohesionless soil due to internal erosion induced by one dimensional upward seepage flow. *Soils Found.*, **52**, 698–711.
- Ke, L. and Takahashi, A. (2015). Drained monotonic responses of suffusional cohesionless soils. *Journal of Geotechnical and Geoenvironmental Engineering* **10**.1061
- Kenney, T.C. and Lau, D. (1985). “Internal stability of granular filters”. *Can. Geotech. J.*, **22**, 215-225.
- Marot, D., Bendahmane, F., Rosquoët, F. and Alexis, A. (2009). Internal flow effects on isotropic confined sand-clay mixtures. *Soil & Sediment Contamination, an International Journal*, **18**(3), 294-306.
- Marot, D., Regazzoni, P.L. and Wahl, T. (2011). Energy based method for providing soil surface erodibility rankings. *J. Geotech. Geoenviron. Eng.*, **137**(12), 1290-1294.
- Marot D., Rochim A., Nguyen H.H., Bendahmane F., Sibille L. (2016). Assessing the susceptibility of gap graded soils to internal erosion: proposition of a new experimental methodology. *Natural Hazards* **83**(1): 365-388
- Muir Wood D., Maeda K., Nukudani, E. (2010). Modeling mechanical consequences of erosion. *Géotechnique* **60**(6), 447–457
- Nguyen, H.H., Marot, D. and Bendahmane, F. (2012). Erodibility characterisation for suffusion process in cohesive soil by two types of hydraulic loading. *La Houille Blanche, International Water Journal*, **6**, 54-60.
- Reddi, L.N., Lee, I. and Bonala, M.V.S. (2000). Comparison of internal and surface erosion using flow pump test on a sand-kaolinite mixture. *J. ASTM Geotech Test.*, **23**(1), 116-122.

- Rochim A., Marot D., Sibille L. and Le V.T. (2017). Effect of hydraulic loading history on the characterization of suffusion susceptibility of cohesionless soils. *Journal of Geotechnical and Geoenvironmental Engineering*. Accepted, in press. DOI: 10.1061/(ASCE)GT.1943-5606.0001673.
- Scholtès L., Hicher P.Y., Sibille L. (2010). Multiscale approaches to describe mechanical responses induced by particle removal in granular materials. *Comptes Rendus Mécanique (CRAS)* **338** (10-11): 627-638
- Skempton, A.W. and Brogan, J.M. (1994). Experiments on piping in sandy gravels. *Géotechnique*, **44**(3), 440-460.
- Sterpi D. (2003). Effects of the erosion and transport of fine particles due to seepage flow. *International Journal of Geomechanics* **3**(1): 111-122
- Wan, C.F. and Fell, R. (2008). Assessing the potential of internal instability and suffusion in embankment dams and their foundations. *J. Geotech. Geoenviron. Eng* **134**(3); 401-407.
- Zhong C., Le V.T., Bendahmane F., Marot D., Zhenyu Y. Investigation of spatial scale effects on suffusion susceptibility. *Journal of Geotechnical and Geoenvironmental Engineering*. Submitted

# Resistance to erosion of lime treated soils and perspectives for coastal dikes

M. De Baecque

*IFSTTAR, GERS, Marne-la-vallée & Salon de Provence, France*

C. Chevalier<sup>1</sup>, S. Palma Lopes<sup>1</sup>, M. Le Feuvre<sup>1</sup>, P. Reiffsteck<sup>1</sup>, I. Charles<sup>2</sup> & G. Herrier<sup>3</sup>

<sup>1</sup>*IFSTTAR, Marne-la-vallée, Bouguenais & Salon de Provence, France*

<sup>2</sup>*Cerema Nord Picardie / BEE – AB, Sequedin,, France*

<sup>3</sup>*Lhoist R&D, Nivelles, Belgium*

**Abstract:** Fluvial and coastal dikes are the primary protection for human life from natural hazards like flooding or wave action. To build these hydraulic earthworks requires many materials with specific performances in terms of workability, mechanical strength, permeability, resistance to erosion, etc. Very often, local material does not meet requirements imposed by standards, and the transportation of material over long distances is only a short-term solution from an environmental point of view. Lime is used for construction purposes because it decreases the plasticity index and water content of soil, which facilitates compaction and improves its mechanical performance over time. However, the resistance to erosion of lime-treated earthwork remains little known and this is one of the reasons why lime has not been applied to dikes yet.

The engineering behavior of lime-treated dikes depends on the lime-soil interaction and environmental impacts. This study focuses on the comparison between raw and treated material behaviors regarding erosion processes and the effects of water. Erosion tests were carried out on two full-scale experimental dry dikes and laboratory samples for different curing times. Three types of tests were performed: Mobile Jet Erosion Test (an apparatus that can be used either in the laboratory or in the field), Hole Erosion Test (an efficient and convenient laboratory apparatus) and Enhanced Crumb Test (an evolution of the ASTM Crumb Test). In all configurations (soil and apparatus), this study reports a great increase in the resistance to erosion of the treated materials, which leads to a significant reduction in the risk of both internal and surface erosion of earthworks. Last, we discuss the application of these materials for building coastal dikes (characterization of the sustainability of lime treated soil versus saline environment, wetting-drying cycles etc.), and the possible monitoring of such a full-scale coastal dike by geophysical methods.

Keywords: lime treatment, soil, erosion, dike

## 1 INTRODUCTION

Lime treatment of soil is a widely applied technique throughout the world for improvement and soil stabilization of road works, embankments, railroad beds, etc. Soil workability and mechanical strength are increased for lime treated soil compared to natural compacted soil. Nevertheless the use of lime treated soils in hydraulic earthwork is very restricted, especially at the European level.

In this context Lhoist Group in collaboration with academic research institutes has initiated a project to study lime treated soil behavior with regard to erosion processes. A part of this projet was carried out by IFSTTAR which performed laboratory erosion tests and also erosion test on an experimental full-scale lime treated hydraulic structure (Chevalier et al., 2015). Quicklime CL-90Q with 90.9% available lime content and  $t_{60}=3.3\text{min}$  reactivity (norm EN 459-1) was used.

Initially, experimental studies were carried out in the lab using compacted samples of natural lime-treated and untreated soils with mastered protocols. Then, in situ tests were performed on two full-scale structures built in the Experimental and Research Center in Rouen (Charles et al., 2012).

## 2 METHODS

To study the soils resistance to erosion and water sensitivity three devices were used, the Mobile Jet Erosion Test (Reiffsteck et al., 2012) , Hole Erosion Test (Haghighi, 2013) and Enhanced Crumb Test (Haghighi et al., 2012b).

### 2.1 Mobile Jet Erosion Test (MoJET)

The MoJET is a rotating erosion test apparatus, which can be used both in the lab and in-situ (Reiffsteck et al., 2012; Haghighi, 2013). MoJET results can be compared with other laboratory tests such as the Hole Erosion Test (HET) (Chevalier et al., 2010).

The MoJET is made up of one mechanical part, named “eroding unit” with 6 rotating water jets, a water supply tank with the possibility of pressurization, and a few additional parts (pump, flowmeter etc.). The eroding unit projects water jets with 0.5 mm diameter nozzles (Fig. 1a) perpendicular to the soil. The mould is placed on a 10% slope (6 degrees) (Fig. 1.a and 1.b). The outfall ring is inserted around the mould while directing the outfall towards the downstream side of the slope into the top of the measurement container. The ground is then subjected to the action of the water jets with the following test parameters:

- imposed flow rate of 600 ml/min (standard, jet pressure is approximately 36kPa) or 2 000 ml/min (modified, jet pressure is approximately 400 kPa),
- duration of the experiment: 15 minutes (standard, with sampling of the whole effluent at 1, 3, 5, 8, 11 and 15 minutes) or 5 minutes (modified, with sampling at 0.5, 1, 2, 3, 4 and 5 minutes).

After the test, the soil sample generally shows gullies located where the water jets impact its surface (Fig. 1c).

Effluent collected at the different times are placed in the drying oven and measured to determine the mass of dry material eroded (Pham, 2008, Reiffsteck et al., 2012). This solid load (i.e. eroded mass as a function of time) can be used to perform qualitative evaluations of erosion, to establish correlations between the amount of eroded soil and geotechnical properties, or to compare between various soil behaviors.

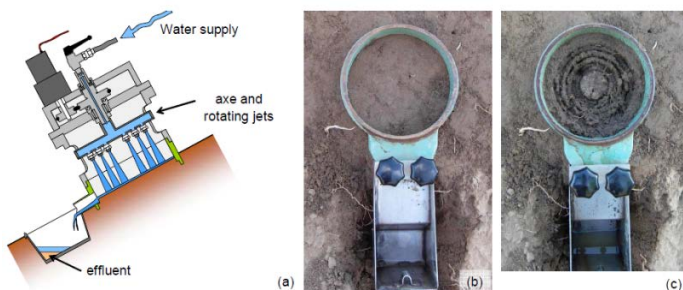


Figure 1. Mobile jets erosion (MoJET) test set-up: (a) Schematic diagram of eroding unit. Image of eroding unit in field (b) before and (c) after test

## 2.2 Hole Erosion Test

In order to quantitatively characterize piping erosion, the Hole Erosion Test recently developed by Wan and Fell (2004) was a great step forward.

We recently designed and developed our own HET device (Pham, 2008; Haghighi et al., 2012a). Similar to the one developed by Wan and Fell, it presents a number of improvements designed to make it easier to use and more comprehensive for measuring erosion parameters on process.

The HET device has three parts: an upstream water tank, an eroding unit where the sample is located and a downstream water exit. The erosion unit is depicted in figure 2 along with the measuring instruments. The soil sample is prepared in a cylindrical Plexiglas mold. The dimensions are 7cm in diameter and 15cm in length (volume: 500 cm<sup>3</sup>), and vertically drilled. The diameter of the initial hole is 3 or 5mm. After bringing water to the system and especially in the sample, the air pressure in the upstream water reservoir is raised gradually until the desired pressure difference is reached. This pressure difference is kept constant after the erosion occurred. During the test, from the increase of head charge to the decrease, the data collected by flow meter (flow rate  $Q$ ), pressure transducers (pressure drop  $\Delta P$ ) and turbidimeter (turbidity  $T$ ) are stored on a computer using a data-logger. The acquisition frequency is generally 1 Hz. These measurements and data on initial and final radii allow us to calculate erosion curves (interpretation method detailed in Pham (2008) and Haghighi et al. (2012a)) i.e. the relationship between the two following physical quantities:

- the shear stress  $\tau$ , applied to the interface by the flowing liquid applies (SI unit: Pa),
- the erosion rate  $\dot{\epsilon}$ , defined as the mass of soil eroded per unit area and time (SI unit: kg.m<sup>-2</sup>.s<sup>-1</sup>).

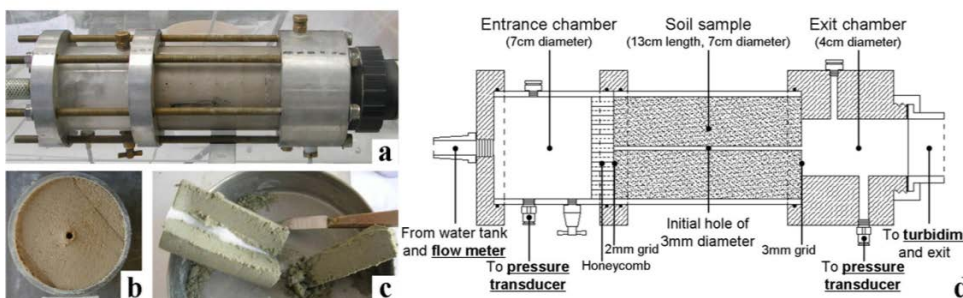


Figure 2. Experimental set-up and soil sample treatment. (a) Image of eroding unit. (b) Sample before test with 3mm diameter hole. (c) Cut sample after test with wax mold. (d) Drawing of eroding unit. Sensors are indicated in bold and underlined characters.

## 2.3 Enhanced Crumb Test (ETC)

The aim of this experimental method is to quantify the disaggregating geometry of an immersed unsaturated soil specimen as a function of time (Haghighi et al., 2012b). With this purpose in mind, a soil specimen of 15 mm in diameter and 20 mm high is placed in a large water container and monitored by two digital cameras (Figure 2).

The general behavior of the soil specimens, after being placed in water, is almost the same but with different characteristics for different soil textures. This behavior can be divided into two different phases: (a) hydration and (b-c) dispersion. Nevertheless detailed characteristics (height of swelling, disaggregation time, etc.) vary between different soil textures.

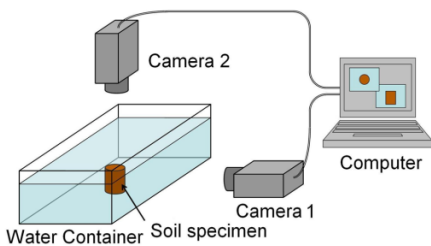


Figure 3. General layout of the experimental setup

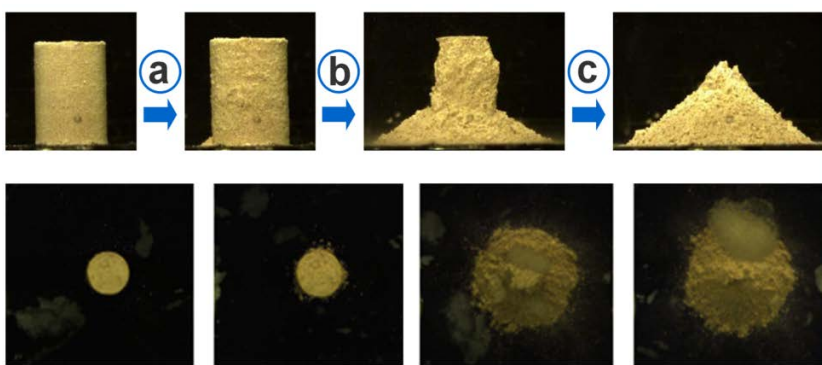


Figure 4. General behavior of a specimen

### 3 RESULTS AND INTERPRETATIONS

#### 3.1 Erosion test on laboratory rebuilt sample

Two different fine graded soils, a silty and a clayey soils, from Héricourt (Haute-Saône, France) were used to perform the tests. Test results on both the silty and the clayey soils showed a considerable increase in all aspects of erosion resistance for treated soils. Results are detailed in Chevalier et al (2012) and Haghghi (2013).

Regarding HET tests, the critical shear stress cannot be measured for treated soil: for the silty treated soil it is higher than 800Pa, being at least 2 times greater than shear stress for untreated silt.

Images of an example of an untreated silt sample and a treated one are given on figure 5.

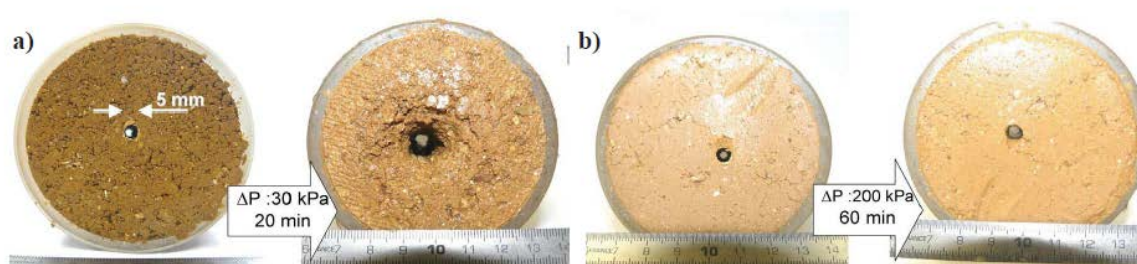


Figure 5: Typical HET results on materials. (a) Untreated silt before and after test (pressure difference of 30KPa during 20 minutes), (b) treated silt before and after test (pressure difference of 200KPa during 60 minutes).

The MoJET tests using the standard protocol do not cause erosion on treated soil. Using the modified protocol, eroded masses are at least 80 times lower for treated soil compared to untreated soil.

Treated soils therefore are virtually water insensitive according to ECT tests. The swelling is very low and crumbling almost nonexistent (Figure 6).

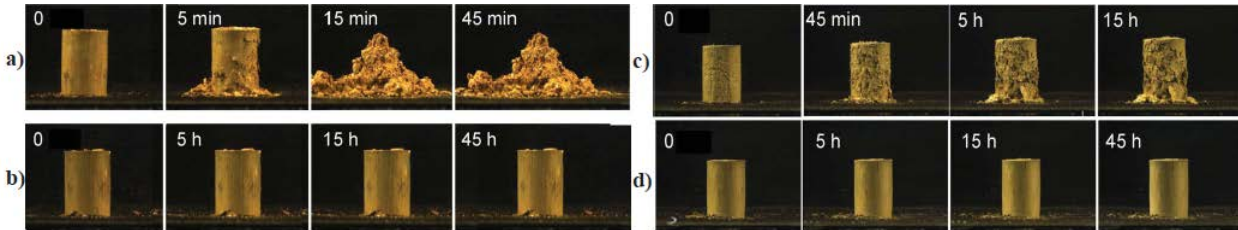


Figure 6: Evolution of the geometry of ECT soil specimen during test. (a) Untreated silty soil, (b) treated silty soil, (c) untreated clayey soil, (d) treated clayey soil.

To make an assessment, lime treated fine soils present a considerable increase in erosion resistance compared to untreated clay and silty soil. Nevertheless, samples were built in the laboratory under strictly controlled conditions especially regarding homogeneity and compaction. In practice, on the building site and under industrial conditions of construction, parameter states of soil and special homogeneity are less controlled and can vary significantly. Therefore, a study on a full-scale dike was performed and is presented below.

### 3.2 Tests on experimental full scale structures

In this section, in situ and laboratory tests performed with soil from two full-scale experimental hydraulic structures built in the Rouen CER (Experimentation and Research Center) are presented (Charles et al. 2012). The structures were two dry dikes built with silty soil from “Marche-les-Dames”(Belgium), one had been treated with 2.5% lime and the other was untreated. The treatment was performed using a mobile mixing plant. Materials were compacted in the wet state, at 17% water content (wOPN+2%) in the case of the untreated silt structure, and at 19.4% (wOPN+1.6%) in the case of the treated soil structure. Pictures of the two dikes are presented in figure 7. The treated soil homogenization was guaranteed throughout the production using the mixing plant, and its compaction was performed by a sheepfoot roller (kneading compaction). Consequently, laboratory conditions of preparation are well reproduced in situ.



Figure 7. View of the experimental dry dikes built at the Rouen Experimentation and Research Center: on left the lime treated dike and on right the untreated dike.

To compare natural soil and lime treated soil behavior regarding erosion, specimens were sampled from the two dikes to perform the Hole Erosion Test (HET) and the Crumb test (ECT). MoJET tests were directly performed on the dikes (treated and natural).

### 3.2.1 Mobile Jet Erosion Test (MoJET)

Tests were performed in situ 28, 180 and 368 days after the building. In most cases, two repeatability tests were carried out for each configuration (soil constitution, protocol and curing time). Tests were performed under temperate climate (15°C mean at 28 days, 20°C mean at 180 days and 15°C mean after 365 days) and without intense rainfalls. Nevertheless, dikes spent winter without superficial protection and at 180 days, a few millimeters of flaky crust had appeared on the free surface of the lime treated dike (Figure 8). That crust was not there after 28 days curing. The two erosion protocols were used on each dike (classic: 600mL/min during 12min; and modified: 2L/min during 5min).



Figure 8: On left the flaky crust which appeared between 28 and 180 days after the construction. On right, this crust is removed using a brush.

Figure 9 shows treated and untreated dike surfaces after tests using the normal protocol. First, we note a large difference in erosion depth and water penetration between tests performed on the treated and untreated dike. Because of the very low permeability of treated dikes, the water stream around the mould and the infiltration depth were only a few millimeters. Removing the superficial layer, the soil water content below was still the same as before solicitation.

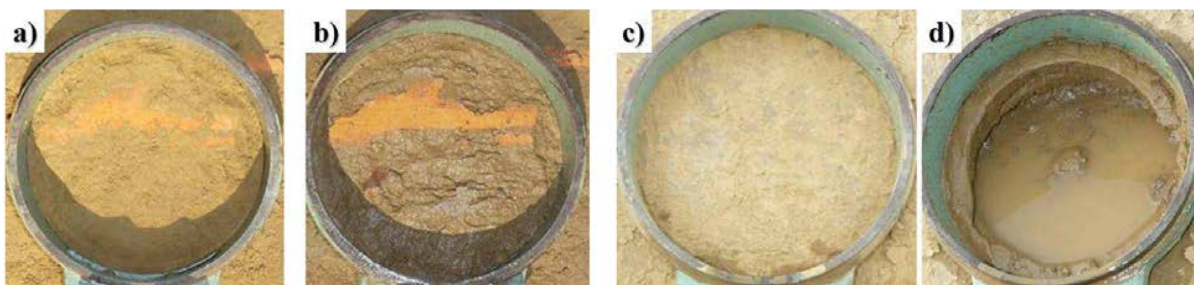


Figure 9. Soil surfaces before and after normal protocol MoJET tests, 28 days after the construction. Soil treated before test (a) and after test (b); untreated soil before test (c) and after test (d).

Results from the 28 curing days test program are shown in figure 10. The repeatability tests are also plotted. The total eroded mass with the classical protocol is on average 900g for the natural soil, against 35g for the lime treated soil. With the modified protocol these values reach 1000 and 80g.

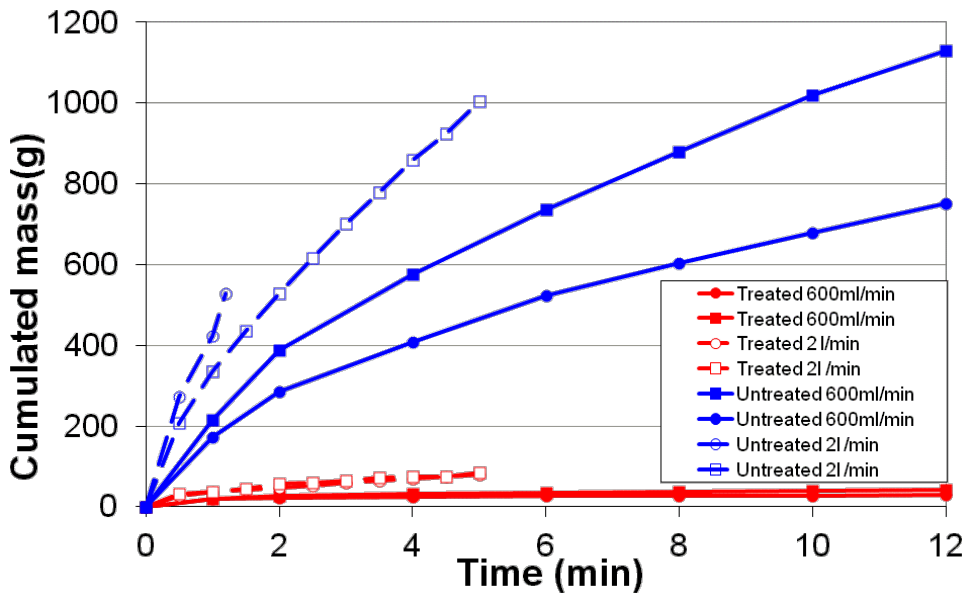


Figure 10. Cumulated mass versus time for the tests 28 day after the construction

The test performed on the natural soil dike gave the same results at 28 and 180 curing days. For the soil treated dike, systematic differences were observed in the eroded masses with and without the flaky crust (Figure 11). The crust showed a low resistance to erosion and was eroded during the 2 first minutes of the test. After the crust was removed the erosion rate from the two layers became similar. Apart from this difference, the results followed similar trends between 28 and 180 days: 1130g natural soil eroded and 40g treated soil eroded in the configuration without the flaky layer, using the classical protocol (600mL/min).

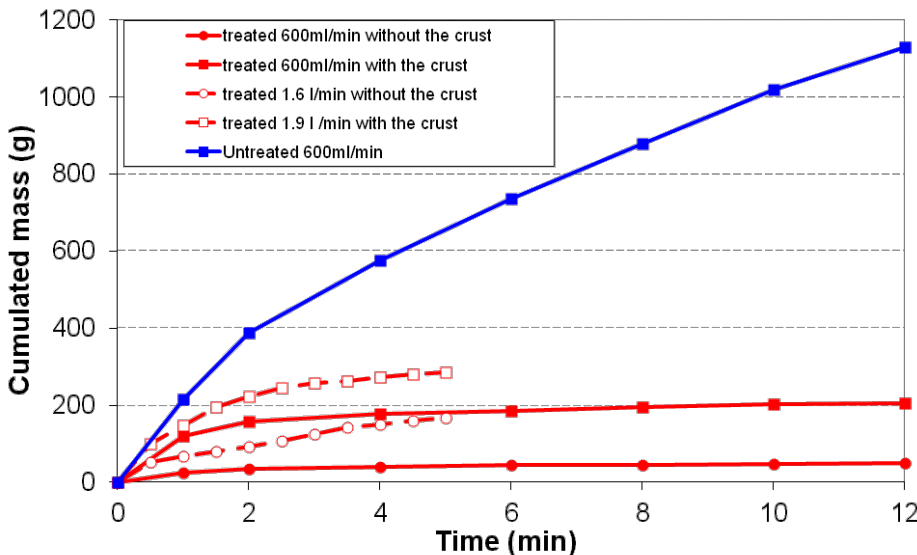


Figure 11 : Effect of the flaky crust on the eroded mass for the tests 180 day after the construction.

After 365 days of curing, tests were only performed on the soil treated embankment, at different depths (surface, 2 and 5cm deep), and on one surface covered by a vegetated layer. The classical protocol was used.

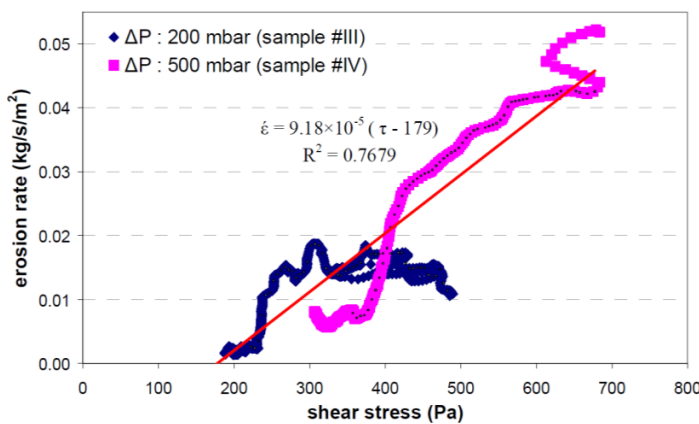
As for the 180 day tests, we note a difference between the uncleaned surface (crust not removed) and the other configurations (surface cleaned, 2 and 5cm deep), especially during the 2 first minutes, the time needed to totally erode the superficial crust. After that the erosion rates remained similar. The results follow trends close to the 28 and 180 days tests. At 2 and 5cm deep the cumulated eroded masses are respectively 80 and 15g. Under the vegetated surface, the cumulated eroded mass is 50g.

Plants seem to protect treated soil from surface degradation, often caused by hydric and temperature variations.

Erosion resistance is therefore higher on the construction using lime treated soil than on the one using natural soil: whatever the protocol, the finale eroded mass is at least 10 times lower. This resistance is obtained after 28 days and is maintained over time, except for the superficial crust observed after the winter. Nevertheless this crust does not appear if the embankment is protected by plants, which is a current esthetic technique to integrate embankments into their environment.

### 3.2.2 Hole Erosion Test (HET)

For this test, soil was sampled from the two dikes 28, 180 and 365 days after the construction, using a PVC cutting edge in the case of the natural construction (500mm long and 80mm external diameter), and a double envelope core drill on the treated embankment. Samples were cut (diameter 68mm, height 150mm) and sealed in a mould using silicone gel to avoid parasitic erosion between the sample and the mould. Two tests were performed using untreated 28 days curing soil, of which one with 20kPa hydraulic solicitation and the other with 50kPa hydraulic solicitation. Experimental curves are given in Figure 12. The critical shear stress for natural soil is about 180Pa.



$$\tau_c = 179 Pa \quad k_{er} = 9.18 \times 10^{-5} s / m$$

Figure 12 Tests result performed with core sampling from the untreated dike, with 20 and 50 mbar hydraulic solicitations

Regarding the lime treated embankment, tests show a very high erosion resistance at 28, 180 and 365 curing days. Note that 180 and 365 days old samples are ductile. Therefore, during sampling and preparation, these samples have more risk of being disturbed or cracked.

Among the 8 tests carried out on treated soil, only two may have shown weak initiation of erosion for a critical shear stress lower than 800Pa.

Results again reveal that treated and untreated soils have very different behaviors. There is at least a factor 4 increasing in critical erosion shear stress values between treated and untreated embankments.

### 3.2.3 Enhanced Crumb Test (ECT)

For the test after 28 days of curing, the typical visual aspect of the sample geometrical evolution is presented in figure 14. Final morphology is reached after 10 minutes of immersion. Contrary to lab rebuilt soil, samples taken from the treated dike present very low water sensitivity. They crumble slowly and less intensively than the untreated samples. Moreover, the aggregates which come off are bigger than those from the untreated soil.

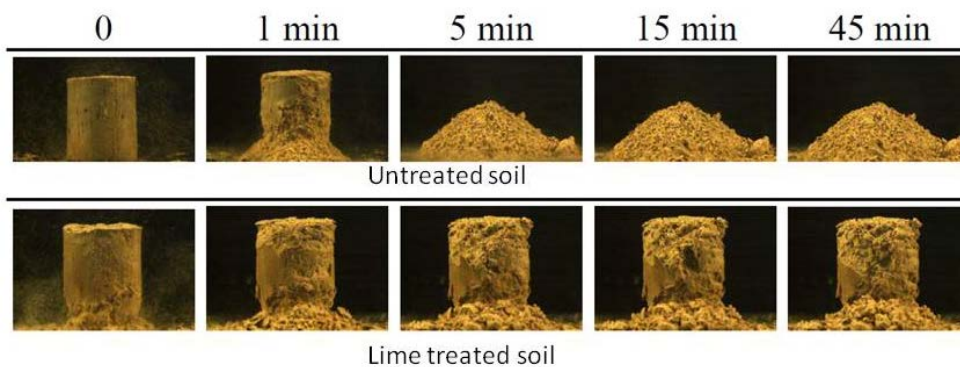


Figure 13. Representative tests results for cores sampled in the treated dike (down), and untreated (above) after 28 days of curing. No evolution observed beyond 45 minutes.

Tests performed at 6 months and 1 year curing times on samples removed from the treated embankment gave similar results to those at 28 days of curing.

In the case of soil treated samples, surface and volume behavior must be differentiated. Surface behavior is largely impacted by the way of sampling. Because of the material high mechanical strength, the cutting edge has a strong effect on the soil structure. It impacts the short-term behavior (i.e. 1 to 5 min) but not the long term behavior. On the other hand, volume behavior does not show any water sensitivity.

To conclude, sampled materials from the treated embankment have a very low water sensitivity compared to those from the untreated dike. In particular, there is less swelling and the sample does not totally collapse after the hydratation phase.

## 4 CONCLUSION

After a lab parametric study (Chevalier et al. 2012), sensitivity to erosion was studied in two full scale flood protection dikes in order to characterize and to compare behaviors of lime treated and untreated soils.

Test results on treated and untreated dikes proved a considerable increase in all aspects of erosion resistance for treated soils. Treated soil properties seem to be maintained over time and during long loading periods which is not the case for the untreated soil. Results obtained are in line with tests performed on lab-reconstituted soil. The increase in resistance to erosion is lower in situ than in the lab sample. Among possible explanations, we can cite: differences in soil preparation, weathering due to climate and material damage caused by in situ sampling. Nevertheless, in any case, differences between lime treated and untreated soils are significant.

In this study, soil sensitivity to erosion is described for materials, which have not suffered strong degradations. Future studies will focus on the durability of the lime treated soil in coastal environments. The first tests will be performed using lab-reconstituted samples. We will stimulate the aging of the materials by imposing wetting-drying cycles. These cycles will be chosen to reproduce as closely as possible the real-life climatic effects of a marine environment. The impact of sea water will be studied.

Erosion tests will be completed by geophysical characterization at the lab-scale, in order to yield existing correlations to the resistance to erosion (e.g. critical shear stress, erosion rate). Then, erosion tests and geophysical measurements will be performed on a full scale experimental lime-treated coastal dike which will be built on the Mediterranean coast (*Digue 2020* project). The soils used for the coastal dike and for the lab study will be the same. First lab results are expected in the autumn 2017.

## ACKNOWLEDGMENTS

Digue 2020 is financed as a part of CPER 2015-2020, with the participation of the French State, PACA region and French department council 13.

Digue 2020 is financed with the participation of the European Union. The Europe commit in Provence-Alpes-Côte d'Azur with the European Found for Regional Development (FEDER)

## REFERENCES

- Charles, I., Herrier G., Chevalier C., and Durand E. (2012). An experimental full-scale hydraulic earthen structure in lime treated soil . *Proceedings of the Sixth International Conference on Scour and Erosion (ICSE)*, 181–188.
- Chevalier, C., Haghghi I., Pham T.L., and Reiffsteck P., (2010). Two complementary tests for characterizing the soil erosion. *Scour and Erosion*, 152-161.
- Chevalier, C., Haghghi I., and Herrier G. (2012). Resistance to erosion of lime treated soils: a complete parametric study in laboratory. *Proceedings of the Sixth International Conference on Scour and Erosion (VI ICSE)*, 161-168.
- Chevalier, C., Herrier, G. and Charles, I. (2015) Resistance to erosion of lime treated soils. *Proceedings of the 16th European Conference on Soil Mechanics and Geotechnical Engineering (XVI ECSMGE)*, 2773-2779
- Haghghi, I. (2013). *Caractérisation des phénomènes d'érosion et de dispersion : développement d'essais et applications pratiques*. PhD-thesis Université Paris-Est.
- Haghghi, I., Chevalier C., Duc M., Guédon S., and Reiffsteck P. (2012a). Improvement of hole erosion test and results on reference soils. *Journal of Geotechnical and Geoenvironmental Engineering* 139 (2): 330-39.
- Haghghi, I., Martin T., Reiffsteck P., and Chevalier C., (2012b). An “Enhanced Crumb Test” for better characterizing water sensitivity of soils. *6th International Conference on Scour and Erosion (VI ICSE)*, 1049-1056.
- Pham, T.L. (2008). *Erosion et dispersion des sols argileux par un fluide*. PhD-thesis Ecole des Ponts ParisTech.
- Reiffsteck, P., Haghghi I., and Chevalier C., (2012). Erodibility diagnostic of existing hydraulic earthworks by Mobile Jets Erosion Test. *6th International Conference on Scour and Erosion (IV ICSE)*, 1105-1112.
- Wan, C.F., Fell, R., (2004). Investigation of rate of erosion of soils in embankment dams. *Journal of geotechnical and geoenvironmental engineering* 130 (4): 373-80.

# Experiences on the use of polymer coated steel net for the protection of dykes against the intrusion of beavers

P. Di Pietro

*Officine Maccaferri S.p.A.*

**Abstract:** Recent studies show an increase in the population of beavers, nutria and other rodents in vast regions of central Europe over the last 15 years. Unfortunately, this caused in many instances considerable damage on large rivers along dykes and earthworks in the floodplain areas, leading to an increased risk of bank failures. However, most of these mammals belong to protected species. This work is aimed at showing positive experience in cooperation with universities, research institutes and environmental agencies regarding measures to permanently safeguard the banks using composite erosion control systems with polymer coated steel wire net (as flexible reinforcement component) and a geosynthetic (to promote vegetation growth). The steel mesh component works as an effective long-term barrier against the intrusion of mammals, discouraging them from digging inside the core of the dyke. An analysis of the sensitive areas to be protected led also to definition of the characteristics of these interventions (length, shape, escape ways, population areas, etc.). The study will present several additional benefits when using polymer steel nets along dykes, such as: high and durable erosion protection in overflow areas, promotion of fast and effective vegetation growth (increasing stability), surface protection against ice impacts (in northern regions), ease of installation, maintenance, ability to conform to irregular shapes of the slope. This work will also present the positive outcome of research studies along dykes in Germany, Austria and in Italy.

Keywords: beavers, nutria, steel net, dykes, erosion control.

## 1 INTRODUCTION

Beavers, nutria and other rodents can sometimes cause fairly large damage on bank slopes, along dykes or in earth-filled embankments.

In isolated cases, such damage caused by these mammals could lead to an increased risk of global slope failures with serious consequences of over flooding for the communities living in the area. Cavities created by beavers can be of high risk for the stability of the dyke. The highest risk is beavers digging through full or semi-impermeable layers. An opening through these layers leads to increased flow through the dyke, ultimately causing erosion and water seeping through the embankment all the way to the dry side. Although rodents can cause these damages, on the other side they shall be considered part of the protected wildlife living in these habitats, and hunting them to simply eliminate the problem cannot be considered as a solution.

According to a study published in 2011 [1, 2] by the Bavarian State Office in charge of environmental protection, authors have shown that the beaver population across Germany was estimated at around 25,000 units, with an increasing trend. An estimate across Europe in the same year was of approximately 800,000 beavers (Figs. 1 and 2).

Measures to be undertaken to permanently prevent such effects depend on the sensitiveness of local authorities for potential hazards caused to people and to infrastructure, as well as on costs required for the interventions and on the sensitiveness for the endangered species. Most critical failures consist in partial or total collapse of the embankment by sliding. The correct approach consists in identifying critical areas of the dyke by observing the effects of their action in the encroachment zone (Fig.3).

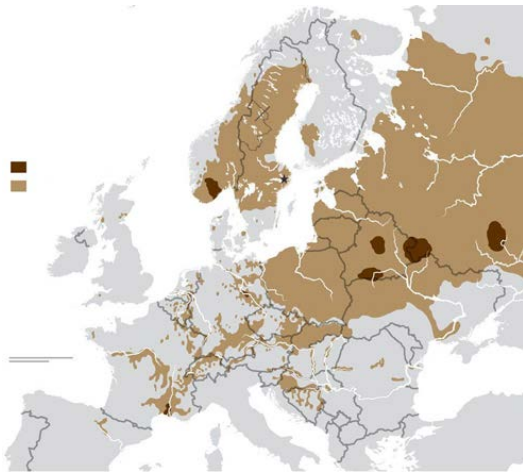


Figure 1. Presence of beavers (brown & dark brown) Fig.2 Beaver population expected to grow to 7000 in 2032.

The prevention against the intrusion of beavers, nutria, rodents and other protected species on dykes has been discussed for over 15 years and documented in studies carried out by academic Institutes and in works developed by technical expert groups [6].



Figure 3. Effects of beavers in floodway encroachment zones along the Odra river in Sophienthal (Germany)

## 2 CONCEPT AND SUMMARY OF RESEARCH

Safe and durable protection against intrusion in dykes consists in identifying a suitable environmentally friendly barrier system. Steel meshes have been used to this purpose for decades. In recent times, steel meshes were developed to combine the strength of the steel with the ability to vegetate provided by a three-dimensional geomat extruded during manufacture. The wire used for the steel mesh is protected

with a zinc-aluminum alloy and additionally by a polymer coating. The strength of the steel mesh will act as the impenetrable barrier for the rodents who will not be able to dig a hole through the steel net. The geomat will combine the anti-erosion function during flooding events and, by holding moisture, it will promote vegetation during the low flow season. These erosion mats may be delivered in rolled form and require very simple installation steps (Fig. 4).



Figure 4. Installation of beaver netting

In order to gain confidence about the effectiveness of steel meshes as beaver protection, several trials were carried out in channels and dykes, some of which were under the monitoring of technical universities, as described in the following chapters. To date, there is wide experience that steel mesh systems perform satisfactorily to this purpose.

## **2.1 Italy: Guidelines from Ministry of Environment and Long-Term Studies after 10 Years of Observation**

Italy has had a flourishing fur industry over the last century. In the 1920s, the population of beavers and nutria actually grew, to feed this sector of the industry. As fashions changed in the 70's, and awareness of protecting endangered species grew, factories were shut down and the animals released into the wild. This caused an increase of this population, which consequently led to more damage occurring to embankments. Observations on slopes previously protected by stone-filled mattresses, showed no damage due to rodents, as opposed to other sections nearby where damage was visible. This was deemed as proof that rodents were actually living in the area, but they could not damage slope sections protected with an armored lining.

Based on these observations, the Ministry of the Environment, in coordination with the "National Institute for the Wild Fauna" and the ISPRA (Institute for the Protection and Environmental Research) financed a long-term research study aimed at monitoring canal banks after the installation of barrier systems against the intrusion of rodents [3]. A section of a drainage canal (Zabarelle) located in the Province of Rovigo (in an open floodplain of the river Po) was chosen as affected by significant presence of rodents and damages (Fig. 5).



Figure 5. Installation of beaver netting along Zabarelle Canal

Steel meshes, with and without an extruded geomat, were installed in test sections in 2003. The initial survey allowed the capture and marking of a number of nutria, and attachment of a GPS-transmitter, in order to trace their movements. Results soon indicated that marked animals had moved to other sections.

In 2013, a second survey was arranged by ISPRA, to inspect these sections.

Observations showed that, where steel meshes with the extruded geomat had been applied, neither loss of fine material in the water change zones nor damage to the steel net due to grass cutting were detected.

Where steel nets had been applied without the extruded geomat, loss of fines was noted. This was presumably due to the lack of the geomat at some locations, where the eroded soil bank lost contact with the steel net, resulting in some damage during the grass cutting. The erosion function was not sufficiently provided by the open structure of the steel mesh alone. However, no intrusion of rodents was detected.

## 2.2 Austria: Tests on Effectiveness and Implementation of 300,000 m<sup>2</sup> of Protection

For decades, Austria experienced damage in waterways due to the intrusion of beavers. In 2008, the design of the protection measures along the river March (tributary of the Danube) took into consideration for the first time the effect of the beaver population with special reference to prevention of potential damage. The analysis considered the variability of the species and types of rodents (quite large), hence, the required strength characteristics of the protection netting, to resist to the animal's bite and discourage even the strongest species from attempting to penetrate the protection.

Following these early studies, a first trial project was built using double twisted steel netting (300,000 m<sup>2</sup>) in a river bank application. The scientific study was part of a diploma thesis done for the Institute for Applied Geotechnics at the Technical University in Vienna under the guidance and coordination of the Prof. Dipl.-Ing. Dr. H. Brandl [4]. Along with the observations and the experiences of the previous cases, the study encompassed an actual test carried out at the Research Center for Ethology at the Institute Konrad-Lorenz in Vienna.

The measures adopted were divided in two sections, where different protection systems (with and without steel nets) were used. The non-metallic systems showed that, after a short time, a fairly large area of damage occurred due to biting of the rodents. Based on these findings, the technical university in Vienna observed that the steel nets with the extruded geomat were the most recommended protection measure against beaver intrusion. The 5-year research study was between 2008 and 2013. It confirmed the expectations that steel nets with an extruded geomat perform as a permanent protection against the intrusion of rodents into the bank.

The ever increasing population of rodents along the banks of large rivers has increased the interest for the use of effective protection measures in Germany and Austria. Data about the beaver population

confirm that both in Upper Austria (Linz region) and in Carinthia (southern region) the beaver population has more than doubled [4].

### 2.3 Germany: Protective Measures against Beavers along the Odra Dyke, District Sophienthal, Brandenburg 2013

Between October and December 2013, in cooperation with the State Agency for Environment, Health and Consumer Protection Frankfurt/Oder and the Water and Dike Association Oderbruch, a beaver protection netting was installed in a trial section approximately 200 m long, near the community of Sophienthal (Fig. 6).

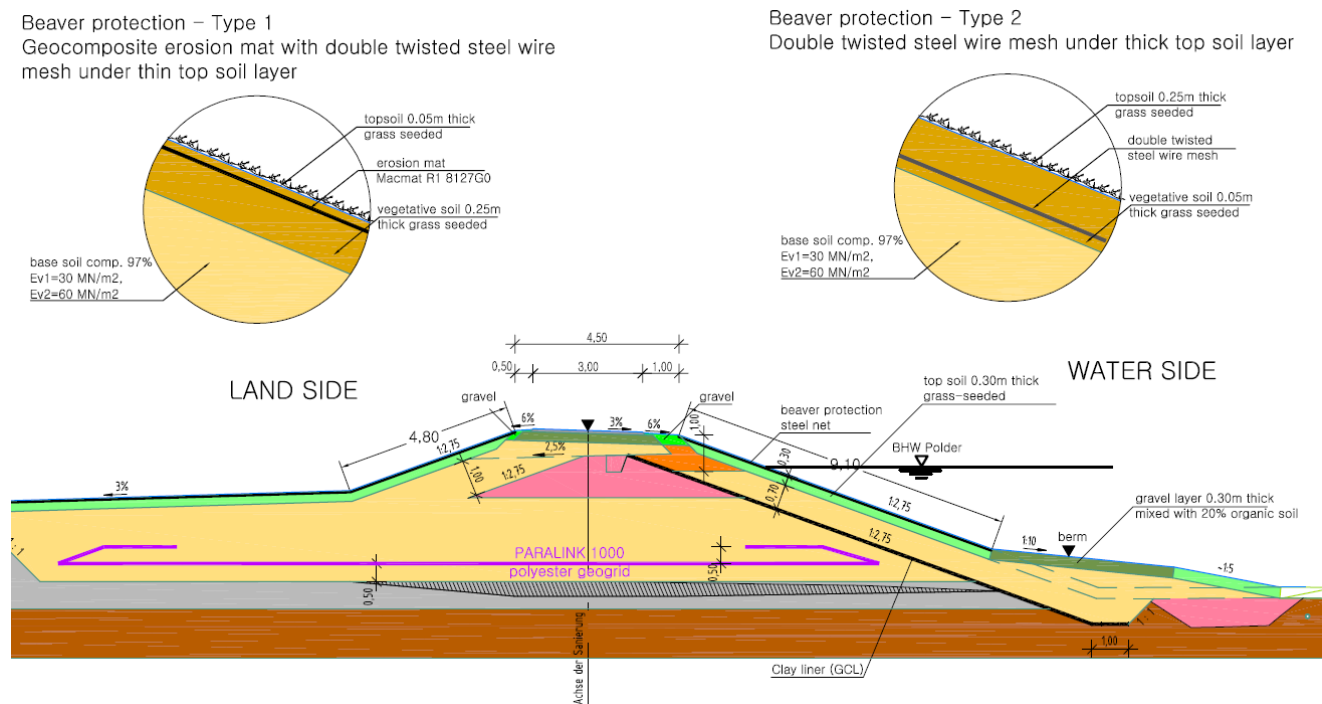


Figure 6. Odra Dyke, Sophienthal – Typical cross section

Three different protection systems were installed:

1. hexagonal steel wire mesh with integrated three-dimensional polymer matrix (MacMat R), covered by 5 cm top soil layer (Fig. 6, left bank);
2. hexagonal steel wire mesh, covered by 20 cm top soil layer;
3. hexagonal steel wire mesh, covered by 20 cm top soil layer, connected to a stone mattress layer below in the water section.

The erosion net starts from the top of the dyke and ends on the waterside, in the last case connected to the stone mattress below. Since further tunnels dug by beavers were detected in other sections nearby, the interventions were extended to these sections as well.

The execution of the works was under the supervision of the Institute of Hydraulic Engineering and Applied Hydromechanics (IWD) of the TU Dresden. IWD has been working for several years on the task and supervised a master diploma thesis on this topic in 2013.

### **3 NORMATIVE REQUIREMENTS FOR LONG LIFE OF STEEL WIRE MESHES**

The use of steel nets in geotechnical and hydraulic applications pose questions of performance in relation to corrosion. Galvanization (using zinc-aluminum alloys) provides an extended life, as the protection acts as a retardant to corrosion by sacrificial nature. Additional polymer coatings applied on the galvanized wire provide a further extended protection. A newer generation of polyamide (PA6) recently introduced a further step up in the life expectancy, allowing tests in severe saline conditions (ISO 9277) to exceed 6,000 h of exposure without trace of red rust on the inner steel core.

An important reference in Europe is the EN 10223-3:2013 [5] for double twisted steel wire meshes in civil engineering applications. Annex A in this standard provides (informative) guidance concerning the life expectancy of woven wire steel mesh, which defines, for polymer coated steel wire mesh, a minimum life of 120 years. In addition, 10-year-old guidelines in Germany [6] and Austria already provide guidance concerning the use of steel nets as protection systems against beavers in dams and dykes.

However, DVWK (Deutsche Vereinigung für Wasserkraft - German Association for Hydropower) 247/1997 has a requirement for beaver nets with respect to corrosion protection and effectiveness as vertical barrier not very effective over time. Experience shows that in numerous sections of the dykes where vertical galvanized steel nets were used burrows were still present between the embankment and the vertical barrier, with evidence of flooding and partial collapse.

Additionally, the progressive erosion into the bank required vertical barriers to work as supporting elements. This caused unexpected deformation of the nets, and an accelerated corrosion with loss of functionality;

Tunnels ended in proximity of the vertical barrier. However, this actually forced beavers to move and dig their tunnels beyond the vertical barriers into the upper berm, up to the toe of the main dyke.

During high flows, the stability of the main dyke became critical along few some sections, triggering initial failure.

### **4 OTHER FEATURES OF BEAVER NETTINGS**

#### **4.1 Increased Water Conveyance**

In accordance with the State Authority for Waterways (BAW) in Germany, erosion protection systems mainly consist of a layer of loose stones laid on a sand mat (a thin layer of sand between two layers of geotextiles) acting as an intermediate filter to prevent under piping through the voids of the larger rocks. Specifications for the stone size and for the layer thickness (0.50~1.0 m) are provided by BAW according to their design recommendations [7]. As an alternative to loose stones, steel meshes with the integrated geomat could be in many cases a viable and sound alternative. Tests performed on these reinforced erosion blankets have shown the ability to resist even high flows for a given period of time [8, 9]. The advantage of using a thin layer is also in the increased water conveyance, allowing a larger discharge in the river section.

#### **4.2 Ease of Maintenance**

In case of accidental damage to the beaver erosion protection blanket, repair works would simply consist in the replacement of the damaged parts by attaching a panel of steel mesh on the surface. Connections are made with conventional steel rings, used for connecting rolls together.

#### **4.3 Vegetation Enhancement**

In hydraulic works, the ability to develop a self-sustained vegetative layer, with a solid rooting system, to blend with the surrounding ecosystem is of particular importance. Newly built sections are highly

Extensive observations in areas protected by beaver nettings show that they protect against several other types of wildlife (rabbits, wild pigs, etc.) who are also frequently endangering the embankment stability. Beavers are discouraged from digging into the embankment and migrate to other areas.

However, these results raise questions concerning how beavers can populate in floodway areas without compromising structures designed to protect human lives. An answer could be to create environmentally friendly structures to allow them to populate safe floodway encroachment zones where they could establish their habitat without compromising the embankment's stability.

Trial projects have already started, and few authorities and research institutes have already positively responded to the initiative. These are first steps towards the development of a correct and more balanced approach to preserve our natural eco-systems and to promote development in harmony with human needs.

## REFERENCES

- [1] Kumutat, C. 2011. *Beaver in Bavaria —Biology and Management*. 2nd ed. Augsburg: Praesident des Bayerischen Landesamtes fuer Umwelt. (in German)
- [2] Schwab, G. 2011. Managing Beavers in South Bavaria. Extract from Conference in Künzell 09-2011, (in German).
- [3] Cocchi, R., and Riga, F. 2005. *Guidelines for the control of Nutria (Myocastor Coypus)*: Ministry of Environment, Rome —INFS. (in Italian)
- [4] Brandl, H., and Szabo, M. 2012. *Notes on the theme of the protection and safety of levees, dams and reservoirs*, Vol. IV, Siegen. (in German)
- [5] EN 10223-3: 2013. *Hexagonal Steel Mesh Products for Civil Engineering Purposes*.
- [6] DVWK. 1997. *Guideline 247/1997, Muskrat, Beaver and Nutria distinctive features and mode of life-style and safety of the endangered banks in levees and dams*. Bonn : DVWK. (in German)
- [7] BAW. 2010. *BAW Code of Practice—Principles for the Design of Bank and Bottom Protection for Inland Waterways (GBB)*. Karlsruhe: Bundesanstalt für Wasserbau.
- [8] Di Pietro, P., and Urroz, G. 1999. "Performance Testing on a Three-Dimensional Composite High Strength Soil Erosion Mat." In *Proceedings from IECA Conference 1999 Nashville*, P.163-174.
- [9] Nemeth, E., and Zanzinger, H. 2009. *Development and verification of selection criteria for geosynthetic erosion control systems* AiF Research Project, SKZ/LWG 2009-2011. (in German)
- [10] Di Pietro, P., Scotto, M., and Guastini, U. 2002. *Stabilizing and Waterproofing a Levee in Italy*. Geotechnical fabric report, August 2002, USA

# Merging criteria for the definition of a local pore and the CSD computation of granular materials

F. Seblany

<sup>1</sup>Université de Lyon, Ecole centrale de Lyon, LTDS, UMR CNRS 5513, 36 av Guy de Collongue 69134 ECULLY CEDEX, France

U. Homberg<sup>2</sup>, E. Vincens<sup>1</sup>, P. Winkler<sup>3</sup> & K.J. Witt<sup>3</sup>

<sup>2</sup>Zuse Institute Berlin, Department Visual Data Analysis, Takustr. 7, 14195 Berlin-Dahlem, Germany

<sup>3</sup>Bauhaus-Universität Weimar, Chair of Geotechnical Engineering, Coudraystrasse 11c, 99421 Weimar, Germany

**Abstract:** Granular filters are materials used to avoid mass transport under seepage flow. They are installed in zoned dams or on the downstream slope of levees to prevent the wash out of soil particles through the core of the earth structures or through its foundation. This migration is stopped if the particles are blocked on their pathway by a constriction smaller than their own size. In that sense, the constriction size distribution is closely related to the filtering capability of the granular filter. Different numerical methods exist to study and divide the pore space into local pores and then constrictions. However, they all require a statement of what a local pore is. Al-Raoush et al. (2003) noticed that the partition of the void space may lead to an over-segmentation of the pore space and merging criteria may be used to define more physical local pores. Conversely, merging may require thresholds that may influence the final degree of the segmentation. In this paper, we compare different merging criteria and discuss their implication on both the local pore definition and the constriction sizes statistical distribution. Moreover, since the constriction size distribution is often used in probabilistic approaches for filtration, we insist on the necessary consistency of the choice of a given merging criterion with other possible statements related to these probabilistic approaches.

Keywords: constriction, sphere packing, probabilistic approach, filtration

## 1 INTRODUCTION

Internal erosion is one of the leading causes of failure of earth structures used in hydraulic engineering and for flood protection (earth dams, levees). This phenomenon occurs when fine particles are detached and transported through the porous medium due to a seepage flow. Granular filters are installed during the construction works in hydraulic structures or on their downstream slopes when repairing in order to avoid or to limit the migration of fine particles. In such a circumstance, they are supposed to mitigate internal erosion.

A granular medium includes a set of connected pores between solid particles that form a continuous network through which a fluid can flow. The constrictions are the narrowest sections linking larger volumes (pores) and are statistically described by means of a cumulative constriction size distribution (CSD).

The retention capacity of a granular filter is mainly related to the geometrical characteristics of its void space. More precisely, the performance of a granular filter can be evaluated and characterized using the information provided by the CSD. Indeed, based on the probabilistic concepts of Silveira (1965), the CSD is related to the probability for a fine particle of diameter  $d$  to cross a constriction having the same size. In fact, fine particles smaller than the smallest constriction  $d_{Cmin}$  can cross the entire filter

(probability of passing = 1). Conversely, all particles larger than the largest constriction  $d_{Cmax}$  will not enter the filter (probability of passing = 0) (Fig. 1.1).

There are different ways to obtain the CSD: experiments (Witt, 1986; Soria et al., 1993), analytical approaches (Locke et al., 2001; Reboul et al., 2010) and numerical approaches (Reboul et al., 2008; Homberg et al., 2012; O'Sullivan et al. 2015).

To overcome some limitations associated with experimental methods, a powerful numerical tool, the Discrete Element Method (DEM), can be used to study modelled granular materials such as packings of spheres and to numerically generate them. The pore space of such packings can be extracted by combining the DEM with spatial partitioning techniques: the Delaunay tessellation or its dual, the Voronoi algorithm. In the Delaunay tessellation, the primary definition for a local pore is the Delaunay cell, i.e., a tetrahedron. The associated void volume can then be deduced for example by computing the largest void sphere inscribed between the four particle vertices of the tetrahedron. Constrictions are found on the four faces of each tetrahedron and are defined as the largest empty discs that can be inscribed between the three particle vertices of a tetrahedron face (Fig. 1.2) (Al-Raoush et al., 2003; Reboul et al., 2008). Obviously, the derived partition of the void space is artificial and a Delaunay cell is merely related to the underlying mathematical process of finding the three closest neighbors of a given particle to generate a tetrahedron. The computation of pores and constrictions are feasible for a granular material made of spheres but is very difficult to handle in the case of irregularly shaped particles.

To solve this issue, Homberg et al. (2012) have developed a voxel-based approach that computes a Voronoi-like decomposition based on a distance mapping on the pore space and the particle regions and extracts the median paths of the void space. Along these paths, the center of pores, the pore diameters and the local minima associated to constriction sizes can be determined.

One of the obstacles related to these methods is to identify pore structures that may hold a physical meaning. In this context, Al-Raoush et al. (2003) were using a Delaunay tessellation and found that the inscribed void sphere confined in each tetrahedron is not necessarily entirely included inside that tetrahedron, and two inscribed void spheres from two neighboring tetrahedra may overlap. According to these authors, it signifies that the opening size between two adjacent tetrahedra may be high enough to indicate a strong interconnection between them which is reflected by this overlapping. As a result, the tetrahedral tessellation would tend to abusively subdivide a complete pore structure into zones.

For the same reason, Homberg et al. (2012) considered that a merge between two adjacent pores may be required when the constriction size linking these pores is very close to that of the smallest pore. In fact, in such a case, pores are interconnected and seem to belong to a single entity. Figure 1.1(b) illustrates such a case where two adjacent pores (hatched and shaded area) are going to be merged.

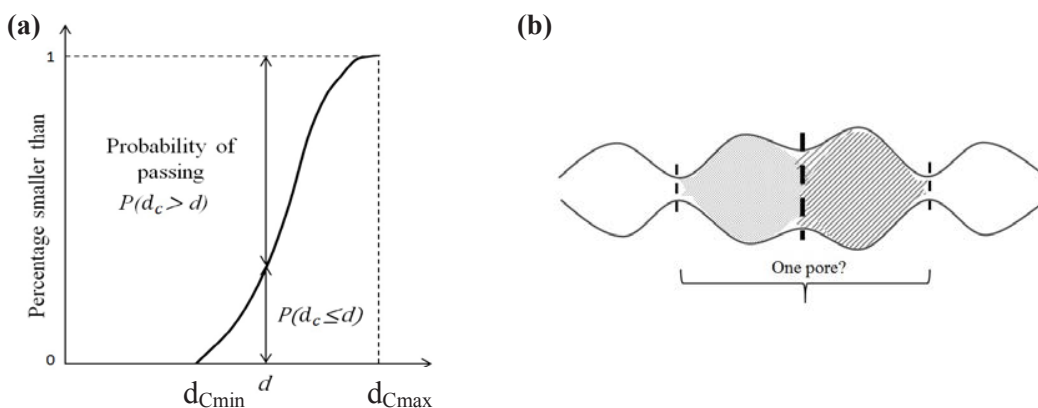


Figure 1.1. (a): Constriction size distribution and probability for a fine particle of diameter  $d$  to pass a constriction of its own size; (b): Scheme of a typical case encountered during pore merging.

Because different methods may lead to different pore structures and as a consequence to a different set of constriction sizes, this study aims to understand better the implications of using a given merging criterion on the pore and constriction statistics. Conversely, this paper does not address the definition of what a physical local pore should be since no clear definition for a local pore can be stated. In a second part, the impact of the merging criteria on the estimate of the average unit path distance (average distance between consecutive throats through the granular filter) is addressed.

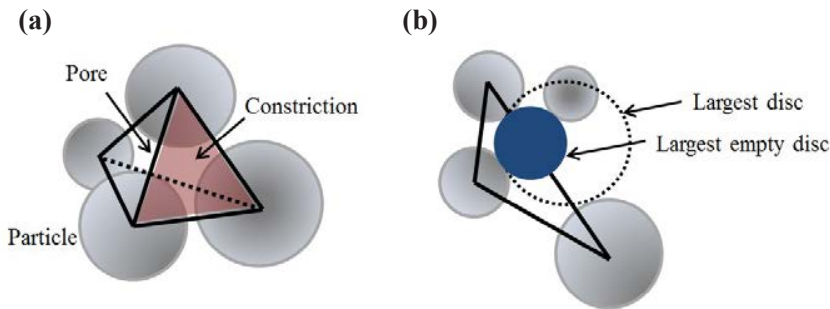


Figure 1.2. **(a)**: Tetrahedron built from the centers of four neighboring spheres; **(b)**: Definition of a constriction: the largest disc included in the void space for a given face.

## 2 GENERATION OF NUMERICAL SAMPLES

The open-source code Yade-DEM (Smilauer et al., 2010) was used to generate the numerical samples. The grading of the material is given in Figure 2.1 and is merely the one used in a previous study (Vincens et al., 2015). The minimum and maximum diameters  $D_0$  and  $D_{100}$  for this material are respectively equal to 3 and 12 mm, and the coefficient of uniformity is equal to 1.7. Particles are represented by spheres that can move according to Newton's laws. The interaction between particles are governed by elastic-frictional contact forces with normal and tangential stiffness ( $K_n$  and  $K_t$ ) and Coulomb friction angle ( $\varphi$ ). A sample composed of 630 particles is created by isotropic compression which produces a homogeneous sample in terms of porosity and CSD. Periodic boundary conditions are used to eliminate the wall effect, which disturbs the self-order of the spheres. Two samples are generated, one corresponding to the loosest state (UGL) and another one for the densest state (UGD) for the uniformly graded material. The coefficient for inter-particles friction is initially set to 0.7 and then decreased to reach the desired porosity (0.38), i.e., the porosity obtained by experiments on similar materials for the loosest state (Biarez and Hicher, 1994). The densest state, with a porosity of 0.34, is obtained by setting the friction value at contact to zero and allowing the system to equilibrate.

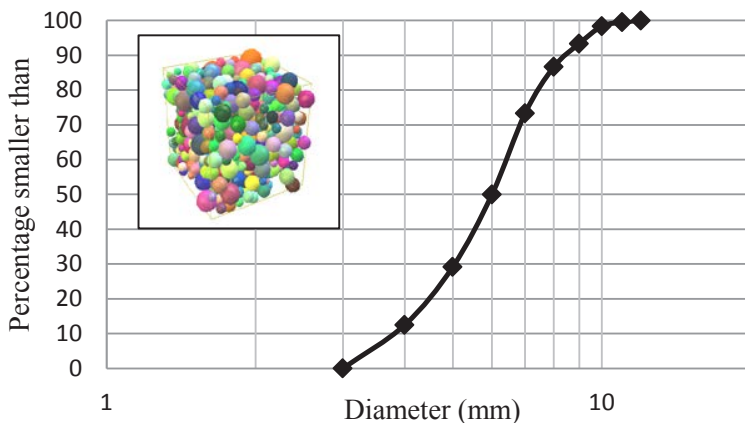


Figure 2.1. Particle size distribution for the studied material (the numerical sphere packing corresponds to the UGL material).

### 3 OVERLAPPING INSCRIBED VOID SPHERES APPROACH

Once the locations and radii of the spherical particles are known, a modified (weighted) tetrahedral tessellation is performed. The space is then partitioned into tetrahedra with vertices on the center of neighborhood spheres.

Such a 3D tessellation provides an essential step for spatial analysis of the packing. Thus, each tetrahedron represents a local pore (which volume is estimated by the largest inscribed void sphere) and four throats (the largest empty discs on tetrahedron faces). They are obtained using optimization algorithms; more details can be found in Al-Raoush et al. (2003) and Reboul et al. (2010). The resultant CSD corresponds to level 0 ( $L_0$ ) by Reboul et al. (2008).

However, the direct computation from Delaunay tessellation includes configurations where constrictions are larger than pores (constrictions formed by non-touching particles) and other configurations where two adjacent inscribed void spheres are superimposed. Such cases correspond to tetrahedra of undesirable shape (e.g., flat tetrahedra). Level  $L_0'$  guarantees the removal of these degenerated constrictions.

As mentioned before, two adjacent inscribed spheres may overlap and then should be distinguished from those which are completely separated. Different merging criteria of pores are then defined as shown in Figure 3.1.

Level 1-p% ( $L_{1-p\%}$ ) is a user controlled merging step applied when two adjacent inscribed void spheres with diameters  $d_{P_i}$  and  $d_{P_j}$  overlap each other and are connected by a constriction  $C_{ij}$  with a diameter  $d_{C_{ij}} \geq (p/100) \times \min(d_{P_i}, d_{P_j})$ ,  $p$  being a given percentage. For Level 1 ( $L_1$ ), the overlap of the inscribed void spheres is the only condition required to merge adjacent pores.

A further level of merging is studied (Level 2b ( $L_{2b}$ ) and Level 2 ( $L_2$ )) where the merging criterion is not only applied to the adjacent local pore but also to the next adjacent local pore. A restriction of  $L_2$  is introduced and is denoted  $L_{2b}$  where the inscribed void spheres must be arranged in decreasing orders to induce a merging. This criterion takes into account the geometric constraints to define the pore entity. Indeed, the transition between pores is characterized by constricted regions followed by more expanded regions.

It should be noted here that after merging two neighboring pores (three neighboring pores in case of  $L_{2b}$  and  $L_2$ ), the interconnection between the newly formed pore with its neighboring pores is not checked, since an extra level of merging tends to create ducts within the granular medium.

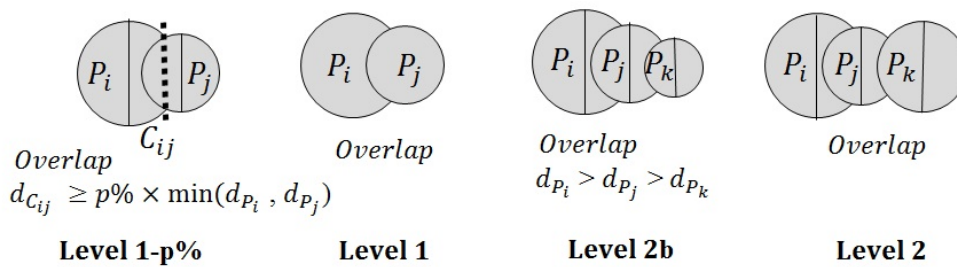


Figure 3.1. Definitions of different merging criteria based on the overlapping of inscribed spheres associated to adjacent pores.

### 4 HIERARCHICAL MERGE

The hierarchical merge method requires a graph data structure representing the pore network. For this study, the graph is obtained from a voxel-based approach (Homberg et al., 2012) that represents the medial paths of a distance mapping of the pore space to the surrounding particles. The graph vertices are located at local maxima and are assumed to represent pore centers, while the edges represent the pore paths running along the maximal distances between two adjacent pores centers. The distance information is tracked along the edges, where the constriction is defined as the point having the smallest distance

along an edge (Fig. 4.1(a-b)). To extract the graph from the studied samples, the sphere packings were scan-converted into voxel data sets with a voxel size of  $0.02 \times 0.02 \times 0.02 \text{ mm}^3$  ( $0.02 \text{ mm} = D_0/150$ ). The discrete nature of the voxelization and the Voronoi-typical degenerated cases produce additional pore centers and constrictions in the graph that do not correspond to real maxima. Such cases have no diameter differences between constriction and smaller pore and will be merged at the beginning of the hierarchical merge, which then corresponds to the result of  $L_0'$ .

This hierarchical method evaluates the separation of a pair of pores  $P_i$  and  $P_j$  by their constriction  $C_{ij}$  based on the relative diameter difference  $t_{diff}(P_i, C_{ij}, P_j) = (d_P - d_{C_{ij}})/d_P$  with  $d_P = \min(d_{P_i}, d_{P_j})$  and  $i \neq j$ . The value  $t_{diff}$  will be used to build hierarchical neighbors of pores according to their degree of separation, which is specified by a user-defined threshold  $t$ . Note,  $t$  corresponds to  $p$  with  $t=1-p/100$ , the threshold introduced in  $L_1-p\%$ . This approach was developed for materials with irregular particles and does not consider sphere overlaps in order to include pairs within elongated pores.

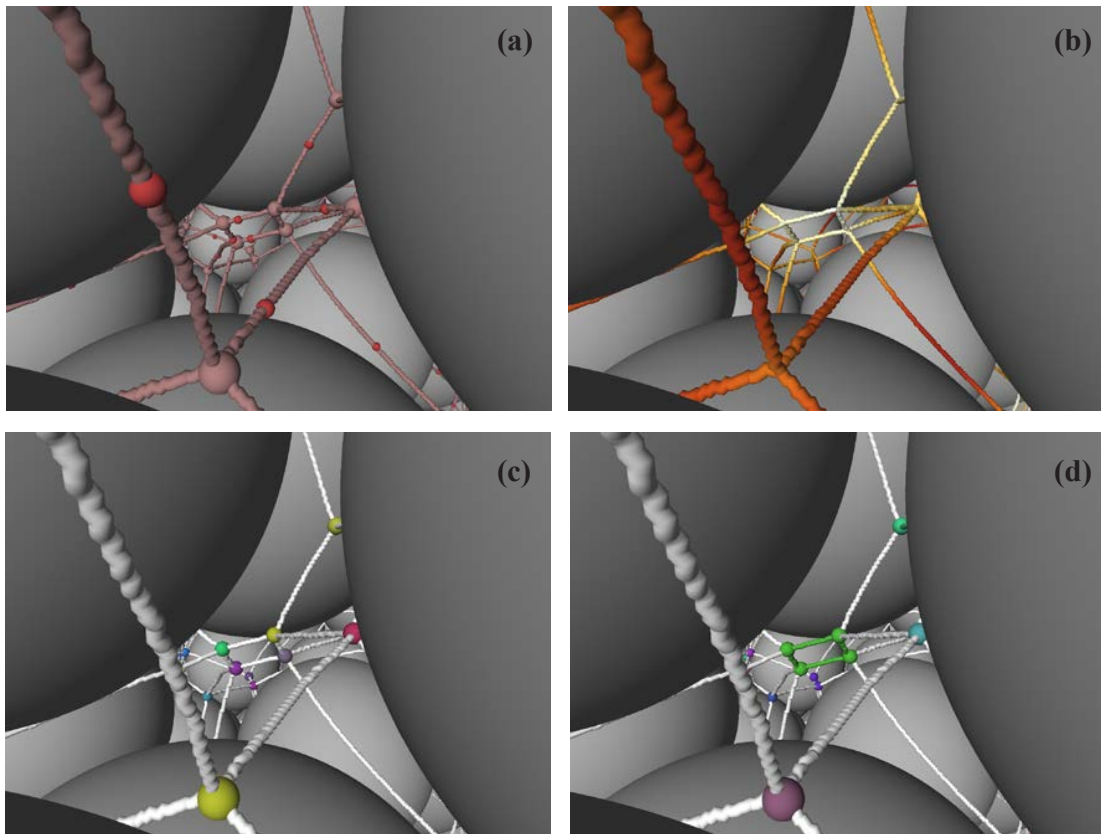


Figure 4.1. Detail of spheres and graph extracted from the voxelization of the UDG material. For visibility, the radius of the particle spheres was reduced to 90%. **(a)**: Larger spheres at crossings indicate pore centers; smaller, darker spheres indicate constrictions. **(b)**: The diameter is attached to each edge point and color-coded with yellow (large) to red (small). **(c)**: Unmerged pore centers are randomly colored by their label id. **(d)**: Merged pore centers and their connection paths and constrictions will be labeled as belonging together ( $t=1\%$ ).

The hierarchical manner arises from specifying tuples  $T_{ij} = (P_i, C_{ij}, P_j, t_{diff}(P_i, C_{ij}, P_j))$  of two pores, their constriction and the difference threshold  $t_{diff}$  and from the order of processing them. The approach starts from tuples of direct neighbors in the unmerged graph (Fig. 4.1(c)) and evaluates them in increasing order of the difference thresholds. Each step assigns the smaller pore and its constriction to the larger pore. The neighbor tuples that contain the merged pore will be updated by replacing the smaller pore by the larger one as well as by re-computing  $t_{diff}$  accordingly. For example, if  $d_{P_i} < d_{P_j}$ , then all neighbor tuples  $T_{ik}$  with  $k \neq j$  will be converted to  $T_{jk} = (P_j, C_{jk}, P_k, t_{diff}(P_j, C_{jk}, P_k))$  to be neighbors of  $P_j$ .  $P_i$  and  $C_{ij}$  are labeled on the graph as belonging to  $P_j$  (Fig. 4.1(d)) and will be discarded from further

considerations. This is then repeated until all (newly created) tuples that have a difference threshold  $t_{diff} \leq t$  are processed. More algorithmic details can be found in Homberg et al. (2014).

The remaining tuples represent hierarchical neighbors rather than direct neighbors where each pore represents all hierarchically assigned pore centers. The constriction and  $t_{diff}$  represent the most significant separation between the two representative pores, which increase their life time as separated pores compared to the direct neighbor relations and avoids an inappropriate merge propagation.

## 5 RESULTS AND DISCUSSION

The initial CSDs ( $L_0$ ) derived from the Delaunay and the voxel-based methods are almost congruent for a sufficient small voxel size (Vincens et al., 2015). For convenience, we only present in the following the results corresponding to the UGL material, but similar results were found for the UGD material. The evolution of the number of constrictions (normalized to the initial total constrictions in the sample before merging) corresponding to different criteria is presented in Figure 5.1. Then, Figure 5.2 and Figure 5.3 show the CSDs and the estimated probability density of constriction sizes for different merging criteria described in sections 3 and 4 respectively. It should be noted that the CSD corresponding to  $L_0'$  is located between the CSDs associated to  $L_0$  and  $L_1$ -99% and is not shown in Figure 5.1.

First, one can note that merge involving overlapping adjacent inscribed spheres (Fig. 5.1(a)) tends to limit the possibility for merging contrary to the hierarchical merge (Fig. 5.1(b)), which guaranties that no pore structure such as ducts would be identified. Any less restrictive criterion than  $L_1$ -90% does not provide further merging and the resulting pore structure is similar to that provided by  $L_1$  merging which means that such cases are generally not present in the packing of spheres. Moreover,  $L_2$  merging just provides few further merged pores than  $L_1$ .

Another feature is observed in Figure 5.2(b) and Figure 5.3(b). Merging tends to let appear a clear and single mode while vanishing a coupled second higher mode. When merging, the first mode for the constriction size almost stabilizes irrespective of the kind of level (Level 1-p%, Level 1 or Level 2) or the threshold value  $t$  in the hierarchical approach if this latter one remains smaller than 10% (not shown herein). If the threshold value  $t$  is too high, for example 30% in Figure 5.3(a), one can note that the CSD shifts towards the smallest diameters. In this case, it implies that the deduced pore structure is changing of kind.

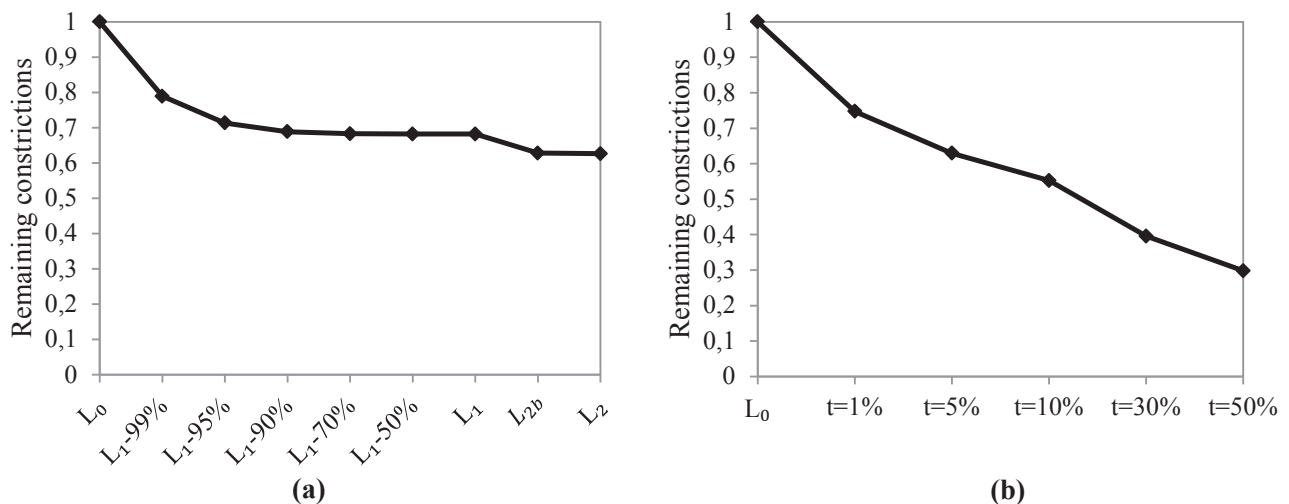


Figure 5.1. Evolution of the relative number of constrictions for different merging criteria. (a): merge associated to overlapping inscribed void spheres; (b): Hierarchical merge.

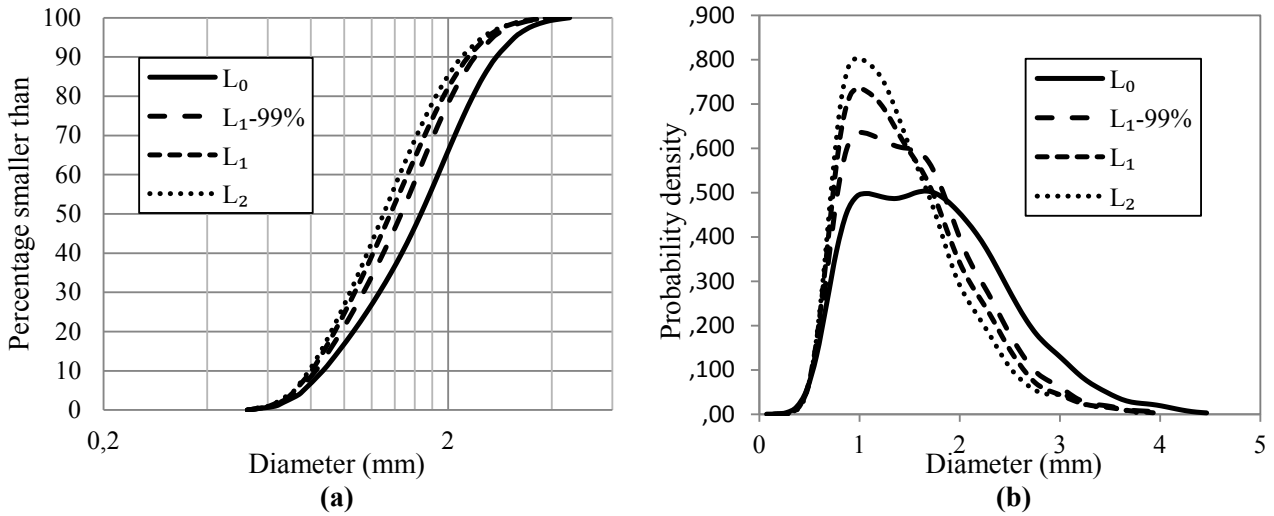


Figure 5.2. (a): CSDs for the UGL material; (b): underlying probability density function for different merging criteria defined in the overlapping inscribed void spheres approach.

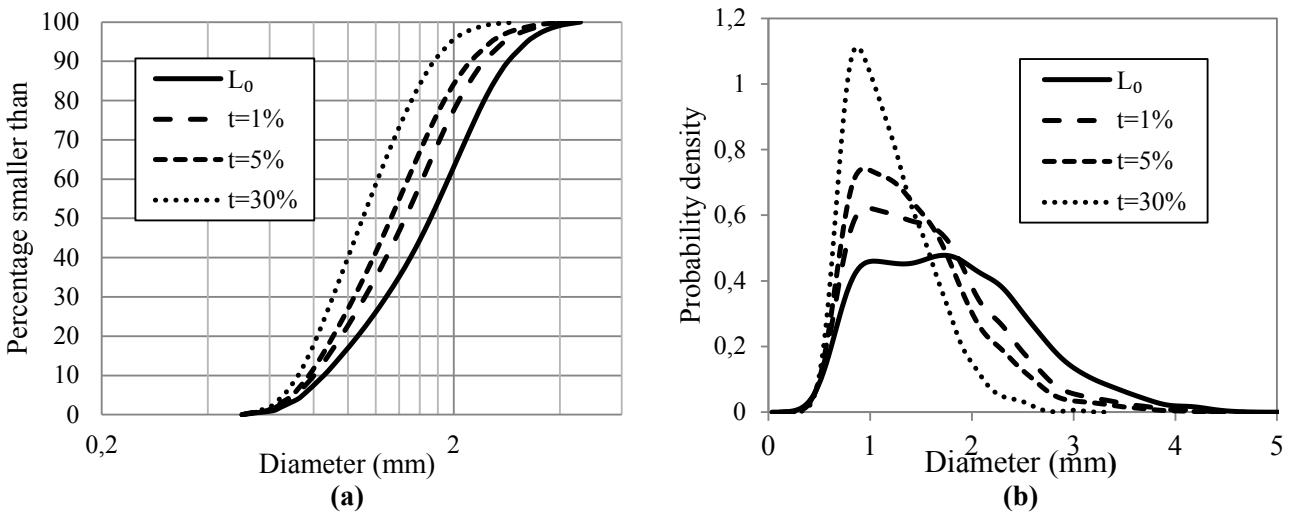


Figure 5.3. (a): CSDs for the UGL material; (b): underlying probability density function of the constriction diameter for different steps of hierarchical merge.

When analyzing in more detail the different approaches for merging, first, the  $L_{1-p\%}$  considers two local properties to evaluate the constrictions: the overlap between adjacent pores and the comparison of the size of constriction connecting two pores to the size of the smallest one, while the hierarchical approach evaluates the degree of separation between pores in a global scope, independently of overlaps. The combination of the overlap and the constriction criterion imply a criterion based on the distance between pores which seems to be more reasonable according to Al-Raoush et al. (2003) where neighboring pores are merged if the center of a void inscribed sphere lies within the adjacent inscribed sphere. In fact, a statistical study over all tuples  $(P_i, C, P_j)$  shows that both properties are verified when  $p=99-95\%$  ( $t=1\%-5\%$  in hierarchical merging). By decreasing the merging threshold  $p$ , more constrictions linking non-overlapping pores are found. In this case, the number of deleted constrictions increases dramatically in the hierarchical merge. That is to say that the comparison between the two merging methods should be restricted to the smallest thresholds ( $t=1\%-5\%$ ).

Furthermore, one should expect that more constrictions can be removed in the hierarchical merge steps, since it allows merging multiple pairs as long as the newly created neighbors also meet the specified difference threshold, in contrast to  $L_{1-p\%}$  where the merging criterion is only applied to the

first neighbor as explained in sections 3 and 4. Figure 5.4 shows that the CSD derived from  $L_1$ -99% and that corresponding to  $t=1\%$  are approximately similar while the CSD ( $t=5\%$ ) is closer to that of  $L_2$ .

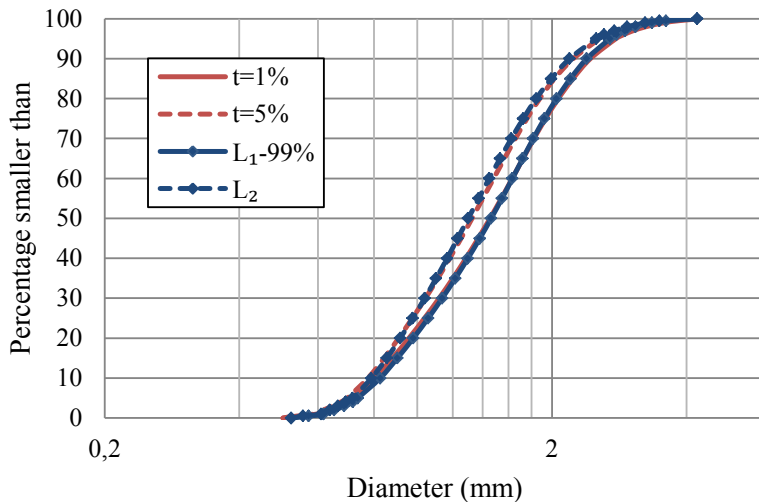


Figure 5.4. Comparison of the CSDs resulting from different merging processes.

After comparing different merging criteria and their associated CSDs, it is important to study how the choice of a certain criterion impacts the processing of the filtration probabilistic theory which assigns the coordinate of the CSD curve to the capture probability of a fine particle by a constriction of its own size.

In the framework of the filtration theory proposed by Silveira (1965), filter constriction sizes are related to the possibility for the transport of base particles of a given diameter. Stating that the pore network is organized according to a regular cubic model forming unit layers (Schuler, 1996) and that the displacement of particles is mainly unidirectional, the probability of passing one unit layer  $P_u$  is equal to that of passing one constriction  $P$ .  $P'$  is the probability to be stopped after a path corresponding to  $n$  layers. The total distance covered by a fine particle having diameter  $d$  is given by Equation (1).

$$L = n \times s = \log(1 - P') \times s / \log P_u \quad (1)$$

where  $s$  is in that case the average distance between two confrontations, which is also the average unit layer thickness. The estimate of  $s$  is a challenging problem and different proposals are found in the literature:  $D_{50}$  by mass (Soria et al., 1993),  $D_{50}$  by number (Locke et al., 2001),  $D_{50}$  by surface area (Indraratna et al., 2007) or the mean pore inscribed sphere computed from the Delaunay method (Sjah et al., 2013). In fact, there is little evidence so far for the choice of one between these options.

A quick estimate of the average thickness of a unit layer  $s$  can be given by the mean distance between centers of adjacent pores computed from the initial statistics over the entire sample (non-directional approach using either overlapping inscribed void spheres approach or the hierarchical method). When applying the merging criteria, the number of constrictions is reduced and then the value of  $s$  tends to increase. In other words, each merging criterion must be associated with a corresponding average unit layer. The results of this calculation are given in the second column of Table 1 and Table 2 for merging criteria associated to the overlapping inscribed void spheres approach and hierarchical approach respectively.

It should be noted that the estimated  $s$  corresponding to  $L_0$  for the different merging processes are slightly different ( $s=2$  mm in Tab 1. and  $s=1.7$  mm in Tab 2.). This is can be justified by the fact that the CSDs resulting from  $L_0$  using a Delaunay tessellation or a voxelization plus a distance mapping approach are not strictly identical. Moreover, the use of a specified merging criterion may lead to a  $s$  value that is greater than the reference  $s$  value found for  $L_0$  by an amount of 90%, which is significant.

On the other hand, the maximum path length  $L_{max}$  for a particle of a given diameter  $d$  (e.g., 1.16mm herein), using Equation (1) was computed. We consider a confidence level of  $P'=95\%$  (Locke et al.,

2001) and  $P$  (equal to  $P_u$  if a unidirectional pathway is stated) is obtained directly from the CSDs associated to different merging criteria (Fig. 1.1(a)). Thus, for the different merging criteria mentioned in Table 1,  $P$  is equal to 0.75, 0.69, 0.65 and 0.62 for  $L_0$ ,  $L_1$ -99%,  $L_1$  and  $L_2$  respectively. In Table 2,  $P$  corresponds to 0.76, 0.69, 0.64 and 0.59 for  $L_0$ ,  $t=1\%$ ,  $t=5\%$  and  $t=10\%$  respectively.

A consistent method would imply to use the  $s$  value corresponding to a merging criterion to compute  $L_{max}$ , which is not generally the case in the literature. In Table 1 and Table 2, one can note that if a consistent value for  $s$  is used, the maximum length  $L_{max}$  computed by the probabilistic approach is rather stable (around 21 mm for merging criteria associated to the overlapping inscribed void spheres approach (see diagonal line in Tab. 1) and 19 mm for the hierarchical merging method (see diagonal line in Tab. 2)).

On the contrary,  $L_{max}$  is considerably underestimated ( $L_{max}=12.8$  mm) if  $P$  value corresponding to  $L_2$  ( $P=0.62$ ) is combined with  $s$  value estimated from  $L_0$  ( $s=2$  mm) in Equation (1). The same holds true in the case of the hierarchical method. If the  $s$  value ( $s=1.7$  mm) for  $L_0$  is used together with a CSD computed with a merging threshold  $t=10\%$ , the error made for the estimate of  $L_{max}$  approximates 45%.

Table 1. The longest distance  $L_{max}$  traversed by a particle of diameter  $d=1.16$  mm for the merging criteria associated with the overlapping inscribed void spheres approach.

Merging criterion		$L_{max}$ (mm)			
		$L_0$	$L_1$ -99%	$L_1$	$L_2$
$L_0$	$s=2.0$ mm	21.2	16.5	14.2	12.8
$L_1$ -99%	$s=2.6$ mm		21.0	18.1	16.3
$L_1$	$s=3.0$ mm			20.9	18.8
$L_2$	$s=3.3$ mm				20.4

Table 2. The longest distance  $L_{max}$  traversed by a particle of diameter  $d=1.16$  mm for the hierarchical merging approach.

Merging criterion		$L_{max}$ (mm)			
		$L_0$	$t=1\%$	$t=5\%$	$t=10\%$
$L_0$	$s=1.7$ mm	19.0	13.5	11.7	9.9
$t=1\%$	$s=2.3$ mm		18.8	15.6	13.2
$t=5\%$	$s=2.8$ mm			18.6	15.7
$t=10\%$	$s=3.2$ mm				17.9

## 6 CONCLUSION

Two techniques for computing the void characteristics of sphere packings (pore and constriction sizes) are compared. Both methods provide the same initial CSD. Different merging criteria can be adopted to associate the interconnected local pores, and consequently different final CSDs can be prescribed. Since there is no clear definition for a local pore, no definite criterion can be prescribed. Nevertheless, one can note that if a  $L_1$  level criterion or a threshold value  $t$  equal or smaller than 1% (hierarchical merge) is chosen, the resulting CSD will be similar and the first mode of the probability density function that tends to emerge due to the merging process is not modified. Such criteria are recommended to define the average opening size of the filter from the CSD often associated to this mode.

In the other hand, if one needs to estimate, in the light of the probabilistic theory, the distance traveled by a fine particle through the filter, based on the CSD, attention must be paid to the choice of a consistent spacing between constrictions. The preliminary results have shown that the CSD and  $s$  must be concertedly and properly chosen, otherwise, the probabilistic method leads to significant errors for the estimate of the maximum travelled distance  $L_{max}$ .

## ACKNOWLEDGEMENTS

Part of this work belongs to a project funded by *Compagnie Nationale du Rhône* (CNR). F. Seblany and E. Vincens acknowledge CNR for its interest and its financial support.

## REFERENCES

- Al-Raoush, R., Thompson, K., and Willson, C.S. (2003). Comparison of network generation techniques for unconsolidated porous media. *Soil Science Society of America Journal*, 67(6):1687–1700
- Biarez, J., and Hicher, P.Y. (1994). *Elementary mechanics of soil Behavior, Classification of and correlations between parameters*. A.A. Balkema: Rotterdam, 81–106
- Homberg, U., Baum, D., Prohaska, S., Kalbe, U. and Witt, K.J. (2012). Automatic Extraction and Analysis of Realistic Pore Structures from  $\mu$ CT Data for Pore Space Characterization of Graded Soil. *Proceedings of the 6th International Conference Scour and Erosion (ICSE-6)*, 66–73
- Homberg, U., Baum, D., Wiebel, A., Prohaska, S. and Hege, H.C. (2014). Definition, Extraction, and Validation of Pore Structures in Porous Materials. *Topological Methods in Data Analysis and Visualization III*, Springer, 235–248
- Indraratna, B., Raut, A.K. and Khabbaz, H. (2007). Constriction-based retention criterion for granular filter design. *Journal of Geotechnical and Geoenvironmental Engineering*, 133(3): 266–276
- Locke, M., Indraratna, B. and Adikari, G. (2001). Time-dependent particle transport through granular filters. *Journal of geotechnical and geoenvironmental engineering*, 127(6):521–529
- O’Sullivan, C., Bluthé, J., Sejpar, K., Shire, T. and Cheung, L. Y. G. (2015). Contact based void partitioning to assess filtration properties in DEM simulations. *Computers and Geotechnics*, 64, 120–131
- Reboul, N., Vincens, E. and Cambou, B. (2008). A statistical analysis of void size distribution in a simulated narrowly graded packing of spheres. *Granular Matter*, 10(6):457–468
- Reboul, N., Vincens, E. and Cambou, B. (2010). A computational procedure to assess the distribution of constriction sizes for an assembly of spheres. *Computers and Geotechnics*, 37(1):195–206
- Silveira, A. (1965). An analysis of the problem of washing through in protective filters. *Proceedings of the 6th International Conference on Soil Mechanics and Foundation Engineering, Montréal, Que*, 551–555
- Sjah, J. and Vincens, E. (2013). Determination of the constriction size distribution of granular filters by filtration tests. *International Journal for Numerical and Analytical Methods in Geomechanics*, 37(10):1231–1246
- Šmilauer, V., Catalano, E., Chareyre, B., Dorofeenko, S., Duriez, J., Gladky, A., Kozicki, J., Modenese, C., Scholtès, L., Sibille, L., Stránský, J. and Thoeni, K. (2010). Yade Reference Documentation. In *Yade Documentation* (V. Šmilauer, ed.).
- Soria, M., Aramaki, R. and Viviani, E. (1993). Experimental determination of void size curves. *Filters in geotechnical and hydraulic engineering*, 43–48
- Vincens E., Witt K.J., Homberg U. (2015) Approaches to determine the Constriction Size Distribution for understanding filtration phenomena in granular materials, *Acta Geotechnica*, 10(3):291–303
- Witt, K.J. (1986). *Filtrationsverhalten und Bemessung von Erdstoff-Filtern*, volume 104. Institut für Bodenmechanik und Felsmechanik der Universität Fridericiana in Karlsruhe.

## Online Alarming for Internal Erosion

J. Dornstädter

*GTC Consult GmbH*

A. Fabritius & B. Heinemann

*GTC Kappelmeyer GmbH*

**Abstract:** Internal erosion is one of the most frequent reasons of failure and deterioration of embankment dams. Internal erosion is controlled by construction properties (e.g. filter and drain design, grain and pore sizes) and hydrodynamic conditions within the dam. While construction properties are usually known, poor information is available on the local hydrodynamic situation inside the embankment. Hydrodynamic parameters vary strongly inside the dam due to local inhomogeneities and the most critical hydrodynamic parameter inducing internal erosion (material transportation phenomena) is the pore velocity of the seeping water. The onset of internal erosion starts at low pore velocities. Thus a method for the detection of seepage zones of low pore velocities can help to prevent the development of damages.

Using the temperature of seepage water as a tracer, applied to dams since 1953, has demonstrated to be a reliable method to detect and monitor in-situ the seepage flow conditions, even at extremely low velocities, i.e. detecting internal erosion at an early stage of development. Nowadays it is even used to automatically measure the in-situ flow velocity and its change over time. The development of this technique is presented. The paper demonstrates how to measure in-situ flow velocities along an array of temperature probes and alternatively along optical fibre - now even retrofits inside existing dams are possible - applying a remote condition monitoring system releasing automatic alarms when flow velocities are increasing over time or exceeding thresholds. Examples from different installations in dams are presented.

Keywords: ground temperature measurement, leak detection, flow velocity, remote condition monitoring, alarm for internal erosion.

### 1 INTRODUCTION

The onset of internal erosion starts at low pore velocities. Present research state that the critical pore velocity initiating material transportation phenomena inducing deterioration of dams is of the order of  $10^{-3}$  m/s. Using the temperature of seepage water as a tracer has demonstrated to be a reliable method to detect leakage zones and monitor in-situ flow velocities of orders  $> 10^{-7}$  m/s (pore velocity). The monitoring of the seepage flow conditions leads to the detection of internal erosion at an early stage of development.

The computation of flow velocities is the qualification for the automatic release of an alarm – either by indicating a change in flow velocities, i.e. in flow conditions, or by exceeding a threshold of a fixed critical velocity. The detection of seepage zones of low pore velocities and their monitoring can prevent the development of damage and possible failure of the structure.

### 2 TEMPERATURE MEASURING METHODS

The use of seepage water temperature as a tracer, applied to dams first in 1953 by Kappelmeyer (1953), has shown to be a reliable method to detect and monitor in-situ the seepage flow conditions and to detect

internal erosion at an early stage of development. With the ability to record temperatures over a period of time the technique can also be used to estimate the leakage flow velocities.

## 2.1 Temperature probes

The development of this technique started in the 1950s with temperature measurements in boreholes and piezometer stand pipes. In 1992 GTC Kappelmeyer introduced greater accuracy and reliability by measuring in-situ ground temperatures with an array of purposed-designed small diameter temperature probes. The temperature probes are composed of high grade steel tubes of less than 25 mm outer diameter which are vibrated into the earth fill dam and its foundation along the dam's axis from its crest. Maximum depth ever reached is 45 m. The probes are rammed vertically into the dam at regular intervals (Dornstädter, 1997). Electrical chains connecting temperature sensors (typically PT-100-sensors spaced at 1 m interval) are inserted into the tubes to constitute the temperature probe. The intervals between probes are reduced at places where temperature anomalies reveal seepage flow, to precise the location of maximum flow velocity. A schematic design of an array of temperature probes is seen in figure 1.

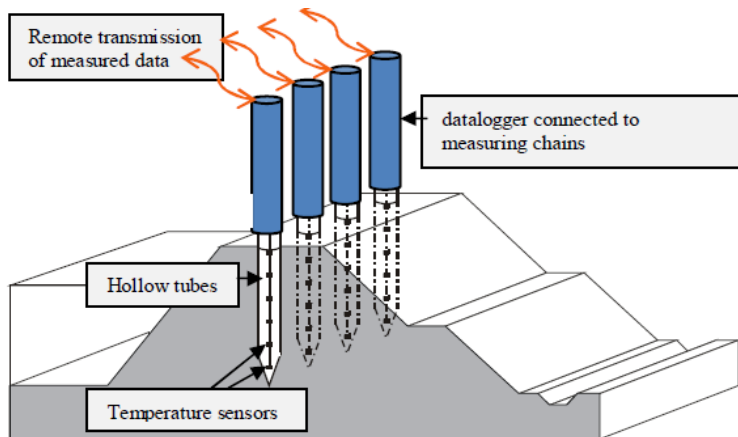


Figure 1. Schematic illustration of an array of temperature probes rammed into the dam from its crest equipped with dataloggers.



Figure 2. Array of temperature probes along the downstream side of the dam's crest, equipped with protecting devices containing dataloggers sending the monitored data to the office via remote transmission.

Dataloggers are protected in larger tubes screwed on top of the small diameter temperature probes. Connected to the temperature measuring chains they record ground temperatures at the positions of the sensors at a given sampling rate over time. The temperature evolutions at different depths are transferred by remote transmission to the office for analysis and release of the alarm. Figure 2 shows an example on site.

## 2.2 Temperatures by optical fibres

As an alternative measurement technique, since 1995, optical fibres have been incorporated into dams and into foundations during construction or major refurbishment (Aufleger et al., 1998). They can provide a continuous record of temperature and can be remotely monitored. In 2014 GTC Kappelmeyer developed a new fibre optic cable with optimized fibres which could be inserted into the small diameter tubes used for the temperature probes (Dornstädter et al., 2016). The development combines temperature probes with fibre optic and thus facilitates temperature measurements along fibre optic cables in existing dams and allows a retrofit of 2 dimensional seepage monitoring based on fibre optic (Patent DE19621797, 2011).

The key to the new solution are bend optimized fibres which can be bent to a very small radius without too much attenuation of light intensity when a laser pulse travels through them. The cable with typical outer diameter of 4 to 6 mm including armouring and water tight protection has a minimum of two fibres inside. At the far end of such a cable one of the internal fibres is bent through 180° and welded to a second fibre by fusion splicing. This optic loop is then protected against mechanical damage by a cover with a typical outer diameter of 8 mm. The cable with fibre optic loop at the end is inserted into the small diameter tube of a temperature probe that has been previously installed into the dam.

Individual fibre optic cables are inserted in each probe and a connecting cable runs in a shallow cable trench from probe to probe and finally to the instrumentation cabinet. The fibres of each individual probe are spliced to the fibres of the connecting cable in a way that allows the laser pulse from the Distributed Temperature Sensing instrument (DTS) to travel along the connecting cable, running down and up each probe from one end of the dam to the other as shown in figure 3.

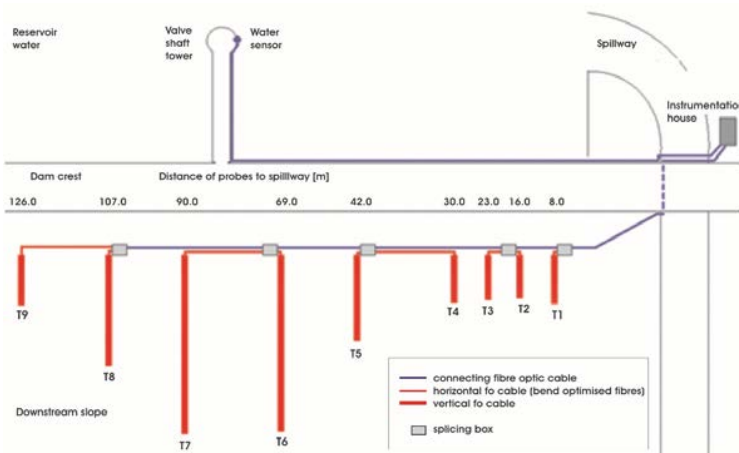


Figure 3. Sketch of a typical layout of fibre optic cabling.

Since the attenuation loss of light on each bend is not negligible this must be taken into account when selecting the laser power of the DTS instrument. When many probes are to be monitored along a dam, there is the option of creating different light passes by using a connecting cable with a large number of fibre pairs each connected to a group of probes forming a separate light pass. Typically 8 to 10 probes can be put together in one pass. Several light passes require multi-channels in the DTS system and are measured one by one by multiplexing. This layout has been applied to the in-situ installation seen in figure 4a and 4b.

The new cables are available in two versions, one for absolute temperature measurements with fibres in a central stainless steel tube, and the other for artificially induced temperature increases with additional coaxial layers of electrical conductors. The electrical conductors are used to heat the cable to apply the heat pulse method (active method) for leakage detection if needed (Dornstädter et al., 2010).

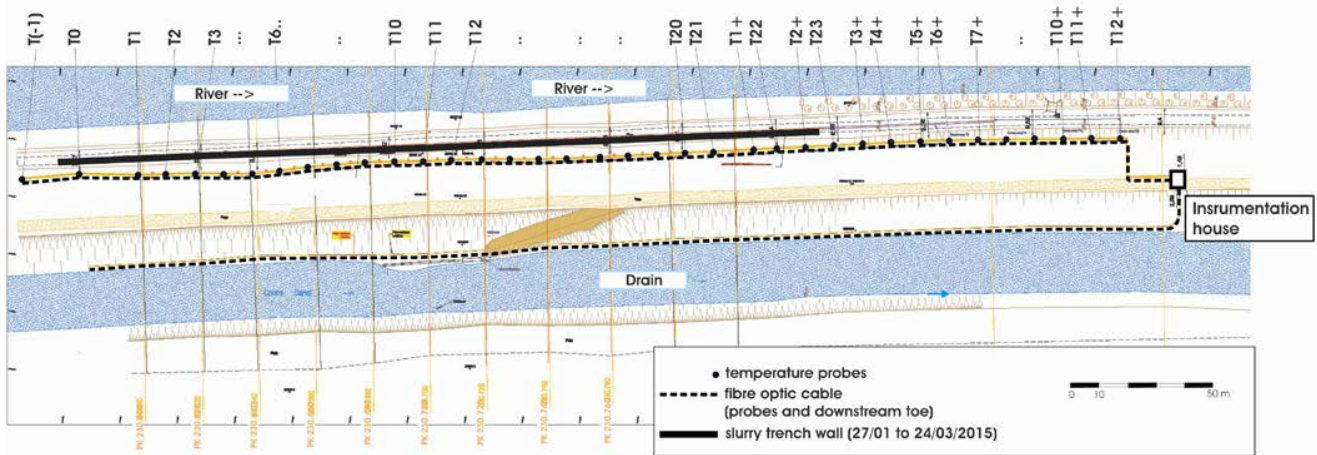


Figure 4a. Example floor plan for a fibre optic retrofit installation showing the connecting cable ending at the instrumentation house/cabinet.

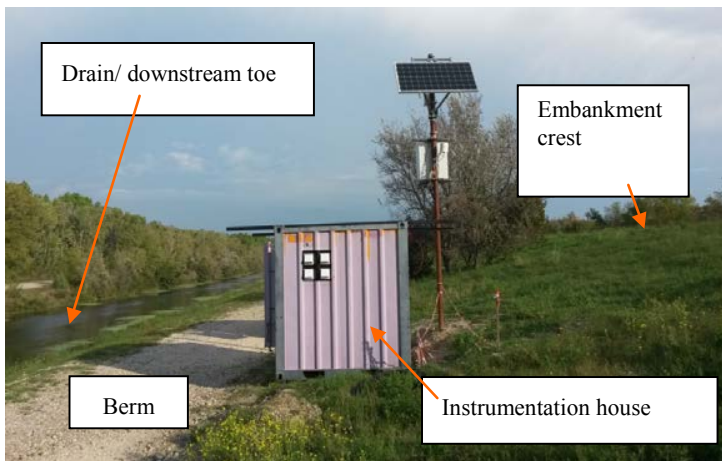


Figure 4b. Visible on site is the instrumentation house in which the remote controlled DTS instrument gathers all temperatures measured along the buried fibre optic cables.

### 3 DATA ANALYSIS

#### 3.1 Remote monitoring of change in flow condition

At the end of 2014 a first site was equipped with the retrofit technique on an embankment river (see figures 4a and 4b; CNR et al., 2013).

The embankment of the river is about 11 m high and has a long history of leakage and transport of fines. For the detection of the leakage zones inside the embankment and its foundation a total of 37 temperature probes were installed to a depth of 16 m along a 430 m long section of the dam. The array runs along the downstream edge of the embankment's crest (figure 4a). Fibre optic cables were installed in all probes and connected by a connecting cable in a small trench. Four light passes were built each ending at the instrumentation house (figure 4b). Since the site was having leakage problems combined with transport of fines the client decided to build a slurry trench cut-off wall in Spring 2015.

The temperature evolution before, whilst and after the construction of the cut-off wall was remotely monitored with automatic data analysis. During the construction work the client followed the success of the procedure by the automatic temperature monitoring system (remote condition monitoring).

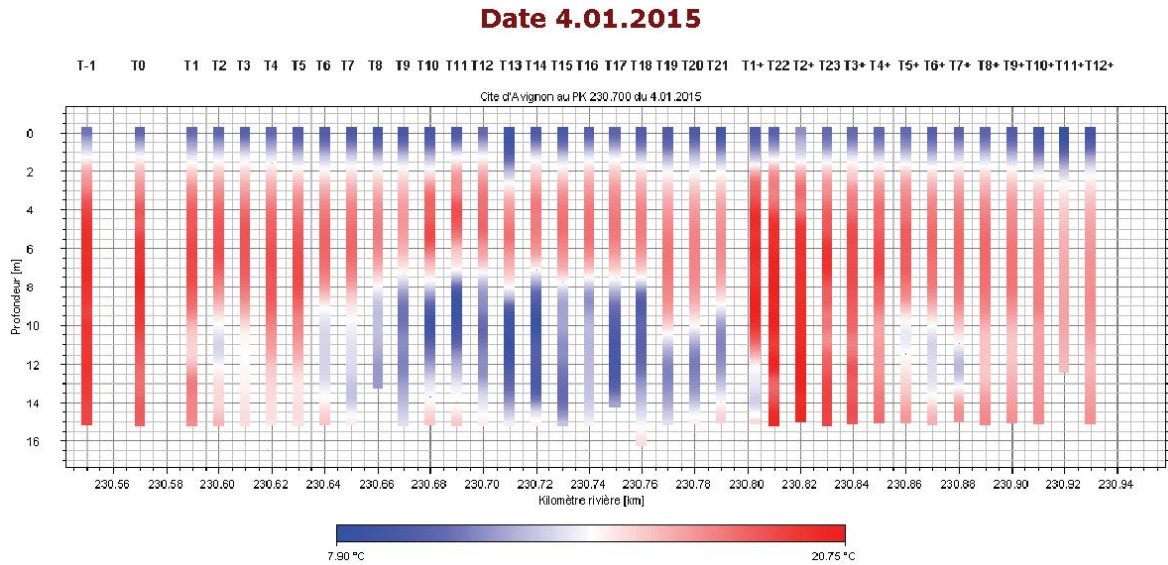


Figure 5a. Temperature distribution before construction of the cut-off wall in January; low water temperatures (blue) bring out the percolated area at depth between 7 m and 14 m.

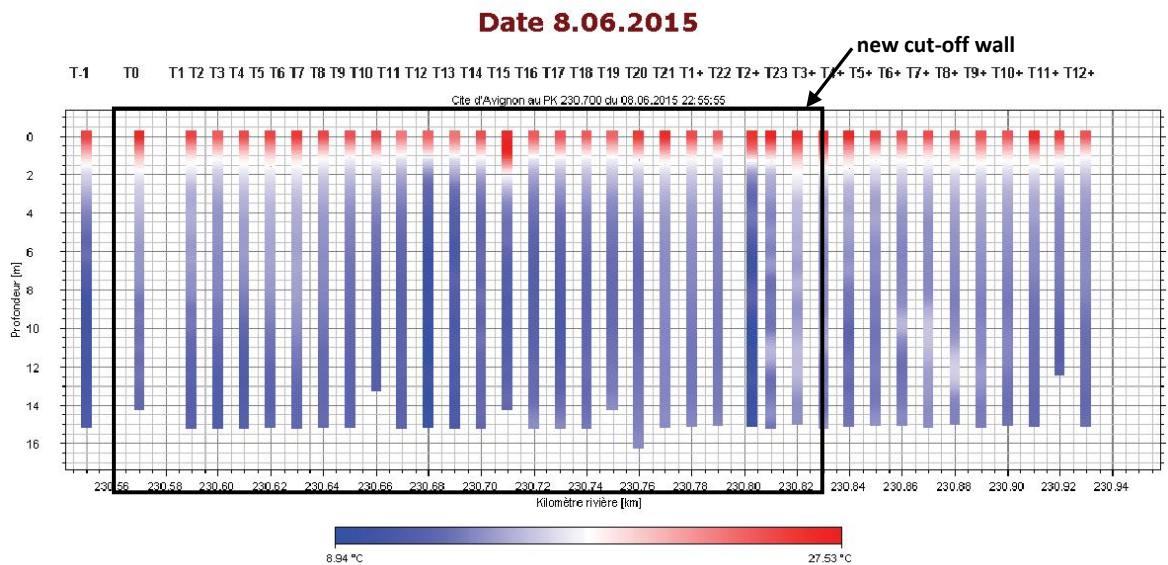


Figure 5b. Temperature distribution after construction of the cut-off wall in June; high water temperatures (red) at depth would bring out a percolated cut-off wall.

The 2-dimensional temperature distribution about 3 weeks before the beginning of the construction of the cut-off wall is shown in figure 5a. A strong temperature anomaly is indicated in the centre by blue colors corresponding to low water temperatures of the river in winter. The strongly percolated area extends from probe T6 to Probe T21 from 7 m to 14 m depth below crest level, showing severe leakage flow through the lower part of the dam and through its foundation. Two minor percolated areas are seen at T2/T3 and from T5+ to T7+ at the interface of the embankment and its foundation.

Figure 5b shows the temperature distribution some months after completion of the cut-off wall constructed from probe T0 to probe T2+. The results show the disappearance of the anomalies seen before and confirm the successful installation of the new cut-off wall.

### 3.2 Automatic alarm release for onset of internal erosion

Besides visual tracing of flow conditions in an embankment, the correlation of ground temperatures with water temperature are computed and the phase shifts of both evolutions calculated for an estimate of pore velocities (Dornstädter et al., 2010; Garandet et al., 2012). The integration of these features in the monitoring software allows a release of an alarm by text message or e-mail as asked for.

In the end of 2015 a 2 km long section of a canal embankment was investigated by temperature probes for leak detection as seen in figure 2. The client was concerned about water losses onto the rail way next to the canal. A leakage section was vaguely known and a remote condition monitoring was required along the delimited seepage zone to follow the situation of the dam and to be alerted in case of aggravation of flow conditions.

An important seepage zone could be limited by an investigation of temperature probes to a 35 m long section on which the space between probes was reduced to 1.25 m to find the maximum seepage flow locally at one single probe (N07). Twelve probes numbered from N01 to N12 were installed at distances between 1.25 m to 10 m depth along the 35 m long section and they were equipped with dataloggers as seen on figures 1 and 2. The depths of the probes vary between 3 m and 4 m, dictated by geological structures. For the probe showing the maximum anomaly a special measuring chain was built with sensors spaced at 0.5 m (typically the sensors are spaced at 1 m intervals).

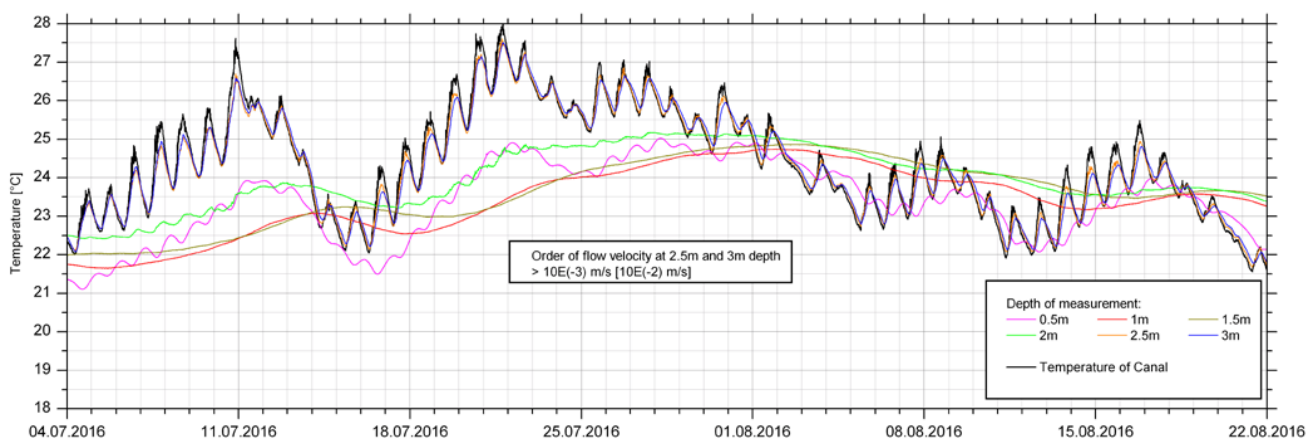


Figure 6a. Temperature evolutions at different depths monitored for probe N07 showing maximum correlation with water temperature for the temperatures at 2.5 m and 3 m depth.

The ground temperatures are measured with a sampling rate of 10 minutes and they are sent to the GTC office via remote transmission once a week. The automatic analysis of the datasets produce graphs of the temperature evolutions for each probe which are presented on an internet site to be consulted by the client. The more the ground temperature evolutions reveal to correlate with the water temperature evolution, the more the situation becomes critical and velocities might induce internal erosion. Figure 6a show the evolutions of the ground temperatures measured during a summer period at different depths at probe N07 being the probe revealing maximum seepage flow at 2.5 and 3 m depth. Figure 6b show the evolutions of the ground temperatures measured during the same period at different depths at probe N01 being the probe revealing the minimum seepage flow along the considered section.

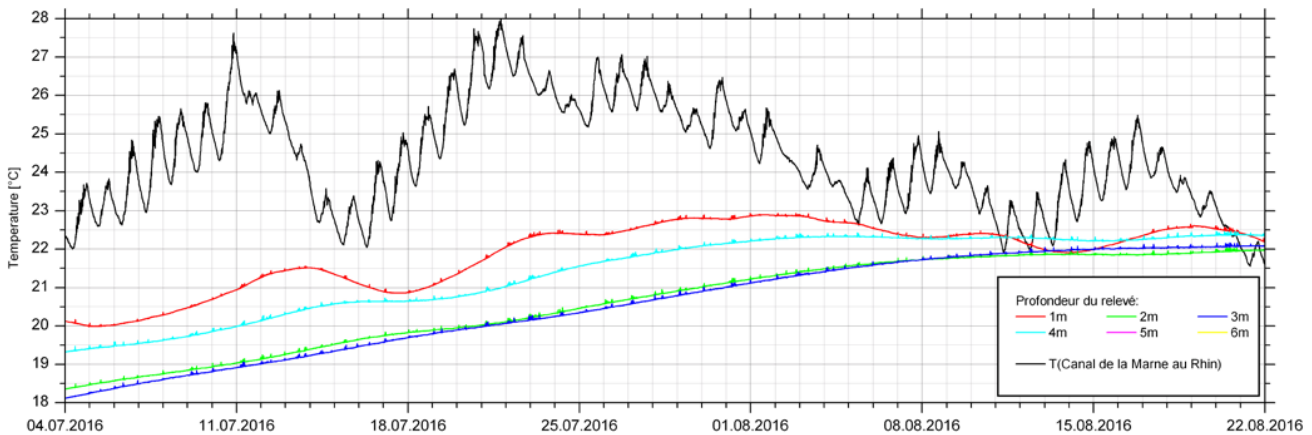


Figure 6b. Temperature evolutions at different depths monitored for probe N01 showing no evident correlation with water temperature for the ground temperatures.

In a non percolated embankment the correlation of ground temperatures with surface or water temperature decreases with depth as indicated in figure 6b. Correlation analysis of all probes results in a table as shown in figure 7.

Probe -->	N01	N02	N03	N04	N05	N06	N07	N08	N09	N10	N11	N12
Depth	results from 01-08-2016											
0.5							0.542					
1												
1.5												
2							1.479					
2.5							0.035					
3							0.097	0.424	0.597			
4					0.41				0.896			

Figure 7. Table representing the importance of flow velocities resulting from correlation analysis between ground temperatures and water temperatures as described in the text. The indicated values are the calculated phase shifts in [d].

The columns correspond to the temperature probes N01 to N12 and the lines to the different depths of temperature sensors. Orange coloured cells represent the measuring points at which the correlation factor exceeds a threshold value for which a phase shift to the water temperature is evaluable. A red coloured cell points out that the estimated pore velocity at that location is of the order greater or equal to  $10^{-3}$  m/s. As soon as a cell turns red an alarm is released by text message.

Figure 8 show the evolutions of the ground temperatures measured during a winter-spring period at different depths at probe N07 being the probe revealing maximum seepage flow until 07/03/2017 when repair works took place. The temperature increase induced by injection works are immediately recognized at 2.5 m and 3 m depth indicating the maximum flow velocities before sealing works. The temperatures at 2 m, 2.5 m and 3m strongly diverge from water temperature several weeks after the injections were realised and the automatic release of an alarm stopped. This evolution is also seen at the surrounding probes and the success of the repair work is retraced. The obvious correlation of ground temperatures at 0.5 m depth with water temperatures is evidently due to heat conduction by the surface.

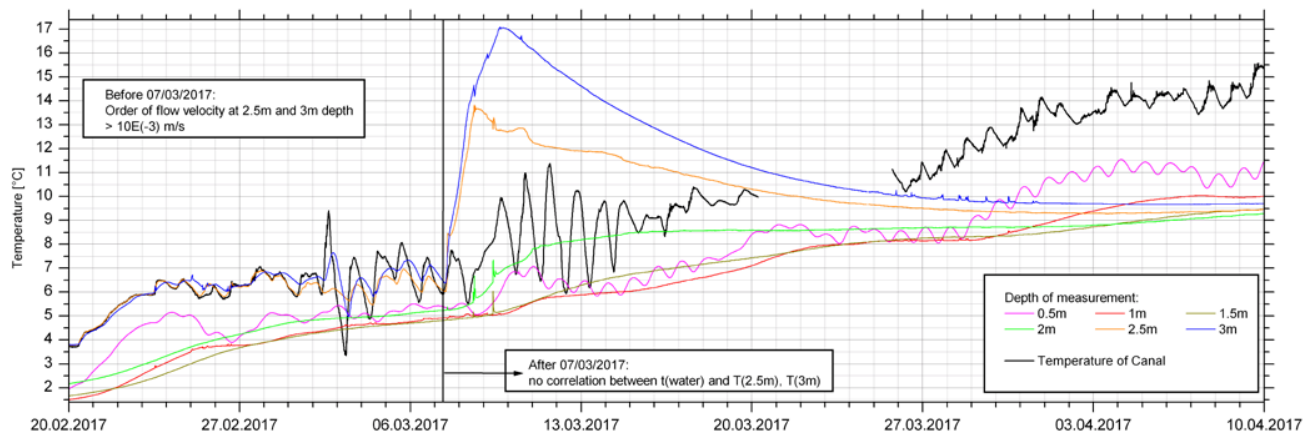


Figure 8. Temperature distribution after construction of the cut-off wall.

## 4 CONCLUSION

Recent developments in ground temperature measurements, data analysis and its computation have enabled the automatic estimation of orders of flow velocities. The pore velocity being the critical hydrodynamic parameter inducing internal erosion is now evaluable and traceable and its calculation provides the possibility to release an alarm at the early onset of internal erosion by text message or e-mail as asked for.

A general remote flow condition monitoring of dams and embankments is practicable by automatically and continuously visualizing the ground temperature measurements on an internet site or another transmission medium, exclusively for the client. Aggravation or amelioration of seepage zones might be followed.

## REFERENCES

- Aufleger, M., Dornstädter, J., Fabritius, A. and Strobl, Th. (1998). *Fibre optic temperature measurements for leakage detection - applications in the reconstruction of dams*. 66th ICOLD annual meeting, New Delhi, International Commission on Large Dams, Paris, 181-189.
- CNR avec partenaires GTC, IRSTEA et Cementys (2013) ; *Mise en œuvre de fibre optique en 3 dimensions pour l'auscultation renforcée de zones d'érosion interne*
- Dornstädter, J. (1997). *Detection of internal erosion in embankment dams*. 19th International Congress on Large Dams, Florence, International Commission on Large Dams, Paris, Q.73R.7.2: 87-101.
- Dornstädter, J. and Heinemann B. (2010). *In Situ Detection of Internal Erosion*. 8th ICOLD European Club Dam Symposium, Innsbruck, 481-485.
- Dornstädter J. and Dutton D. (2016). *Retrofit of Fibre Optics to existing Dams - Permanent Monitoring of Leakage and Detection of Internal Erosion*. 19th Biennial Conference of the British Dam society, Lancaster, 165-172.
- Garandet, A., Duchesne, L., Dornstädter, J., Heinemann, B. and Frappin, P. (2012). *Approches comparées de la thermométrie et des mesures de résistivité pour caractériser les écoulements d'une digue*. Colloque CFBR, Chambéry, 242-255.
- Kappelmeyer, O. (1957). *The use of near surface temperature measurements for discovering anomalies due to causes at depth*. Geophysical Prospecting, The Hague, Vol. 3: 239-258.
- Patent DE19621797 (2011). *Verfahren und Vorrichtung zur Leckageüberwachung an Objekten und Bauwerken*. Deutsches Patent- und Markenamt, Munich.



